

Departamento de Tecnología y Química Farmacéuticas  
Facultad de Farmacia y Nutrición

UNIVERSIDAD DE NAVARRA



TESIS DOCTORAL

**“IMAGING AND THERAPY OF BRAIN CANCER USING  
THERANOSTIC NANOPARTICLES”**

Trabajo presentado por Eurne Luque Michel para obtener el  
Grado de Doctor

Fdo. Eurne Luque Michel  
Pamplona, 2018





UNIVERSIDAD DE NAVARRA  
FACULTAD DE FARMACIA Y NUTRICION  
Departamento Tecnología y Química Farmacéuticas

DÑA. MARÍA JOSÉ BLANCO PRIETO, Doctora en Farmacia y Catedrática del Departamento de Farmacia y Tecnología Farmacéutica de la Universidad de Navarra.

Certifica:

Que el presente trabajo, titulado **“IMAGING AND THERAPY OF BRAIN CANCER USING THERANOSTIC NANOPARTICLES”**, presentado por **DÑA EDURNE LUQUE MICHEL** para optar al grado de Doctor en Farmacia, ha sido realizado bajo su dirección en el Departamento de Tecnología y Química Farmaceuticas de la Universidad de Navarra. Considerando finalizado el trabajo autorizan su presentación a fin de que pueda ser juzgado y calificado por el Tribunal correspondiente.

Y para que así conste, firma la presente:

Fdo.: Dra. María José Blanco Prieto

Pamplona, 2018



This project has been performed thanks to the economic support of different grants:

- ***Asociación de Amigos (University of Navarra) (2014-2016)***  
Dissertation research fellowships
- **Ministry of Education. Navarra Government (2016-2018)**  
Dissertation research fellowships
- **Short-term scientific missions (STSM)**  
**European Cooperation in Science & Technology (COST). COST Action TD1004 (2015)**  
Thanks to this grant I could learn how to perform the cellular model of the human blood brain barrier in the laboratory of Dr Karine Andrieux, University of Descartes, Paris (France)
- **Excellence Grant Program. Mobility scholarship for doctoral students**  
**Caja Navarra Bank Foundation (2018)**  
Thanks to this grant I could perform the *in vivo* studies by magnetic resonance imaging in the laboratory MINT (Micro et Nanomédecines Translationnelles) University of Angers, Angers (France).

The project presented configures an active collaboration with the Dr Victor Sebastian from the Institute of Nanoscience of Aragon (INA) who is an expert in microscopy images acquisition and has provided us the metallic NP and all the chemical knowledge that they involve.



*A mis padres,*





*Para los débiles es lo inalcanzable.*

*Para los temerosos, lo desconocido.*

*Para los valientes es la oportunidad.*

*Victor Hugo*



## *AGRADECIMIENTOS/ ACKNOWLEDGMENTS*

En primer lugar, me gustaría dar las gracias a María Blanco quien me aceptó en su grupo de investigación y me dio la oportunidad de trabajar en este desafiante proyecto. Gracias por los consejos y por guiarme, espero que te estén por venir muchos logros científicos. A mi profesora de Tecnología farmacéutica Rosa Hernández, quien me empujó sin saberlo a desarrollar esta tesis. A M<sup>a</sup> Angeles Solinís con quien empecé mis primeros pasos en la investigación y a quien siempre guardaré en muy buena estima. A Edurne Imbulzqueta quien me enseñó tanto en mis primeros años en la Universidad de Navarra. A la Universidad de Navarra y a todo su personal que nos acoge, se preocupa y nos guía para que obtengamos tesis doctorales de excelencia. Un agradecimiento muy especial a Víctor Sebastian quien sin importar la hora del día o la noche resuelve nuestras dudas y siempre me contagió la curiosidad científica que todos nosotros llevamos por vocación. Agradecer también a Marta Alonso y su grupo (Montse Puigdelloses y Marisol González) por aportarme las líneas celulares que necesité para desarrollar mi proyecto. *Thanks to Karine Andrieux for accepting me in the laboratory at the University of Descartes and to Caroline Roques for teaching me how to perform the blood brain barrier model. Thanks to Patrick Soulner for accepting me in the laboratory MINT and allowing me to get the international doctorate. Special thanks go to Laurent Lemaire for his care, for all that I learnt about MRI and glioma and for the excellent human quality.*

Un agradecimiento especial a todos mis compañeros y ya amigos por las conversaciones científicas y personales, por el apoyo y la motivación y por los muchísimos buenos momentos en los cafés, las sidrerías, las cenas, las cañas, las juergas, las excursiones, las bodas, los viajes, los conciertos... A todos los que aún siguen y a los que ya han emprendido un nuevo camino. ¡Ha sido un gran placer que todavía no ha acabado!

Un agradecimiento a toda mi gente con especial mención a quienes he involucrado más en la tesis: mi hermano, consejero y amigo, mi compañero de vida y mis amigas, quienes sin ser científicos ni estar interesados en ello han compartido conmigo largas conversaciones sobre mis progresos, fracasos y preocupaciones en estos primeros años de investigación. Y por último, los más importantes, mis padres Manolo y Blanca quienes siempre se han desvivido por darnos lo mejor. Gracias por los valores, por estar siempre, por querernos y por decirlo, por enseñarnos que es la vida y sobre todo, por habernos hecho libres y felices, muy felices. ¡Gracias!



# TABLE OF CONTENTS

<b>TABLE OF CONTENTS</b> .....	i
<b>ABBREVIATIONS</b> .....	iii
<b>INTRODUCTION</b> .....	1
<b>HYPOTHESIS AND OBJECTIVES</b> .....	43
<b>CHAPTER 1</b> .....	51
<hr/>	
Index .....	51
I. A simple approach to obtain hybrid Au-loaded polymeric nanoparticles with a tunable metal load	
Abstract .....	53
1. Introduction .....	54
2. Results and discussion .....	57
3. Experimental .....	69
4. Conclusions .....	72
5. Notes and references .....	72
II. Visualization of hybrid gold-loaded polymeric nanoparticles in cells using scanning electron microscopy	
Abstract .....	77
1. Introduction .....	78
2. Materials and methods .....	79
3. Results and discussion .....	82
4. Conclusions .....	87
5. References .....	88
<b>CHAPTER 2</b> .....	95
<hr/>	
Co-encapsulation of superparamagnetic nanoparticles and doxorubicin in PLGA nanocarriers coated with surfactants for glioma theragnosis	
Abstract .....	95
Index .....	96

---

1. Introduction .....	96
2. Material and methods .....	98
3. Results and discussion .....	103
4. Conclusions .....	115
5. References .....	115
<b>CHAPTER 3</b> .....	<b>125</b>
<hr/> <b>Magnetic enhancement into brain tumor and MRI monitoring of SPION and doxorubicin-loaded PLGA nanocarriers with different surfactants</b>	
Abstract .....	125
Index .....	127
I. Introduction .....	126
II. Material and methods .....	127
III. Results and discussion .....	134
IV. Conclusions .....	147
V. References.....	147
<b>DISCUSSION AND OUTLOOK</b> .....	<b>155</b>
<b>CONCLUSSIONS</b> .....	<b>185</b>
<b>CONCLUSIONES</b> .....	<b>187</b>
<b>ANNEX 1</b> .....	<b>191</b>
<hr/> <b>Supplementary Material of chapter 2: A simple approach to obtain hybrid Au-loaded polymeric nanoparticles with tunable metal load.</b>	
<b>ANNEX 2</b> .....	<b>199</b>
<hr/> <b>Optimization of doxorubicin (DOX) encapsulation into polymeric nanoparticles (PNP) using Lactic-co-Glycolic Acid (PLGA) as polymer.</b>	
<b>ANNEX 3</b> .....	<b>205</b>
<hr/> <b>Efficient production of hybrid bio-nanomaterials by continuous microchannel emulsification: Dye-doped SiO<sub>2</sub> and Au-PLGA nanoparticles</b>	

## *ABBREVIATIONS*

<b>AIDS</b>	Acquired Immunodeficiency Syndrome
<b>ANOVA</b>	Analysis of variance
<b>ATCC®</b>	American type culture collection
<b>Au</b>	Gold nanoparticles
<b>Au NP</b>	Gold nanoparticles
<b>BBB</b>	Blood brain barrier
<b>CH50</b>	Complement consumption
<b>C</b>	Carbon
<b>C-dots</b>	Cornell dots
<b>CMC</b>	Critical micelle concentration
<b>CT</b>	Computed tomography
<b>DACH-Pt</b>	Diaminocyclohexane-platinum
<b>DDS</b>	Drug delivery systems
<b>DHAD</b>	Dihydroxyanthracenedione
<b>DLS</b>	Dynamic light scattering EFG (epidermal growth factor)
<b>DMEM</b>	Dulbecco's Modified Eagle's medium
<b>DMSO</b>	Dimethyl sulfoxide
<b>DOX</b>	Doxorubicin
<b>EPR</b>	Enhanced permeability and retention
<b>FBS</b>	Fetal Bovine Serum
<b>FDA</b>	Administración de Alimentos y Medicamentos Estadounidense
<b>Fe</b>	Iron
<b>FGF-2</b>	basic Fibroblast Growth Factor
<b>FOV</b>	Field of view
<b>FTIR</b>	Fourier-Transform Infrared Spectroscopy
<b>GBM</b>	Glioblastoma
<b>HCl</b>	Hydrochloric acid
<b>HPMA</b>	N-(2-hydroxypropyl) methacrylamide)
<b>IC<sub>50</sub></b>	Inhibitory concentration 50
<b>LY</b>	Lucifer yellow
<b>MDR</b>	Multidrug resistance
<b>MICRO-CT</b>	Microcomputed tomography

## ABREVIATIONS

<b>MRI</b>	Magnetic resonance imaging
<b>MTT</b>	CellTiter 96® AQueous One Solution Cell Proliferation Assay
<b>MWCO</b>	Molecular weight cut-off
<b>NaOH</b>	Sodium hydroxide
<b>NCT</b>	Nationa Clinical Trial. ClinicalTrials.gov identifier
<b>NIR</b>	Near-infrared
<b>NIRF</b>	Near-infrared fluorescence
<b>NP</b>	Nanoparticles
<b>NPs</b>	Nanoparticles
<b>PBS</b>	Phosphate-buffered saline
<b>PDI</b>	Polydispersity index
<b>O</b>	oxygen
<b>OCM</b>	Optical coherence microscopy
<b>OCT</b>	Optical coherence tomography
<b>OI</b>	Optical imaging
<b>P-gp</b>	P-glycoprotein
<b>PAA</b>	Poly (aspartic acid)
<b>PACA</b>	Poly (alkyl cyanoacrylate)
<b>PBCA</b>	Poly (butyl cyanoacrylate)
<b>PDC</b>	Polymer-drug conjugates
<b>PEG</b>	Polyethylene glycol
<b>PET</b>	Positron-emission tomography
<b>PGA</b>	Poly (glutamic acid)
<b>PIHCA</b>	Poly (isohexyl cyanoacrylate)
<b>PLA</b>	Poly (lactic acid)
<b>PLGA</b>	Polymer Lactic-co-Glycolic Acid
<b>PM</b>	Polymeric micelles
<b>PMMA NP</b>	poly (methyl methacrylate) nanoparticles
<b>PNP</b>	Polymeric nanoparticles
<b>PPO</b>	Polypropylene oxide
<b>PSMA</b>	Prostate-specific membrane antigen
<b>PVA</b>	Polyvinyl alcohol
<b>r1</b>	Longitudinal relaxivity
<b>r2</b>	Transversal (r2) relaxivity
<b>ROS</b>	Reactive oxygen species



## ABREVIATIONS

<b>SC</b>	Sodium cholate
<b>SD</b>	Standard deviation
<b>SEM</b>	Scanning electron microscope
<b>SI</b>	Signal intensity
<b>SLN</b>	Solid lipid nanoparticles
<b>SPECT</b>	Single photon emission computed tomography
<b>SPIO</b>	Superparamagnetic iron oxide
<b>SPION</b>	Superparamagnetic iron oxide nanoparticles
<b>SPR</b>	Surface plasmon resonance
<b>STC</b>	Sodium taurocholate
<b>SWI</b>	Susceptibility weighted images
<b>T1</b>	Longitudinal relaxation time
<b>T2</b>	Transversal relaxation time
<b>T</b>	Telsa
<b>T80</b>	Tween 80
<b>TE</b>	Time echo
<b>TEER</b>	Transendothelial electrical resistance
<b>TEM</b>	Transmission electronic microscope
<b>TC</b>	Taurocholic acid sodium salt hydrate
<b>TPGS</b>	Tocopheryl polyethylene glycol 1000 succinate
<b>TR</b>	Repetition time
<b>UHPLC MS/MS</b>	Ultrahigh performance liquid chromatography tandem mass spectrometry
<b>USPIO</b>	Ultra-small superparamagnetic iron oxide
<b>UV/vis</b>	Ultraviolet/visible
<b>v/v</b>	Volume/volume
<b>VBS2+</b>	Veronal Buffered Saline containing 0.15 mM Ca <sup>2+</sup> and 0.5 mM of Mg <sup>2+</sup>
<b>w/v</b>	Weight/volume
<b>W<sub>1</sub>/O/W<sub>2</sub></b>	Water-in-oil-in-water (double emulsion)
<b>W/O</b>	Oil-in-water (single emulsion)
<b>WHO</b>	World Health Organization



# INTRODUCTION

---

**Clinical advances of nanocarrier-based cancer therapy and  
diagnostics**

Expert Opin Drug Deliv, 14, 75-92, 2017. IF: 5,657  
PHARMACOLOGY, TOXICOLOGY AND  
PHARMACEUTICS: 85/783, Q1  
<http://dx.doi.org/10.1080/17425247.2016.1205585>





## Clinical advances of nanocarrier-based cancer therapy and diagnostics

Edurne Luque-Michel<sup>a,b</sup>, Edurne Imbuluzqueta<sup>a,b</sup>, Víctor Sebastián<sup>c,d</sup> and María J. Blanco-Prieto<sup>a,b</sup>

<sup>a</sup>*Department of Pharmacy and Pharmaceutical Technology, School of Pharmacy and Nutrition, University of Navarra, Pamplona, Spain.*

<sup>b</sup>*IdiSNA, Fundación Instituto de Investigación Sanitaria de Navarra, Recinto del Complejo Hospitalario de Navarra, Pamplona, Spain.*

<sup>c</sup>*Institute of Nanoscience of Aragon (INA) and Department of Chemical, Engineering and Environmental Technology, University of Zaragoza, Zaragoza, Spain.*

<sup>d</sup>*CIBER de Bioingeniería, Biomateriales y Nanomedicina (CIBER-BBN), Centro de Investigación Biomédica en Red, Madrid, Spain.*

### ABSTRACT

**Introduction:** Cancer is a leading cause of death worldwide and efficient new strategies are urgently needed to combat its high mortality and morbidity statistics. Fortunately, over the years, nanotechnology has evolved as a frontrunner in the areas of imaging, diagnostics and therapy, giving the possibility of monitoring, evaluating and individualizing cancer treatments in real-time.

**Areas covered:** Polymer-based nanocarriers have been extensively studied to maximize cancer treatment efficacy and minimize the adverse effects of standard therapeutics. Regarding diagnosis, nanomaterials like quantum dots, iron oxide nanoparticles or gold nanoparticles have been developed to provide rapid, sensitive detection of cancer and, therefore, facilitate early treatment and monitoring of the disease. Therefore, multifunctional nanosystems with both imaging and therapy functionalities bring us a step closer to delivering precision/personalized medicine in the cancer setting.

**Expert opinion:** There are multiple barriers for these new nanosystems to enter the clinic, but it is expected that in the near future, nanocarriers, together with new 'targeted drugs', could replace our current treatments and cancer could become a nonfatal disease with good recovery rates. Joint efforts between scientists, clinicians, the pharmaceutical industry and legislative bodies are needed to bring to fruition the application of nanosystems in the clinical management of cancer.

### INDEX

1. Introduction.....	2
2. Clinical status of polymer-based nanocarriers for cancer therapy .....	4
2.1. Polymeric micelles .....	5
2.2. Polymer-drug conjugates.....	9
2.3. Polymeric nanoparticles.....	14
3. Cancer diagnostics and nanotechnology .....	18
3.1. Magnetic resonance imaging.....	18
3.2. Positron-emission tomography.....	23
3.3. Positron-emission tomography.....	24
4. Cancer theranostics and nanotechnology.....	26
5. Conclusion .....	29
6. Expert opinion .....	30

### 1. INTRODUCTION

Cancer is one of the most alarming diseases of all human disorders. According to the WHO World Cancer Report 2014, this disease was responsible for 8.2 million deaths in 2012, with 14 million new cases in the same year. In fact, it is expected that within the next 2 decades, annual cancer numbers will reach 22 million (1). Cancer is a heterogeneous group of malignant diseases that begins when a DNA mutated cell that should die does not do so. With fatal consequences, this cell triggers abnormal cancer cell growth, forming a tumor (except in the case of hematologic cancers) that invades healthy tissues and then spreads to other parts of the body creating secondary tumors named metastases, which are the major cause of death from cancer (2, 3). The methods globally used for cancer therapy are surgery, radiation, chemotherapy and immunotherapy. However, efficient new treatments are urgently needed to combat the high mortality and morbidity statistics. Regarding conventional chemotherapy, its inconveniences include high toxicity and the inadequate bio-distribution and pharmacokinetics profile of the cytostatic drugs (4, 5). On the other hand, early detection of cancer significantly increases patient survival. Nonetheless, current diagnostic methods (biopsies, imaging procedures and detection of markers) are often invasive, present low sensitivity or detect cancer only in its later stages, which

is the main reason for the high mortality rate. Although new biomarkers are being investigated, it is still necessary to develop new, faster, highly specific and more sensitive diagnostic technologies alongside new therapy strategies (6, 7). At present, two main research lines are being developed to improve cancer management. The first one involves the use of genomics and proteomics studies for the identification of specific targets in order to synthesize therapeutically active drugs without side effects (“targeted drugs”). Several are already on the market and are producing good results, such as the tyrosine kinase inhibitor Glivec® (Gleevec® in the USA). However, it is important not to forget the drug resistance they induce (8, 9). The second one, which will form the object of this review, is the design of nanomaterials to transport and deliver biomedical compounds through biological systems for the treatment, diagnosis, and for the theranostics of cancer (with the combination of diagnostic and therapeutic compounds into multifunctional nanoplatforms) (10). The use of nanotechnology to develop these systems has been well established over the past decade, both in pharmaceutical research and the clinical setting. Nanosystems have tuneable size, shape and surface characteristics, and they offer two mechanisms to reach cancerous tissue: passive and active targeting. The passive accumulation of nanocarriers in solid tumors is based on the so-called enhanced permeability and retention (EPR) effect that consists in their retention due to increased leakiness of neovascularization as well as impaired lymphatic drainage in tumor tissues (5, 11). On the other hand, active targeting is possible through the functionalization of the surface of the nanocarriers with biological targeting moieties (ligands), the main targets being the specific receptors expressed on cancer cells and/or tumor endothelial cells (4, 12).

At present, one of the most frequent applications of biomedical nanotechnology is to enhance the efficacy of anticancer drugs already used in clinical settings by improving their bioavailability and safety, and their targeting at the cancer cells, without damaging healthy tissues. It is known that drugs carried by nanoparticles (NP) evade the efflux mechanism (over-expressed in tumors), maintain a high concentration within tumor cells, and therefore avoid drug resistance in the cells, which is one of the biggest challenges in cancer chemotherapy (5). On the other hand, the application of diagnostic nanomedicines allows the early detection and identification of tumor cells

which is indispensable to improve the prognosis of the disease. Therefore, theranostics nanocarriers could personalize the treatment of cancer, avoiding the over- and underdosing that currently occurs as a result of the high interindividual variability of this disease (10, 13). In fact, with these nanosystems it is expected to bring about significant improvements, offering early diagnosis, lower toxicity and reduced treatment costs (14). To date, the medical use of nanomaterials in oncology has made good progress, with some nano-based products already on the market and others in various stages of preclinical and clinical development. This review highlights the clinical status and recent advances of nanotechnology based products in cancer, encompassing organic and inorganic-based systems.

## **2. CLINICAL STATUS OF POLYMER-BASED NANOCARRIERS FOR CANCER THERAPY**

Nanomaterials designed for cancer therapy can be as diverse as micelles, dendrimers, inorganic NP, carbon NP and nanotubes, nanodiamonds, nanoemulsions, viral nanocarriers, peptide NP, solid lipid NP (15-18), etc., although most clinically available nanomaterials for human use are liposomes and polymer-based nanoformulations (11, 12). In fact, the first nanotechnology-based cancer drugs on the market was Doxil<sup>®</sup>, a pegylated liposome with the drug doxorubicin encapsulated (5), which was approved in 1995 by the Food and Drug Administration (FDA) for the treatment of AIDS-related Kaposi's sarcoma, and in 1997 in Europe under the brand name Caelyx<sup>®</sup> (now also indicated for the treatment of metastatic breast cancer, ovarian cancer and multiple myeloma) (5, 12). However, despite the clinical progress made using liposomes, they present difficulties when it comes to modulating drug release *in vivo*, as well as stability problems and a limited capacity for drug loading (12). Fortunately, polymer-based nanostructures have been developed to overcome these problems (10, 12) and nowadays polymer therapeutics are being developed with a wide variety of architectures and chemical properties. Polymers used in drug delivery systems (DDS) can be synthetic, like poly(esters), poly(alkyl cyanoacrylates) and poly(ethers) or natural, like proteins (such as albumin) and polysaccharides (12, 19). Synthetic polymers have the advantage of being prepared with tailored compositions and have



properties that are easily adjustable to specific applications. Therefore, although there are some natural polymer-based DDS already on the market for cancer treatment, owing to the great versatility that synthetic polymers offer, this section will focus on the clinical status of the most relevant synthetic polymer-based DDS, including polymeric micelles (PM), polymer-drug conjugates (PDC) and polymeric nanoparticles (PNP) (Figure 1).

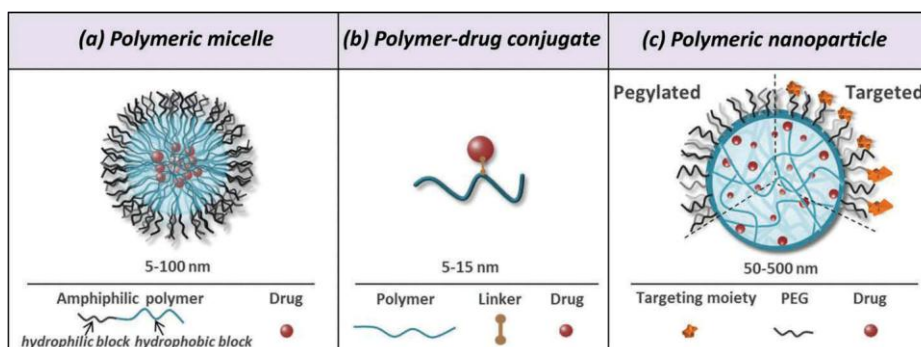


**Figure 1.** - Illustration of the most relevant synthetic polymer-based drug delivery systems in clinical trials. PEG = Poly(ethylene glycol)

## 2.1 POLYMERIC MICELLES

PM are promising vehicles for the controlled delivery of poorly water soluble drugs, and therefore offer great potential to improve the therapeutic window of lipophilic antitumor drugs such taxanes or platinates. With a mean diameter ranging from 5 to 100 nm, PM are nano-sized supramolecular constructs made of amphiphilic block copolymers that self-assemble in an aqueous environment above a polymer concentration known as critical micelle concentration (CMC) (20). They present a core-shell architecture in which the hydrophobic block of the copolymer forms a semi-solid core and the hydrophilic segment a coronal layer (see Figure 1 a). Within this structure, the active molecules can be physically entrapped in the hydrophobic core, avoiding the requirement of functional groups for drug encapsulation, or may also be chemically conjugated to the amphiphilic polymer, enhancing drug loading and preventing premature drug release. On the other hand, the hydrophilic corona provides good stability for the micellar structure as well as protection against rapid clearance from the body (21). Regarding the polymers used for the formulation of PM, although alternatives are being explored, poly (ethylene glycol) (PEG) is the most

frequent hydrophilic block in the copolymer structure. In fact, this polymer is widely used in the synthesis of nanosystems because it prevents recognition of the carrier as a foreign body by the mononuclear phagocyte system, increasing the blood circulation time. Conversely, there are various polymers used to form the micellar core, poly(ethers), poly(esters), poly(amino acid)s and N-(2-hydroxypropyl) methacrylamide (HPMA) being the ones that have a longer development track record.

PM have been under intense investigation for cancer therapy purposes during the past few decades, and some of them are currently undergoing clinical evaluation or are already on the market. A summary is presented in table 1. To date, there are two PM on the market: Genexol-PM<sup>®</sup>, and Nanoxel-PM<sup>™</sup>, two monomethoxy PEG-b-poly(D,L lactic acid) (PLA) formulations which were specifically designed to improve the solubility of paclitaxel and docetaxel, respectively, and avoid the need to use toxic solubilizing agents such Cremophor<sup>®</sup> EL or Tween 80<sup>®</sup>. Genexol-PM<sup>®</sup> is available in South Korea and other Asian countries for the treatment of breast, non-small cell lung and ovarian cancer (22, 23) and is currently undergoing bioequivalence testing to gain marketing approval in the USA. Genexol-PM<sup>®</sup> will probably be registered in the USA and European markets under the name Cynviloq<sup>™</sup> as a bioequivalent to Abraxane<sup>®</sup> (24, 25). Regarding Nanoxel-PM<sup>™</sup>, which is also commercialized in South Korea, it is under clinical evaluation for pharmacokinetic equivalence with Taxotere<sup>®</sup> as well as for safety and antitumor efficacy (NCT01336582 and NCT02639858).

**Table 1:** Polymeric micelles on the market or clinical trials for cancer therapy. Asp = aspartic acid; GEJ = gastroesophageal junction; HNSCC = head and neck squamous cell carcinoma; JapicCTI# = clinicaltrials.jp registry number, clinical trials information of the Japan Pharmaceutical Information Center; mPEG = methoxy-poly(ethylene glycol); NCT# = ClinicalTrials.gov registry number; NSCLC = non-small cell lung cancer; PGA = poly(L-glutamic acid); PLA = poly (D,L lactic acid); SCLC = small cell lung cancer

Product name	Company	Drug	Polymer	Indication	Clinical status
IG-001 (Genexol-PM <sup>®</sup> ) (Paxus-PM <sup>®</sup> ) (Cynviloq <sup>™</sup> ) (Paclitaxel-PM)	Samyang Biopharmaceutic als Corporation	Paclitaxel	mPEG-PLA	Breast cancer, ovarian cancer and NSCLC	Marketed in South Korea and other Asian countries (NCT02064829)
				Metastatic or locally recurrent breast cancer	Bioequivalence study versus Nab-paclitaxel
				Recurrent or metastatic breast cancer	Phase III (NCT00876486)
				Taxane-pretreated recurrent breast cancer	Phase IV (NCT00912639)

				Unresectable locally advanced or metastatic pancreatic cancer	Phase II (NCT00111904)
				Advanced NSCLC in combination with carboplatin	Phase II (NCT01770795)
				Locally advanced HNSCC in combination with cisplatin	Phase II (NCT01689194)
				Advanced Urothelial Cancer	Phase II (NCT01426126)
				Advanced ovarian cancer in combination with carboplatin	Phase I (NCT00877253)
Nanoxel-PM™ (Docetaxel-PM) (Nanoxel® M)	Samyang Biopharmaceuticals Corporation	Docetaxel	mPEG-PLA	Breast, NSCLC, prostate, ovarian, head and neck, gastric and esophageal cancer	Marketed in South Korea
				Advanced solid tumor or NSCLC, biliary tract, and bladder cancer	Phase I (NCT01336582)
				Recurrent or metastatic HNSCC	Phase II (NCT02639858)
SP1049C	Supratek Pharma Inc.	Doxorubicin	Pluronic® P-61 and F-127 block copolymers	Advanced refractory adenocarcinoma of the esophagus or GEJ	Phase II (26)
NK911	Nippon Kayaku Co., Ltd	Doxorubicin	PEG-poly(α,β-Asp)	Solid tumors	Phase I (Japan)(106)
				Metastatic pancreatic cancer	Phase II (14)
NK105	NanoCarrier Co., Ltd Nippon Kayaku Co., Ltd	Paclitaxel	PEG-modified poly(α,β-Asp)	Recurrent or metastatic breast cancer	Phase III (NCT01644890)
				Advanced gastric cancer	Phase II (JapicCTI-090769)
NC-6300 K-912	NanoCarrier Co., Ltd. Kowa Company, Ltd	Epirubicin	PEG-poly (aspartate-hydrazone)	Advanced or metastatic solid tumors	Phase I (JapicCTI-132221)
				Triple negative breast cancer	Phase II (NCT00951054)
				Refractory solid tumors	Phase I (NCT00542958)
				Relapsed SCLC	Phase II (NCT00951613)
NK012	Nippon Kayaku Co., Ltd	SN38	PEG-modified PGA	Metastatic colorectal cancer in combination with 5-fluorouracil	Phase II (NCT01238939)
				Unresectable advanced colorectal cancer	Phase II (JapicCTI-090780)
				Multiple myeloma	Phase I/II (JapicCTI-111652)
NC-4016	NanoCarrier Co., Ltd.	Oxaliplatin	mPEG-PGA	Advanced solid tumors or lymphoma	Phase I (NCT01999491)
Nanoplatin® (NC-6004)	NanoCarrier Co., Ltd.	Cisplatin	mPEG-PGA	Locally advanced or metastatic pancreatic cancer in combination with gemcitabine	Phase III (NCT02043288); Phase I/II (NCT00910741)
				Advanced solid tumor	Phase I/II (NCT02240238)
Cripec® - docetaxel	Cristal Therapeutics	Docetaxel	Thermosensitive PEG-β-poly(N-(2-hydroxypropyl)-methacrylamide-lactate)	Solid tumors	Phase I (NCT02442531)

Besides PLA micelles, other PM undergoing clinical trials are Pluronic® and poly(amino acid) micelles. Pluronic® or poloxamers are amphiphilic PEG-poly(propylene oxide) (PPO)-PEG tri-block copolymers that present temperature

dependent self-assembling and thermo-gelling behavior. Pluronic L61 (PEG<sub>2</sub>-PPO<sub>30</sub>-PEG<sub>2</sub>) is a potent Pgp inhibitor and sensitizer of multidrug resistant (MDR) cancer cells and Pluronic F127 (PEG<sub>100</sub>-PPO<sub>65</sub>-PEG<sub>100</sub>) can improve the physical stability and increase the blood circulation time of the carrier due to its long PEG hydrophilic chain. SP1049C is a mixed micelle formulation of Pluronic® L61 and F127, which physically encapsulate doxorubicin. It is particularly active in MDR and metastatic cancers and has successfully completed a phase II clinical trial demonstrating safety and efficacy in patients with advanced adenocarcinoma of the esophagus and gastroesophageal junction, and has achieved FDA orphan drug approval (20, 26). Moreover, an international phase III study designed for this formulation has been reviewed and agreed to with the FDA under a Special Protocol Assessment procedure (27). On the other hand, micelles made of block copolymers of poly(amino acid)s are very attractive due to their high biocompatibility and flexibility to carry drugs by chemical conjugation to the polymer. There are two types of PEG-poly(amino acid) micelles that have been evaluated in clinical trials, PEG-poly (glutamic acid) (PGA) and PEG-poly (aspartic acid) (PAA) micelles. The first PEG-poly(amino acid) micelle to advance into clinical evaluation was NK911 (14, 21), a PEG-PAA micelle in which doxorubicin is chemically conjugated to increase the affinity of the core for physically encapsulated doxorubicin, improving the stability of the micellar structure and achieving high drug loading (28). Similarly, in the paclitaxel containing NK105, the PEG-PAA copolymer was modified by an esterification reaction with 4-phenyl-1-butanol to increase its core hydrophobicity and enhance its affinity for the drug. This formulation is already far advanced in clinical studies in patients with metastatic or recurrent breast cancer (phase III) (NCT01644890) (29). Along the same lines, before the self-assembly of the micelle, hydrophobic drugs can be conjugated to this type of PEG-poly(amino acid) copolymers via linkages dissociable under the desired conditions that trigger the drug delivery (14, 21). Using this method, stimuli-responsive micellar systems are obtained. NK012, currently in phase II development, is prepared by conjugating the active metabolite of irinotecan hydrochloride SN-38 to the PGA copolymer segment via an ester bond that can be cleaved by hydrolysis under physiological conditions (30). The same occurs with NC-6300, a pH sensitive micellar system. In this case, the cytostatic drug epirubicin has been covalently bonded to the copolymer through a hydrazone linkage to be selectively released at

the low pH of intracellular and tumor environments (20, 31, 32). In addition, PEG-poly(amino acid) micelles have also reached clinical trials using the major component in chemotherapy regimens, platinum drugs. After showing low bloodstream stability with PAA, PGA was used as hydrophobic block in NC-4016 and NC-6004 (Nanoplatin®). These systems encapsulate diaminocyclohexane platinum (DACH-Pt, the active metabolite of oxaliplatin) and cisplatin, respectively, presenting a prolonged blood circulation time and a safer profile than the active molecules they encapsulate (33, 34).

Finally, another type of PM that have entered clinical trials are core-cross-linked PM, which have been designed to enhance micelle stability and prevent the premature dissociation of the micelle and consequent drug release at concentrations below CMC, as occur in the bloodstream (35). Cripec®-docetaxel is a PM composed of methoxy PEG-b-poly (HPMA lactate) thermosensitive block copolymers cross-linked through the conjugation of the core with the docetaxel itself by hydrolysis-sensitive covalent linkages. This core cross-linked PM is under clinical trial to find the highest safe dose in the treatment of solid tumors (35-38).

Therefore, even though there are still certain difficulties in controlling micelle dissociation and drug release rate, PM hold promise as an effective DDS in cancer therapy (19, 20, 39). Indeed, on the basis of the ongoing efforts, it is expected that in the coming years more PM will go on the market (21, 37).

## **2.2 POLYMER-DRUG CONJUGATES**

Polymer-drug conjugates (PDC) are macromolecular prodrugs of 5-15 nm comprising a chemotherapeutic agent covalently attached, usually through a peptidyl or ester linkage, to a polymeric carrier used to improve the performance of the drug (see Figure 1 b). The PDC formed is a new entity with different solubility, toxicity and pharmacokinetic profile and with the ability to overpass drug resistance mechanisms and to accumulate in the tumor by the EPR effect (40). Polymer-drug/protein conjugates are the most extensively studied polymeric carriers in the clinical setting, and three polymer-protein conjugates are already being marketed for cancer therapy: Zinostatin Stimalamer®, Oncaspar® and Neulasta® (40, 41). However, although, a large

number of studies have been carried out in the field of PDC, unfortunately none has yet reached the market (Table 2). The most advanced PDC in clinical trials is Opaxio® (Xyotax®), a paclitaxel-PGA conjugate which is being studied alone or in combination with others antineoplastics in phase III clinical trials. In this conjugate, paclitaxel is bound to PGA through a glycinate ester linkage and is only released by the action of cathepsin B, an intracellular lysosomal protease enzyme up-regulated in many tumor types (12). Likewise, peptidyl linkages are stable in plasma and cleavage by lysosomal proteases. They are commonly used in the synthesis of HPMA copolymer–drug conjugates. Some examples include PK1, the first PDC to proceed to clinical trials in 1994. PK1 consists of a HPMA copolymer covalently conjugated to doxorubicin via a glycyl–phenylalanyl–leucyl–glycine linker (42) which is under two phase II clinical trials for the treatment of breast, lung and colorectal cancer (14). The same conjugate with active targeting ability has also been developed under the name of PK2 (FCE28069), in which galactosamine moieties were added to target the asialoglycoprotein receptor present in hepatocytes and hepatoma cell lines (43). Phase I studies of this conjugate have demonstrated liver-specific doxorubicin delivery (44), but the accumulation of PK2 in normal liver tissue is still a serious concern and therefore, currently, PK2 is not under an active development program. AP5280 is another HPMA polymer conjugated to cis-NH<sub>3</sub> platinum via a tetrapeptide linker that has provided promising phase I clinical results (45); however, the company, Access Pharmaceuticals, focused on ProLindac™ (AP5346), discontinuing the development of AP5280. This conjugate has already completed a phase II clinical trial for advanced recurrent ovarian cancer and has been shown to release DACH-Pt from HPMA at acidic environments, such as the tumor microenvironment or the intracellular lysosomal compartment (46). It is important to highlight the importance of using linkers that ensure the stability of the conjugate in the systemic circulation, as some PDC have failed in early clinical studies due to this issue. This is the case with the HPMA conjugate of camptothecin (PNU 166148), a conjugate with bladder toxicity due to its urine labile linker and high urinary excretion, or paclitaxel (PNU 166945), which caused same neurotoxicity as the free drug due to the fast drug release from the conjugate (47, 48). PEG is another polymer commonly used to synthesize PDC. PEG possesses two functional –OH groups suitable for conjugation and it can be modified to obtain more sites of drug binding, giving place to PDC with a

higher drug loading capacity while the molecular weight is simultaneously increased. Most of the drugs in PEG-drug conjugates under clinical trials are from the camptothecin family (camptothecin, SN38 and irinotecan). Pegamotecan is a camptothecin-PEG conjugate whose development was discontinued because it had a similar toxicological profile to native drug due to quick *in vivo* hydrolysis of its alaninate ester linkage (49). The company therefore focused on improving the formulation: the new conjugate, named EZN-2208 is made up of a camptothecin derivative SN38 and a 4-arm PEG polymer, and has improved drug loading with slower hydrolysis of the ester linker. All these improvements allow the new formulation to accumulate in the tumor by the EPR effect. This last architecture of multi-arm PEGs was also exploited for the preparation of docetaxel-PEG (NKTR-105) conjugate, currently under dose-escalation phase I study and irinotecan-PEG (NKTR-102) conjugate, which is highly advanced in phases I, II and III of clinical trials. As in the case of other polymer conjugates, there is a PEG conjugate with failed clinical development. This is paclitaxel-PEG conjugate, which completed a phase I clinical trial but the company Enzon unfortunately discontinued its development without apparent reasons (49, 50). Similarly, more PDC studies appear to have been discontinued without sufficient information, such as the dextran bioconjugates of the topoisomerase I inhibitor exatecan (DE-310) and doxorubicin (AD-70, DOX-OXD) (51, 52).

Finally, XMT-1001 is a novel active camptothecin analogue conjugated to the biodegradable polyacetal polymer Fleximer® (poly(1-hydroxymethylethylene hydroxymethylformal)), which has successfully completed a phase I clinical trial and is currently in phase Ib clinical trial for the treatment of gastric and non-small cell lung cancer. Specifically, this conjugate is a polymeric pro-drug derivative of camptothecin with a dual release mechanism; first the active camptothecin analogue is released non-enzymatically, enters cells readily because of its lipophilicity and then, mostly intracellularly, the analogue can be further converted into another active analogue or camptothecin through hydrolysis. Therefore, PDC enhance the efficacy of camptothecin by increasing accumulation of the drug and its active analogues in the tumor. Furthermore, due to the low level of camptothecin in blood, its urinary excretion is low and its bladder toxicity is avoided. In addition, the use of this

## INTRODUCTION

analogue avoids the gastrointestinal toxicity associated with other camptothecin analogues such as irinotecan or SN-38 (53-55).

Although some PDC clinical trials failed, showing us the importance of a careful design of polymer-drug linkers, more than 10 anticancer conjugates are currently in clinical development and it is expected that they will enter the market in the near future. Indeed, a future PDC generation will reach clinical development, meeting challenges such as the development of novel polymers with high molecular weight and the development of versatile conjugation chemistry to allow accurate control of therapy as well as the delivery of different or multiple drugs.

**Table 2: Polymer-drug conjugates on clinical trials for cancer therapy.** DACH = diaminocyclohexane; EudraCT Number = Clinical trial registry number of the European Union Drug Regulatory Authorities Clinical Trial System; GFLG = Gly-Phe-Leu-Gly; HNSCC =Head and Neck Squamous Cell Carcinoma; HPMA = N-(2-Hydroxypropyl)methacrylamide; NCT = ClinicalTrials.gov registry number; NSCLC= non-small cell Lung Cancer; PEG = poly(ethylene glycol); PGA = Poly-L-glutamic acid; PHF = Poly(1-hydroxyl-methylethylene hydroxyl-methyl-formal); SCLC= small cell lung cancer

Product name	Company	Drug	Polymer (linker/spacer)-targeting moiety	Indication	Clinical status
Opaxio® (Xyotax®) (paclitaxel poliglumex) (CT-2103)	Cell Therapeutics, Inc	Paclitaxel	PGA (Ester)	Advanced NSCLC	Phase III (NCT00054197 and NCT00269828); Phase II (NCT00487669) (in combination with pemetrexed); Phase III (NCT00576225, NCT00054210 and NCT00551733)(in combination with carboplatin)
				Progressive NSCLC	Phase III (NCT00054184)
				Metastatic breast cancer	Phase I (NCT00270907) (in combination with gemcitabine); Phase II (NCT00148707); Phase II (NCT00265733) (in combination with capecitabine)
				Advanced HNSCC in combination with cetuximab	Phase I/II (NCT00660218)
				Epithelial ovarian, primary peritoneal, or fallopian tube carcinoma	Phase I/II (NCT00017017); Phase I (NCT00060359) (in combination with carboplatin)
				Maintenance therapy in advanced ovarian, primary peritoneal or fallopian tube cancer	Phase III (NCT00108745)
				Recurrent or persistent epithelial ovarian or primary peritoneal cancer	Phase II (NCT00045682); Phase II (NCT00069901) (in combination with carboplatin)
				Advanced hormone refractory prostate cancer	Phase II (NCT00446836)
				Androgen Independent Prostate Cancer	Phase II (NCT00459810) (in combination with transdermal estradiol)
				Esophageal cancer in	Phase II (NCT00522795)



				combination with cisplatin and radiation	
				Metastatic colorectal cancer	Phase I (NCT00598247)
				newly diagnosed brain tumors in combination with temozolomide and radiation	Phase II (NCT00763750)
				Newly diagnosed glioblastoma multiforme in combination with radiation therapy	Phase II (NCT01402063)
				Advanced ovarian cancer	Phase II (NCT00291837)
CT-2106	Cell Therapeutics, Inc	Camptothecin	PGA (Ester)	Metastatic colorectal cancer in combination with 5-FU and folic acid	Phase I/II (NCT00291785)
				Unspecified adult advanced solid tumor	Phase I (NCT00059917)
PK1 (FCE28068)	Pharmacia and Upjohn	Doxorubicin	HPMA copolymer(Amide / GFLG)	Advanced breast cancer	Phase II (NCT00003165)
				Breast, lung and colorectal cancer	Phase II (98)
PK2 (FCE 28069)	Pharmacia and Upjohn	Doxorubicin	HPMA copolymer (Amide/GFLG)-galactosamine	Liver cancer	Phase I(44)
AP5280	Access pharmaceuticals, inc	Platinum	HPMA copolymer (Aminomalonate/ GFLG)	Solid tumors	Phase I(45)
ProLindac® (AP5346)	Access pharmaceuticals, inc	DACH platinite	HPMA copolymer (Aminomalonate/ GGG)	Head and neck cancer	Pilot study (NCT00415298)
				Advanced recurrent ovarian cancer	Phase II (EudraCT Number: 2010-020030-25)
PNU 166148 (MAG-CPT)	Pfizer; Cancer Research Campaign UK	Camptothecin	HPMA copolymer (ester)	Solid tumors	Phase I (NCT00004076); discontinued
PNU 166945	Pfizer; Cancer Research Campaign UK	Paclitaxel	HPMA copolymer (ester)	Solid tumors	Phase I; discontinued (107)
Prothecan® (Pegamotecan, EZ-246)	Enzon Pharmaceuticals, Inc	Camptothecin	PEG (Ester)	Locally advanced or metastatic adenocarcinoma of the stomach or gastroesophageal junction	Phase II (NCT00080002); Discontinued
				Metastatic colorectal carcinoma in combination or not with Cetuximab	Phase II (NCT00931840)
				Metastatic breast cancer	Phase II (NCT01036113)
EZN-2208	Enzon Pharmaceuticals, Inc	SN-38	4-arm PEG (Glycinamidoester)	Refractory solid tumors in combination with Bevacizumab	Phase I (NCT01251926)
				Pediatric patients with relapsed or refractory solid tumors	Phase I/II (NCT01295697)
				Advanced solid tumors or lymphoma	Phase I (NCT00520637, NCT00520390)
NKTR-105	Nektar Therapeutics	Docetaxel	4-arm PEG	Refractory solid cancers	Phase I
				Locally advanced or metastatic second-line colorectal cancer	Phase II (NCT00856375), (NCT00598975) (in combination with cetuximab)
				Metastatic or locally recurrent breast cancer	Phase III (NCT01492101)
Etirinotecan pegol (NKTR-102)	Nektar Therapeutics	Etirinotecan	4-arm PEG (Glycinamidoester)	Refractory brain metastases and advanced lung cancer or metastatic breast cancer	Phase II (NCT02312622)
				Relapsed SCLC	Phase II (NCT01876446)
				Advanced or metastatic solid tumors in patients	Phase I (NCT01991678)

				with hepatic impairment	
				Metastatic or locally advanced platinum-resistant ovarian cancer	Phase II (NCT00806156)
				Bevacizumab-resistant high grade glioma	Phase II (NCT01663012)
				Metastatic and recurrent NSCLC	Phase II (NCT01773109)
PEG-paclitaxel	Enzon Pharmaceuticals, Inc	Paclitaxel	PEG (Ester)	Advanced solid tumors or lymphoma	Phase I (NCT00023166); discontinued
DE-310, DX-8951	Daiichi Pharmaceuticals, Japan	Exatecan mesylate	Carboxymethyl dextran (GFLG)	Solid tumors	Phase I; discontinued (108)
AD-70; DOX-OXD	Mitsubishi Tanabe Pharma	Doxorubicin	Oxidized dextran (Schiff's base)	Refractory solid tumors	Phase I; discontinued (109)
XMT-1001	Mersana Therapeutics	Camptothecin	PHF (Succinamidoester)	Advanced solid tumors	Phase I (NCT00455052)

### 2.3 POLYMERIC NANOPARTICLES

Polymeric NP (PNP) are submicron-sized colloidal systems much larger than PM (50-500 nm) that have proved to be efficient carriers for the sustained and prolonged release of anti-cancer drugs (Figure 1 c). These carriers can be prepared using different biocompatible polymers. In fact, the release of anti-cancer drugs can be easily modulated by the type of polymer used (4, 19). PNP are usually prepared by two main approaches; starting from initial monomers that are polymerized (e.g., by emulsion polymerization); or starting from presynthesized polymer (e.g., by nanoprecipitation, emulsification/solvent evaporation, etc.) (56). These polymeric nanocarriers can be matrix systems in which the anticancer agent is dissolved or dispersed (nanospheres), or reservoir systems in which the anticancer agent is in a cavity surrounded by the polymer (nanocapsules) (19); the conjugation of anticancer agent to the surface or core of the particle is also possible.

Among nanosystems made of natural polymer or biopolymers, Abraxane<sup>®</sup>, used in the treatment of breast, lung and pancreatic cancer, is the only formulation currently on the market. This nanosystem consists of paclitaxel bound albumin NP which allows the administration of high drug doses (57). On the other hand, there are no PNP made of synthetic polymers being marketed, and only a few are under clinical evaluation (Table 3), even though they are usually more stable in biological media than nanocarriers based on natural polymers (56).

As far as passive targeting is concerned, NP formed with the biodegradable polymer poly (alkyl cyanoacrylate) (PACA) have been extensively used for drug delivery based on their ability to encapsulate small hydrophobic drugs and to improve the oral bioavailability of small molecular weight drugs (58). In fact, Livatag® (doxorubicin Transdrug™) is produced by the emulsion polymerization method using anionic surfactants and consists in a PIHCA ((poly (isohexyl cyanoacrylate))) nanosphere formulation loaded with doxorubicin. Currently, although only for one indication, it is the most advanced PNP in clinical evaluation. It is an orphan drug in Europe and the US and is in phase III for i.v. treatment of advanced hepatocellular carcinoma. Moreover Onxeo Company is already exploring new indications and its combination with other drugs to achieve a synergistic effect (59, 60). Another PACA NP prepared by the emulsion polymerization method is DHAD-PBCA NP which consists of mitoxantrone (dihydroxyanthracenedione, DHAD) loaded into poly (butyl cyanoacrylate) (PBCA), a biodegradable polymer that has been used as a medical adhesive for decades. It is in phase II clinical trials and has slightly improved the survival rates in patients with hepatic cancer (61, 62). Other polymers that have also been used for PNP preparation are poly(esters). This is the case with Docetaxel-PNP, a formulation comprised of a mixture of monovalent metal salts of PLA, amphiphilic diblock copolymers of monomethoxy PEG-PLA and the drug docetaxel. It is being developed by Samyang Pharmaceuticals and is under phase I clinical trials for advanced solid tumors in South Korea (63). On the other hand, CRLX101, a camptothecin nanosystem used in various clinical trials, which is showing enhanced pharmacokinetic efficacy in various solid tumors, and CRLX301, a docetaxel nanosystem in phase Ib/IIa, are both NP-drug conjugates. Between PDC and PNP, they are composed of a co-polymer, formed with  $\beta$ -cyclodextrins (a macrocyclic oligosaccharide) and PEG, which self-assembles into NP of 30-40 nm after its previous covalent glycinate linkage with the active drug (64-66).

Regarding active targeting, and following the pioneering work of Langer and Farokhzad, only BIND-014 has reached clinical development (67). BIND-014 is a docetaxel PNP targeted to Prostate-Specific Membrane Antigen (PSMA), a tumor antigen expressed on prostate cancer cells and on the neovasculature of most non-prostate solid tumors. BIND-014 has a biodegradable polymeric core of PLA, PEG and

PLGA, and a pseudo-mimetic dipeptide as the PSMA-targeting ligand. This formulation is in various phase II clinical trials for treatment of solid tumors and in phase I for advanced and metastatic cancer (21, 40).

Despite the poor clinical development of PNP, there are promising candidates currently under preclinical investigation which appear to offer prolonged and effective control of drug delivery. Indeed, despite their more complicated methods of synthesis compared to micelles and conjugates, PNP show better stability and a more controlled drug release (via diffusion through the polymeric matrix or by the erosion and degradation of the particles) (2). Moreover, like some PM, PNP can also overcome the mechanisms of chemo resistance developed by tumor cells that affect standard chemotherapy agents. Thus, although PNP provide promising new therapeutic properties (59), pharmaceutical companies are still cautious about the clinical study of these nanosystems with more complex production processes. Their arrival on the market is thus being delayed, as are their expected benefits in cancer therapy.

**Table 3: Polymeric nanoparticles on clinical trials for cancer therapy.** DHAD = dihydroxyanthracenedione (mitoxantrone); HNSCC = Head and neck squamous cell carcinoma; mPEG = methoxy-poly(ethylene glycol); NCT = ClinicalTrials.gov registry number; NSCLC = non-small cell lung cancer; PBCA = poly(butyl cyanoacrylate); PIHCA = poly(isohexyl cyanoacrylate); PLA = poly (D,L lactic acid); PLGA = poly (D,L lactic-co-glycolic acid); PMSA = prostate-specific membrane antigen; SCLC = small cell lung cancer

Product name	Company	Drug	Polymer/ targeting moiety	Indication	Clinical status
<i>Non-targeted polymeric nanoparticles</i>					
Livatag® (Doxorubicin Transdrug™)	Onxeo (BioAlliance Pharma)	Doxorubicin	PIHCA	Advanced hepatocellular carcinoma	Phase III (NCT01655693)
DHAD- PBCA-NP	-	Mitoxantrone	PBCA	Hepatocellular carcinoma	Phase II (61)
Docetaxel- PNP	Samyang Biopharm aceuticals	Docetaxel	mPEG-PLA	Advanced solid tumors	Phase I (NCT02274610; NCT01103791)
				NSCLC	Phase II (NCT01380769)
				SCLC	Phase II (NCT01803269)
CRLX101 (IT-101)	Cerulean Pharma Inc.	Camptothecin	Cyclodextrin- PEG	Locally advanced rectal cancer in combination with capecitabine and radiation therapy	Phase Ib/II (NCT02010567)
				Recurrent ovarian, tubal and peritoneal cancer	Phase II (NCT01652079) (with bevacizumab); Phase I

					(NCT02389985) (with paclitaxel)
				Solid tumors	Phase I (NCT02648711); Phase Ib/IIa (NCT00333502)
				Advanced or metastatic stomach, gastroesophageal, or esophageal cancer	Pilot study (NCT01612546)
				Metastatic renal cell carcinoma in combination with bevacizumab	Phase II (NCT02187302)
CRLX301	Cerulean Pharma Inc.	Docetaxel	Cyclodextrin- PEG	Advanced solid tumors	Phase I/IIa (NCT02380677)
<i>Targeted polymeric nanoparticles</i>					
				Urothelial carcinoma, cholangiocarcinoma, cervical cancer and HNSCC	Phase II (NCT02479178)
				NSCLC	Phase II (NCT01792479)
				KRAS mutation positive or squamous cell NSCLC	Phase II (NCT02283320)
				Metastatic castration-resistant prostate cancer	Phase II (NCT01812746)
				Advanced or metastatic cancer	Phase I (NCT01300533)
BIND-014	Bind Therapeutic	Docetaxel	PEG-PLGA/ PSMA		

### 3. CANCER DIAGNOSIS AND NANOTECHNOLOGY

Imaging tumorous tissue is of paramount importance to early identify the tumor type, location and stage of cancer. A precise tumor depiction enables specialists to establish accurate judgments about the tumor's distribution and its response to surgical removal and adjuvant therapies (68). There are a wide variety of imaging modalities to depict cancer tissue, including positron-emission tomography (PET), X-ray computed tomography (CT) and magnetic resonance imaging (MRI).

#### 3.1. MAGNETIC RESONANCE IMAGING

MRI is an essential imaging technique in medicine devised to achieve a detailed submillimetre-level spatial resolution and soft tissue contrast without the use of ionizing radiation or potentially harmful radiotracers (68). MRI contrast agents contain paramagnetic or superparamagnetic metal ions that affect the MRI signal properties of surrounding tissue. The aim of these contrast agents is to increase the sensitivity of MRI for detecting various pathological processes and to characterize various pathologies. Superparamagnetic iron oxide nanoparticles (SPION) have

generated great interest in the field of cancer diagnosis owing to their intrinsic magnetic property that enables them to be used as contrast agents in MRI (Figure 2 a and 3 a, b) SPION are extremely good enhancers of proton relaxation and do not self-aggregate when the external magnetic field is terminated. SPION are categorized as negative contrast agents, decreasing  $T_2$  signals and thus the signal intensity. Stability, biocompatibility and blood half-life are the three key design considerations for SPION. Once SPION are administered (Figure 3 c) and cleared from blood by phagocytosis, they are metabolized in the lysosomes into a soluble and non-superparamagnetic form of iron that becomes part of the normal iron pool (69). At present there are 18 nanoparticle formulations under clinical investigation for MRI imaging, which are producing notable results (see Table 4) (70). For instance, the accuracy of SPIO-enhanced MRI imaging for the detection of local hepatic lesions is higher than that achieved with non-enhanced MRI (71). The early marketed SPION based MRI contrast agents were clinically available under the name of Feridex<sup>®</sup> and Resovist<sup>®</sup>. Feridex<sup>®</sup> is a SPIO colloid with a dextran coating and a particle size in the range 120-180 nm. Hypotension and lumbar pain/leg pain represent the most frequent symptoms associated with Feridex<sup>®</sup>. On the other hand, Resovist<sup>®</sup> is a carboxydextrane-coated SPIO colloid with a particle size between 40-60nm. Unlike Feridex<sup>®</sup>, the incidence of cardiovascular adverse events and back pain is significantly less with Resovist<sup>®</sup>. Although Feridex<sup>®</sup> and Resovist<sup>®</sup> were previously clinically approved, on-going concern was focused on the long term toxicity of these SPION based MRI contrast agents and they were withdrawn from use in humans (72). Endorem<sup>®</sup>, 5 nm SPION coated with dextran, is efficiently accumulated in the liver and spleen within minutes of administration and its blood, liver and spleen half-life is 6 min, 3 days and 4 days, respectively (73). The recommended administration dose is 15 mmol/kg (71). Oral SPIO preparations such as Lumirem<sup>®</sup> (300 nm), GastroMARK<sup>®</sup> (300 nm) and Abdoscan (3.5  $\mu$ m) contain larger particles than the injectable contrast agents to prevent their being absorbed in the bowel (71). These contrast agents enhance the ability to distinguish the loops of the bowel from other abdominal structures, as well as the bowel from adjacent tissues and organs in the upper gastrointestinal tract (74). The recommended clinical dose concentration is 1.5-3.9 mM (75). Ultrasmall superparamagnetic iron oxide (USPIO) agents make it possible to prolong the blood half-life and cross the capillary wall in order to achieve more

widespread tissue distribution (Figure 2 a and 3 d). Ferumoxtran-10, commercialized as Combidex® in Europe and Sinerem® in USA, is a USPIO composed of 4-6 nm magnetic NP surrounded by a hydrophilic dextran coating to promote wide circulation in the intravascular space. Postcontrast imaging is usually obtained 24 h after administration of the contrast agent (71). Their clinical dose depends on the type of MIR imaging and can range from 13.8- 44.7 mmol/kg (69). However, the significantly high number of false positives in the identification of lymph node metastases has stopped the clinical development (76). NC100150 is also a type of USPIO surrounded by a carbohydrate-PEG coating and with a vascular half-life in the range of 3-4 h. The recommended clinical dose is 50-100 mmol/kg (77).

Finally, Ferumoxytol (Feraheme®) is a 30 nm SPION formulation with a magnetite core covered by a polyglucose sorbitol carboxymethylether coating. It is an approved iron replacement therapy agent that has also shown potential for use as a contrast agent in imaging studies for tumors, especially involving lymph nodes that have been affected by cancer. Ferumoxytol is taken up by normal lymph nodes, but excluded from cancerous lymph node tissue (74).

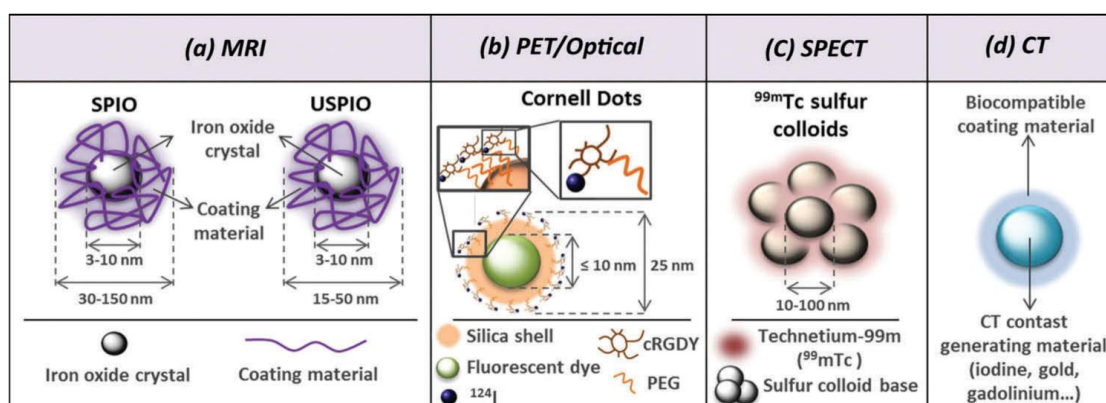


**Figure 2. - Illustration of the most relevant nanosystems in clinical trials for cancer imaging.** cRGDY = Cyclic arginine–glycine–aspartic acid peptide; CT = X-ray computed tomography; MRI = Magnetic resonance imaging; PEG = Poly(ethylene glycol); PET = Positron-emission tomography; SPECT = Single photon emission computed tomography; SPION = Superparamagnetic iron oxide nanoparticles; USPIO = Ultrasmall superparamagnetic iron oxide nanoparticles

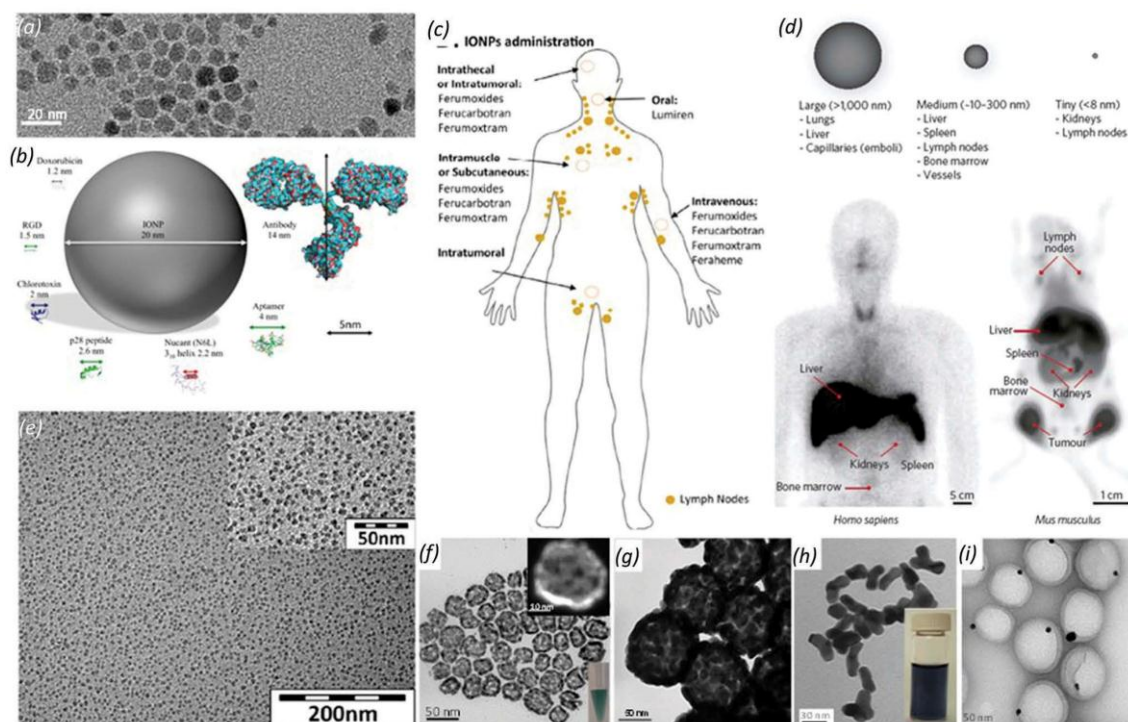


**Figure 3.-Nanoparticles applied for cancer imaging.** a) TEM image of SPION. b) Schematic representation to scale of SPION and the structure of different molecules used for their functionalization. Adapted from ref(110) under CC license. c) Routes of administration of marketed SPION: intrathecal, intratumor, intravenous and intramuscular or subcutaneous methods. Adapted from ref(110) under CC license. d) Common organ distribution of nanoparticles as a function of particle size. Most nanoparticles for *in vivo* use fall into the intermediate category (10–300 nm), where distribution to liver, spleen, lymph nodes and bone marrow is common. Bottom: CT images of nanoparticles used in a human patient (Tc-labelled NP) and mouse mode (Zr-labelled cross-linked dextran nanoparticles). Adapted from ref(111) with permission of Nature Publishing group. e) TEM image of Cornell dots. Adapted from ref(112) with permission of American Chemical Society. f) Normalized absorbance and emission spectra of Cornell dots with different dyes. Adapted from ref(112) with permission of American Chemical Society. g) Photograph showing the solution appearance of C' dots derived from different color dyes (from left to right: RhG, TMR, Cy5, Cy5.5, DY782, and CW800). Adapted from ref(112) with permission of American Chemical Society. h) Hollow gold nanoparticles. Adapted from ref(113) with permission of Royal Society of Chemistry. i) Au-SiO<sub>2</sub> nanoshells. Adapted from ref(114) with permission of Royal Society of Chemistry. j) Au nanorods. Adapted from ref(115) with permission of Royal Society of Chemistry. k-l) Au-NP loaded in polymeric PLGA NP. Adapted from ref(93) under CC license. C`dots=Cornell dots; CW800=Infrared dye 800 CW; Cy5=Fluorescent dye Cy5; DY782= Dynamics 782 fluorescent dye; IONP= Iron Oxide Nanoparticle; RGD= Peptide arginylglycylaspartic acid; RhG= Rhodamine Green Fluorescent Dye; TMR= Tetramethylrodamine fluorescent dye



**Table 4: Nanoparticles on the market or in clinical trials for cancer imaging.** C-dots=Cornell dots; cRGDY= cyclic arginine–glycine–aspartic acid peptide; CT= X-ray computed tomography; FDA= Food and Drug Administration in USA; GU= Genito-Urinary; MRI = Magnetic resonance imaging; NCT = ClinicalTrials.gov registry number; NIRF= Near-infrared fluorescence; NP=Nanoparticles; HNSCC= Head and Neck Squamous Cell Carcinomas; I.V=Intravenous; OCT= Optical coherence tomography; PEG= poly(ethylene glycol); PET= positron-emission tomography; SPECT= photon emission computed tomography; SPIO= Superparamagnetic Iron Oxides; USPIO= Ultrasmall Superparamagnetic Iron Oxides

Imaging modality	Agent	Nanopatform and composition	Trade name	Company	Imaging indication	Status
	Ferucarbotran (SHU-555)	SPIO NP coated with carboxydextran	Resovist®	Bayer Schering Pharma AG	Liver/spleen malignancies	Approved in Europe.
	Ferumoxyde (AMI-25)	SPIO nanoparticles coated with dextran	Feridex I.V.®	Bayer Schering Pharma AG	Liver/spleen malignancies	FDA-approved.
			Endorem®	Guerbet	Liver/spleen malignancies	Approved in Europe
	Ferumoxsil (AMI-121)	SPIO NP	Sienna+®	Endomagnetics Ltd	Sentinel nodes mapping in breast cancer	NCT01790399 (Feasibility study); NCT02336737 (comparison study)
			Lumirem®	Guerbert	Gastrointestinal tract	FDA-approved
			GastroMA RK®	Advanced Magnetics	Gastrointestinal tract	FDA-approved
			Abdoscan	Nycomed (now GE Healthcare)	Gastrointestinal tract	Approved in Europe. Taken off the market
			Sinerem®	Guerbet	Lymph node metastasis	Approved in Europe
<b>MRI</b>	Ferumoxtran-10 (AMI-227)	USPIO NP coated with dextran	Combindex®	AMAG Pharmaceuticals	Lymph node metastasis in different neoplasms	Phase I/II (NCT00188695)(uterine, cervix, bladder and prostatic neoplasms), (NCT00416455) (cervical or endometrial cancer); Phase II (NCT00107484) (breast cancer); Phase IV (NCT00185029) (prostatic neoplasms)
	NC100150	USPIO NP coated with carbohydrate-polyethylene glycol	Clariscan	Nycomed (now GE Healthcare)	Angiography-Perfusion	Clinical trials stopped
	Ferumoxytol (Code 7728)	USPIO NP coated with poly (glucose sorbitol carboxymethylether)	Feraheme® (USA and Canada)/ Rienso® (Europe)	AMAG Pharmaceuticals/ Takeda Pharmaceutical Company Ltd.	Brain neoplasms	Phase II (NCT00103038), (NCT00659126)
					Primary and nodal tumor in HNSCC	Phase 0 (NCT01895829)
					Lymph node metastasis in prostate cancer and GU cancers	Phase I (NCT01296139) (prostate cancer); Phase II (NCT02141490)

					(GU cancers)	
					Pre-operative staging of pancreatic cancer	Phase IV (NCT00920023)
<b>PET</b>	SiO <sub>2</sub>	<b>124I-cRGDY-PEG-dots (Cornell dots, core-shell silica NP)</b>	C-dots	-	Melanoma, malignant brain tumors, pituitary adenoma and hepatic metastasis	NCT01266096, (82)
<b>Optical imaging</b>	SiO <sub>2</sub>	<b>cRGDY-PEG-Cy5.5-C-dots (Cornell dots, core-shell silica NP)</b>	C-dots	-	Sentinel Lymph Node Mapping in Head and Neck Melanoma, Breast and Cervical/ Uterine Cancer	NCT02106598
<b>SPECT</b>	-	Technetium Tc 99m sulphur colloid NP	Nanocoll <sup>®</sup> / Nanocis <sup>®</sup>	GE Health Care	sentinel lymph node mapping in invasive breast cancer	Preliminary clinical study (NCT00438477 (Breast cancer) NCT00070317 (cervical cancer))
<b>CT</b>	Au-SiO <sub>2</sub> colloid	Heavy metals (gold, lanthanide, tantalum...) nanoparticles coated with compounds that yield solubility in biological media and biocompatibility	Aurolase <sup>®</sup>	Nanospectra Biosciences	Solid tumors	NCT02680535 (Phase I)

### 3.2 POSITRON-EMISSION TOMOGRAPHY

PET is a highly sensitive (down to picomolar level) and non-invasive nuclear imaging tool widely applied for preclinical and clinical imaging of diseases. However, the resolution is relatively low (typically < 1 mm). Upon the injection of either a radiotracer or a radiolabeled NP, PET can monitor its distribution and accumulation. Radiolabeled NP are paramount in the field of cancer imaging (78). Beyond the development of radiolabeled nanoprobe suitable for PET alone, recent tendencies aim at the synthesis of bimodal imaging probes applicable in PET as well as optical imaging (OI) in order to exploit the potential of both imaging techniques (79). The combination of PET and OI provides clinical advantages: 1) PET possesses a high tissue penetration, allowing quantitative imaging able to identify and visualize tumors and metastases in the whole body. 2) OI is based on light scattering and exhibits only a limited tissue penetration but enables the identification of tumor margins and infected lymph nodes during surgery without bearing a radiation burden

for the surgeon (79). Although an extensive number of fluorescent particle nanoplatforms have been investigated (80), only Cornell dots (C-dots) have received the first FDA-approved investigational new drug approval for human clinical trials (Figure 2 b and 3 e, f). This type of core-shell silica NP shows clear advantages in comparison with single fluorophore labeling in diagnostics and theranostics. In addition, they also provide higher brightness and photostability than the single fluorophore moieties, two key points in fluorescent imaging (80). Most interestingly, these NP are non-toxic, have a fast cellular uptake and complete clearance. In addition, it is considered that complete renal clearance is achieved when the NP have a particle size under the effective renal glomerular filtration size cut-off (approx. 10 nm) (81). The use of 6 nm C-dots was reported for the imaging of cancer in human clinical trials (82). C-dots were labeled with  $^{124}\text{I}$  for PET imaging and modified with cyclo-(Arg-Gly-Asp-Tyr) peptides, cRGDY, for sentinel lymph node mapping (83) and molecular targeting to cancer cells: melanoma, hepatic metastasis and pituitary adenoma. C-dot whole-body clearance half-time values range from 13 to 21 hours, which is smaller than for large NP ie, 90 nm liposomes which have median clearance half-time values ranging from 40 to 103 hours (82). *In vivo* PET imaging was able to accurately estimate the fraction of the injected particle load that accumulates at tumor sites, in addition to monitoring time-varying particle uptake and clearance.

Advanced imaging techniques such as single photon emission computed tomography (SPECT) coupled with additional techniques such as Near-infrared fluorescence (NIRF) make it possible to detect the sentinel lymph nodes to detect an image at the primary site of lymphatic metastasis (84). Nanocoll®,  $^{99\text{m}}\text{Tc}$ -labeled sulphur-colloid (USA) and  $^{99\text{m}}\text{Tc}$  colloid albumin (Europe) were selected as tracer (see Figure 2 c). After subcutaneous injection, Nanocoll® colloid particles are filtered into lymphatic capillaries, then transported along the lymphatic vessels and trapped in functionary lymph nodes. This technique has been evaluated for tumor resection, showing improved and accurate sentinel lymph node identification in oral cancer patients.

### 3.3 X-RAY COMPUTED TOMOGRAPHY

X-ray computed tomography (CT) is one of the leading radiology technologies applied in the field of biomedical imaging. The basic process of CT is to detect the X-rays that pass through a sample. CT is among the most convenient imaging tools in terms of availability, efficiency and cost. CT, unlike PET and MRI, can provide three-dimensional (3D) anatomic details with high spatial and temporal resolution, even to capture cardiac motion (84). The higher the atomic number of the CT contrast agent, the better the resulting CT contrast. As a result, iodinated contrast agents are widely used as CT contrast agents in clinical practice (85). Gold nanoparticles (Au-NP) have demonstrated greater contrast than iodinated agents, as well as reduced toxicity and prolonged circulation times (86). Lanthanides with high atomic number can be also used as CT contrast agents, i.e. gadolinium. However, free lanthanide ions are toxic and must be chelated to obtain FDA-approval. Au-NP are by far the most widely investigated noble metal type NP as CT contrast agent (Figure 2 d and 3 h-l). In addition, Au-NP are used also in optical coherence tomography (OCT) and optical coherence microscopy (OCM). OCT can generate a signal based on refractive index mismatches and scattering events (86). Au-NP make it possible to achieve an extra scattering because they possess both unique absorption and scattering properties in the near-infrared (NIR) region that have generated promise in differentiating normal from diseased tissue (86). However, no Au-NP products have been clinically approved. AuroLase<sup>®</sup>, silica-gold nanoshells coated with PEG (Figure 3 i), developed by Nanospectra to thermally ablate solid tumors, is also being considered for cancer imaging (87). AuroLase<sup>®</sup> still faces certain technical and biological challenges before clinical approval, such as determining the biological fate and long-term biocompatibility and proving that this nanosystem can be used intravenously utilizing the EPR effect (88). The optical behavior of gold nanoshells in the NIR is noteworthy, as they show scattering and/or absorption cross-sections that are often several times higher than the particle geometric cross-section (87). Gold nanoshells can efficiently lower the photon reflectance in comparison with gold colloid, enhancing reflectance signatures through absorption for spectroscopic detection modalities (87). This considerable change in reflectance is observed with only a very small concentration of nanoshells and it is rarely observed with other type of Au-NP. In addition, gold nanoshells can be used in numerous bioconjugate applications as

their surfaces are virtually chemically identical to universally used gold colloid (89). This implies that gold nanoshells can selectively be targeted to cancer cells.

In the past decade, enormous advances have been made in the research of imaging sciences, and many new technologies (PET, CT and MRI) and imaging agents based on nanosystems have been applied to oncology research and clinical trials. The translation of these nanosystems and technologies from the laboratory to the clinic has been much slower than was initially hoped. The main reasons for this could be summarized as: 1) Lack of reliable technology to scale up the production of advanced nanomaterials (90), 2) Considerable regulatory hurdles and market forces (90, 91), 3) lower profit margins for imaging than for therapeutic drugs (90), 4 ) Low target selectivity (high number of false positives) for imaging and ultrasensitive detection of near and distant metastases and 5) Toxicity and side effects in patients. Despite these hurdles, several new nanosystems in clinical trials show that they are more robust and versatile, since they can enhance and improve current imaging and diagnostic techniques. For instance, PET nanoparticle tracers could complement the information that is not acquired by nonspecific radiopharmaceuticals.

#### **4. CANCER THERANOSTICS AND NANOTECHNOLOGY**

Originally introduced by Funkhouser in 2002, the term “theranostics” describes any “material that combines the modalities of therapy and diagnostic imaging” into a single package (92). Nowadays, nanomedicine theranostics for cancer is progressing with the design of multifunctional platforms that consist of colloidal NP ranging in sizes from 10 to 1000 nm in which the diagnostic and therapeutic agents are adsorbed, conjugated, entrapped or encapsulated (91, 93). The same therapeutic agent has not the same effect on all patients with the same diagnosis. The objective of nanotheranostic is therefore to achieve real-time traceable drug distribution and delivery, and monitor the therapeutic efficacy non-invasively. Therefore, with theranostic nanosystems, patients would have better treatment regimens based on each individual’s responses and needs, which would enhance their quality of life by lowering the adverse side effects and the therapeutic efficacy of over- or under-dosed antitumor drugs (10, 94).

In the development of theranostic nanoplatfoms it should be consider that the optimal concentration for the desired therapy is generally much higher than that required for imaging (95). Furthermore, it is necessary to have an equilibrium between the desired long circulation time for therapeutic efficacy and the short time frame for the imaging agent, which is enough to evaluate the disease with low toxicity (96). Consequently, to achieve clinical translation, increased regulatory barriers that depend on each function of the nanosystem need to be included (97). In this way, despite the successful introduction of the therapeutic and diagnostic nanosystems already discussed into clinical trials and even onto the market, most of the results for theranostic nanomedicines reported in the literature are *in vitro* studies and only a few *in vivo* data are available to demonstrate their potential clinical application (94). In this sense, it is important to highlight that there are some proof-of-principle clinical studies of therapeutic NP in which biodistribution proofs have been obtained through their self-imaging properties (inherent or added), which have shown the promising possibilities of theranostic nanosystems.

Various nanocarriers are being investigated for sustained, controlled and targeted co-transport of diagnostic and therapeutic agents. Two different strategies are being investigated, each one with strengths and weaknesses. The first one is an "All in One" approach in which the nanosystem carries both agents (see Figure 4 a). The most commonly used are liposomes and polymer-based nanocarriers such as PMs, polymer conjugates, PNP or dendrimers (94, 95). They carry, at the same time, the therapeutic drug and the diagnostic agent such as radionuclides, different NIR dyes, MRI agents or inorganic NP. They are excellent theranostic carriers owing to their biocompatibility, protection of loaded drug/diagnostic agent and controlled drug release. However, it should be borne in mind that physicochemical and drug loading properties could change after adding the imaging agent; and also, that the imaging agent could be lost from nanoplatfoms during systemic circulation (96). Nevertheless, there are already proof-of-principle clinical studies of "All in One" strategy in PK1 (doxorubicin-HPMA conjugate) and PK2 (hepatocellular carcinoma targeted doxorubicin-HPMA conjugate) clinical studies. Theranostic studies with the radiolabeled PK1 were carried out in phase I and II clinical studies. They showed a significant tumor accumulation of PK1, also in metastatic lesions, in a large number of patients. It

should therefore be possible to visualize the efficacy of the treatment in real-time with a mixture of trace amounts of radiolabeled PK1 with regular PK1 (42, 98). On the other hand, in similar studies with radiolabeled PK2, the conjugate was primarily accumulated in healthy liver tissue, rather than in the tumors. This result indicates that the targeting of PK2 may not be very effective. In fact, antitumor responses in patients were modest (only 3 out of 31 patients with advanced liver cancer responded) (44, 96). This study shows the usefulness of monitoring therapeutic NP to understand and explain the therapeutic efficacy of nanocarriers.

The second strategy used to produce theranostic nanosystems, is a “One for All” approach in which the nanocarrier, such as inorganic NP and carbon nanotubes, have inherent imaging properties and can transport the therapeutic agent, or can even also act as a therapeutic agent by photothermal (such as Au-NP or SPION) or photodynamic (such as silicon NP or quantum dots) therapy (94, 99, 100) (see Figure 4 b). As we have seen in the previous section, metallic and magnetic NP are excellent diagnostic tools for imaging applications. Nevertheless, they are commonly coated with organic polymers (dextran, chitosan, polysorbate, PEG, polyaniline), organic surfactants (oleate and dodecylamine) or other metallic materials (gold, silica or carbon), providing limited cargo space for therapeutic payloads within the protective coatings (10, 101). However, if the nanosystem has both therapeutic and diagnostic functionalities, this drug loading problem is avoided. This occurs, for example, with Au-NP which, due to their unique surface characteristics, can act as CT imaging agents at the same time as they can act as radiotherapy sensitizers and photothermal agents (102). However, although Au-NP show low toxicity (5) and the coating of SPION covers the oxidative sites and reduces their toxicity (94), it is believed that “hard” materials such as gold, silver, and ceramics (silica) formulation, are not biodegradable and may aggregate in the liver and lymph system causing long-term adverse effects (97). Fortunately, the potential of theranostic nanomedicine in cancer using the strategy of “One for All” can be appreciated, as the proof-of-principle clinical study, in the Aurimune® (CYT-6091) biodistribution studies. Aurimune® was a first multifunctional NP system combining both imaging and therapeutic functionalities to progress into clinical trials. It is composed of a PEGylated colloidal- Au-NP core conjugated to recombinant human tumor necrosis factor alpha as a tumor growth

inhibitor. (103). In phase 0 (NCT00436410) and I (NCT00356980) clinical trials the imaging properties of colloidal gold particles were used for the analysis of tumor biopsies. The detection of Au-NP in tissue biopsy samples via transmission electron microscopy was used as initial proof of concept of the tumor targeting ability of CYT-6091 (104).

Nanotheranostic technologies are therefore showing their potential to personalize the management of cancer through the monitoring, evaluation and individualization of treatments in real-time. Moreover, nanotheranostics can facilitate clinical efficacy and toxicity studies and a better understanding of various important aspects of the drug delivery process such as the efficacy of targeting or stimuli drug release. The employment of clinically validated nanomaterials could possibly accelerate the clinical translation of theranostic NP (95). However, to achieve safe, efficacious clinical platforms, further *in vivo* research efforts are needed (105).

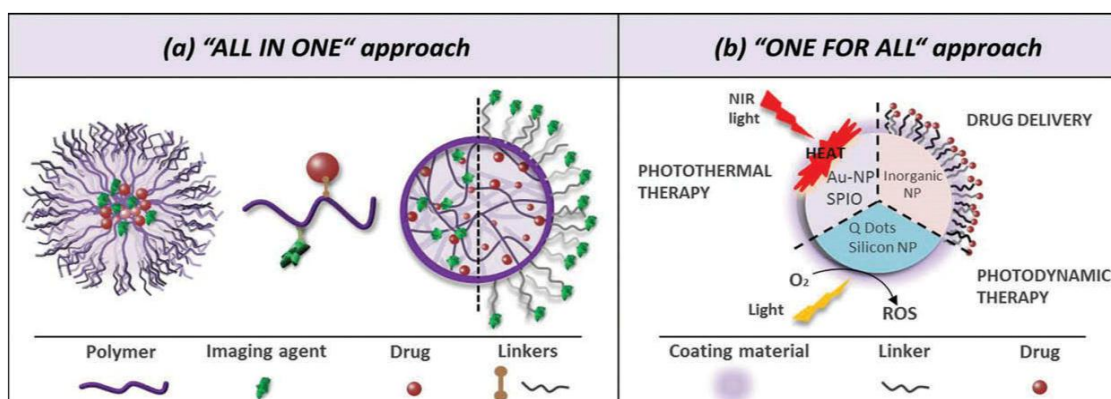


**Figure 4. - Illustration of the most relevant strategies used to develop theranostic nanosystems for cancer imaging and therapy.** Au-NP = Gold nanoparticles; NIR = Near-infrared; NP = Nanoparticles; Q Dots = Quantum dots; ROS= Reactive oxygen species; SPIO = Superparamagnetic iron oxides

## 5. CONCLUSION

The application of nanotechnology in cancer, including drug delivery, diagnostic and theranostic nanosystems, is changing current diagnosis and therapy concepts. The possibility of manipulating nanocarriers' properties, such as their size, shape, charge or surface functionality, is the best strategy to achieve the desired *in vivo* behavior.



Polymer-based nanocarriers have shown excellent therapeutic potential in both preclinical and clinical development. In fact, owing to their favourable physicochemical properties, polymeric DDS have been shown to be excellent carriers of therapeutic agents, increasing the therapeutic efficacy with better pharmacokinetic profiles and fewer side effects. At present there are several PM going through late stages of clinical trials and two, Genexol PM<sup>®</sup> and Nanoxel PM<sup>™</sup>, are already available for use. Moreover, a large number of PDC are under clinical development and some of them are even being investigated simultaneously in different trials for the treatment of various types of cancer. Likewise, PNP are promising nanocarriers with high versatility. Unfortunately, in spite of the large number of preclinical research projects being carried out, there is little clinical investigation in this area. Regarding nanosystems for diagnosis, some are already on the market (Lumirem<sup>®</sup>, GastroMARK<sup>®</sup> or Endorem<sup>®</sup>). Theranostic nanomedicine opens up the door to personalized medicine. Some proof-of-principle in primary clinical trials of therapeutic nanocarriers have shown the possibility of monitoring, evaluating and individualizing cancer treatments in real-time. However, no theranostic nanosystem is currently undergoing clinical trials, and still further *in vivo* work will be required prior to clinical application. Indeed, despite the revolutionary impact of potential applications of nanosystems in medicine; their clinical translation is progressing slowly and only a few nanosystems have reached the marketplace.

## 6. EXPERT OPINION

Two of the major challenges in cancer therapy are the early diagnosis of cancer cells and their selective eradication. Both challenges could be met with nanomedicine. Nanocarriers have the potential for significant improvements in disease prevention, diagnosis and treatment. Nevertheless, in spite of the variety of nanosystems investigated, only a few, such as Doxil<sup>®</sup>, Abraxane<sup>®</sup>, Genexol-PM<sup>®</sup>, Nanoxel PM<sup>™</sup>, Endorem<sup>®</sup> and Lumirem<sup>®</sup>, have been given approval for use in the treatment and diagnosis of cancer. The translation of oncological nanomedicines into clinical practice has been slow. As previously stated, some major reasons could be the lack of reliable technology to scale up the production of advanced nanomaterials and the

regulatory hurdles and market forces. In fact, the challenge of ensuring the quality of the nanosystems, and our knowledge gaps about the disease, are delaying the development of new systems of this kind, and better understanding of the interaction between the NP and tumor microenvironment is urgently needed, especially of the internalization and trafficking of NP into tumor cells. In this sense, the identification of new molecular targets would advance the active targeting in nanomedicine in order to attain clinical success. Up to now, no targeted nanocarrier has come onto the market, and only a few clinical trials (such as the PM for gene therapy CALAA-01) are under development. This clinical failure can be attributed to various barriers that the nanosystems have to cross before they are recognized by the cells, which may explain why targeted and untargeted NP *in vivo* behave in the same way. For these reasons, to ensure successful clinical evaluation and connect the needs of cancer medicine to the enormous potential of nanotechnology, we need to integrate a wide variety of disciplines (scientific, technological and legal) and to make rules for clinical studies and production of nanocarriers. All of this could speed up the progress of nanomedicine, and address concrete problems such as the prediction of new side effects not associated with either the drug or the carrier, as in the case of Doxil® and certain cases of Abraxane®, which have the dose-limiting “hand and foot syndrome” (or Palmar-Plantar erythrodysesthesia) because of their long circulation and their deposition in the peripheral tissues.

Overall, this is an exciting time in the field of nanotherapeutics, with advances being made in diagnostics, therapeutics and theranostics. There are multiple barriers for these new nanosystems to enter the clinic, but it is expected that in the near future, nanocarriers, together with new “targeted drugs”, could replace our current treatments and cancer could become a nonfatal disease with good recovery rates. Joint efforts between scientists, clinicians, the pharmaceutical industry and legislative bodies are needed to bring to fruition the application of new nanosystems in the clinical management of cancer.

## 7. REFERENCES

1. WHO: Cancer, 2015. Available at: <http://www.who.int/mediacentre/factsheets/fs297/es/> [Last accessed 27 January 2016]
2. Perez-Herrero E, Fernandez-Medarde A. Advanced targeted therapies in cancer: Drug nanocarriers, the future of chemotherapy. *Eur J Pharm Biopharm* 2015;93:52-79
3. Estanqueiro M, Amaral MH, Conceicao J, et al. Nanotechnological carriers for cancer chemotherapy: The state of the art. *Colloids Surf B Biointerfaces* 2015;126:631-48
4. Masood F. Polymeric nanoparticles for targeted drug delivery system for cancer therapy. *Mater Sci Eng C Mater Biol Appl* 2016;60:569-78
5. Gopalakrishna Pillai. Nanomedicines for cancer therapy: An update of FDA approved and those under various stages of development. *SOJ Pharm Pharm Sci* 2014;2:1-13
6. Siminska E, Koba M. Amino acid profiling as a method of discovering biomarkers for early diagnosis of cancer. *Amino Acids*, 2016; DOI: 10.1007/s00726-016-2215-2
7. Ravi Kumar MN, Blanco-Prieto MJ, Waterhouse DN. Nanotherapeutics. *Cancer Lett* 2013;334(2):155-6
8. Al-Hadiya BM, Bakheit AH, Abd-Elgalil AA. Imatinib mesylate. *Profiles Drug Subst Excip Relat Methodol* 2014;39:265-97
9. Li C, Wallace S. Polymer-drug conjugates: Recent development in clinical oncology. *Adv Drug Deliv Rev* 2008;60(8):886-98
10. Luk BT, Zhang L. Current advances in polymer-based nanotheranostics for cancer treatment and diagnosis. *ACS Appl Mater Interfaces* 2014;6(24):21859-73
11. Bregoli L, Movia D, Gavigan-Imedio JD, et al. Nanomedicine applied to translational oncology: A future perspective on cancer treatment. *Nanomedicine* 2016;12(1):81-103
12. Sanna V, Pala N, Sechi M. Targeted therapy using nanotechnology: Focus on cancer. *Int J Nanomedicine* 2014;9:467-83
13. Mura S, Couvreur P. Nanotheranostics for personalized medicine. *Adv Drug Deliv Rev* 2012;64(13):1394-416
14. Cabral H, Kataoka K. Progress of drug-loaded polymeric micelles into clinical studies. *J Control Release* 2014;190:465-76 \*Excellent review of drug-loaded polymeric micelles and their performance in human studies
15. Jebar AH, Errington-Mais F, Vile RG, et al. Progress in clinical oncolytic virus-based therapy for hepatocellular carcinoma. *J Gen Virol* 2015;96:1533-50
16. Yang H. Targeted nanosystems: Advances in targeted dendrimers for cancer therapy. *Nanomedicine* 2016 ;12(2):309-16

17. Lim DJ, Sim M, Oh L, et al. Carbon-based drug delivery carriers for cancer therapy. *Arch Pharm Res* 2014;37(1):43-52
18. Lasa-Saracibar B, Estella-Hermoso de Mendoza A, Guada M, et al. Lipid nanoparticles for cancer therapy: State of the art and future prospects. *Expert Opin Drug Deliv* 2012;9(10):1245-61
19. Fonseca AC, Serra AC, Coelho JF. Bioabsorbable polymers in cancer therapy: Latest developments. *EPMA J* 2015;6(22): DOI: 10.1186/s13167-015-0045-z
20. Biswas S, Kumari P, Lakhani PM, et al. Recent advances in polymeric micelles for anti-cancer drug delivery. *Eur J Pharm Sci* 2015;83:184-202
21. Van Gaal E.V.B., Crommelin D.J.A. Polymeric micelles. *Non-Biological Complex Drugs*. Switzerland: Springer, 2015. p. 11-76 \*Comprehensive chapter book of polymeric micelles and their performance in human studies.
22. Genexol PM injection. Seoul: Samyang Biopharm, 2013. Available at: <https://www.samyangbiopharm.com/eng/ProductIntroduce/injection01> [Last accessed 13 February 2016]
23. Paclitaxel polymeric micelle formulation - samyang. *Adis Insight News: Springer International Publishing AG*, 2015 Available at: <http://adisinsight.springer.com/drugs/800034369> [Last accessed 13 February 2016]
24. Sorrento announces first patient dosed in registration trial to evaluate bioequivalence between cynviloq and abraxane. United States: Sorrento Therapeutics, 2014 Available at: <http://sorrentotherapeutics.com/sorrento-announces-first-patient-dosed-in-registration-trial-to-evaluate-bioequivalence-between-cynviloq-and-abraxane/> [Last accessed 13 February 2016]
25. Bioequivalence study of IG-001 versus nab-paclitaxel in metastatic or locally recurrent breast cancer (TRIBECA). *clinicaltrials.gov*: Sorrento Therapeutics, Inc, 2016 Available at: <https://clinicaltrials.gov/ct2/show/NCT02064829> [Last accessed 13 February 2016] \*\* Bioequivalence study of Genexol-PM® versus Abraxane® for its registration in the USA and European markets under the name of Cynviloq™
26. Valle JW, Armstrong A, Newman C, et al. A phase 2 study of SP1049C, doxorubicin in P-glycoprotein-targeting pluronics, in patients with advanced adenocarcinoma of the esophagus and gastroesophageal junction. *Invest New Drugs* 2011;29(5):1029-37
27. PRODUCTS. Supratek website: Supratek Pharma Inc, 2016. Available at: <http://www.supratek.com/pipeline/products> [Last accessed 7 April 2016]
28. Nakanishi T, Fukushima S, Okamoto K, et al. Development of the polymer micelle carrier system for doxorubicin. *J Control Release* 2001;74(1-3):295-302
29. A phase III study of NK105 in patients with breast cancer. *ClinicalTrials.gov*: Nippon Kayaku Co.,Ltd, 2016 Available at: <https://clinicaltrials.gov/ct2/show/NCT01644890?term=NCT01644890&rank=1> [Lat accessed 22 March 2016]
30. Hamaguchi T, Doi T, Eguchi-Nakajima T, et al. Phase I study of NK012, a novel SN-38-incorporating micellar nanoparticle, in adult patients with solid tumors. *Clin Cancer Res* 2010;16(20):5058-66

31. Takahashi A, Yamamoto Y, Yasunaga M, et al. NC-6300, an epirubicin-incorporating micelle, extends the antitumor effect and reduces the cardiotoxicity of epirubicin. *Cancer Sci* 2013;104(7):920-5.
32. IND application for NC-6300 (K-912) epirubicin micelle in japan. EvaluateTM: EvaluateClinicalTrialsTM, 2013 Available at: <http://www.evaluategroup.com/Universal/View.aspx?type=Story&id=425130> [Last accessed 14 February 2016]
33. Plummer R, Wilson RH, Calvert H, et al. A phase I clinical study of cisplatin-incorporated polymeric micelles (NC-6004) in patients with solid tumours. *Br J Cancer* 2011;104(4):593-8
34. Cabral H, Nishiyama N, Okazaki S, et al. Preparation and biological properties of dichloro(1,2-diaminocyclohexane)platinum(II) (DACHPt)-loaded polymeric micelles. *J Control Release* 2005;101(1-3):223-32
35. Hu Q, Rijcken CJ, Van Gaal EV, et al. Core-cross-linked polymeric micelles: A highly versatile platform to generate nanomedicines with divergent properties. Thesis, Chapter 2. Core-cross-linked polymeric micelles: A versatile nanomedicine. China, 2015. p. 19-60
36. Hu Q, Rijcken CJ, Bansal R, et al. Complete regression of breast tumour with a single dose of docetaxel-entrapped core-cross-linked polymeric micelles. *Biomaterials* 2015;53:370-8
37. Ke X, Ng VW, Ono RJ, et al. Role of non-covalent and covalent interactions in cargo loading capacity and stability of polymeric micelles. *J Control Release* 2014;193:9-26
38. Talelli M, Barz M, Rijcken CJ, et al. Core-crosslinked polymeric micelles: Principles, preparation, biomedical applications and clinical translation. *Nano Today* 2015;10(1):93-117
39. Thipparaboina R, Chavan RB, Kumar D, et al. Micellar carriers for the delivery of multiple therapeutic agents. *Colloids Surf B Biointerfaces* 2015;135:291-308
40. Prabhu RH, Patravale VB, Joshi MD. Polymeric nanoparticles for targeted treatment in oncology: Current insights. *Int J Nanomedicine* 2015;10:1001-18
41. Vicent MJ, Duncan R. Polymer conjugates: Nanosized medicines for treating cancer. *Trends Biotechnol* 2006;24(1):39-47 \*Good revision of current status of polymer conjugates
42. Vasey PA, Kaye SB, Morrison R, et al. Phase I clinical and pharmacokinetic study of PK1 [N-(2-hydroxypropyl)methacrylamide copolymer doxorubicin]: First member of a new class of chemotherapeutic agents-drug-polymer conjugates. Cancer research campaign phase I/II committee. *Clin Cancer Res* 1999;5(1):83-94 \*\*Proof-of-principle theranostic clinical study of PK1 in which the biodistribution proof has been obtained through radiolabeled conjugate
43. Zhong YJ, Shao LH, Li Y. Cathepsin B-cleavable doxorubicin prodrugs for targeted cancer therapy (review). *Int J Oncol* 2013;42(2):373-8
44. Seymour LW, Ferry DR, Anderson D, et al. Hepatic drug targeting: Phase I evaluation of polymer-bound doxorubicin. *J Clin Oncol* 2002;20(6):1668-76 \*\*Proof-

of-principle theranostic clinical study of PK1 in which the biodistribution proof has been obtained through radiolabeled conjugate

45. Rademaker-Lakhai JM, Terret C, Howell SB, et al. A phase I and pharmacological study of the platinum polymer AP5280 given as an intravenous infusion once every 3 weeks in patients with solid tumors. *Clin Cancer Res* 2004;10(10):3386-95

46. Nowotnik DP, Cvitkovic E. ProLindac (AP5346): A review of the development of an HPMA DACH platinum polymer therapeutic. *Adv Drug Deliv Rev* 2009;61(13):1214-9

47. Duncan R. Nanomedicine(s) and their regulation. *Handbook of Safety Assessment of Nanomaterials: From Toxicological Testing to Personalized Medicine*. Florida: Pan Stanford Publishing, 2015. p. 1-43

48. Bissett D, Cassidy J, de Bono JS, et al. Phase I and pharmacokinetic (PK) study of MAG-CPT (PNU 166148): A polymeric derivative of camptothecin (CPT). *Br J Cancer* 2004;91(1):50-5

49. Pasut G, Veronese FM. PEG conjugates in clinical development or use as anticancer agents: An overview. *Adv Drug Deliv Rev* 2009;61(13):1177-88

50. Wenjun Li, Peng Zhan, Erik De Clercq, et al. Current drug research on PEGylation with small molecular agents. *Prog Polym Sci* 2013;38:421-4

51. Scomparin A, Salmaso S, Bersani S, et al. Novel folated and non-folated pullulan bioconjugates for anticancer drug delivery. *Eur J Pharm Sci* 2011;42(5):547-58

52. Wente MN, Kleeff J, Buchler MW, et al. DE-310, a macromolecular prodrug of the topoisomerase-I-inhibitor exatecan (DX-8951), in patients with operable solid tumors. *Invest New Drugs* 2005;23(4):339-47

53. Walsh MD, Hanna SK, Sen J, et al. Pharmacokinetics and antitumor efficacy of XMT-1001, a novel, polymeric topoisomerase I inhibitor, in mice bearing HT-29 human colon carcinoma xenografts. *Clin Cancer Res* 2012;18(9):2591-602

54. Mersana therapeutics initiates phase 1b extension study of XMT-1001 in gastric cancer and non-small cell lung cancer. Mersana Press Releases: Mersana Therapeutics, Inc., 2011 Available at: <http://www.mersana.com/news-events/pr-2011-03-25.php> [Last accessed 24 February 2016]

55. Yurkovetskiy AV, Fram RJ. XMT-1001, a novel polymeric camptothecin pro-drug in clinical development for patients with advanced cancer. *Adv Drug Deliv Rev* 2009;61(13):1193-202

56. Yordanov G. Advanced strategies for drug delivery in nanomedicine. *Colloid and interface chemistry for nanotechnology*. Florida: CRC Press, 2014. p. 3-27

57. Kundranda MN, Niu J. Albumin-bound paclitaxel in solid tumors: Clinical development and future directions. *Drug Des Devel Ther* 2015;9:3767-7

58. D. Hubbard, D.J. Brayden, H. Ghandehari. Nanopreparation for oral administration. *Handbook of nanobiomedical research: Fundamentals, Applications and Recent Developments*. Northeastern University, USA: World Scientific, 2014. p. 153-202

59. Onxeo files application for key livatag® patent — onxeo indleverer ansøgning om vigtigt patent for livatag®. Onxeo Press Releases: Onxeo, 2015 Available at: <http://www.onxeo.com/en/onxeo-files-application-key-livatag-patent-onxeo-indleverer-ansogning-om-vigtigt-patent-livatag/> [Last accessed 18 February 2016]
60. Orphan oncology products.livatag. ONXEO website, 2016; Available at: <http://www.onxeo.com/en/nos-produits/portefeuilles-produits/orphelins-oncologie/> [Last accessed 11 April 2016]
61. Zhou Q, Sun X, Zeng L, et al. A randomized multicenter phase II clinical trial of mitoxantrone-loaded nanoparticles in the treatment of 108 patients with unresected hepatocellular carcinoma. *Nanomedicine* 2009;5(4):419-23
62. Zhang Z, Liao G, Nagai T, Hou S. Mitoxantrone polybutyl cyanoacrylate nanoparticles as an anti-neoplastic targeting drug delivery system. *Int J Pharm* 1996;139:1-8
63. Zhang L, Zhang N. How nanotechnology can enhance docetaxel therapy. *Int J Nanomedicine* 2013;8:2927-41
64. Conley SJ, Baker TL, Burnett JP, et al. CRLX101, an investigational camptothecin-containing nanoparticle-drug conjugate, targets cancer stem cells and impedes resistance to antiangiogenic therapy in mouse models of breast cancer. *Breast Cancer Res Treat* 2015; 150(3):559-67.
65. Pham E, Birrer MJ, Eliasof S, et al. Translational impact of nanoparticle-drug conjugate CRLX101 with or without bevacizumab in advanced ovarian cancer. *Clin Cancer Res* 2015; 21(4):808-1.
66. Young C, Schlupe T, Hwang J, Eliasof S. CRLX101 (formerly IT-101)-A novel nanopharmaceutical of camptothecin in clinical development. *Curr Bioact Compd* 2011;7(1):8-14
67. Farokhzad OC, Jon S, Khademhosseini A, et al. Nanoparticle-aptamer bioconjugates: A new approach for targeting prostate cancer cells. *Cancer Res* 2004;64(21):7668-72
68. Revia R.A., Zhang M. Magnetite nanoparticles for cancer diagnosis, treatment, and treatment monitoring: Recent advances. *Materials Today* 2016;19(3):157-68
69. Wang YX, Hussain SM, Krestin GP. Superparamagnetic iron oxide contrast agents: Physicochemical characteristics and applications in MR imaging. *Eur Radiol* 2001; 11(11):2319-31 \* Excellent description of current clinical applications of SPION
70. Search of: Nanoparticles MRI. *ClinicalTrials.gov*: National Institutes of Health, 2016 Available at: [https://clinicaltrials.gov/ct2/results?term=nanoparticles+MRI&no\\_unk=Y](https://clinicaltrials.gov/ct2/results?term=nanoparticles+MRI&no_unk=Y) [Last accessed 01 March 2016]
71. Wang YX. Superparamagnetic iron oxide based MRI contrast agents: Current status of clinical application. *Quant Imaging Med Surg* 2011;1(1):35-40
72. Fadeel B, Garcia-Bennett AE. Better safe than sorry: Understanding the toxicological properties of inorganic nanoparticles manufactured for biomedical applications. *Adv Drug Deliv Rev* 2010;62(3):362-74

73. Weissleder R, Stark DD, Engelstad BL, et al. Superparamagnetic iron oxide: Pharmacokinetics and toxicity. *AJR Am J Roentgenol* 1989;152(1):167-73
74. Ryan SM, Brayden DJ. Progress in the delivery of nanoparticle constructs: Towards clinical translation. *Curr Opin Pharmacol* 2014;18:120-8
75. Hahn PF, Stark DD, Lewis JM, et al. First clinical trial of a new superparamagnetic iron oxide for use as an oral gastrointestinal contrast agent in MR imaging. *Radiology* 1990;175(3):695-700
76. Heesakkers RA, Jager GJ, Hovels AM, et al. Prostate cancer: Detection of lymph node metastases outside the routine surgical area with ferumoxtran-10-enhanced MR imaging. *Radiology* 2009;251(2):408-14
77. Saeed M, Wendland MF, Engelbrecht M, et al. Value of blood pool contrast agents in magnetic resonance angiography of the pelvis and lower extremities. *Eur Radiol* 1998;8(6):1047-53.
78. Sun X, Cai W, Chen X. Positron emission tomography imaging using radiolabeled inorganic nanomaterials. *Acc Chem Res* 2015;48(2):286-94
79. Seibold U, Wängler B, Schirmacher R, Wängler C. Bimodal imaging probes for combined PET and OI: Recent developments and future directions for hybrid agent development. *BioMed Res Int* 2014; DOI:10.1155/2014/153741
80. Arap W, Pasqualini R, Montalti M, et al. Luminescent silica nanoparticles for cancer diagnosis. *Curr Med Chem* 2013;20(17):2195-211
81. Choi CH, Zuckerman JE, Webster P, Davis ME. Targeting kidney mesangium by nanoparticles of defined size. *Proc Natl Acad Sci U S A* 2011;108(16):6656-61
82. Phillips E, Penate-Medina O, Zanzonico PB, et al. Clinical translation of an ultrasmall inorganic optical-PET imaging nanoparticle probe. *Sci Transl Med* 2014;6(260):260ra149 \*A first-in-human clinical trial of ultrasmall inorganic hybrid nanoparticles C-dots is described
83. Bradbury MS, Phillips E, Montero PH, et al. Clinically-translated silica nanoparticles as dual-modality cancer-targeted probes for image-guided surgery and interventions. *Integr Biol (Camb)* 2013;5(1):74-86
84. Christensen A, Juhl K, Charabi B, et al. Feasibility of real-time near-infrared fluorescence tracer imaging in sentinel node biopsy for oral cavity cancer patients. *Ann Surg Oncol* 2016;23:565-572
85. Lee N, Choi SH, Hyeon T. Nano-sized CT contrast agents. *Adv Mater* 2013 May 21;25(19):2641-60
86. Bao C, Conde J, Polo E, et al. A promising road with challenges: Where are gold nanoparticles in translational research? *Nanomedicine (Lond)* 2014;9(15):2353-70
87. Lin AW, Lewinski NA, West JL, et al. Optically tunable nanoparticle contrast agents for early cancer detection: Model-based analysis of gold nanoshells. *J Biomed Opt* 2005;10(6): DOI:10.1117/1.2141825



88. Anselmo AC, Mitragotri S. A review of clinical translation of inorganic nanoparticles. *AAPS J* 2015;17(5):1041-54 \*Detailed discussion on the preclinical success of inorganic nanoparticles for therapeutic or diagnostic applications
89. Loo C, Hirsch L, Lee MH, et al. Gold nanoshell bioconjugates for molecular imaging in living cells. *Opt Lett* 2005;30(9):1012-4
90. Sebastian V, Arruebo M, Santamaria J. Reaction engineering strategies for the production of inorganic nanomaterials. *Small* 2014;10(5):835-53
91. Garbayo E, Estella-Hermoso de Mendoza A, Blanco-Prieto MJ. Diagnostic and therapeutic uses of nanomaterials in the brain. *Curr Med Chem* 2014;21(36):4100-31 \*Excellent discussion of future direction and commercialization problems of nanotechnology
92. Funkhouser J. Reinventing pharma: The theranostic revolution. *Current Drug Discovery* 2002;2:17-19
93. Luque-Michel E, Larrea A, Lahuerta C, et al. A simple approach to obtain hybrid au-loaded polymeric nanoparticles with a tunable metal load. *Nanoscale* 2016;8(12):6495-506
94. Muthu MS, Leong DT, Mei L, Feng SS. Nanotheranostics - application and further development of nanomedicine strategies for advanced theranostics. *Theranostics* 2014;4(6):660-77 \*Interesting review regarding nanotheranostics form the view of experts in the topic
95. Ryu JH, Lee S, Son S, et al. Theranostic nanoparticles for future personalized medicine. *J Control Release* 2014;190:477-84
96. Xi,Zhu, Emma L.B. Anquillare, et al. Polymer- and protein-based nanotechnologies for cancer theranostics. *Cancer theranostics*. San Diego, USA: Elsevier, 2014. p. 419-36
97. Clancy M K. Clinical translation and regulation of theranostics. *Polymer- and Protein- Bades Nanotechnology for Cancer Theranostics*. San Diego, USA: Elsevier, 2014. p. 439-546
98. Seymour LW, Ferry DR, Kerr DJ, Rea D, et al. Phase II studies of polymer-doxorubicin (PK1, FCE28068) in the treatment of breast, lung and colorectal cancer. *Int J Oncol* 2009;34(6):1629-36
99. Agostinis P, Berg K, Cengel KA, et al. Photodynamic therapy of cancer: An update. *CA Cancer J Clin* 2011;61(4):250-81
100. Huang YY, Sharma SK, Dai T, et al. Can nanotechnology potentiate photodynamic therapy? *Nanotechnol Rev* 2012;1(2):111-46
101. Singh A, Sahoo SK. Magnetic nanoparticles: A novel platform for cancer theranostics. *Drug Discov Today* 2014;19(4):474-81
102. Kim TH, Lee S, Chen X. Nanotheranostics for personalized medicine. *Expert Rev Mol Diagn* 2013;13(3):257-69
103. Babu A, Templeton AK, Munshi A, Ramesh R. Nanodrug delivery systems: A promising technology for detection, diagnosis, and treatment of cancer. *AAPS PharmSciTech* 2014;15(3):709-21

104. Libutti SK, Paciotti GF, Byrnes AA, et al. Phase I and pharmacokinetic studies of CYT-6091, a novel PEGylated colloidal gold-rhTNF nanomedicine. *Clin Cancer Res* 2010;16(24):6139-4 \*\*Proof-of-principle theranostic clinical study of Aurimune® in which the biodistribution proof has been obtained through TEM images
105. Lammers T, Kiessling F, Hennink WE, Storm G. Nanotheranostics and image-guided drug delivery: Current concepts and future directions. *Mol Pharm* 2010;7(6):1899-912
106. Matsumura Y, Hamaguchi T, Ura T, et al. Phase I clinical trial and pharmacokinetic evaluation of NK911, a micelle-encapsulated doxorubicin. *Br J Cancer* 2004;91(10):1775-81
107. Meerum Terwogt JM, ten Bokkel Huinink WW, Schellens JH, et al. Phase I clinical and pharmacokinetic study of PNU166945, a novel water-soluble polymer-conjugated prodrug of paclitaxel. *Anticancer Drugs* 2001;12(4):315-23
108. Soepenbergh O, de Jonge MJ, Sparreboom A, et al. Phase I and pharmacokinetic study of DE-310 in patients with advanced solid tumors. *Clin Cancer Res* 2005;11(2 Pt 1):703-11 \*\*Article where a phase II dose study is recommended although the development of DE-310 appear to have been discontinued
109. Danhauser-Riedl S, Hausmann E, Schick HD, et al. Phase I clinical and pharmacokinetic trial of dextran conjugated doxorubicin (AD-70, DOX-OXD). *Invest New Drugs* 1993;11(2-3):187-95
110. Cortajarena A. L., Ortega D., Ocampo S.M., et al. Engineering iron oxide nanoparticles for clinical settings. *Nanobiomedicine*, 2014;1(2): DOI: 10.5772/58841
111. Weissleder R, Nahrendorf M, Pittet MJ. Imaging macrophages with nanoparticles. *Nat Mater* 2014;13(2):125-38
112. Ma K., Mendoza C., Hanson M., et al. Control of ultrasmall sub-10 nm ligand-functionalized fluorescent Core-Shell silica nanoparticle growth in water. *Chem Mater* 2015;27(11):4119-33
113. Gomez L, Sebastian V, Irusta S, et al. Scaled-up production of plasmonic nanoparticles using microfluidics: From metal precursors to functionalized and sterilized nanoparticles. *Lab Chip* 2014;14(2):325-32
114. Gomez L., Arruebo M., Sebastian V., et al. Facile synthesis of SiO<sub>2</sub>-Au nanoshells in a three-stage microfluidic system. *J Mater Chem* 2012;22:21420-5
115. Sebastian V, Lee SK, Zhou C, et al. One-step continuous synthesis of biocompatible gold nanorods for optical coherence tomography. *Chem Commun (Camb)* 2012;48(53):6654-6





# **HYPOTHESIS AND OBJECTIVES**

---



Glioma is a general term used to describe primary brain tumors, the most neoplasms common in the central nervous system (CNS). Glioblastoma multiforme (GBM) is the most malignant and accounts for more than 60 % of all brain tumors in adults. Despite the variety of therapies researched to treat GBM, it is still a deadly disease with extremely poor prognosis (average survival of 18 months). One of the main strategies to achieve lower mortality is early detection, localization and typing, as well as the precise therapy and monitoring of the tumor. In the field of diagnosis, nanotechnology plays an important role and several nanosystems have improved the accuracy of different imaging techniques. This is the case of superparamagnetic iron oxide nanoparticles (SPION) for magnetic resonance imaging (MRI) or gold nanoparticles (AuNP) for computed tomography (CT). From the therapeutic point of view, doxorubicin (DOX) is a potent antineoplastic drug widely used in the treatment of cancer. Administered in a free form it does not target the tumor and high doses are needed, which cause cardiotoxicity. Nanomedicine is also considered an interesting alternative since the encapsulated drug offers improved bioavailability, decreased toxicity and more effective treatment. On the top of that, numerous studies such as those carried out by our research group have shown that by modifying the surface of the nanocarriers with, for example, the surfactant Tween® 80 or the apolipoprotein E, they are able to cross the blood brain barrier (BBB). Failure to do so is the main cause of chemotherapy failure in CNS diseases. It is indeed well acknowledged that magnetic nanoparticles, as the SPION already mentioned, could also improve the specificity of the treatment since they can be attracted by magnets. All in all, it is possible to combine the application of nanotechnology to the diagnosis and treatment of diseases such as glioma, leading to what is known as theragnosis. As a matter of fact, diagnostic/therapeutic nanoplatfoms are a new and promising step towards early diagnosis and personalized medicine.

On the basis of the foregoing, the initial hypothesis of this thesis is as follows:

The primary hypothesis is that the coencapsulation of DOX (as a treatment agent) and AuNP or SPION (as a diagnostic agents) in the same nanosystem will allow NP monitoring and therefore tumor monitoring. Apart from that, the encapsulation of DOX in polymeric nanoparticles coated with different surfactants along with magnetic targeting of SPION will allow BBB permeation and therefore glioma therapy improvement.

Objectives:

The main objective of this project is to design and develop nanosystems for the treatment and diagnosis of glioma.

In order to achieve this general objective, the following partial objectives have been formulated:

1. Design, optimization and characterization of polymeric nanoparticles that encapsulate a contrast agent (AuNP or SPION) and/or a cytostatic drug (DOX) using different types of surfactants.
2. In vitro study of the theranostic efficacy of the nanoparticles developed: study of their use as contrast agents by micro-CT or MRI, and study of their use as therapeutic agents in the treatment of glioma cells.
3. Study of the influence of the surfactant-coating in the passage through a cellular BBB model of the nanoparticles developed.
4. Biodistribution and efficacy studies by MRI of nanoparticles synthesized with T80 and targeted magnetically to the brain in a glioma murine model.

In the long term, the results obtained could be used at a later stage as a theranostic platform and could be transferred to treat diseases that require crossing BBB.







# CHAPTER 1

---

## **I. A simple approach to obtain hybrid Au-loaded polymeric nanoparticles with a tunable metal load**

Nanoscale 016, 8, 6495-6506. IF: 7.367  
NANOSCIENCE AND NANOTECHNOLOGY: 11/88, Q1  
DOI: 10.1039/C5NR06850A

## **II. Visualization of hybrid gold-loaded polymeric nanoparticles in cells using scanning electron microscopy**

Journal of Drug Delivery Science and Technology, 42, 315-320,  
2017. IF: 2.297  
PHARMACOLOGY, TOXICOLOGY AND PHARMACEUTICS: 356/783, Q2  
DOI: 10.1016/j.jddst.2017.04.008



## INDEX

<b>I. A simple approach to obtain hybrid Au-loaded polymeric nanoparticles with a tunable metal load</b>	
Abstract .....	53
1. <b>Introduction</b> .....	54
2. <b>Results and discussion</b> .....	57
2.1 Encapsulation of preformed AuNP – double W/O/W emulsion .....	58
2.2. Encapsulation of preformed AuNP – single emulsion .....	59
2.3. In situ formation of AuNP inside PLGA NP .....	61
3. <b>Experimental</b> .....	69
3.1 Materials .....	69
3.2 Synthesis of AuNP .....	69
3.3 Synthesis of hybrid-PLGA NP by direct encapsulation using a double-emulsion W/O/W .....	70
3.4 Synthesis of hybrid-PLGA NP by direct encapsulation using a simple-emulsion O/W .....	70
3.5 Synthesis of hybrid-PLGA NP by <i>in situ</i> reduction using a double-emulsion W/O/W .....	70
3.6 Characterization .....	71
4. <b>Conclusions</b> .....	72
5. <b>Notes and references</b> .....	72
<b>II. Visualization of hybrid gold-loaded polymeric nanoparticles in cells using scanning electron microscopy</b>	
Abstract .....	77
1. <b>Introduction</b> .....	78
2. <b>Materials and methods</b> .....	79
2.1 Materials .....	76
2.2 Au – PLGA NP synthesis and characterization .....	80
2.3 Cellular internalization assay of Au - PLGA NP .....	81
2.4 Viability assay .....	81
2.5 <i>In vivo</i> tracking test .....	82
3. <b>Results and discussion</b> .....	82
3.1 Au-PLGA NP characterization .....	82
3.2 Cellular internalization of Au - PLGA NP .....	84
3.3 Viability assay .....	85
3.4 <i>In vivo</i> tracking .....	86
4. <b>Conclusions</b> .....	87
5. <b>References</b> .....	88



## A simple approach to obtain hybrid Au-loaded polymeric nanoparticles with a tunable metal load

Edurne Luque-Michel,<sup>‡a,b</sup> Ane Larrea,<sup>‡c</sup> Celia Lahuerta,<sup>‡c,d</sup> Víctor Sebastian,<sup>\*c,e</sup> Edurne Imbuluzqueta,<sup>a,b</sup> Manuel Arruebo,<sup>c,e</sup> María J. Blanco-Prieto<sup>\*a,b</sup> and Jesús Santamaría<sup>c,e</sup>

<sup>a</sup>Department of Pharmacy and Pharmaceutical Technology, School of Pharmacy, University of Navarra, C/Irunlarrea 1, E-31008 Pamplona, Spain. E-mail: mjblanco@unav.es; Fax: +34 948 425 649; Tel: +34 948 425 600 ext. 6519

<sup>b</sup>IdiSNA, Fundación Instituto de Investigación Sanitaria de Navarra, Recinto del Complejo Hospitalario de Navarra, Calle Irunlarrea, 3. Pamplona 31008, Spain

<sup>c</sup>Institute of Nanoscience of Aragon (INA) and Department of Chemical, Engineering and Environmental Technology, University of Zaragoza, C/Mariano Esquillor, s/n, I+D+i Building, 50018 Zaragoza, Spain. E-mail: victorse@unizar.es; Fax: +34 976 761879; Tel: +34 876555441

<sup>d</sup>Minimally Invasive Techniques Research Group (GITMI), Universidad de Zaragoza, C/Miguel Servet, 177, 50013 Zaragoza, Spain

<sup>e</sup>CIBER de Bioingeniería, Biomateriales y Nanomedicina (CIBER-BBN), Centro de Investigación Biomédica en Red, C/Monforte de Lemos 3-5, Pabellón 11, 28029 Madrid, Spain

<sup>‡</sup>These authors contributed equally.

### Abstract

A new strategy to nanoengineer multi-functional polymer-metal hybrid nanostructures is reported. By using this protocol the hurdles of most of the current developments concerning covalent and noncovalent attachment of polymers to preformed inorganic nanoparticles (NP) are overcome. The strategy is based on the *in situ* reduction of metal precursors using the polymeric nanoparticle as a nanoreactor. Gold nanoparticles (AuNP) and poly(DL-lactic-co-glycolic acid), PLGA, are located in the core and shell, respectively. This novel technique enables the production of PLGA NP smaller than 200 nm that bear either a single encapsulated AuNP or several smaller NP with tunable sizes and a 100% loading efficiency. *In situ* reduction of Au ions inside the NP was achieved on demand by using heat to activate the reductive effect of citrate ions. In addition, we show that the loading of the resulting AuNP inside the PLGA NP is highly dependent on the surfactant used. Electron microscopy, laser irradiation, UV-Vis and fluorescence spectroscopy characterization techniques confirm the location of Au nanoparticles. These promising results indicate that these hybrid nanomaterials could be used in theranostic applications or as contrast agents in dark-field imaging and computed tomography.

## 1. Introduction

An important advance concerning the production of polymeric nanoparticles (PNP) is the ability to nanoengineer biocompatible polymer–metal hybrid nanostructures with remarkable optoelectronic and biomedical properties.<sup>1</sup> Metal and metal oxide nanoparticles (NP), as well as quantum dots, can endow NP with unique properties which make them potentially useful as Surface-Enhanced Raman Scattering (SERS) probes, contrast agents or advanced drug carriers [2, 3]. To date, most of the developments concerning polymer–hybrid nanomaterials that encapsulate metal NP are based on covalent and non-covalent attachment [4] of polymers to preformed inorganic NP. Covalent attachment is achieved by the polymerization of monomers using mainly the “grafting-from” [5] and the “*in situ* polymerization” [6] techniques. In a typical “grafting-from” approach, polymer brushes are grown outwardly *in situ* from the functional surfaces of the preformed inorganic NP by means of different surface-initiated polymerization techniques such as Atom Transfer Radical Polymerization (ATRP) and Reversible Addition–Fragmentation chain Transfer (RAFT). In the “*in situ* polymerization” approach, inorganic NP are surface-functionalized and trapped in a “micelle reactor” containing the necessary chemicals such as the monomer and the catalyst. After initiating the polymerization, the inorganic NP become trapped within the polymeric network. These strategies have proven to be effective in generating core/shell inorganicpolymer hybrids, but they typically require complex preparation procedures, including surface functionalization, a delicate control over the reaction conditions, and time-consuming purification processes. On the other hand, non-covalent immobilization requires the use of as-made polymers using the “layer by layer” (LBL) [7], “direct encapsulation” [3, 8-11] and “template-assisted” approaches [12, 14]. The “layer by layer” procedure is based on the consecutive adsorption of alternating layers of positively and negatively charged polyelectrolytes on the inorganic NP surfaces, forming core/shell nanostructures. Although the main advantage of the LBL technique is its ability to precisely control the thickness of the polymer shell by controlling the number of polyelectrolyte layers, it is also a complex multi-step process and the shell often faces serious stability issues [4].



The direct encapsulation approach consists of mixing preformed metal NP separately prepared along with the oil or aqueous phase to produce an O/W or W/O/W emulsion, respectively. After synthesis, the organic phase is usually removed by solvent evaporation and then the NP precipitate along with the encapsulated metal NP. Although this one-pot procedure is easy to implement, the core encapsulation control is poor and its reproducibility limited, requiring a suitable core functionalization process if the core particles were dispersed in the organic phase [15-16]. A new approach based on the direct encapsulation of gold (Au) NP by the supercritical emulsion extraction (SEE) technique was successfully applied, obtaining sub-micron polylactic-Au particles (ca. 200 nm) [17]. However, although a good Au dispersion was achieved, the loading efficiency was limited (around 50 %). Finally, the template-assisted approach is intrinsically a multistep complex procedure, where preformed metal NP are typically coated with a silica shell, which is in turn functionalized with certain groups that promote the growth of a polymeric layer. Afterwards, the removal of the sacrificial silica layer by an etching agent yields polymeric capsules that contain inner single nanoparticle. Although the template-assisted approach is a promising way to create hybrid NP with an excellent control on the loading of inorganic cores, it involves a rigorous regulation of the reaction conditions [18] and a further template removal step that may introduce stability problems and/or induce chemical attachment on the NP cores.

Apart from the use of pre-formed NP, a new strategy based on the *in situ* reduction of metal ions in a polymeric matrix circumvents some of the weaknesses of the previous techniques. The metallic ions are trapped in the polymeric particle and the reduction reaction is *in situ* activated by a reducing agent [19], UV-light [20] or even ultrasounds [21]. Although this is a more effective and lower-cost protocol than the previous one, the control on the loading and selective encapsulation of metal NP must be still considerably improved [10]. In addition, to the best of our knowledge, this technique has only been applied to the production of hybrid microparticles [22, 23], but not to NP. The latter require a higher degree of accuracy regarding encapsulation control especially whenever biomedical applications are considered, where the size of the carriers used in many applications is typically below 200 nm [24, 25].

These aforementioned procedures are not amenable to large scale production due to the lack of control during multistep productions or due to the unavoidable formation of either polymer NP without inorganic cores or inorganic NP without a polymer coating in the one-pot approaches. It is widely recognized that controlling the size, morphology and payloads is one of the main barriers for the development of nanotechnology-based applications [26]. Also, when a sufficiently large production per batch cannot be achieved, combining NP derived from different batches may introduce unwanted variations in the quality and consequently affect the potential applications of the NP [27]. Therefore, it seems clear that developing a robust, scalable process to prepare NP containing tunable inorganic NP payloads would be highly interesting. In particular, the preparation of monodisperse polymer NP containing noble metal NP represents a challenging objective with a multitude of potential applications.

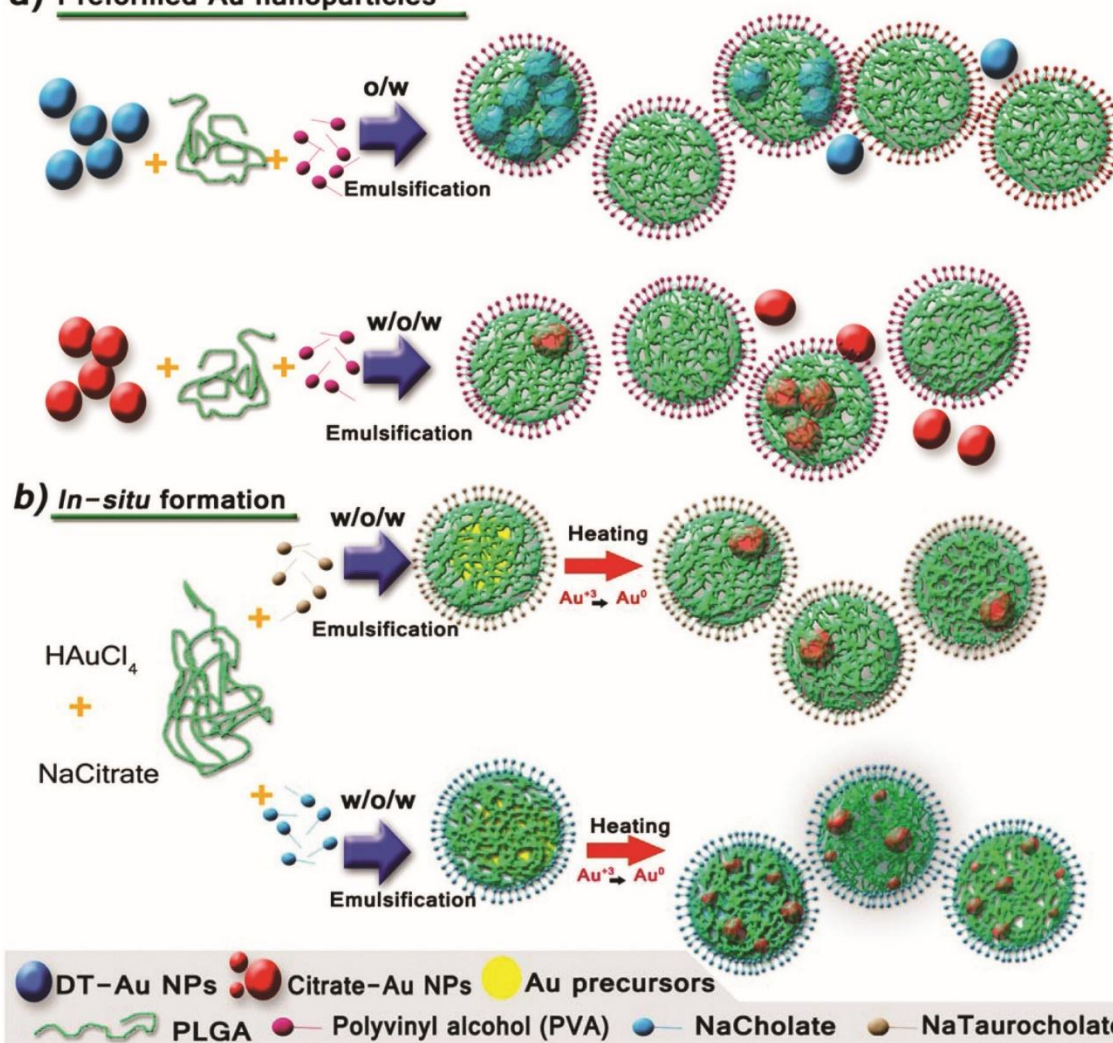
Herein, we report a versatile one-pot protocol based on the *in situ* reduction to produce monodisperse poly(DL-lactic-co-glycolic acid), PLGA NP smaller than 200 nm that bear either a single encapsulated AuNP or several smaller NP with tunable sizes. Chloroauric acid and citrate ions were directly used as reagents and the PLGA polymer NP as nanoreactors. The Au reagent dose within the polymer NP, and consequently the AuNP size, was controlled by the formation of a double-emulsion with the polymer. *In situ* reduction of Au ions inside the NP was achieved on demand by using heat to activate the reductive effect of citrate ions. In addition, we show that the loading of the resulting AuNP inside the PLGA NP is highly dependent on the surfactant used. To the best of our knowledge, this is the first case of a one-pot fabrication of highly monodisperse PLGA NP with a tunable AuNP payload in their interior and an exquisite control over the AuNP loading. PLGA was chosen as the polymeric matrix because of its non-toxic character, biodegradability and high cellular uptake efficiency.<sup>28</sup> PLGA undergoes hydrolysis in the presence of physiological water, releasing the original monomers which are easily metabolized in the body via the Krebs cycle without any systemic toxicity. On the other hand, AuNP are widely used in a variety of biomedical applications, mainly on account of their optical properties [29–31]. Here we use them as a practical example of the potential of the method developed to tailor the encapsulation of noble metal NP in polymeric

matrices for future use in theranostic applications or as contrast agents in dark-field imaging and computed tomography.

## 2. Results and discussion

Two different alternatives to produce hybrid PLGA NP were explored, involving respectively the encapsulation of preformed AuNP (Figure 1a) and the *in situ*

### a) Preformed Au nanoparticles



formation of AuNP inside the PLGA matrix from Au precursors (Figure 1b).

**Figure 1** Schematic illustration of the synthesis of Au-PLGA hybrid NP produced by: (a) direct encapsulation of the preformed hydrophilic (citrate) and hydrophobic (dodecanethiol – DT) AuNP and (b) the *in situ* reduction method. The *in situ* reduction method was performed with different types of surfactants to tune the AuNP payload.

## 2.1 Encapsulation of preformed AuNP – double W/O/W emulsion

PLGA–AuNP were first synthesized by an emulsion evaporation process following a direct encapsulation approach with preformed AuNP (Figure 1a and 2a). To this end, hydrophilic AuNP were separately fabricated according to the well-known Turkevich method (Figure 2b) [32]. Next, PLGA particles entrapping the previously synthesized AuNP were prepared by a water in-oil-in-water (W/O/W) emulsion method followed by solvent evaporation of the volatile organic phase (ethyl acetate) at room temperature (RT) under stirring (Figure 2a). Figure 2d shows that for the PLGA NP containing AuNP, the Au position inside the PLGA matrix was near the surface. It was believed that this preferential location could be derived from the weak interaction of the hydrophilic Au particles with the organic phase in the W/O/W emulsion. It is likely that some citrate molecules located at the surface of AuNP form hydrogen bonds between the hydroxyl groups of citrate and the surfactant used in the synthesis of PLGA NP. On the other hand, the TEM characterization revealed a poor control of the AuNP loading, resulting in the presence of numerous PLGA NP without a Au payload and AuNP without a PLGA coating (Figure 2c and S1a in Annex 1).

To improve the encapsulation of AuNP, the concentration of AuNP at the inner water phase utilized in the W/O/W emulsion was modified. As expected, the encapsulation efficiency increased as the concentration of AuNP was increased, obtaining indifferently limited encapsulation efficiency (Figure S1b in Annex 1). However, it was also observed that a highly concentrated Au colloid was not stable enough due to a concentration-polarization effect and the AuNP tended to aggregate (Figure S1b in Annex 1). This aggregation resulted in PLGA–AuNP with a heterogeneous size distribution.

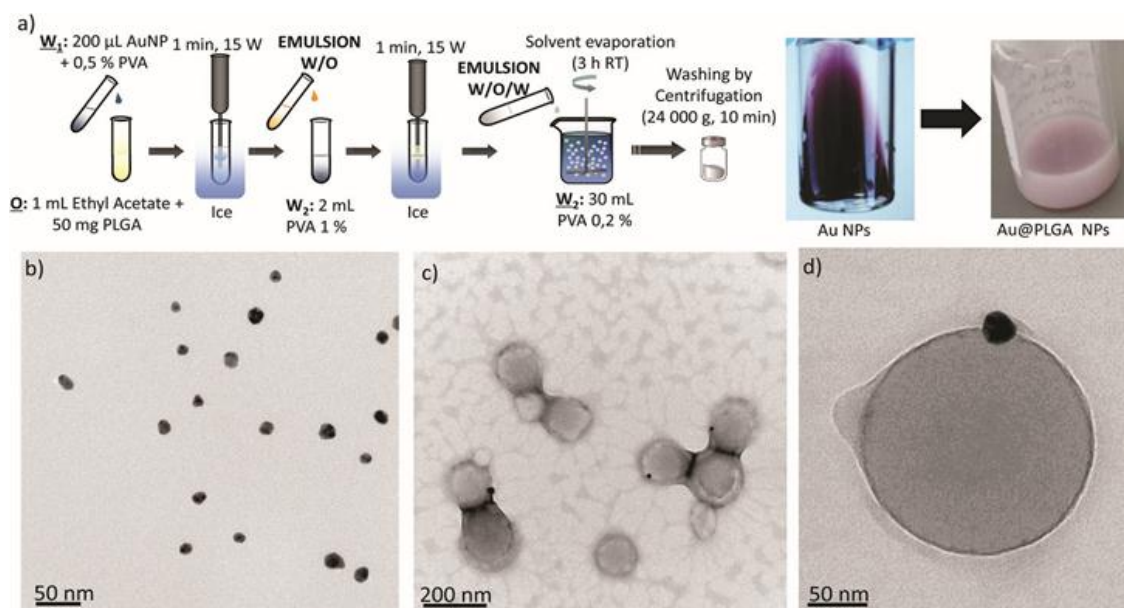


**Figure 2** (a) Synthesis procedure of Au–PLGA hybrid NP by direct encapsulation in W/O/W emulsion and visual appearance of the initial AuNP and the Au–PLGA hybrids. TEM micrographs of: (b) Au-citrate NP, (c) Au–PLGA hybrid NP after solvent evaporation. (d) A detailed image of a Au–PLGA hybrid NP.

## 2.2 Encapsulation of preformed AuNP – single emulsion

Since both the volume (200 µL) and the concentration of Au in the colloid used as an aqueous phase in the W/O/W emulsion had to be limited to get a stable emulsion, we also attempted the encapsulation of the AuNP in a single O/W emulsion (Figure 1a and 3a). To achieve this, the surface of the preformed AuNP was functionalized with non-hydrophilic ligands using a previously described aqueous-to-organic phase transfer protocol (Figure 3b) [33]. It is important to point out that the surface functionalization of AuNP with dodecanethiol (DT) and their dispersion in ethyl acetate led to a dielectric change that resulted in the modification of the Surface Plasmon Resonance (SPR) peak and therefore in the optical properties of the NP (Figure S3a in Annex 1) [34, 35]. Figure 3a shows that, at the same concentration, the typical red-wine colour of the NP produced by the Turkevich method in the water phase (see Figure 2a) turns into a bluish colour after being surface-modified and dispersed in ethyl acetate. The DT-AuNP were then encapsulated in PLGA by preparing an oil-in-water (O/W) emulsion followed by solvent evaporation of the volatile organic phase at RT under stirring (Figure 3a). In this way, the DT-AuNP were

incorporated into the hydrophobic domain of PLGA molecules via hydrophobic interactions, and the PLGA NP were then formed in the presence of polyvinyl alcohol (PVA) as emulsifier. The method produced hybrid structures with AuNP located roughly in a central location inside the PLGA matrix (Figure 3c and d). However, in spite of the fact that the single emulsification process facilitates the encapsulation of NP due to the less restricted volume limitations between the aqueous/organic phases compared with the W/O/W method, the encapsulation yield achieved did not improve the results obtained by the double emulsion approach. In addition, Figure 3c, d and S2 (Annex 1) show that AuNP tended to agglomerate and were unevenly distributed inside the PLGA NP. The agglomerates encapsulated were constituted by a heterogeneous number of NP, ranging from 10 to more than 100 units. This uncontrolled agglomeration inside the hybrid NP prepared by the single emulsion method also gave rise to a non-homogeneous size distribution of Au PLGA NP ( $207 \pm 39$  nm) and to the presence of empty PLGA NP without metal NP.

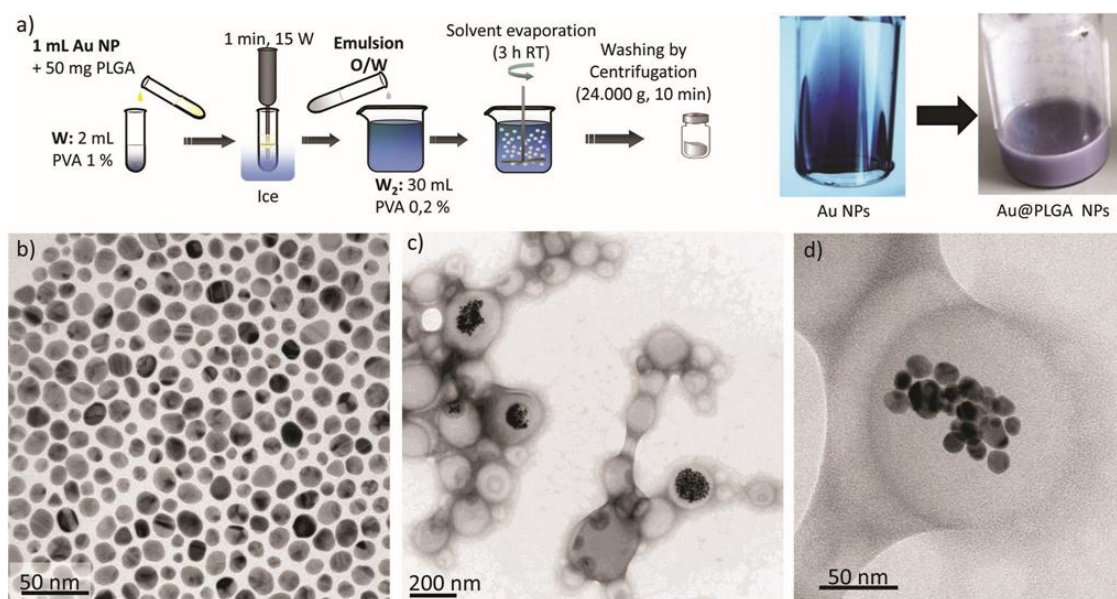


**Figure 3** (a) Synthesis procedure of Au-PLGA hybrid NP by direct encapsulation in O/W emulsion and visual appearance of the initial AuNP and the Au-PLGA hybrids. TEM micrographs of: (b) DT-AuNP, (c) Au-PLGA hybrid NP after solvent evaporation. (d) A detailed image of a Au-PLGA hybrid structure with clustered AuNP.



### 2.3 *In situ* formation of AuNP inside PLGA NP

Considering the problems already described (encapsulation efficiency, homogeneity of the NP load in the PLGA matrix) by the direct encapsulation approach, a new strategy was tested in which the nanoemulsification process was coupled to an *in situ* reduction method to generate AuNP inside the PLGA NP (Figure 1b). In this case, PLGA NP entrapping tetrachloroaurate and citrate ions were prepared by a double emulsion (W/O/W) method (Figure 4a). This procedure was adopted because it could guarantee a similar load of Au<sup>3+</sup> ions provided that the relative amounts of water and oil could be maintained in each PLGA NP. Similarly to a modified Turkevich procedure [36], the reduction of Au<sup>3+</sup> ions to Au could be activated at the desired time by using a temperature increase, since at RT the Au<sup>3+</sup> payload of each PLGA NP is stable enough to avoid reduction by citrate ions. Since PLGA 50: 50 has a low vitreous transition temperature, 45–50 °C [37], 40 °C was selected as a suitable temperature to activate the redox reaction while keeping sufficient polymer rigidity to minimize the outward diffusion of the encapsulated chemicals. Then, the hybrid Au– PLGA NP were formed by allowing evaporation of the organic phase at RT under stirring.

Three different types of surfactants, with different ionic natures, were selected to stabilize the double W/O/W emulsion: anionic sodium taurocholate (STC), anionic sodium cholate (SC), and non-ionic Tween 80. After 20 minutes of heating at 45 °C, the colour of the PLGA double emulsion prepared with STC as the surfactant gradually changed from pale yellow to dark purple. This colour change was a clear indication that the reduction of Au<sup>3+</sup> ions was occurring. The UV-Vis spectra showed a noticeable peak associated with the surface plasmon resonance of AuNP around 520 nm, supporting the AuNP growth (see Figure S3b in Annex 1). Figure 4b depicts the TEM micrograph of the Au–PLGA NP formulation obtained with STC. It can be observed that every PLGA NP contains a single AuNP, as indicated by the dark sharp contrast associated with Au. A higher magnification is shown in Figure 4b (below) where a single AuNP of 10 ± 2 nm in diameter was encapsulated in each PLGA NP, achieving a 100 % selectivity in the encapsulation. This remarkable achievement confirms the effectiveness of the encapsulation of AuNP precursors. The containment of precursors was so efficient that Au reduction only occurred inside the PLGA NP,

using the PLGA micelle itself as a nanoreactor. On the other hand, the location of AuNP was close to the surface of the PLGA NP, as shown by the TEM images.

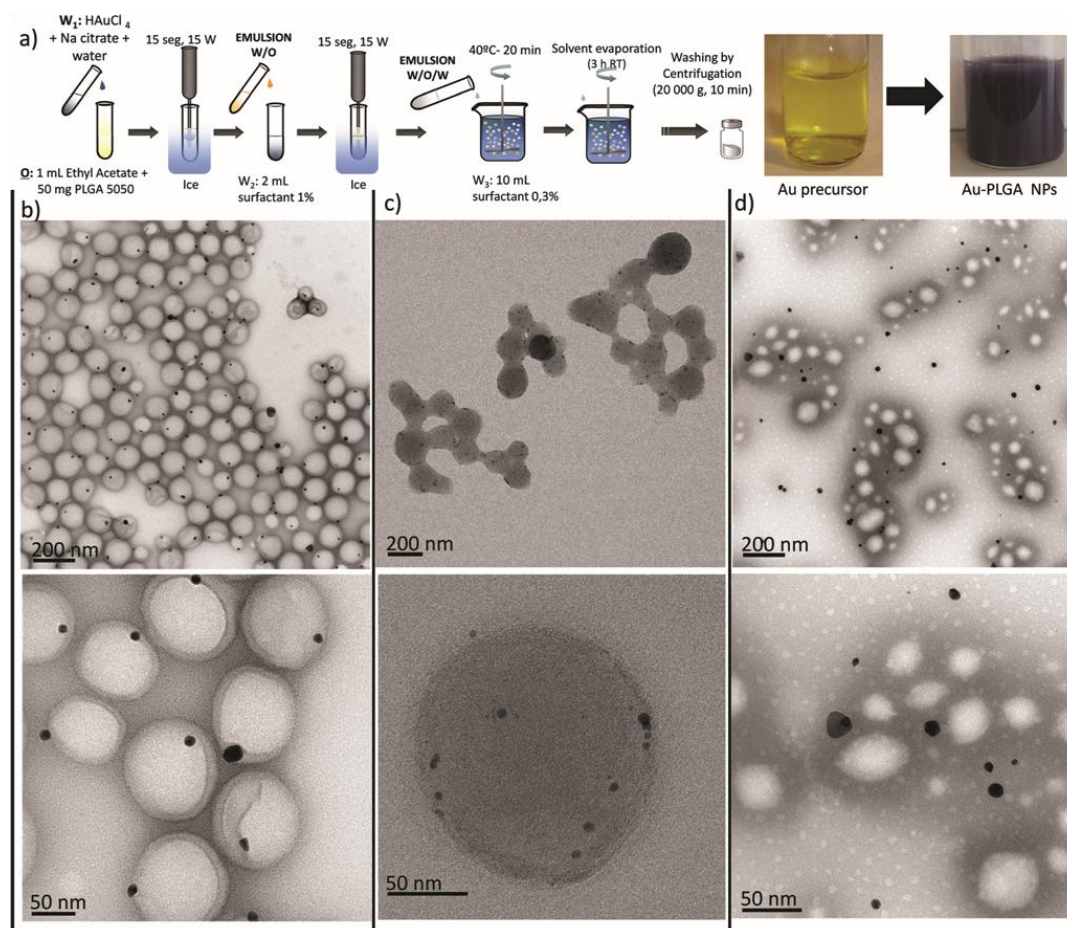


**Figure 4** (a) Synthesis procedure of Au-PLGA hybrid NP by the *in situ* reduction method in W/O/W emulsion and visual appearance of the initial AuNP and the Au-PLGA hybrids. TEM micrographs of Au-PLGA NP produced with different stabilizers: (b) taurocholate, (c) sodium cholate, (d) Tween 80.

Finally, the loading of AuNP by the procedure developed here was reproduced in 20 independent syntheses with nearly 100 % reproducibility regarding the encapsulation of a single AuNP inside the PLGA NP (see Figure S4 in Annex 1).

The type of surfactant applied in the formation of emulsions is a key variable for directing the production of PLGA NP in a controlled manner [38]. The changes in



physico-chemical interactions between the hydrophobic and hydrophilic parts of the PLGA molecules produced by a change in the surfactant have an immediate effect on the final dimension of the resulting PLGA NP and on the confinement of the Au precursor. Thus, when SC was used instead of STC during the double emulsion formation, the reduction of  $\text{AuCl}_4^-$  by citrate ions gave rise to multiple encapsulated AuNP with a size under 5 nm (Figure 4c). The presence of SC directs the growth of  $\text{Au}^{3+}$  ions to tiny NP randomly distributed in the PLGA matrix rather than producing a single, larger Au nanoparticle (Figure 4).

The influence of the surfactant on the size of noble metal NP has previously been described in the literature. It is well known that the stabilizers used in the reduction of  $\text{Au}^{3+}$  ions can control the size of the resulting AuNP by lowering their high surface energy, leading to small AuNP with strong stabilizers such as thiols and amines and to larger NP with weaker stabilizers such as citrate ions [35]. Although we do not have a direct measurement of the interaction, it can be speculated that the adsorption energy of SC is higher than the one of TSC. Again, the UV-Vis characterization showed a tiny SPR peak which is in full agreement with the AuNP size (see Figure S3b in Annex 1), since when the size of AuNP reaches dimensions below 5 nm their SPR band become very weak or even non-existent, because for these sizes the electron density in the conduction band becomes very small [39].

SEM characterization using secondary and back-scattered electrons was performed in order to confirm the location of the AuNP. Figure 5a shows a SEM image obtained with secondary electrons where spherical PLGA NP containing AuNP are depicted. When the same PLGA NP are analyzed through back-scattered electrons (Figure 5b) the random presence of AuNP, already observed by TEM, is clearly revealed. These pictures indicate that the location of AuNP is close to the surface but they are still immersed in the PLGA matrix, in agreement with TEM results. Further evidence of the presence of the AuNP inside the PLGA NP will be provided by the experiments carried out with pyrene (see below).

Finally, Tween 80, a non-ionic surfactant, was also used to obtain Au-PLGA hybrid NP. Compared to the anionic SC and STC surfactants, the use of Tween allows one to study the effect of surfactant polarity on the synthesis of hybrid Au-PLGA NP by the *in situ* reduction method. Figure 4d shows that Tween 80 neither stabilizes the PLGA

molecules during the emulsification process nor the AuNP during the *in situ* reduction process. It can be observed that PLGA NP suffer from a lack of control of the shape and size after the solvent evaporation step and that a wide size distribution was obtained (Figure 4d). On the other hand, most AuNP were also located outside the PLGA NP with an uncontrolled size distribution. These results imply that, in this case, the Au precursor and citrate ions were not properly encapsulated inside the double emulsion.

The above results support the double role played by the surfactant as a stabilizer of the polymer molecules during micelle formation and of the AuNP during the *in situ* reduction process. In this study ionic surfactants (STC and SC) were preferred over non-ionic ones (Tween 80) because the former could provide electrostatic stabilization to both polymeric and AuNP. Also, the size of AuNP loaded into PLGA NP can be effectively tuned over 10 nm using STC or under 5 nm selecting SC. STC stabilizes the AuNP inside the PLGA, likely due to the enhanced colloidal stabilization that the amino and the sulfur groups provide to the AuNP. Electron-rich nitrogen donates electron density to the 5d and 6s orbitals of Au via its lone pairs. Au can also play the role of a proton acceptor and form nonconventional H-bonds with amine and hydroxyl groups [40], and strongly bonds to sulfur. It has been previously demonstrated that the S–Au bond is partially covalent (35%) and mostly electrostatic (65%) [41]. In addition, it is reported that both surfactants [42,43] can provide electrons (reducing agent) to Au<sup>3+</sup> ions through the hydroxyl groups and direct the formation of AuNP. However, the reduction time required is higher than 4 days at RT. The higher electron affinity between STC and AuNP might be responsible for a successful controlled single AuNP encapsulation. The slow action of citrate and STC as weaker reducing agents also helps to avoid the formation of multiple single crystals. Thus, after the initial nucleation/reduction leading to the formation of crystal seeds, as Au<sup>3+</sup> species are reduced, the concentration of reduced species does not reach the threshold required for a new nucleation, and instead they incorporate into growing crystals.

We found from a detailed analysis of the PLGA NP' size distribution that the PLGA NP obtained with STC had the narrowest size distribution of the three tested after solvent evaporation, rendering a mean particle size with STC and SC of 102 ± 13 nm

and  $175 \pm 33$  nm, respectively (Figure 5c). The corresponding mean NP sizes measured by Dynamic Light Scattering (DLS) in Au-PLGA hybrid NP produced with STC and SC were  $128 \pm 6$  nm (PDI  $0.065 \pm 0.006$ ) and  $197 \pm 4$  nm (PDI  $0.101 \pm 0.031$ ), respectively. Notwithstanding some degree of agglomeration (slight in any case, as shown by the electron microscopy images). The observed differences in size between DLS and TEM may also arise from the drying process and the subsequent shrinkage that polymeric chains underwent during TEM sample preparation. It should be highlighted that according to previous reports, NP with sizes less than 200 nm have shown great potential for both *in vitro* and *in vivo* applications [24, 25]. From the obtained results we can conclude that both SC and STC can stabilize AuNP in the PLGA matrix to achieve 100 % selectivity in the encapsulation by the double emulsion evaporation method with *in situ* reduction. Nevertheless, the different stabilization and reductibility during the nucleation-growth process of AuNP enable the encapsulation of either big AuNP (size > 10 nm) with STC or small AuNP (size < 5 nm) with SC. On the other hand, PLGA NP obtained with STC are more homogeneous in size and smaller than the ones produced with SC. Consequently, a balance between the stabilization of PLGA and Au atoms is required in the formation of Au-PLGA hybrid NP.

A further microscopy analysis from a single Au-PLGA hybrid NP, using a STEM microscope with a HAADF detector sensitive to the atomic number, confirms the location of AuNP close to the surface but embedded in the PLGA matrix (Figure 5d and g). Although this observation was already inferred from the TEM images, in some cases there was some doubt as to whether the NP were inside the PLGA particle or on its surface. It must be taken into account that the electron beam radiation that receives the PLGA NP makes them shrink a few nanometers, and that may be enough to bring the AuNP to the surface. This behavior can be observed in the halo which remains as shown in Figure 5g after the shrinkage. AuNP stabilized with SC are highly crystalline with the presence of twin defects as can be observed from the HR-STEM image in Figure 5e. Similarly to AuNP stabilized with SC, the use of STC gave rise to highly crystalline AuNP (Figure 5h). The energy-dispersive X-ray spectroscopy analysis (EDS) of the brightest NP encapsulated in the hybrid Au-PLGA NP produced with both surfactants confirms the presence of Au and not W crystals from the

contrast agent, this could also be originated during the staining process and give a similar contrast (Figure 5f and i).

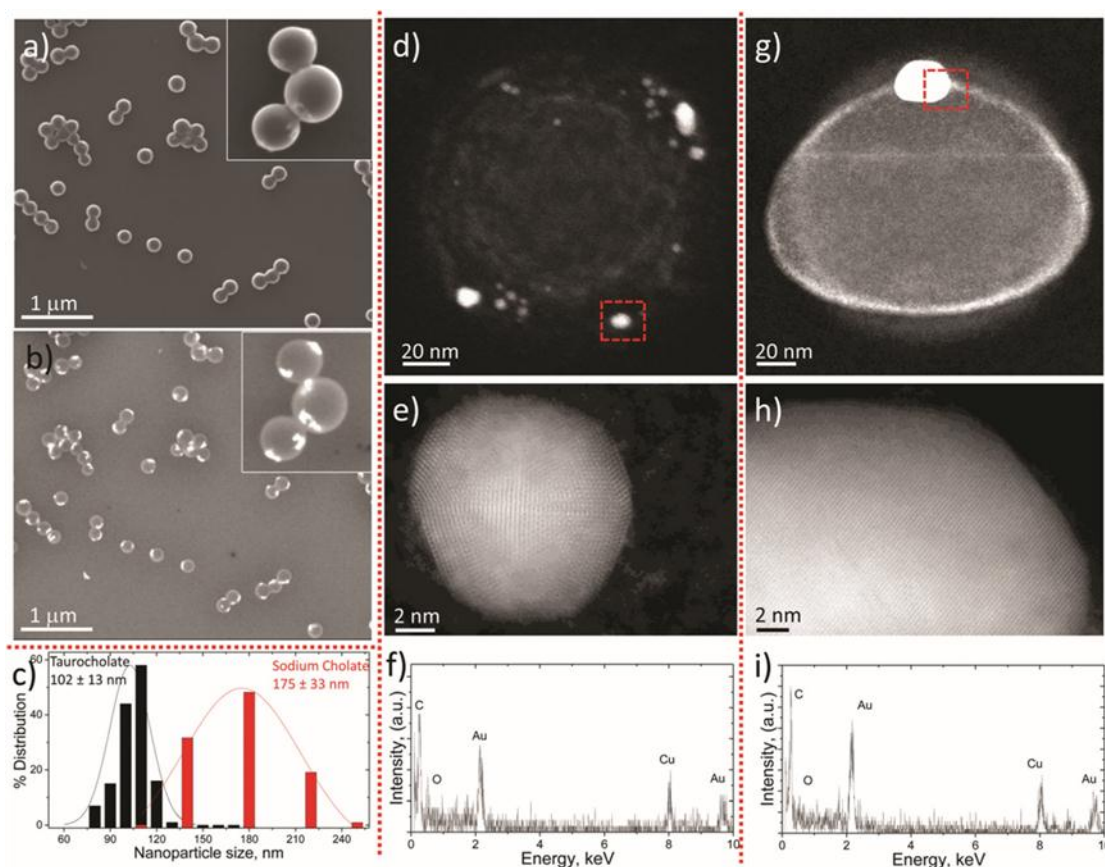


**Figure 5** Au–PLGA hybrid NP produced by the *in situ* reduction method in W/O/W emulsion with SC. (b) Back scattered electron micrograph to show the location of AuNP in the same area as (a). (c) NP size distribution of Au–PLGA hybrid NP produced with STC and SC as surfactants (data obtained from TEM analysis). (d) HAADF-STEM micrograph of representative Au–PLGA hybrid NP produced with SC to show by Z-contrast the location of AuNP inside representative Au–PLGA NP. (e) HAADF-HR STEM image to show the crystal fringes of an AuNP located inside a PLGA NP. (f) HAADF-EDS analysis of the area selected in (d) to confirm the presence of a AuNP. (g) HAADF-STEM micrograph of a representative Au–PLGA hybrid NP produced with STC to show by Z-contrast the location of the single AuNP entrapped inside a PLGA NP. (h) HAADF-HR STEM image of the AuNP depicted in figure (g) to show the crystal fringes of the AuNP located inside the PLGA NP. (i) HAADF-EDS analysis of the area selected in (g) to confirm the presence of AuNP.

Pyrene is a photoactive fluorophore that can be considered as a good hydrophobic model molecule because of its low water solubility, well-defined fluorescence spectra, and a well-established method to statistically analyze its transfer rate from its carrier to the surrounding medium [44]. Moreover, it is reported that the binding of pyrene to AuNP renders organic–inorganic hybrid nanoassemblies suitable for light harvesting and optoelectronic applications [45, 46]. We therefore used this system as a final direct proof of the presence of Au inside the PLGA matrix. Pyrene has different peak signals between 360 and 500 nm depending on solvent polarity. The intensity of the peaks in the absorption and emission spectra has often been used to sense the polarity of the microenvironment. Thus, the defined I/III emission intensity is usually related to the intensities of the peaks at 373 (I1) and 384 (I3) nm and it is used as a scale for solvent polarity [47]. When pyrene is present in a polar solvent such as water, the I/III ratio equals 1.87; when pyrene is present in a non-polar solvent such as hexane, the I/III ratio equals 0.58 [47]. Figure 6a shows the fluorescence spectrum of pyrene moieties encapsulated in PLGA NP without Au. In this case the calculated I/III ratio equals 1.3, which corresponds to the ratio associated with ethyl acetate [47]. Then, it can be inferred that pyrene moieties are located close to the PLGA polymer, where the ethyl acetate moieties, which still remain after the 3 h evaporation step, are adsorbed since the solubility of ethyl acetate in water is relatively low (8.3 g per 100 mL at 20 °C).

On the other hand, the fluorescence spectrum of the pyrene moieties encapsulated in the hybrid Au–PLGA NP did not show the typical emission peaks of pyrene and no peaks were detected. This fact can be explained as a consequence of the quenching effect that AuNP produce on pyrene due to the modification of electron and energy transfer processes, which deactivate the excited states of this fluorophore [48]. Isopropyl alcohol (IPA) can be used to extract the pyrene from the pyrene-loaded PLGA NP. We used this property to show that, in spite of the absence of the characteristic signals for the Au containing PLGA NP (Figure 6a), the hydrophobic interior of the PLGA NP was loaded with pyrene. Indeed, after extraction with IPA the fluorescence signal of the solubilized pyrene was clearly shifted corroborating the presence of pyrene moieties associated with Au inside the PLGA NP. This displacement could be an added advantage to the potential uses of the Au– PLGA hybrid NP as biological tracers as well as in optoelectronic devices.

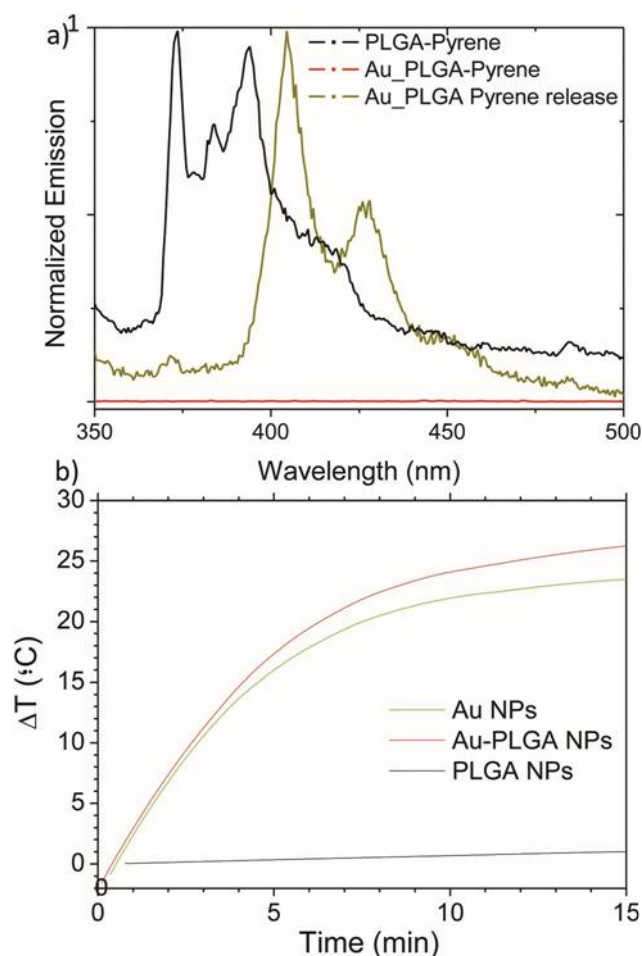


**Figure 6** (a) Fluorescence spectra of pyrene: encapsulated in PLGA NP, encapsulated in hybrid Au–PLGA NP and dispersed in IPA after release from hybrid Au–PLGA NP. [Au]  $0.29 \text{ mg mL}^{-1}$ ; [Pyrene] = 4.6 ppm. (b) Temperature increase as a function of time under laser irradiation (wavelength = 532 nm and power density of  $4.2 \text{ W cm}^{-2}$ ) of AuNP, PLGA NP and the hybrid Au–PLGA NP. [Au] =  $0.29 \text{ mg mL}^{-1}$ .

Since the UV-Vis characterization was able to show the interesting optoelectronic properties of the hybrid Au–PLGA nanoplateforms, they were exposed to continuous illumination to demonstrate that the AuNP synthesized inside the PLGA matrix are crystalline enough to act as efficient light absorbers. The exposure of aqueous suspensions of Au–PLGA produced with SC to continuous illumination at a laser power of  $4.2 \text{ W cm}^{-2}$  (wavelength 532 nm) for 15 min resulted in an elevation of the dispersion mean temperature of *ca.* 26 °C (Figure 6b), while a blank experiment with PLGA NP without AuNP inside showed temperature increases around 1 °C under the same conditions. On the other hand, a very similar heating (23 °C) was achieved when aqueous dispersions of AuNP containing the same nominal Au loading (measured by ICP),  $0.29 \text{ mg mL}^{-1}$ , were subjected to irradiation (Figure 6b). These results clearly

indicate that the Au encapsulated in the hybrid nanoplatforms are still efficient light absorbers. In addition, at this wavelength the attenuation by the PLGA shell was negligible and the hybrid Au-PLGA NP achieved the same temperature elevation as a pure Au colloid. This may also be helped by the position of the AuNP near the PLGA edge. The morphology of the hybrid Au-PLGA NP after laser irradiation was conserved, as observed by TEM images (see Figure S5 in Annex 1).

### 3. Experimental

#### 3.1 Materials

The following chemicals were obtained from commercial suppliers and used as received: the polymer poly(D,L-lactic-co-glycolic acid) 50 : 50 (PLGA;  $M_w$  38 000– 54 000 Da,  $T_g$  46–50 °C), under the commercial name of Resomer® RG 504 was purchased from Boehringer Ingelheim (Ingelheim, Germany) and Evonik Industries (Evonik Röhm GmbH, Germany). Sodium cholate, chloroauric acid ( $\text{HAuCl}_4 \cdot 3\text{H}_2\text{O}$ ), sodium citrate tribasic dehydrate  $\geq 99.0$  % ( $\text{Na}_3\text{C}_6\text{H}_5\text{O}_7 \cdot 2\text{H}_2\text{O}$ ), PVA (polyvinyl alcohol)  $M_w$  85 000– 124 000 Da, 97–99 % hydrolyzed, taurocholic acid sodium salt hydrate  $\geq 95$  % (TLC), ethyl acetate ACS reagent, dodecanethiol, phosphotungstic acid hydrate as a contrast agent for microscopy and fluorescent molecule pyrene  $\geq 99.0$  % were purchased from Sigma Aldrich (St Louis, MO, USA).

#### 3.2 Synthesis of AuNP

Citrate-capped AuNP were synthesized according to the Turkevich method but by decreasing the synthesis temperature [32], using  $\text{HAuCl}_4$  as a Au precursor and sodium citrate as both reducing agent and stabilizer. Briefly, 100 ml of a  $\text{HAuCl}_4$  solution containing 2.9 mg of Au was added to 50 ml of distilled water and kept at 70 °C. Afterwards, 5 mL of 1% sodium citrate solution was added while stirring vigorously. After continuous stirring for 30 minutes, the dispersion was allowed to cool down.

The dodecanethiol (DT)-capped AuNP were synthesized using the previously prepared citrate capped AuNP and using a phase transfer ligand exchange method

[33]. Citrate-AuNP at high concentrations ( $2 \times 10^{-8}$ – $5 \times 10^{-8}$  M) in water were put into contact with DT. After addition of acetone, NP were extracted into DT by swirling the solution for a few seconds, upon which the aqueous phase became clear, indicating that no AuNP remained. Excess DT was removed by diluting the DT coated AuNP in ethyl acetate and performing several centrifugation cycles.

### **3.3 Synthesis of hybrid Au–PLGA NP by direct encapsulation using a double-emulsion W/O/W**

AuNP were encapsulated into PLGA NP by the water-in-oil-in-water emulsion solvent evaporation method. Briefly, an aqueous phase composed of 200  $\mu$ L Au colloid NP (4 mM– 50 mM) and PVA (0.5 % w/v) was mixed by ultrasonication (15 W, 1 min, Branson Sonifier 450, Branson Ultrasonics Corp., Danbury, USA) with the organic phase containing 50 mg of PLGA dissolved in 1 mL of ethyl acetate. This w/o emulsion was emulsified again by ultrasonication (15 W, 1 min) with 2 mL of a 1 % (w/v) PVA aqueous solution to form a W/O/W emulsion. This final emulsion was then poured into a 30 mL solution of 0.2 % (w/v) PVA and continuously stirred for at least 3h at RT to allow solvent evaporation and NP formation. Particles were collected by centrifugation (24 000g, 15 min) (Sigma Laboratory Centrifuges, 3K30, Rotor no. 12150-H, Osterode am Harz, Germany) and washed three times with ultrapure water.

### **3.4 Synthesis of hybrid Au–PLGA NP by direct encapsulation using a single-emulsion O/W**

DT functionalized AuNP were encapsulated into PLGA NP by the oil-in-water emulsion solvent evaporation method. Briefly, 50 mg of PLGA was dissolved in 1 mL of DT-AuNP (4 mM– 50 mM) dispersed in ethyl acetate. This organic phase was emulsified with 2 mL of a 1 % (w/v) PVA aqueous solution by ultrasonication at 15 W for 1 min in an ice bath. The formed O/W emulsion was then poured into a 30 mL solution of 0.2 % (w/v) PVA and continuously stirred for at least 3 h at room temperature to allow solvent evaporation and NP formation. Particles were collected by centrifugation (24 000 g, 15 min) and washed three times with ultrapure water.



### 3.5 Synthesis of hybrid Au–PLGA NP by *in situ* reduction using a double-emulsion W/O/W

AuNP precursors were encapsulated into PLGA NP by the double emulsion solvent evaporation method. Once the emulsion was formed, the temperature was increased to activate the reduction of the Au precursor by sodium citrate. Briefly, 5 mg of Au (III) chloride hydrate and 25 mg of sodium citrate tribasic dihydrate were dissolved in 50  $\mu$ L of MilliQ water. This aqueous phase was emulsified with 1 mL of ethyl acetate containing 50 mg of PLGA by ultrasonication (Branson Sonifier 450, Branson Ultrasonics Corp., Danbury, CT, USA) at 30% amplitude for 15 seconds in an ice bath. The formed w/o emulsion was emulsified likewise with 2 ml of a 1% (w/v) surfactant aqueous solution (sodium cholate, taurocholate or Tween 80) to obtain a W/O/W emulsion that was added into a 10 ml of 0.3 % (w/v) surfactant solution. Then to promote the reduction of Au<sup>3+</sup> ions to Au<sup>0</sup> and consequently the formation of AuNP inside the PLGA NP, the temperature was increased to 45 °C for 20 minutes in a closed vessel to avoid solvent evaporation. Finally the vessel was opened and the formulation was stirred for at least 3h at RT to allow solvent evaporation. Particles were collected by centrifugation (20 000 g, 10 min) and washed three times with ultrapure water.

### 3.6 Characterization

The UV-Vis spectra of AuNP and Au–PLGA hybrid NP were measured using a Jasco V-670 spectrophotometer. The fluorescence spectra of the hybrid NP containing pyrene were measured using a fluorimeter (Perkin-Elmer LS55). Average particle size and size distributions were determined by DLS with a particle size analyzer (Zeta Plus, Brookhaven Instruments Corporation, NY) at a fixed angle of 90° at room temperature. The surface morphology of the nanocomposites was investigated by using a FE-SEM (Inspect F-50, FEI, Eindhoven) at an accelerating voltage of 10–15 kV. The NP were immobilized on a silicon chip, stained with phosphotungstic acid hydrate, dried and coated with a platinum layer. Preliminary transmission electron microscopy observations were carried out at the LMA-INA-Universidad Zaragoza facilities using a T20-FEI microscope with a LaB6 electron source fitted with a “SuperTwin®” objective lens allowing a point-to-point resolution of 2.4 Å. Aberration corrected scanning transmission electron microscopy (Cs-corrected STEM) images were acquired using a high angle annular dark field detector in a FEI XFEG Titan

electron microscope operating at 300 kV and equipped with a CETCOR Cs-probe corrector from the CEOS Company allowing the formation of an electron probe of 0.08 nm. Elemental analysis was carried out with an EDS (EDAX) detector which allows performing EDS experiments in the scanning mode. A 2.5  $\mu\text{L}$  suspension of stained hybrid Au-PLGA NP was pipetted onto a TEM copper grid with a holey carbon film. Samples were allowed to evaporate completely and then analyzed.

Irradiation experiments were performed with a collimated VIS light at 532 nm and a power density of  $4.2 \text{ W cm}^{-2}$ . Measurements were carried out in 24-cell culture insert plates made of polycarbonate and with a fixed volume of 1 ml of dispersion. The distance between the laser head and the sample was approximately 1 cm. In all the assays the sample concentration used was  $0.29 \text{ mg ml}^{-1}$  of Au and  $5 \text{ mg ml}^{-1}$  of PLGA.

#### **4. Conclusions**

Novel hybrid Au-PLGA NP under 180 nm in size have been synthesized by coupling the nanoemulsion and the *in situ* reduction techniques in a one-pot procedure. This protocol enables the complete encapsulation of AuNP inside PLGA NP, which is much more efficient than the direct encapsulation method that has usually been employed so far. In addition, the Au load distribution (as a single NP or multiple smaller NP) can be tailored by the appropriate choice of a surfactant. The electrostatic nature of the surfactants used and the presence of electron-rich nitrogen and sulfur in the STC structure are deemed to be responsible for the successful stabilization and consequent encapsulation. The presence of AuNP close to the surface but still inside the PLGA matrix was confirmed by electron microscopy observations (SEM, TEM, STEM), laser irradiation and pyrene fluorescence tracking. Also this protocol can potentially be extrapolated to other reduction reactions used for the synthesis of metal NP at low temperatures. Interestingly, the developed NP could be used in theranostic applications or as contrast agents in dark-field imaging and computed tomography.

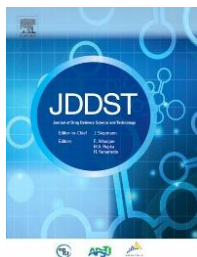
## 5. Notes and references

1. S. Y. Li and M. Wang, *Mater. Lett.*, 2013, 92, 350–353.
2. B. P. Timko, K. Whitehead, W. W. Gao, D. S. Kohane, O. Farokhzad, D. Anderson and R. Langer, *Annu. Rev. Mater. Res.*, 2011, 41, 1–20.
3. A. J. Mieszawska, A. Gianella, D. P. Cormode, Y. M. Zhao, A. Meijerink, R. Langer, O. C. Farokhzad, Z. A. Fayad and W. J. M. Mulder, *Chem. Commun.*, 2012, 48, 5835–5837.
4. H. Q. Li, J. V. John, S. J. Byeon, M. S. Heo, J. H. Sung, K. H. Kim and I. Kim, *Prog. Polym. Sci.*, 2014, 39, 1878–1907.
5. M. Zeltner, R. N. Grass, A. Schaetz, S. B. Bubenhofer, N. A. Luechinger and W. J. Stark, *J. Mater. Chem.*, 2012, 22, 12064–12071.
6. L. Quaroni and G. Chumanov, *J. Am. Chem. Soc.*, 1999, 121, 10642–10643.
7. G. Schneider, G. Decher, N. Nerambourg, R. Praho, M. H. V. Werts and M. Blanchard-Desce, *Nano Lett.*, 2006, 6, 530–536.
8. A. Topete, M. Alatorre-Meda, E. M. Villar-Alvarez, S. Carregal-Romero, S. Barbosa, W. J. Parak, P. Taboada and V. Mosquera, *Adv. Healthcare Mater.*, 2014, 3, 1309–1325.
9. J. L. Geng, K. Li, K. Y. Pu, D. Ding and B. Liu, *Small*, 2012, 8, 2421–2429.
10. M. Gajendiran, S. M. J. Yousuf, V. Elangovan and S. Balasubramanian, *J. Mater. Chem. B*, 2014, 2, 418–427.
11. E. R. Swy, A. S. Schwartz-Duval, D. D. Shuboni, M. T. Latourette, C. L. Mallet, M. Parys, D. P. Cormode and E. M. Shapiro, *Nanoscale*, 2014, 6, 13104–13112.
12. K. Kamata, Y. Lu and Y. N. Xia, *J. Am. Chem. Soc.*, 2003, 125, 2384–2385.
13. M. Kim, K. Sohn, H. Bin Na and T. Hyeon, *Nano Lett.*, 2002, 2, 1383–1387.
14. D. M. Cheng, X. D. Zhou, H. B. Xia and H. S. O. Chan, *Chem. Mater.*, 2005, 17, 3578–3581.
15. I. Andreu, E. Natividad, L. Solozabal and O. Roubeau, *ACS Nano*, 2015, 9, 1408–1419.
16. Y. Qiu, R. Palankar, M. Echeverria, N. Medvedev, S. E. Moya and M. Delcea, *Nanoscale*, 2013, 5, 12624–12632.
17. R. Campardelli, G. Della Porta, L. Gomez, S. Irusta, E. Reverchon and J. Santamaria, *J. Mater. Chem. B*, 2014, 2, 409–417.
18. H. Q. Li, C. S. Ha and I. Kim, *Macromol. Rapid Commun.*, 2009, 30, 188–193.
19. F. Wen, W. Zhang, G. Wei, Y. Wang, J. Zhang, M. Zhang and L. Shi, *Chem. Mater.*, 2008, 20, 2144–2150.

20. T. Tamai, M. Watanabe, Y. Hatanaka, H. Tsujiwaki, N. Nishioka and K. Matsukawa, *Langmuir*, 2008, 24, 14203–14208.
21. V. G. Pol, H. Grisar and A. Gedanken, *Langmuir*, 2005, 21, 3635–3640.
22. J. Q. Xi, X. D. Qian, K. H. Qian, W. Y. Zhang, W. He, Y. Chen, J. Han, Y. Z. Zhang, X. J. Yang and L. Fan, *J. Mater. Chem. B*, 2015, 3, 4213–4220.
23. F. Wen, W. Q. Zhang, G. W. Wei, Y. Wang, J. Z. Zhang, M. C. Zhang and L. Q. Shi, *Chem. Mater.*, 2008, 20, 2144–2150.
24. Q. Tian, C. N. Zhang, X. H. Wang, W. Wang, W. Huang, R. T. Cha, C. H. Wang, Z. Yuan, M. Liu, H. Y. Wan and H. Tang, *Biomaterials*, 2010, 31, 4748–4756.
25. K. Y. Win and S. S. Feng, *Biomaterials*, 2005, 26, 2713–2722.
26. V. Sebastian, M. Arruebo and J. Santamaria, *Small*, 2014, 10, 835–853.
27. Q. Zhang, C. Cobley, L. Au, M. McKiernan, A. Schwartz, L. P. Wen, J. Y. Chen and Y. N. Xia, *ACS Appl. Mater. Interfaces*, 2009, 1, 2044–2048.
28. K. Li, J. Pan, S. S. Feng, A. W. Wu, K. Y. Pu, Y. T. Liu and B. Liu, *Adv. Funct. Mater.*, 2009, 19, 3535–3542.
29. X. H. Huang, I. H. El-Sayed, W. Qian and M. A. El-Sayed, *J. Am. Chem. Soc.*, 2006, 128, 2115–2120.
30. A. G. Tkachenko, H. Xie, D. Coleman, W. Glomm, J. Ryan, M. F. Anderson, S. Franzen and D. L. Feldheim, *J. Am. Chem. Soc.*, 2003, 125, 4700–4701.
31. I. C. Sun, D. K. Eun, H. Koo, C. Y. Ko, H. S. Kim, D. K. Yi, K. Choi, I. C. Kwon, K. Kim and C. H. Ahn, *Angew. Chem., Int. Ed.*, 2011, 50, 9348–9351.
32. J. Turkevich, P. C. Stevenson and J. Hillier, *J. Phys. Chem.*, 1953, 57, 670–673.
33. A. Wijaya and K. Hamad-Schifferli, *Langmuir*, 2008, 24, 9966–9969.
34. K. S. Lee and M. A. El-Sayed, *J. Phys. Chem. B*, 2005, 109, 20331–20338.
35. S. Nath, S. Jana, M. Pradhan and T. Pal, *J. Colloid Interface Sci.*, 2010, 341, 333–352.
36. C. F. Li, D. X. Li, G. Q. Wan, J. Xu and W. G. Hou, *Nanoscale Res. Lett.*, 2011, 6.
37. H. Kranz, N. Ubrich, P. Maincent and R. Bodmeier, *J. Pharm. Sci.*, 2000, 89, 1558–1566.
38. C. Bouissou, J. J. Rouse, R. Price and C. F. van der Walle, *Pharm. Res.*, 2006, 23, 1295–1305.
39. L. Uson, V. Sebastian, A. Mayoral, J. L. Hueso, A. Eguizabal, M. Arruebo and J. Santamaria, *Nanoscale*, 2015, 7, 10152–10161.
40. A. H. Pakiari and Z. Jamshidi, *J. Phys. Chem. A*, 2007, 111, 4391–4396.

41. Y. Ding, Z. W. Jiang, K. Saha, C. S. Kim, S. T. Kim, R. F. Landis and V. M. Rotello, *Mol. Ther.*, 2014, 22, 1075– 1083.
42. Y. Qiao, H. F. Chen, Y. Y. Lin and J. B. Huang, *Langmuir*, 2011, 27, 11090–11097.
43. J. Kasthuri and N. Rajendiran, *Colloids Surf., B*, 2009, 73, 387–393.
44. L. P. Ruan, H. Y. Zhang, H. L. Luo, J. P. Liu, F. S. Tang, Y. K. Shi and X. J. Zhao, *Proc. Natl. Acad. Sci. U. S. A.*, 2009, 106, 5105–5110
45. A. N. Shipway, E. Katz and I. Willner, *ChemPhysChem*, 2000, 47 D. C. Dong and M. A. Winnik, *Can. J. Chem.*, 1984, 62, 1, 18–52. 2560–2565
46. K. G. Thomas and P. V. Kamat, *J. Am. Chem. Soc.*, 2000, 48 B. I. Ipe, K. G. Thomas, S. Barazzouk, S. Hotchandani and 122, 2655–2656. P. V. Kamat, *J. Phys. Chem. B*, 2002, 106, 18–21.
47. D. C. Dong and M. A. Winnik, *Can. J. Chem.*, 1984, 62, 2560–2565.
48. B. I. Ipe, K. G. Thomas, S. Barazzouk, S. Hotchandani and P. V. Kamat, *J. Phys. Chem. B*, 2002, 106, 18–21





## Visualization of hybrid gold-loaded polymeric nanoparticles in cells using scanning electron microscopy

Edurne Luque-Michel<sup>1</sup>, Víctor Sebastián<sup>2,3</sup>, Boguslaw Szczupak<sup>4,5</sup>, Edurne Imbuluzqueta<sup>1</sup>, Jordi Llop<sup>4</sup>, María J. Blanco Prieto<sup>1</sup>

<sup>1</sup> Department of Pharmacy and Pharmaceutical Technology, School of Pharmacy and Nutrition, University of Navarra, Pamplona, Spain

<sup>2</sup> IdiSNA, Fundación Instituto de Investigación Sanitaria de Navarra, Recinto del Complejo Hospitalario de Navarra, Pamplona, Spain

<sup>3</sup> CIBER de Bioingeniería, Biomateriales y Nanomedicina (CIBER-BBN), Centro de Investigación Biomédica en Red, Madrid, Spain

<sup>4</sup> Molecular Imaging Unit, CIC biomaGUNE, Paseo Miramón 182, 20009 San Sebastián, Guipúzcoa, Spain

<sup>5</sup> Present Address: Department of Telecommunications and Teleinformatics, Wrocław University of Science and Technology, Wybrzeże Wyspińskiego 27, 50-370 Wrocław, Poland

### ABSTRACT:

Nanotechnology is growing quickly, with great advances in the area of nanomedicine. Opening the door to personalized medicine, a considerable number of nanosystems have been synthesized for the diagnosis, treatment and monitoring of diseases. Specifically, gold nanoparticles (AuNP) have been shown to be good contrast agents. However, they have a limited surface area for the transport of active molecules. In this paper, polymeric nanoparticles encapsulating AuNP have been synthesized by the double emulsion method (W/O/W) and solvent evaporation technique. This approach opens up the possibility of encapsulating hydrophilic and/or lipophilic thermostable biomolecules. The nanoparticles could be monitored in macrophage cells by simple scanning electron microscopy (SEM). Nevertheless, a micro computed tomography (micro-CT) study revealed that they would not be detected in future *in vivo* studies. In short, this paper explains the difficulty of obtaining nanovehicles that are trackable from early investigation stages to their clinical use, and discusses the controversy surrounding the concentration of AuNP needed to obtain enough X-ray attenuation with safe doses.

## 1. Introduction

It is well known that nanotechnology has great potential in the area of biomedicine [1]. Specifically in cancer, nanotechnology promises to resolve the issues of low tumor accumulation and toxicity associated with traditional chemotherapy. In fact, the key advantage of nanobiotechnology is the accumulation of nanovehicles in the tumor mass where the drugs incorporated are released. The transport of active compounds could change not only their biodistribution but also their pharmacokinetic and toxicological characteristics. Nanomedicine thus introduces new neoplasm treatments with lower and more efficient doses, which also could overcome the problem of drug resistance. Additionally, the imaging capacity of nanobiotechnology in cancer diagnosis is also an important issue. Some inorganic nanosystems have shown unique chemical, physical and optical properties at the nanometer scale. These properties make them able to detect tumors at early stages, which is essential to have a good prognosis. At present, various types of nanosystems are being investigated to explore their potential in cancer diagnosis, including gold nanoparticles (AuNP), quantum dots or superparamagnetic iron oxide nanoparticles (SPION) [2]. The combination of nanosystems as drug delivery systems and, at the same time, as imaging agents to detect tumors, is known as theragnosis. This represents a great advance in the management of this heterogeneous disease because it permits individualized antineoplastic therapies with the possibility of localizing, typifying and monitoring the tumor in real-treatment time. It is also exciting to follow simultaneously the drug and its transporter to understand better how the nanosystems release the drug and are distributed throughout the body [3]. It is worth mentioning that one major problem in the interpretation of nanosystem behavior is that, normally, it may be possible to quantify the amount of drug that reaches each organ, but it is very difficult to know if the drug reaches them inside the nanoparticles (NP) or it was released from the NP before.

AuNP have become tools in cancer diagnosis and therapeutics owing to their surface chemistry, relatively low short-term toxicity, high atomic number and high X-ray absorption coefficient [4]. Moreover, these NP are simple to prepare and have easy surface functionalization [5]. Several imaging techniques can be used to detect them [6], for instance, with the use of AuNP the contrast between normal and cancerous tissue can be enhanced using X-ray based computed tomography (CT), one of the



leading radiology technologies applied in hospitals nowadays [7]. In fact, AuNP have revealed higher contrast and longer imaging times than the iodinated contrast agents used in clinical practice [2,7]. Apart from this, due to the high atomic number of Au, AuNP are also good contrast agents for use with the transmission electron microscope (TEM) [8] and scanning electron microscope (SEM) [9] which makes these nanosystems very interesting at early stages of research. These techniques can help us to understand the behavior of nanosystems in different situations, such as their internalization by cells, or the way they cross biological barriers.

Several methods have been developed for the synthesis of theragnostic NP. In general, the “one for all” approach, where metallic NP act as imaging contrast agent and drug transporter at the same time, has a limited drug loading capacity [2,10]. This is worsened by the fact that the surfaces of Au nanostructures are often covered with different materials [11]. In order to overcome this limitation, in this work the “all in one” approach was used. AuNP were internalized inside poly(lactic-co-glycolic acid) (PLGA) NP allowing the encapsulation of several types of thermostable biomolecules (hydrophilic or/and lipophilic) within this polymeric NP. In this work, AuNP were encapsulated into polymeric NP by the double emulsion method (W/O/W) and solvent evaporation technique[8]. Their internalization inside macrophages by SEM was investigated, and a proof of concept of their X-ray attenuation capacity by micro-CT was obtained.

## **2. Materials and Methods**

### **2.1 Materials**

For Au-PLGA NP synthesis, the polymer PLGA 50:50 (MW 38000–54000 Da, Resomer® RG 504) was purchased from Boehringer Ingelheim (Ingelheim, Germany). Sodium cholate, chloroauric acid ( $\text{HAuCl}_4 \cdot 3\text{H}_2\text{O}$ ), sodium citrate tribasic dehydrate  $\geq 99.0\%$  ( $\text{Na}_3\text{C}_6\text{H}_5\text{O}_7 \cdot 2\text{H}_2\text{O}$ ), taurocholic acid sodium salt hydrate  $\geq 95\%$  (TC), ethyl acetate ACS reagent and phosphotungstic acid hydrate, as a contrast agent for microscopy, were purchased from Sigma Aldrich (St Louis, MO, USA).

For cellular studies, RPMI Medium 1640 (1X), 0.25 % trypsin-EDTA (1X), penicillin-streptomycin (Pen Srep), fetal bovine serum (Heat Inactivated FBS) and Collagen I rat tail 3 mg/mL were purchased from Gibco (Invitrogen Inc. Carlsbad, EEUU). Dimethyl sulfoxide (DMSO) and 3-(4,5-dimethylthiazol-2-yl)-2,5-diphenyltetrazolium bromide (MTT) were purchased from Sigma-Aldrich (Barcelona, España). Finally, Dulbecco's Phosphate Buffered saline – 0.0095 M (PO<sub>4</sub>) without Ca and Mg (Biowhittaker DPBS) was purchased from Lonza (Veviers, Belgium).

## **2.2 Au-PLGA NP synthesis and characterization**

Au-PLGA NP were synthesized by an *in situ* reduction method using a double-emulsion W/O/W as described previously [8]. Briefly, AuNP precursors, Au (III) chloride hydrate and sodium citrate tribasic dehydrate, were encapsulated into PLGA NP by the double emulsion solvent evaporation method. Once the emulsion was formed, the temperature was increased to activate the reduction of the AuNP precursors by sodium citrate. After 3 h at room temperature to allow solvent evaporation, particles were collected by centrifugation and washed with ultrapure water. Blank NP were synthesized following the previous procedure but without adding the AuNP precursors. The formulations obtained were lyophilized using mannitol (25 %; w/w with respect PLGA) or glucose (12.5 %) as cryoprotectants.

Au-PLGA NP were characterized with respect to the size, surface charge, morphology and surface plasmon resonance (SPR). The average particle size and polydispersity index (PDI) were determined by dynamic light scattering (DLS) and the surface charge (zeta potential) by laser Doppler electrophoresis using a ZetaSizer Nano ZS analyzer system (Malvern Instruments, UK). The morphology was evaluated at the LMA-INA facilities by an environmental Scanning Electron Microscope Quanta™ FEG-250 (FEI, Hillsboro, Oregon, USA) with an accelerating voltage of 30 kV and by a TEM FEI™ Tecnai T20 at 200 kV. A 5 µL suspension of stained PLGA NP was pipetted onto a TEM copper grid having a continuous carbon film. Samples were let to evaporate completely and then analyzed. The typical SPR peak of AuNP was measured using a UV-visible Agilent 8453 spectrophotometer.

### 2.3 Cellular internalization assay of Au-PLGA NP

The J774 cell line (ATCC TIB-67) was maintained in RPMI 1640 medium supplemented with glutamax®, 10 % of heat-inactivated fetal bovine serum and 1 % of penicillin-streptomycin solution. Cells were cultured at 37 °C in a humidified 5 % CO<sub>2</sub> atmosphere and passaged twice a week at 80 % of confluence.

To visualize the internalization of the nanosystems, J774 cells were grown and treated with Au-PLGA NP on a metallic insert. This insert had an area of growth of 0.38 cm<sup>2</sup> which was collagened before seeding 10000 cells. After 12 hours, they were treated with 1 mg/mL of Au-PLGA NP (theoretically 0.27 mM of Au) or PLGA NP (blank NP). Cells were incubated with the treatments at 37 °C in a humidified 5 % CO<sub>2</sub> atmosphere for 24 hours. Afterwards, they were fixed with para-formaldehyde 4% (for 15 minutes at RT) and prepared to be analyzed by FEG SEM, using secondary and backscattered electrons. The presence of AuNP inside the macrophage cells was confirmed by an elemental analysis with the environmental FEG SEM which is equipped with an energy-dispersive X-ray spectrometer (EDX).

### 2.4 Viability assay

To test the toxicity of Au-PLGA NP, 10000 cells per well were seeded in a 96 well plate. The cytotoxic activity of 1 mg/mL of Au-PLGA NP was analyzed in triplicate with the cellular proliferation test MTT [12]. After 24 hours of treatment, the cells were washed three times with PBS and 100 µL of MTT reactant (0.5 mg/mL in culture medium) were added. After 2 hours of incubation at 37 °C in a humidified 5 % CO<sub>2</sub> atmosphere, all reactant was removed, 100 µL of DMSO were added to each well and the plate was read at  $\lambda = 540$  nm using an iEMS reader (Labsystems, Finland). This experiment was repeated three times on different days.

### 2.5 *In vivo* tracking test

With the aim of checking the capacity of the Au-PLGA NP to be monitored *in vivo* with a micro-CT (eXplore speCZT 120, GE, Healthcare, USA ), the Hounsfield Units (HU) of the NP were measured at 70 kV/32mA/16ms. For the experiment, the AuNP or Au-

PLGA NP were suspended in water at a concentration of 15 mg/mL (which theoretically corresponds to 2.95 mM of Au). These AuNP were synthesized as previously, according to the Turkevich method [8] and similarly to those formed inside the PLGA NP. This AuNP suspension had a theoretical concentration of gold of 50.8 mM.

### 3. Results and discussion

#### 3.1 Au-PLGA NP characterization

The nanosystems formed by the double-emulsion W/O/W with the *in situ* reduction approach showed similar sizes and surface charges independently of the presence of AuNP inside the PLGA NP (Figure 1 a). In the case of the PLGA NP loaded with AuNP, they showed a monodisperse size of 131.7 nm. This size is suitable for cancer therapy. Indeed, due to the enhanced permeability and retention (EPR) effect, the NP can be accumulated in the tumor and release the drug on site. The surface charge of these nanosystems was around -45 mV. Arvizo, R. *et al.* demonstrated that positively charged NP depolarize the membrane to a greater extent and have more uptake [13]; however, this causes a cytotoxic effect due to the presence of cationic surfactants [14]. Moreover, it is well known that all NP get masked by a protein layer when they are in the bloodstream, which has a strong correlation with an enhanced cellular uptake, mainly in the mononuclear phagocytic system. This occurs more in NP with positive charge [15]. Thus, negative NP are expected to have larger circulation times and thereby, greater accumulation at the action site.

SEM and TEM micrographs (Figure 1 b and c) showed a spherical morphology and smooth surface of the Au-PLGA NP. As we demonstrated previously [8], these nanosystems are characterized by the selective location of one AuNP inside each PLGA NP. These AuNP were selectively formed inside PLGA NP by the reduction of tetrachloroauric acid ( $\text{HAuCl}_4$ ) with trisodium citrate, the most common synthesis of colloidal gold in aqueous solution [16]. SEM is normally used to see surface reliefs; however, AuNP had enough contrast to be detected from the interior of the PLGA NP with backscattered electron images (Figure 1 b2). On the other hand, based on

several TEM images (Figure 1 c2), the AuNP formed inside PLGA NP had a relatively large size of  $12.5 \pm 1.3$  nm. In addition, microscopy characterization confirmed that no AuNP were segregated from the PLGA NP. In Figure 1 d the UV-spectra of Au-PLGA NP showed a SPR peak which also confirmed the presence of AuNP inside the PLGA NP. The SPR peak shifts to a longer wavelength when the AuNP size increases and it was slightly above the common 520 nm. Furthermore, the blue-purple color of the formulation formed is characteristic of this size of AuNP [17].

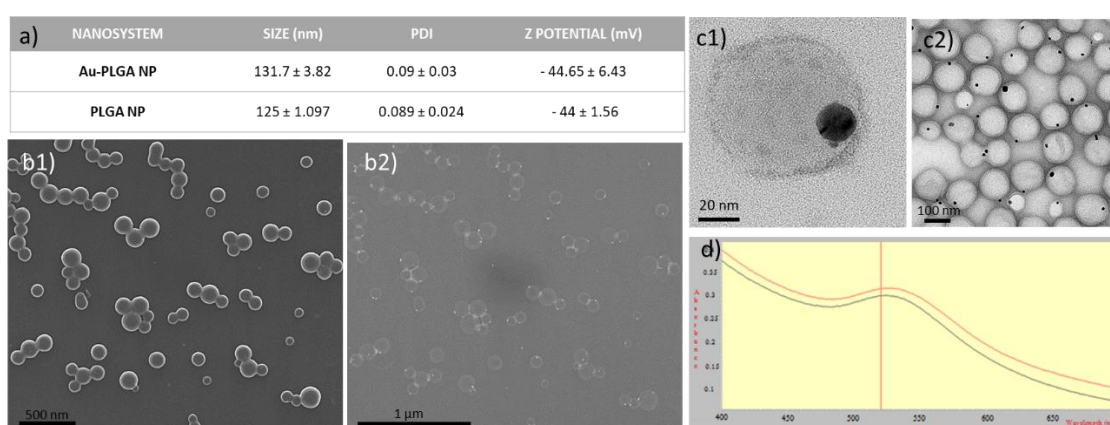


**Figure 1:** Characterization of Au-PLGA NPs: (a) Size, polydispersion and superficial charge (b) SEM micrographs: (b1) secondary electron image (b2) backscattered electron image (c1; c2) TEM micrographs (d) SPR peak of two Au-PLGA NPs batches.

### 3.2 Cellular internalization of Au-PLGA NP

Various techniques can be used to follow nanosystems into cells or living beings [18]. The use of biocompatible metallic NP allows their monitoring by imaging techniques at all stages of the investigation without additional markers and, more importantly, in real-treatment situations. TEM could be used to follow metallic NP in *in vitro* studies. It is worth noting that it is complicated to prepare and cutting thin layers of cells by ultramicrotome [19]. Furthermore, considering the dimensions of cells, few micrometers, the analysis of few-nanometer slices to localize AuNP of  $12.5 \pm 1.3$  nm is challenging and time consuming analysis. The main problem of this procedure is that although several NP would be internalized, each one would be on a different level and

it would be difficult to find a representative image to support the internalization process. On the other hand, as we can see in Figure 1 b2, heavy atoms with a high atomic number are stronger scatterers than light ones. Then, AuNP, with a high atomic number, had enough brightness in backscattered electron images to be differentiated from the other Au-PLGA NP components. Consequently, it would be expected that Au-PLGA NP could be also identified once they were internalized in cells.

The internalization of Au-PLGA NP was studied by secondary and backscattered SEM imaging. As can be seen in Figure 2, the upper row corresponds to secondary electron images while the lower row corresponds to backscattered electron images. Figure 2 a1 shows a control cell which was not treated with NP. This cell is a non-activated macrophage with a smooth-rounded surface in contrast to the rough surface of the cells activated by the treatments with PLGA NP (Figure 2 b1) or Au-PLGA NP (Figure 2 c1). With respect to the backscattered electron images, no different contrast is observed in the control (Figure 2 a2) or the PLGA NP treatment (Figure 2 b2), but dots with high contrast are observed in cells treated with Au-PLGA NP (Figure 2 c2). It is important to note that before the cells were fixed, they were washed three times with PBS in order to eliminate those NP that had not been internalized. Therefore, all white-brilliant contrast in the image corresponds to Au-PLGA NP inside the cell. In the same way, Plascencia-Billa *et al.* studied the internalization of star-shaped AuNP coated with HEPES (2-[4-(2-hydroxyethyl)-1-piperazinyl] ethanesulfonic acid) buffer by macrophages [14]. Although in their study the dose was much lower, they also appreciated membrane projections deployment and granularity, as well as a precise location of each single metallic NP.

With the aim of determining the composition of the elements present in the sample, an EDX analysis was done to the brightest points of the images (data not shown) confirming that they correspond to Au. This confirmed that there were AuNP internalized inside the J744 cells. Therefore, this technique allowed us to confirm that Au-PLGA NP could be tracked in cells by an imaging technique.

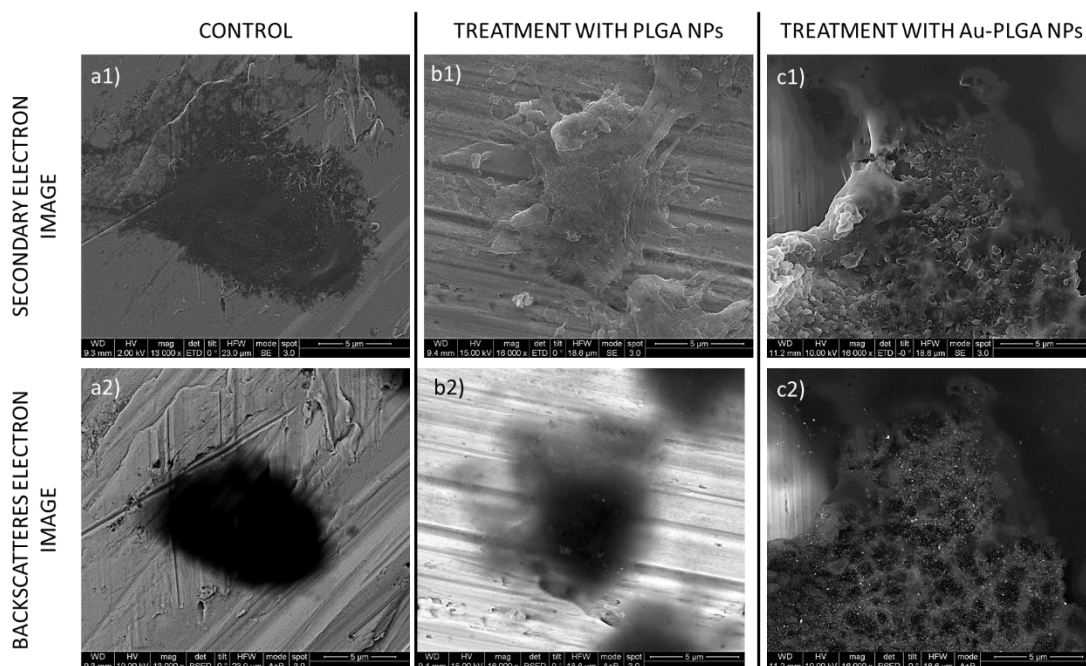


**Figure 2:** SEM micrographs of J774 cells. Upper row corresponds to secondary electron images and lower row corresponds to backscattered electron images. (a1; a2) control cell without treatment; (b1; b2) cell treated with PLGA NP; (c1; c2) cell treated with Au-PLGA NP.

### 3.3 Viability assay

The toxicity of Au-PLGA NP was tested in a macrophage cell line. The polymer used, PLGA, has regulatory acceptance due to its biocompatibility and biodegradability [20]. But, although AuNP are generally thought not to be toxic, a feature which accounts for its long history of use in medicine [7], the studies of toxicity in the literature do not show clear results [21]. For this study, J774 cells were seeded in a 96-well plate and treated with 1 mg/mL of Au-PLGA NP (around 0.27 mM of Au) in the same way as the previous experiment. This assay was done in triplicate and showed good viability of  $70.63 \pm 7.89$  %. Some types of AuNP have shown toxicity, but this largely depends on the size and coating of the surface [14]. In our case, the cellular interaction occurs with a polymeric NP and not with an inorganic NP. Nevertheless, the important question is whether AuNP are toxic at the concentration at which they will be used. According to Boisselier, E. and Astruc D., the safe dose is in the range of 1 and 100 AuNP per cell [6]. These doses are far from the dose used in our experiment, since in **Figure 2 c2** it can be observed that there are many more

AuNP inside the cell. This suggests that the dose should be adjusted to a real situation in future experiments, and also, that these Au-PLGA NP will be safe nanovehicles for their use in theragnostics. Soto, C. *et al.* observed no mortality or sign of toxicity when they studied the bioaccumulation and toxicity of AuNP with a similar size and synthesis method (12.5 nm and citrate reduction of  $\text{HAuCl}_4$ , respectively) in mice [22].

### 3.4 *In vivo* tracking

In contrast to AuNP cytotoxicity studies, X-ray enhancement is less dependent on the size and shape of AuNP [7]. Prior to the *in vivo* assay, the nanovehicles were examined to confirm their capacity as contrast agents by micro-CT. As a reference, soft tissues have typical attenuation values in the range of 0-50 HU [23], although values of 65 and 1000 can be reached in the liver and bones, respectively [24]. An enhancement of 30 HU has been proposed as the lower limit to perceive attenuation [24]; therefore, the X-ray attenuation required for *in vivo* cancer imaging will depend on the signal of the tumor mass. The Au-PLGA NP had a value of 37 HU, which is very similar to that obtained for water (25 HU, used as the control). Because the X-ray attenuation coefficient is determined by the atomic number and electron density (79 and 19.32 g/cm<sup>3</sup> in Au), the only parameter tunable to increase the HU was the total amount of gold per unit volume [23]. The sample had a theoretical Au concentration of 2.95 mM, but in contrast with the above *in vitro* results, this indicated that 10 times higher concentrations of AuNP were still required inside PLGA NP. Galper *et al.* considered that a minimum of 5.8 mM of gold accumulation in the tissue of interest is needed to appreciate contrast [25], a very different conclusion compared to previous studies that had indicated that good contrast images can be obtained at an Au concentration of 100  $\mu\text{g/mL}$  (0.51 mM) [7]. Conversely, Hainfeld *et al.* used successfully small AuNP (1.9 nm) as an X-ray CT contrast agent to detect tumors in mice, but injecting 0.01 mL/g of a high concentrated (1.37 M) solution of AuNP [26]. In our case, a more concentrated AuNP suspension (50.8 mM), which was not encapsulated inside the PLGA NP, was also measured by micro-CT; however, an



attenuation value of 86.0 HU was obtained (with respect to 26.7 HU for water) indicating that these AuNP are not suitable as CT contrast agents.

The most important limitation regarding CT is the relatively high mass concentration of contrast agents necessary at the site of interest, typically a millimolar concentration, in comparison with micromolar concentrations required, for example, with MRI contrast agents [27]. Moreover, *in vivo* cytotoxicity has not been studied rigorously and, generally, it has been investigated at doses below the range utilized in the studies that investigate AuNP as X-ray contrast agents [27]. Hence, due to the AuNP concentration-dependence of both X-ray attenuation and toxicity, it is absolutely necessary to determine the minimum effective and safe dose of AuNP for X-ray imaging. Summing up, these Au-PLGA NP seem to be non-toxic and good contrast agents in *in vitro* techniques; however, they did not have sufficient X-ray attenuation under micro-CT to be used *in vivo*.

#### **4. Conclusions**

From the therapeutic point of view, it cannot be disputed that theragnosis offers the possibility of improving cancer prognosis since it allows early-stage detection and tumor monitoring, and enables specialists to identify the effective drugs to optimize the treatment of each individual patient. Bearing this in mind, in this study we present an investigation of Au-PLGA NP as a theragnostic nanovehicle. These nanosystems have proved to be safe and biocompatible in cells. Au-PLGA NP were efficiently internalized by macrophages, which showed a clear membrane activation. In addition, they were followed inside cells by a simple SEM, suggesting that this nanovehicle might be monitored by imaging techniques. Finally, a micro-CT study revealed that these Au-PLGA NP did not reach enough Au-electron density to be used as *in vivo* diagnostic agents.

## 5. References

1. M. Spivak, R. V Bubnov, I.M. Yemets, L.M. Lazarenko, N.O. Tymoshok, Z.R. Ulberg, Development and testing of gold nanoparticles for drug delivery and treatment of heart failure: a theranostic potential for PPP cardiology, *EPMA J.* 4 (2013) 20. doi:10.1186/1878-5085-4-20.
2. E. Luque-Michel, E. Imbuluzqueta, V. Sebastián, M.J. Blanco-Prieto, Clinical advances of nanocarrier-based cancer therapy and diagnostics, [Http://Dx.Doi.Org/10.1080/17425247.2016.1205585](http://Dx.Doi.Org/10.1080/17425247.2016.1205585). 5247 (2016). doi:10.1080/17425247.2016.1205585.
3. S.D. Jo, S.H. Ku, Y.-Y. Won, S.H. Kim, I.C. Kwon, Targeted Nanotheranostics for Future Personalized Medicine: Recent Progress in Cancer Therapy., *Theranostics.* 6 (2016) 1362–77. doi:10.7150/thno.15335.
4. S.K. Nune, P. Gunda, P.K. Thallapally, Y.-Y. Lin, M. Laird Forrest, C.J. Berkland, Nanoparticles for biomedical imaging, *Expert Opin. Drug Deliv.* 6 (2009) 1175–1194. doi:10.1517/17425240903229031.
5. M. Kodiha, Y.M. Wang, E. Hutter, D. Maysinger, U. Stochaj, Off to the organelles - killing cancer cells with targeted gold nanoparticles., *Theranostics.* 5 (2015) 357–70. doi:10.7150/thno.10657.
6. E. Boisselier, D. Astruc, Gold nanoparticles in nanomedicine: preparations, imaging, diagnostics, therapies and toxicity, *Chem. Soc. Rev.* 38 (2009) 1759. doi:10.1039/b806051g.
7. S. Ahn, S. Jung, S. Lee, Gold Nanoparticle Contrast Agents in Advanced X-ray Imaging Technologies, *Molecules.* 18 (2013) 5858–5890. doi:10.3390/molecules18055858.
8. E. Luque-Michel, A. Larrea, C. Lahuerta, V. Sebastian, E. Imbuluzqueta, M. Arruebo, M.J. Blanco-Prieto, J. Santamaria, A simple approach to obtain hybrid Au-loaded polymeric nanoparticles with a tunable metal load, *Nanoscale.* 8 (2016) 6495–6506. doi:10.1039/c5nr06850a [doi].
9. Z. Fan, D. Senapati, A.K. Singh, P.C. Ray, Theranostic magnetic core-plasmonic shell star shape nanoparticle for the isolation of targeted rare tumor cells from whole blood, fluorescence imaging, and photothermal destruction of cancer., *Mol. Pharm.* 10 (2013) 857–66. doi:10.1021/mp300468q.
10. J. Spadavecchia, D. Movia, C. Moore, C.M. Maguire, H. Moustou, S. Casale, Y. Volkov, A. Prina-Mello, Targeted polyethylene glycol gold nanoparticles for the treatment of pancreatic cancer: from synthesis to proof-of-concept in vitro

- studies., *Int. J. Nanomedicine*. 11 (2016) 791–822. doi:10.2147/IJN.S97476.
11. X. Yang, M. Yang, B. Pang, M. Vara, Y. Xia, Gold Nanomaterials at Work in Biomedicine, *Chem. Rev.* 115 (2015) 10410–10488. doi:10.1021/acs.chemrev.5b00193.
  12. D.M. Morgan, Tetrazolium (MTT) assay for cellular viability and activity., *Methods Mol. Biol.* 79 (1998) 179–83. <http://www.ncbi.nlm.nih.gov/pubmed/9463833> (accessed November 23, 2016).
  13. R.R. Arvizo, O.R. Miranda, M.A. Thompson, C.M. Pabelick, R. Bhattacharya, J.D. Robertson, V.M. Rotello, Y.S. Prakash, P. Mukherjee, Effect of Nanoparticle Surface Charge at the Plasma Membrane and Beyond, *Nano Lett.* 10 (2010) 2543–2548. doi:10.1021/nl101140t.
  14. G. Plascencia-Villa, D. Bahena, A.R. Rodríguez, A. Ponce, M. José-Yacamán, Advanced microscopy of star-shaped gold nanoparticles and their adsorption-uptake by macrophages., *Metallomics*. 5 (2013) 242–50. doi:10.1039/c3mt20202j.
  15. A. Petrizzo, C. Conte, M. Tagliamonte, M. Napolitano, K. Bifulco, V. Carriero, A. De Stradis, M.L. Tornesello, F.M. Buonaguro, F. Quaglia, L. Buonaguro, Functional characterization of biodegradable nanoparticles as antigen delivery system., *J. Exp. Clin. Cancer Res.* 34 (2015) 114. doi:10.1186/s13046-015-0231-9.
  16. M. Wuthschick, A. Birnbaum, S. Witte, M. Sztucki, U. Vainio, N. Pinna, K. Rademann, F. Emmerling, R. Kraehnert, J. Polte, Turkevich in *New Robes: Key Questions Answered for the Most Common Gold Nanoparticle Synthesis.*, *ACS Nano*. 9 (2015) 7052–71. doi:10.1021/acsnano.5b01579.
  17. A. Llevot, D. Astruc, Applications of vectorized gold nanoparticles to the diagnosis and therapy of cancer., *Chem. Soc. Rev.* 41 (2012) 242–57. doi:10.1039/c1cs15080d.
  18. S.S. Kelkar, T.M. Reineke, Theranostics: Combining Imaging and Therapy, *Bioconjug. Chem.* 22 (2011) 1879–1903. doi:10.1021/bc200151q.
  19. C. Tomuleasa, O. Soritau, A. Orza, M. Dudea, B. Petrushev, O. Mosteanu, S. Susman, A. Florea, E. Pall, M. Aldea, G. Kacso, V. Cristea, I. Berindan-Neagoe, A. Irimie, Gold nanoparticles conjugated with cisplatin/doxorubicin/capecitabine lower the chemoresistance of hepatocellular carcinoma-derived cancer cells., *J. Gastrointest. Liver Dis.* 21 (2012) 187–96. <http://www.ncbi.nlm.nih.gov/pubmed/22720309> (accessed December 1, 2016).
  20. R. Jain, N.H. Shah, A.W. Malick, C.T. Rhodes, Controlled drug delivery by biodegradable poly(ester) devices: different preparative approaches., *Drug Dev.*

- Ind. Pharm. 24 (1998) 703–27. doi:10.3109/03639049809082719.
21. N. Khlebtsov, L. Dykman, Biodistribution and toxicity of engineered gold nanoparticles: a review of in vitro and in vivo studies, *Chem. Soc. Rev.* 40 (2011) 1647–1671. doi:10.1039/C0CS00018C.
22. C. Lasagna-Reeves, D. Gonzalez-Romero, M.A. Barria, I. Olmedo, A. Clos, V.M. Sadagopa Ramanujam, A. Urayama, L. Vergara, M.J. Kogan, C. Soto, Bioaccumulation and toxicity of gold nanoparticles after repeated administration in mice., *Biochem. Biophys. Res. Commun.* 393 (2010) 649–55. doi:10.1016/j.bbrc.2010.02.046.
23. R. Popovtzer, A. Agrawal, N.A. Kotov, A. Popovtzer, J. Balter, T.E. Carey, R. Kopelman, Targeted gold nanoparticles enable molecular CT imaging of cancer., *Nano Lett.* 8 (2008) 4593–6. <http://www.ncbi.nlm.nih.gov/pubmed/19367807> (accessed December 21, 2016).
24. Krause, Delivery of diagnostic agents in computed tomography., *Adv. Drug Deliv. Rev.* 37 (1999) 159–173. <http://www.ncbi.nlm.nih.gov/pubmed/10837733> (accessed December 21, 2016).
25. M.W. Galper, M.T. Saung, V. Fuster, E. Roessler, A. Thran, R. Proksa, Z.A. Fayad, D.P. Cormode, Effect of computed tomography scanning parameters on gold nanoparticle and iodine contrast., *Invest. Radiol.* 47 (2012) 475–81. doi:10.1097/RLI.0b013e3182562ab9.
26. J.F. Hainfeld, D.N. Slatkin, T.M. Focella, H.M. Smilowitz, Gold nanoparticles: a new X-ray contrast agent, *Br. J. Radiol.* 79 (2006) 248–253. doi:79/939/248 [pii].
27. L.E. Cole, R.D. Ross, J.M. Tilley, T. Vargo-Gogola, R.K. Roeder, Gold nanoparticles as contrast agents in x-ray imaging and computed tomography, *Nanomedicine.* 10 (2015) 321–341. doi:10.2217/nnm.14.171.





# CHAPTER 2

---

**Co-encapsulation of superparamagnetic nanoparticles  
and doxorubicin in PLGA nanocarriers coated with  
surfactants for glioma theragnosis**





## Co-encapsulation of superparamagnetic nanoparticles and doxorubicin in PLGA nanocarriers coated with surfactants for glioma theragnosis

Eduarne Luque-Michel<sup>1,2</sup>, Víctor Sebastian<sup>4,5</sup>, Ane Larrea<sup>4</sup>, Clara Marquina<sup>4</sup> and María J. Blanco-Prieto<sup>1,2</sup>

<sup>1</sup> Department of Pharmacy and Pharmaceutical Technology, School of Pharmacy, University of Navarra, C/Irunlarrea 1, E-31008 Pamplona, Spain

<sup>2</sup> Instituto de Investigación Sanitaria de Navarra (IdiSNA), Pamplona, Spain

<sup>4</sup> Institute of Nanoscience of Aragon (INA) and Department of Chemical, Engineering and Environmental Technology, University of Zaragoza, C/Mariano Esquillor, s/n, I+D+I Building, 50018 Zaragoza, Spain

<sup>5</sup> CIBER de Bioingeniería, Biomateriales y Nanomedicina (CIBER-BBN), Centro de Investigación Biomédica en Red, C/ Monforte de Lemos 3-5, Pabellón 11, 28029 Madrid, Spain

### Abstract

With a very poor prognosis and no clear etiology, glioma is the most aggressive cancer in the brain. Nanomedicine is an alternative widely studied to solve the limitations of chemotherapy imposed by the blood brain barrier (BBB), mainly thanks to the high versatility it offers. The objective of this chapter was to attain monitored tumor-targeted therapeutic nanoparticles (NP). To that end, theranostic surfactant-coated NP encapsulating doxorubicin hydrochloride (DOX) and superparamagnetic iron oxide nanoparticles (SPION) were developed using poly lactic-co-glycolic acid (PLGA) as polymer. Different non-ionic surfactants (Tween 80, Brij-35, Pluronic F68 or Vitamin E-TPGS) were used to develop 4 types of NP, which were characterized in terms of size and morphology by DLS and TEM. These NP were stable for at least 3 months at 4 °C after their lyophilisation and showed a pH-dependent *in vitro* DOX-release. Importantly, the NP developed showed therapeutic efficacy against different glioma cell lines (U87-MG, 9L/LacZ and patient derived-neuronal stem cells) and could be used as contrast agents in magnetic resonance imaging (MRI), as a relaxivity study revealed.

**Keywords:** SPION, simple and multiple emulsion, TEM, Tween 80, Pluronic F68, Brij-35, Vitamin E-TPGS, PVA, neurospheres, U87-MG, 9L/LacZ

## INDEX

<b>1. Introduction</b> .....	96
<b>2. Material and methods</b> .....	98
2.1 SPION-DOX PNP synthesis .....	98
2.2 SPION-DOX PNP characterization .....	99
2.3 Lyophilization optimization .....	100
2.4 Relaxivity study .....	101
2.5 Stability study .....	101
2.6 <i>In vitro</i> DOX release .....	101
2.7 Cellular studies .....	102
2.7.1 Cell cultures .....	102
2.7.2 Cells internalization .....	102
2.7.3 <i>In vitro</i> efficacy .....	102
<b>3. Results and discussion</b> .....	103
3.1 SPION characterization .....	103
3.2 SPION-DOX PNP optimization .....	104
3.3 SPION-DOX PNP characterization .....	106
3.4 Lyophilization optimization .....	107
3.5 Stability study .....	109
3.6 Relaxivity study .....	111
3.7 <i>In vitro</i> drug release and cellular internalization .....	112
3.8 <i>In vitro</i> efficacy .....	114
<b>4. Conclusions</b> .....	115
<b>5. References</b> .....	115

**Introduction**

Among the several types of cancer that can be developed in the CNS, the glioblastoma (GBM) is considered the most lethal in children and adults even with treatment [1, 2]. Many diagnostic and therapeutic strategies, such as the use of immunotherapy, new drugs or predictive factors of the disease, are being studied in clinical trials [3]. However, until now there has been no real improvement and the glioma treatment protocol has not changed since 2005 [4]. This year a significant benefit survival improvement was demonstrated when initial surgery to remove as much malignant mass as possible was followed by simultaneous radio- and chemotherapy with the alkylating agent prodrug temozolomide (Temodal®) [4]; the antiangiogenic drug

bevacizumab (Avastin®) alone is nowadays used in recurrent GBM [5]. Nevertheless, the improvement was still poor, with a survival increase from 12.2 to 14.6 months [4]. Different difficulties are associated with treatment failure; beginning with the diffuse infiltration of these tumors that complicates their complete removal during surgery, and followed by the existence of cells with stem cell-like properties. These cancer stem cells (CSCs) initiate and foster the tumor by means of the generation of an aberrant GBM cell population and they are resistant to the therapy used after surgery. Consequently, all of this triggers inevitable recurrence of the tumor [5]. On the other hand, it cannot be forgotten that the chemotherapy options are gravely limited by the blood brain barrier (BBB) that protects the brain from foreign toxins. Certainly, at primary tumor sites the rapid expansion of the malignant mass can generate a rapid neoangiogenesis, losing tight junction and disrupting the blood brain tumor barrier (BBTB) [5]. However, drug access is still limited since the brain microenvironment continues to compromise these fenestrations and, additionally, in some cases such as in the diffuse intrinsic pontine glioma (DIPG), which is the most common brainstem tumor of childhood, the tumor conserves an intact BBB [6]. In fact, intact regions can be maintained and the porous areas formed are heterogeneous and smaller than those detected in tumors located in other organs [7, 8]. At this point, nanomedicine is an alternative widely investigated in the treatment of cancer. It works by synthesizing drug nanocarriers targeted to the BBB/BBTB. Interestingly, the composition and the surface properties of these carriers influence the diffusion through the brain and even overcome the size hurdle [9]. In this way a controlled, continued release of the drug in the tumor area could increase the tumor drug concentration and avoid the usual side effects. For instance, it has been widely demonstrated that nanosystems formed with the surfactant Tween 80 (T80) increase the amount of drug that reaches the brain [10–12]. In the bloodstream the T80-nanosystems are covered with apolipoproteins and then endocytosed by the low-density lipoprotein (LDL) receptors, highly expressed in the BBB/BBTB cells [13]. Besides, once inside the cell, the glycoprotein P responsible for returning foreign compounds to the blood is inhibited by this surfactant [14]. Similarly, other surfactants have been demonstrated to increase the BBB passage by inhibiting the action of the glycoprotein P such as poloxomers (Pluronic)[15, 16], Vitamin E-TPGS (Tocopheryl polyethylene glycol 1000 succinate) [17–19] or Brij [14, 20]. Apart from

that, due to the interindividual heterogeneity of the disease, the investigation of its individualized management is nowadays taking on a prominent position. In this area, nanotechnology is also playing a really interesting role. The use of nanosystems capable of being followed by imaging techniques at the same time that they treat the tumour could push medicine forward to reach the desired personalized therapy. Because of that, much of the current research is focused on the combination of therapeutic and diagnostic agents in the same nanosystem, so-named nanotheragnosis [9]. Superparamagnetic iron oxide nanoparticles (SPION) are capable of being followed by magnetic resonance imaging (MRI), as in the clinical trial of the MRI contrast imaging agent Ferumoxytol, which was designed to improve the observation of tumors in patients with high-grade brain tumors or cancers that had spread to the brain [21]. These metallic nanoparticles (NP) modify the signal of the surrounding tissues, increasing the sensitivity of the technique, making their monitoring possible, and therefore facilitating GBM therapy tracking. Moreover, due to the different properties of these magnetic NP they could also be used as hyperthermia or magnetic-targeting agents [22, 23].

In this chapter, we describe the design, development and characterization of theranostic NP formulated with the use of polymers by the simple emulsion and solvent evaporation method. The hypothesis of this paper is that the encapsulation of SPION and the cytostatic drug doxorubicin hydrochloride (DOX) in the same NP should permit fine-tuning of the GBM treatment, according to the patient response. We show the optimizations of the synthesis and lyophilization processes as well as a 3-month stability study of 4 types of polymeric NP (PNP) synthesized with the different surfactants: T80, Pluronic F68, Vitamin E-TPGS and Brij-35.

## **Material and methods**

### **1. SPION-DOX PNP synthesis**

The SPION, synthesized by the thermal decomposition of polyols at high temperature, were supplied by the Institute of Nanoscience of Aragon (INA) [24]; and DOX was purchased from Sigma. Both SPION and DOX were encapsulated in polymeric NP (PNP) using the polymer poly lactic-co-glycolic acid (PLGA) 503H (Resomer® RG

503H, PLGA 50:50). The SPION-DOX PNP were synthesized by two methods: the multiple or the simple emulsion and solvent evaporation methods. The NP developed were synthesized with 4 different surfactants: T80, Brij-35, Pluronic F68 and Vitamin E-TPGS; and the NP formulated without DOX or SPION were synthesized in the same way but without their addition.

To synthesize SPION-DOX PNP by the multiple W/O/W emulsification method, 1 mg of DOX was dissolved in 1 mL of triethyl amine: ethyl acetate (EA: TEA) in the proportion 1: 1000, overnight and in continuous agitation. The following day, 50 mg of polymer PLGA and 50  $\mu$ L of an aqueous suspension of SPION (7445 ppm of Fe) were added to the same solution. The mixture was sonicated for 20 seconds at 20 Watts in an ice bath using a Microson Ultrasonic Cell Disruptor XL (Branson sonifier 450, Branson Ultrasonics corp., EEUU) and then poured into 2 mL of water with 1 % (w/w) surfactant. Quickly, the new mixture was sonicated again under the same conditions and added to 10 mL of an aqueous solution containing 0.3 % (w/w) surfactant. After 1.5 hours under magnetic agitation, the ethyl acetate was evaporated and the NP were purified and collected by three centrifugations at 17000 g for 10 min at 4<sup>o</sup> C.

To synthesize SPION-DOX PNP by the simple O/W emulsification method, the SPION were covered with oleic acid and included in the organic phase. To do this, the SPION were incubated with oleic acid (10 mg of iron/mL of oleic acid) for 24 hours in continuous orbital agitation at room temperature (RT). The following day, they were centrifuged twice at 17000 g for 5 min at 4<sup>o</sup> C and suspended first in the same volume of absolute ethanol and secondly in the same volume of dichloromethane. After that, 0.2 mL of these SPION (7445 ppm) were added to 0.8 mL of EA: TEA (1:1000) containing 1 mg of DOX and 50 mg of PLGA. All of these were added to 2 mL of an aqueous solution containing 1 % (w/w) surfactant; and, as in the previous method, the mixture was sonicated for 20 seconds at 20 Watts in an ice bath before being added to 10 mL of an aqueous 0.3 % (w/w) surfactant solution. Once the ethyl acetate had evaporated after 1.5 hours, the NP were purified and collected by three centrifugations at 17000 g for 10 min at 4<sup>o</sup> C.

## 2. SPION-DOX PNP characterization

The size and surface charge of the PNP developed were characterized using a Zetasizer Nano ZS (Malvern Instruments, UK). Moreover, transmission electronic microscopy (TEM) images were used to confirm the size and study the morphology and the SPION distribution inside the PNP. The DOX loading efficiency was determined by fluorimetry and UV/vis spectrophotometry. DOX fluorescence was measured in a Tecan GENios microplate reader (Tecan Group Ltd, Maennedorf, Switzerland) at an excitation and emission wavelength of 485 and 580 nm; while DOX absorbance was measured at 485 nm in a microplate PowerWave XS Microplate Spectrophotometer (BioTek). The calibration curves consisted in serial dilutions of DOX in DMSO with a matrix of NP synthesized without the drug. As well, the approximate encapsulation of iron was analyzed spectrophotometrically ( $\lambda = 300$  nm). To do this, SPION with a known iron concentration measured by an Agilent 4100 MP-AES (Microwave Plasma - Atomic Emission Spectrometry) system were used to form a calibration curve with a matrix in DMSO containing NP without SPION [25]. Additionally, the SPION's oleic acid cover slip was confirmed with a Fourier-Transform Infrared Spectroscopy (FTIR) analysis.

## 3. Lyophilization optimization

All NP were lyophilized for 2 days in a LyoAlfa 6 -50 laboratory freeze dryer (230 V, 50Hz; Telstar). For that, the composition of the NP was optimized in order to obtain good reconstitution after the lyophilization process. Accordingly, it was studied the influence of adding different amounts of three cryoprotectants (trehalose, glucose and mannitol), the amount of surfactants in the external phase of the emulsion (1 or 2 %) and an extra addition of polyvinyl alcohol (PVA) in the last solvent evaporation step were studied. In all cases, the influence on the size, the superficial charge and the morphology after the reconstitution of the NP was characterized. Moreover, the residual PVA in the formulations was measured following the protocol devised by Sanjeeb K. Sahoo *et al.* who used a colorimetric method based on the formation of a colored complex between two adjacent hydroxyl groups of PVA and an iodine molecule [26]. Briefly, lyophilized NP (2mg) was treated with NaOH (0.5 M, 2 ml) for

15 min at 60 °C. After incubation, they were neutralized with HCl (1N, 0.9 ml) and the volume was adjusted to 5 ml with distilled water. Later, boric acid (0.65 M, 3 ml), and a solution of I<sub>2</sub>/KI (0.05 M/0.15 M, 0.5 ml) and distillate water (1.5 ml) were added to each sample; and after 15 min of incubation the absorbance was measured at 690 nm (Agilent 8453 UV-Vis Spectroscopy System, Agilent Technologies, Waldbronn Germany). The calibration curve of PVA was prepared under identical conditions.

#### **4. Relaxivity study**

The relaxivity for the SPION-DOX PNP was measured by Time Domain Nuclear Magnetic Resonance (TD-NMR) (<sup>1</sup>H-NMR Bruker Minispec Mq60) applying a magnetic field of 1.5 Tesla at 37 °C. Both the longitudinal (T1) and transversal (T2) relaxation time were measured to obtain the longitudinal (r1) and transversal (r2) relaxivity. For the measurement of T1 and T2 the sequences Inversion Recovery (IR) and Carr-Purcell-Meiboom-Gill were used respectively. To check the reproducibility of the results, several measurements were made using each concentration on different days.

#### **5. Stability study**

The physical and chemical stability of lyophilized NPs were studied over 3 months. The same batch of NP was lyophilized and divided for storage under 3 different conditions: RT, 4 °C and 40 °C. The NPs were characterized after being lyophilized and 1, 3, 4, 8 and 12 weeks after lyophilization by the measurement of the size (using a Zetasizer Nano ZS) and the amount of DOX, fluorimetric- and spectrophotometrically.

#### **6. *In vitro* DOX release**

The release of the drug from the SPION-DOX PNP was studied *in vitro* using a Float-A-Lyzer® G2 Dialysis Device (Spectra/Por®; MWCO: 8-10 kD) at pH 7 and 4, similar to

the pH of the blood and the cytoplasmic lysosomes. Keeping sink condition, 1 mL of PBS containing free or encapsulated DOX at 0.2 mg/mL (0.5 mg/mL is the maximal DOX solubility) was placed inside the device and introduced in 24 mL of PBS for 72 hours. During the dialysis, the device was shaken at 300 rpm and at different times the entire volume was replaced with fresh PBS. The cumulative release of DOX was quantified fluorimetrically at an excitation and emission wavelength of 485 and 580 nm and the percentage of drug released was plotted over time.

## **7. Cellular studies**

### **7.1 Cell cultures**

From the American Type Culture Collection (ATCC), 9L/lacZ gliosarcoma rat cell line (ATCC® CRL-2200™) was cultured in DMEM and human glioblastoma U-87 MG (ATCC® HTB-14™) cells were cultured in DMEM/F12, both mediums were complemented with 1 % (v/v) penicillin-streptomycin and 5 % (v/v) Fetal Bovine Serum (FBS), all from Gibco. Human neurosphere stem cell line (NSC-23) obtained from a patient from the hospital *Clínica Universidad de Navarra* (Spain) was grown in DMEM-F12-Glutamax (Thermofisher) completed with 10 % B27 supplement (Gibco), 1 % (v/v) penicillin-streptomycin, FGF-2 (basic Fibroblast Growth Factor) at 20 ng/mL (Immuno Tool) and EFG (epidermal growth factor) at 20 ng/mL (Sigma). Cells were cultured at 37°C and 5% CO<sub>2</sub> and every 3-4 days when cells were approximately 80 % confluent (80 % of surface of flask covered by cell monolayer) or the spheres formed are quite large, a 1:5 split was performed.

### **7.2 Cellular internalization**

The internalization of the drug encapsulated inside the SPION-DOX PNP was studied in the U87-MG cellular line using fluorescence microscopy (Zeiss, 120 Libra). For that,  $1 \times 10^5$  cells were seeded on sterile glass coverslips placed inside a 24-well plate. After 24 h, the cells were treated for 4 h with 30 µg/mL of DOX free or encapsulated inside the different types of NP. After treatment, the cells were fixed with p-



formaldehyde 4 % (5 min), permeabilized with Triton 0.1 % (10 min) and stained with DAPI (1:1000) for 5 min. For fluorescence microscope analysis, cells were washed three times and the slides were prepared with a drop of fluorescence mounting media.

### **7.3 *In vitro* efficacy**

To quantify the cytotoxic effect of SPION-DOX PNP, an *in vitro* cell viability assay was assessed by the CellTiter 96® AQueous One Solution Cell Proliferation Assay (MTS) colorimetric method. This method measures the metabolic activity of the mitochondrial NADPH dehydrogenases by means of MTS-tetrazolium salt reduction into a water soluble formazan product. Three cell lines were tested: the glioma cell line 9L, the human glioma cell line U87 and a human neurosphere stem cell NSC-23 obtained from a patient. First of all, the amount of cells needed of each cell line to perform the experiment was established; to do this, a study of the relation between the color obtained with respect to the amount of cells plated was performed. The number of cells chosen was in the higher third of the first linear curve, before a plateau was reached.

For the adherent cell lines 9L and U87,  $3 \times 10^3$  and  $2 \times 10^3$  cells/well, respectively, were seeded on a sterile 96-plate. After 24 hours of incubation (at 37 °C and 5 % of CO<sub>2</sub>) to allow cell adhesion, the medium was replaced with DOX, SPION, DOX PNP, SPION PNP or SPION-DOX PNP at increasing concentrations (from 0 to 50 µg/mL) of DOX or equivalent. 48 or 72 hours after treatments, the medium was replaced with a dilution of MTS (15µL MTS/100µL cellular medium) and 2 hours later the color that appeared from the produced formazan was measured spectrophotometrically ( $\lambda = 492$  and 690 nm). For the NSC-23 cells, which are cultured in suspension,  $8 \times 10^3$  cells/well were plated and treated on the same day; from that moment the same protocol that was used for adherent cells was followed. At the end of the experiments, the concentration of DOX that killed 50 % of the cells after a specified exposure time, the half maximal effective concentration (EC50), was calculated. The smaller EC50 value, the more effective the treatment is. For EC50 calculation, the data were

adjusted to the logarithmic DOX concentration vs. response curve in GraphPad Prism Software; data were expressed as mean  $\pm$  SD.

## **Results and discussion**

### **1. SPION characterization**

The oleic acid coating of the SPION was confirmed by infrared spectroscopy. Figure 1 represents the FTIR spectrum in the range of 600 to 4000  $\text{cm}^{-1}$  of 3 components: pure oleic acid (Figure 1A), SPION functionalized with oleic acid (oleic acid-SPION) in dichloromethane (Figure 1B) and SPION not functionalized in water (Figure 1C). In the spectrum corresponding to oleic acid-SPION, the peak at 620  $\text{cm}^{-1}$  corresponds to the vibration of the linkage Fe-O which belongs to SPION (Figure 1; square 1); while the peaks at 2924 and 2854  $\text{cm}^{-1}$  denote the vibrational vibration of the functional  $\text{CH}_3$  which belongs to oleic acid (Figure 1; square 2). However, a third peak at 1464  $\text{cm}^{-1}$ , characteristic of the asymmetric tension vibrations of the functional group  $\text{COO}^-$ , is absent in the other two spectra and reveals that the oleic acid is adsorbed chemically on the SPION as a carboxylate (Figure 1; square 3). This is confirmed by the presence of an intense peak at 1710  $\text{cm}^{-1}$  in the pure oleic spectrum corresponding to a C=O functional group (Figure 1; square 4), which would be responsible for the carboxylic linkage between oleic acid and SPION. We should point out that the other two peaks in the spectrum of SPION are typically obtained in aqueous solutions [27, 28].

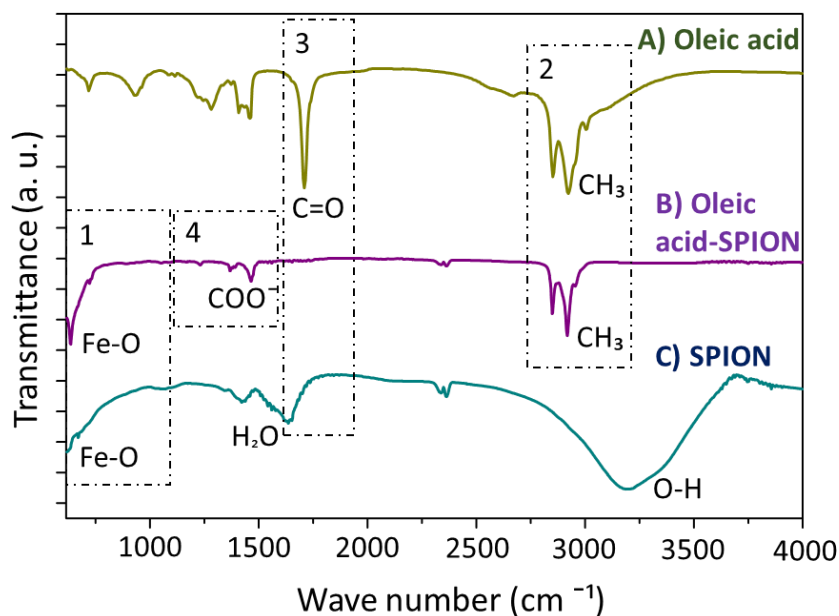


**Figure 1:** FTIR spectra of A) oleic acid, B) SPION covered with oleic acid (in dichloromethane) and C) SPION (in water). FTIR: Fourier-Transform Infrared Spectroscopy; SPION: superparamagnetic iron oxide nanoparticles.

## 2. SPION-DOX PNP optimization

SPION-DOX PNP were formed by the multiple or the simple emulsification and solvent evaporation method. First of all, the encapsulation of DOX and SPION was optimized independently and then the coencapsulation of both components was performed. Based on other papers [29–31], to optimize DOX encapsulation (Annex 2), different PLGAs (Resomer® 502, 503, 752 with free carboxylic or ester end groups), organic solvents (ethyl acetate (EA), dichloromethane or acetone) and the proportions of these or of the surfactant used (1 or 2 %) were tuned. In addition to this, to be able to dissolve the DOX in the organic phase, triethylamine (TEA) or oleic acid was added to the organic phase in different proportions (1:100 or 1:1000). Finally, the best DOX encapsulation efficacy was reached using the simple emulsion method with PLGA 503H, EA: TEA (1:1000) and 1 % of surfactant. Then, from the composition of this formulation, SPION encapsulation was tuned independently. As can be seen in Figure 2, the SPION were selectively encapsulated within PLGA nanoparticles using the simple emulsion method after they had been coated with

oleic acid (Figure 2C) [32, 33]. When the multiple emulsion method was used, the SPION were not encapsulated if they were added to the aqueous phase (Figure 2A). While if they were added to the organic phase after being covered with oleic acid, they were encapsulated in only a few PLGA NP (Figure 2B) and several PLGA NP remained empty.

Importantly, the co-encapsulation of DOX and SPION did not influence the distribution of SPION inside the PNP (Figure 2D), and NP with a uniform size and spherical shape were obtained.

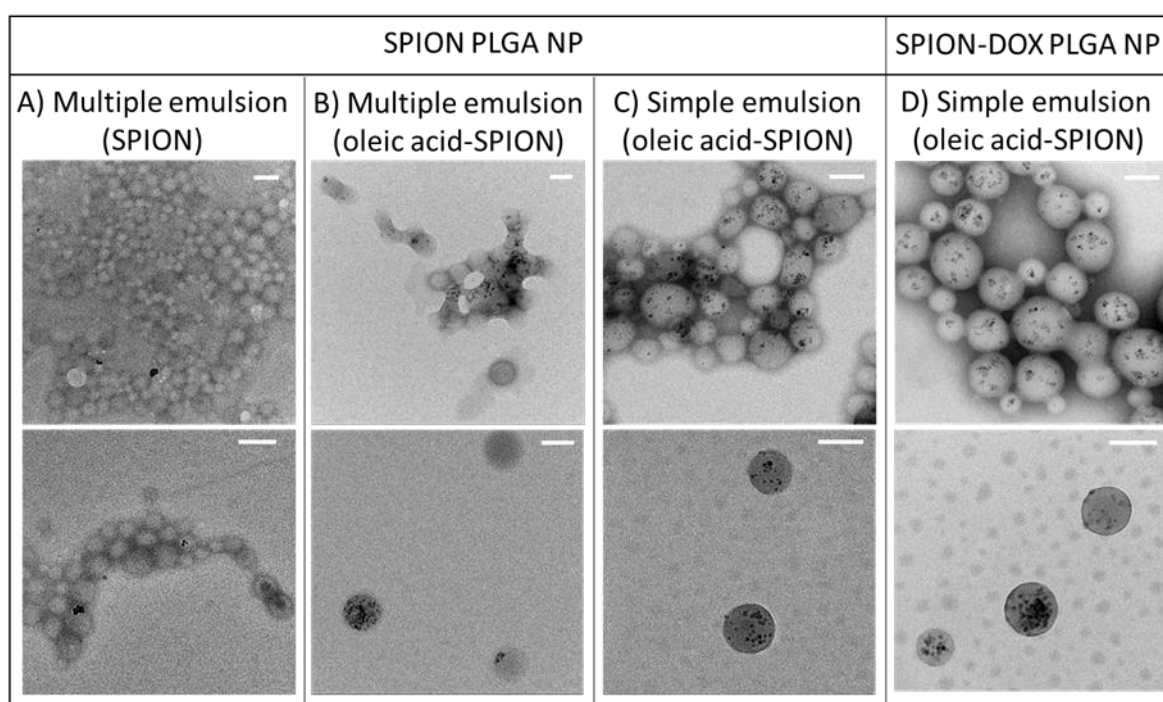


**Figure 2:** TEM images of the NP developed by different synthesis methods in the optimization of the SPION encapsulation inside the PNP. Multiple emulsion method with A) SPION or B) oleic acid-SPION. C) Simple emulsion method with oleic acid-SPION. D) Coencapsulation of oleic acid-SPION and DOX by the simple emulsion method. White scale bars represent the size of 50 nm.

### 3. SPION-DOX PNP characterization

The final characterization of all NP synthesized with the 4 surfactants studied (T80, Brij-35, Pluronic F68 and Vitamin E-TPGS) is shown in Table 1. A homogeneous

distribution of sizes between 209 and 230 nm was presented by DLS. However, the analysis by TEM was mandatory to ensure that the DLS-measured sizes represent primary particle size; and this analysis yielded sizes about 100 nm smaller (Figure 3). This difference could have various causes, such as the drying process during TEM sample preparation [34] or the sensitivity of the DLS technique to particle agglomeration, to DOX fluorescence [35] or to “soft” flexible biological molecules such as polymers (like PVA), which could cause significant frictional drag influencing the particle's motion [36, 37]. With respect to DOX and SPION encapsulation, the results were similar for all the NP developed. The DOX loading, measured fluorimetric- and spectrophotometrically, was around 10  $\mu\text{g}$  DOX/mg of NP, corresponding to an encapsulation efficiency of 80 %; while a loading of around 20  $\mu\text{g}$  Fe/mg of NP showed total SPION encapsulation, as confirmed by TEM images.

Surfactant used	Size (DLS)	PDI	Z potential (mV)	DOX ( $\mu\text{g}/\text{mg}$ formulation)		Fe ( $\mu\text{g}/\text{mg}$ formulation)
				Fluorimetry	UV/vis spectroph.	
<b>T80</b>	227.4 $\pm$ 18.2	0.066 $\pm$ 0.021	-13.8 $\pm$ 3.3	11.2 $\pm$ 1.9	9.9 $\pm$ 1.4	17.8 $\pm$ 1.8
<b>Brij-35</b>	209.1 $\pm$ 26.5	0.077 $\pm$ 0.019	-16.8 $\pm$ 2.9	10.7 $\pm$ 0.8	10.2 $\pm$ 1.3	20.3 $\pm$ 1.5
<b>Pluronic F68</b>	211.9 $\pm$ 7.7	0.076 $\pm$ 0.017	-15.8 $\pm$ 2.1	10.7 $\pm$ 0.9	10.5 $\pm$ 1.0	17.7 $\pm$ 3.9
<b>Vitamin E-TPGS</b>	227.9 $\pm$ 55.8	0.107 $\pm$ 0.019	-17.8 $\pm$ 1.7	11.1 $\pm$ 2.8	10.8 $\pm$ 3.9	21.9 $\pm$ 3.6

**Table 1:** Characterization of the SPION-DOX PLGA NP developed in terms of size, polydispersity index (PDI), Z potential and amount of DOX and Fe encapsulated.

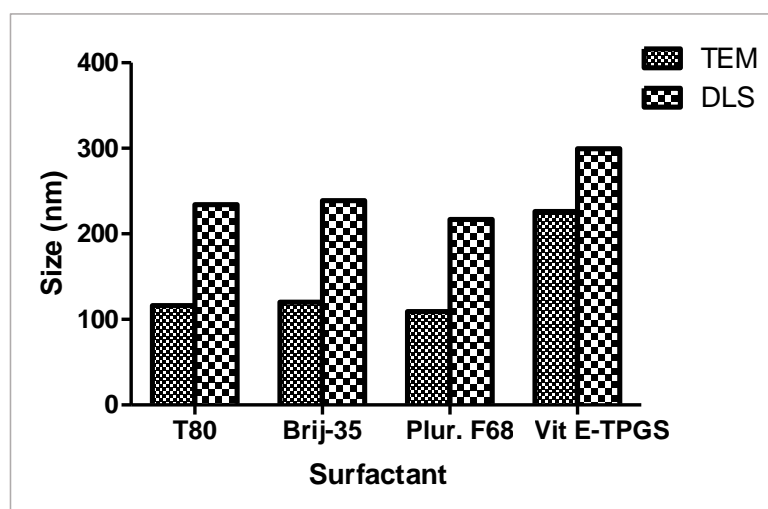


**Figure 3:** Difference in the SPION-DOX PLGA NP sizes measured by DLS or directly using TEM images (minimum 150 NP measured).

#### 4. Lyophilization optimization

Lyophilization (or freeze-drying) is a dehydration process commonly used to preserve nanomedicines over time. After the procedure, the NP were obtained as a powder that was reconstituted before use. As the SPION-DOX PNP developed were not stable during lyophilization, changing their morphology and increasing considerably their size, the addition of cryoprotectants and different surfactant concentrations were tested. By adding 37 % of trehalose (w/w with respect to the amount of PLGA) a small enhancement was appreciated, so this was added to the subsequent formulations. By contrast, a considerable influence on the reconstitution was detected when PVA was added in the last step of the NP synthesis. In fact, as can be seen in the comparison of size before and after lyophilization (Figure 4A), the higher the concentration of PVA the better the reconstitution was, being maintained the good reconstitution at the highest concentrations of 0.4 and 0.6 % of PVA. Besides, when 0.4 % PVA was used the morphology of the NP and the SPION distribution were maintained after lyophilization (Figure 5). The block copolymer character of the partially hydrolysed PVA could interact in the NP formation and explain the considerable improvement in the NP stability during the lyophilization process [38]. In fact, the addition of PVA also affected the physicochemical properties

of the NP, which increased in size and decreased the surface charge (Figure 4B-C); indicating that the PVA was present on the surface of the NP. This PVA represented around 5 % of the total weight of the NP (Figure 4D), less than that found by other groups that used PVA as a surfactant in the external phase (13 %) [26]. Conversely, this small amount of PVA was enough to improve the NP reconstitution after lyophilization and it could be enough to modify other properties like cell internalization or biodistribution. Certainly, the effect achieved could be compared to the effect of coating with a hydrophilic polymers such as polyethylene glycol (PEG), resulting in higher hydrophilicity [26]. But, fortunately, a labile adsorption of PVA on the surface of the NP was appreciated when, in contrast to Murakami H. et al.[39], a decrease of PVA content was observed with the number of washing cycles by centrifugation. Therefore, it is likely that the presence of PVA did not completely cover the surface of the NP and allowed the interaction of the BBB with the 4 surfactants used to synthesize the NP.

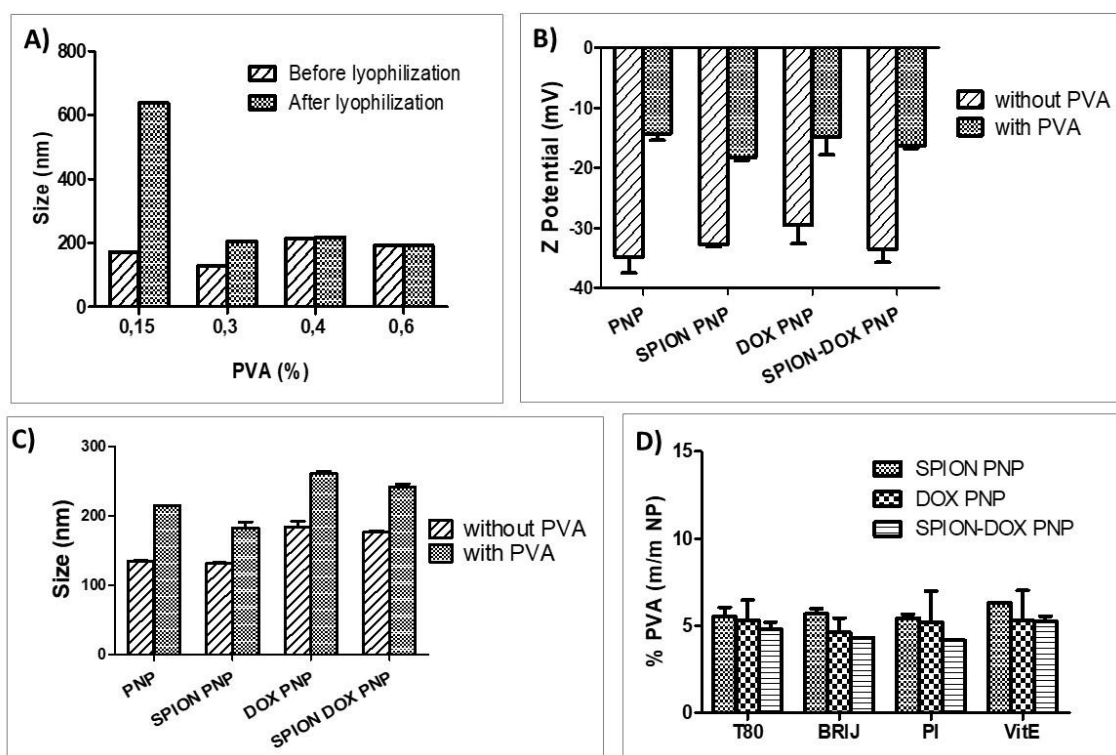


**Figure 4:** Characterization of the PVA addition to the formulation process. A) Influence of PVA on NP size during lyophilization, measured by DLS. B) Influence of PVA on the surface charge of NP formulated with T80. C) Influence of PVA on the size of the NP formulated with T80. D) Residual percentage of PVA with respect to the weight of the NP after their lyophilization.

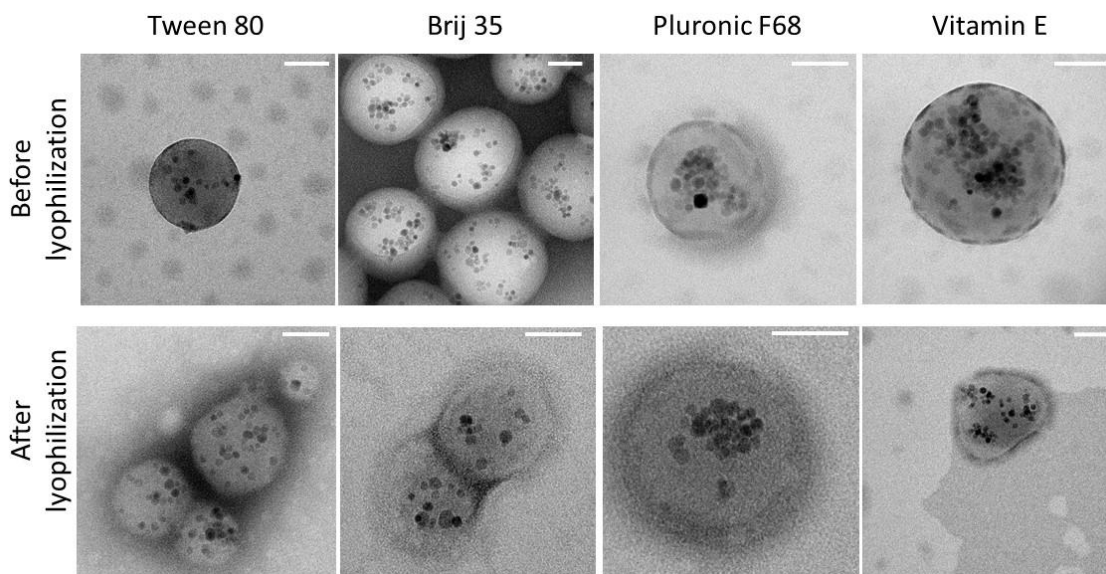


**Figure 5:** TEM images of SPION-DOX PNP before and after their lyophilization and subsequent reconstitution. All NP maintained their morphology and SPION distribution after lyophilization. White bars represent the size of 20 nm.

## 5. Stability study

To improve the long-term stability by avoiding instability in suspension and, simultaneously, facilitating its handling and storage, the NP formulated were lyophilized. A good lyophilizate should maintain the physical and chemical properties of the original product, with a short reconstitution time, low residual moisture content and good long term conservation [40]. To assess this stability and the maintenance of these characteristics, each type of NP was characterized in terms of size and amount of DOX after being formulated and lyophilized; then, these were divided in 3 to be stored at 4, 25 or 40 °C. 1, 3, 4, 8 and 12 weeks later NP were reconstituted in water to measure the size and the amount of DOX. In terms of size, the NP stored at 4 °C remained stable throughout the study (Figure 6); those stored at RT were only stable during the first month; and those stored at 40 °C were not stable since in 1 week the size increased considerably, losing the homogeneity of the reconstituted NP. With respect to the drug stability, the inherent fluorescence of DOX,



associated with the central anthracycline chromophore group has a strong dependence on the microenvironment and the formation of DOX dimers or DOX–iron complexes. Thus, as the degradation of the NP could also decrease the fluorescence intensity, the drug loading was also determined by the optical absorbance of DOX, which is less sensitive but is not influenced by the microenvironment, dimerization or iron-complex formation [41–43]. Figure 6B shows how the amount of DOX encapsulated into the NP is conserved over time at all storage temperatures when measured spectrophotometrically. But interestingly, when DOX was measured fluorimetrically (Figure 6C), the drug load decreased considerably at RT and 40 °C and only at 4 °C was it stable throughout the experiment. Considering that free DOX is a labile molecule which needs to be stored at – 20 °C, the NP developed protected the drug considerably from degradation, when stored at 4 °C.

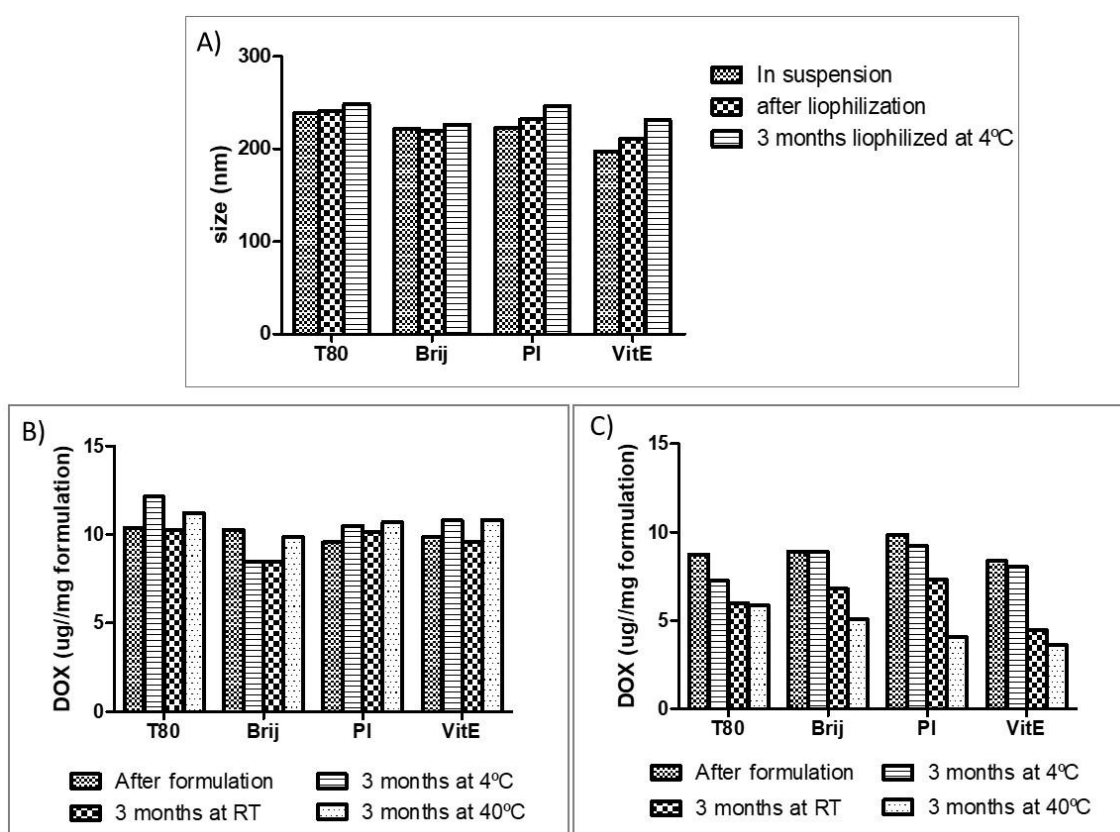


**Figure 6:** Lyophilized NP stability for 12 weeks. A) Size of NP before and after being lyophilized (immediately and 12 weeks later, stored at 4 °C). B) Spectrophotometric or C) fluorimetric measuring of DOX loading before and 12 weeks after being lyophilized and stored at RT, 4 or 40 °C.

## 6. Relaxivity study

Magnetic resonance signals are characterized by two principal kinetic processes governed by the longitudinal ( $T_1$ ) and transversal ( $T_2$ ) relaxation times. In an NMR process, these times characterize the relaxation process of the longitudinal and transversal components of the magnetic moments of the hydrogen protons present in the medium. In this sense, contrast agents modify the NMR signal of the surrounding hydrogen protons by increasing the inverse of the  $T_1$  and  $T_2$ , that is, what is termed the longitudinal and transverse relaxation rate constants. All of this occurs in a concentration-dependent manner so that, for instance, in simple water solutions the longitudinal and transversal relaxation rate constants increase linearly with contrast agent concentration. The slope of these dependences is known respectively as longitudinal and transversal relaxivity ( $r_1$  and  $r_2$ ), a measure of how potent the agent is for accelerating the longitudinal and transversal relaxation processes [44]. Contrast agents increasing mainly the longitudinal relaxation (i.e., decreasing  $T_1$ ) are called  $T_1$  or positive contrast agents, and are made of paramagnetic materials; contrast agents increasing mainly the transversal relaxation (i.e., decreasing  $T_2$ ) are called  $T_2$  or negative contrast agents. Contrast agents synthesised from superparamagnetic NP, as for example our SPION, belong to this type. Thus, the relaxivity for the SPION-DOX PNP in aqueous suspension was obtained measuring the relaxation times of the hydrogen protons of the water at different NP concentrations (from 0.1 to 1 mM  $[\text{Fe}^{+2}]$ ). The results had a good reproducibility and, as expected from a superparamagnetic nanoparticle system, the  $r_2$  was much larger than the  $r_1$  (Table 2). In detail, the  $r_1$  were 1.85, 0.28, 0.20 and 0.14  $\text{mM}^{-1}\text{s}^{-1}$ ; and the  $r_2$  197.80, 172.09, 158.03 and 160.15  $\text{mM}^{-1}\text{s}^{-1}$  for the NP developed with T80, Brij-35, Pluronic F68 or Vitamin E-TPGS, respectively. These results were very similar to those obtained by SPION already commercialized as contrast agents (Feridex  $r_2=120 \text{ mM}^{-1}\text{s}^{-1}$ ; Ferumoxtran  $r_2=65 \text{ mM}^{-1}\text{s}^{-1}$ ; Resovist-Ferucarbotran  $r_2=189 \text{ mM}^{-1}\text{s}^{-1}$ ) and indicate that these NP could be applied on magnetic susceptibility-based acquisitions in  $T_2$ -weighted or  $T_2^*$ -weighted MRI, in which they would produce a hypointense (dark) signal [44].

Surfactant used	r1 (mM <sup>-1</sup> s <sup>-1</sup> )	r2 (mM <sup>-1</sup> s <sup>-1</sup> )
T80	1.85	197.80
Brij-35	0.28	172.09
Pluronic F68	0.20	158.03
Vitamin E-TPGS	0.14	160.15

**Table 2:** Longitudinal (r1) and transversal (r2) relaxivity of the SPION-DOX PLGA NP developed by nuclear magnetic resonance.

### 7. *In vitro* drug release and cellular internalization

In general, NP are internalized inside the cells mainly via clathrin mediated endocytosis and are transported to endosomes and lysosomes. These acidic cell compartments (endosomes with pH 5.5 and lysosomes with pH 4.0–5.0) are important organelles for the intracellular drug release [45]. For that reason, the release of the drug from the different SPION-DOX PNP was studied at pHs 4 and 7 using a dialysis device (8-10 kDa). The sustained release of the DOX from the NP by the dialysis bag diffusion technique was both time and pH dependent (Figure 7). Comparing the release profiles of the drug in solution and encapsulated in SPION-DOX PNP at pH 7, the encapsulation of DOX into SPION-DOX PNP clearly favors the controlled release of the drug. Meanwhile, the same release profile at pH 4 of DOX and NP synthesized with T80 and Pluronic F68 and the clear increase in the case of Brij-35 indicate a rapid release from the NP under acidic conditions. The release could be promoted by the high acidic affinity of DOX along with the degradation of the nanocarrier [45]. In the case of SPION-DOX PNP formulated with Vitamin E-TPGS no release was detected at pH 4. This different behavior could be due to a slower degradation rate [46] or an increment of the DOX stability inside the matrix [47]. However, as acid-sensitive linker between TPGS and DOX has been clearly demonstrated [48], this lack of DOX release effect could be due to the *in vitro* dialysis device model.

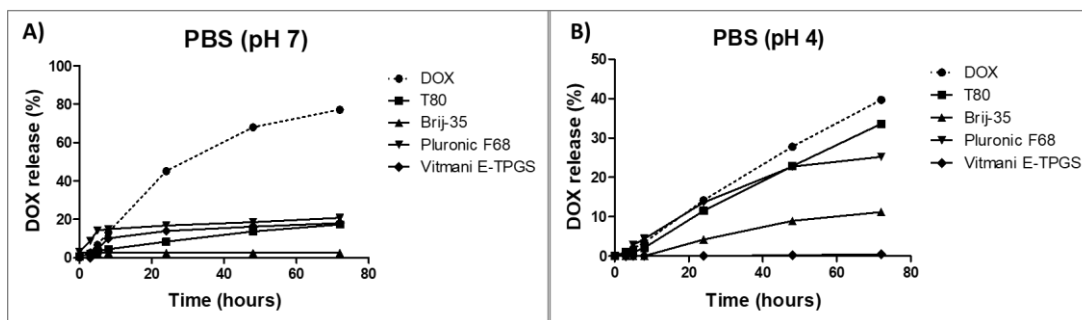


**Figure 7:** Release of DOX from SPION-DOX PNP in PBS at pH 4 (A) and 7 (B).

To confirm all these assumptions, U87 cells were incubated with free or encapsulated drug for 4 hours and fluorescence imaging was used to explore the subcellular localization of the drug. As can be seen in Figure 8, after 4 hours the DOX (in red) was in the nucleus (in blue) of cells, regardless of whether the treatment was by free or encapsulated drug. As suggested by Malinovskaya Y. *et al.* who had similar results, within 1 h DOX could be released from PNP in the acidic environment of endosomes and, once in the cytoplasm, these could reach the target site (the nucleus) without degradation [45].

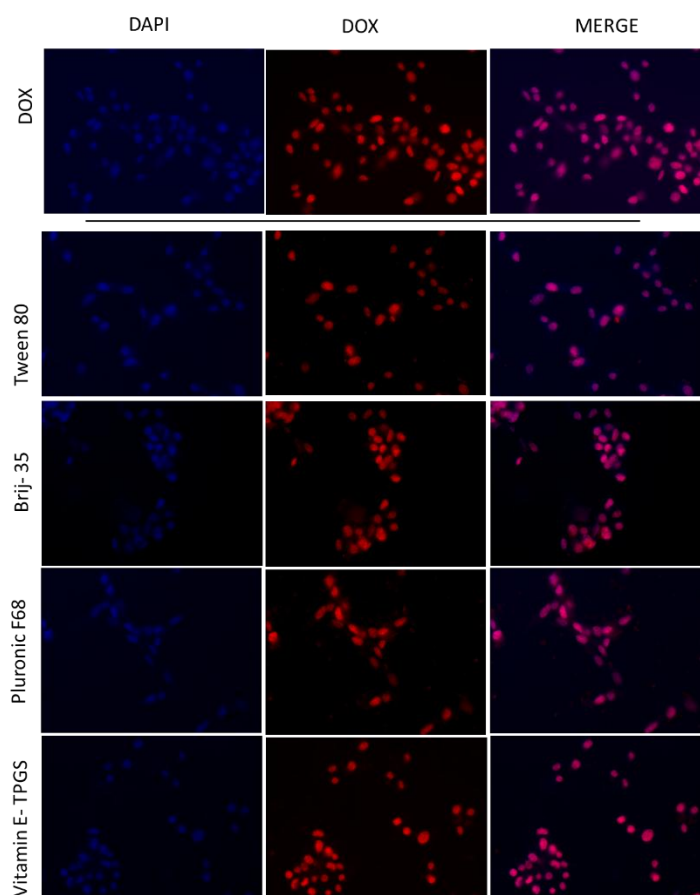


**Figure 8:** Fluorescence microscopy of U87 cells after 4 h incubation with DOX or SPION-DOX PNP developed with the surfactants T80, Brij-35, Pluronic F68 or Vitamin E-TPGS. DAPI indicates nucleus location in blue and DOX fluorescence is detected in red.

### 8. *In vitro* efficacy

The cytotoxic efficacy of SPION-DOX PNP was examined in different glioma cell lines by MTS assay. In the case of the commercial glioma cell lines U87 and 9L (Figure 9A and E), all the SPION-DOX PNP developed were similar in potency to free drug with an EC<sub>50</sub> in a narrow range of 20  $\mu\text{g}/\text{mL}$  at 48 hours. This cytotoxicity maintenance after DOX encapsulation has also been detected by other authors such as Battaglia L. *et al* who encapsulated DOX in solid lipid nanoparticles [49]. In more detail, they found that just the cytotoxic effect against 9L was slightly smaller than the control, matching the same value at 72 hours. This indicated a slight time-dependence cytotoxicity, probably due to the controlled drug release from the NP inside the cells

[50]. On the other hand, as in glioma tumors, neurospheres are a complex group of cells sustained by stem cells [51]. These stem cells are multipotent and have auto-regeneration capabilities; in GBM they are responsible for the initial tumor formation and progression, as well as treatment resistance and later recurrence [52]. This makes it important for us to target the tumor-initiating cells that are resistant to current therapies. Moreover, the three dimensional (3D) culture models (Figure 9B), closely mimic the heterogeneity and the microenvironment of the tumor in *in vivo* conditions, and thus allow a more predictive *in vitro* evaluation of nanomedicines [53]. As in the previous cell lines and Battaglia L. *et al* [49], similar EC50 values were obtained for encapsulated and non-encapsulated DOX at 72 hours of treatment (Figure 9A).

For all of the cells studied, SPION-DOX PNP inhibited cell viability in a dose-dependent manner; the type of surfactant used to form the NP did not influence the cytotoxic effect; and both vehicle-controls, SPION and SPION PNP, proved to be non-toxic at the concentrations used (Figure 9C and D), indicating that the drug alone was responsible for the toxicity. In conclusion, these *in vitro* results suggest that all SPION-DOX PNP developed are potent treatments and thus promising candidates for *in vivo* efficacy studies.

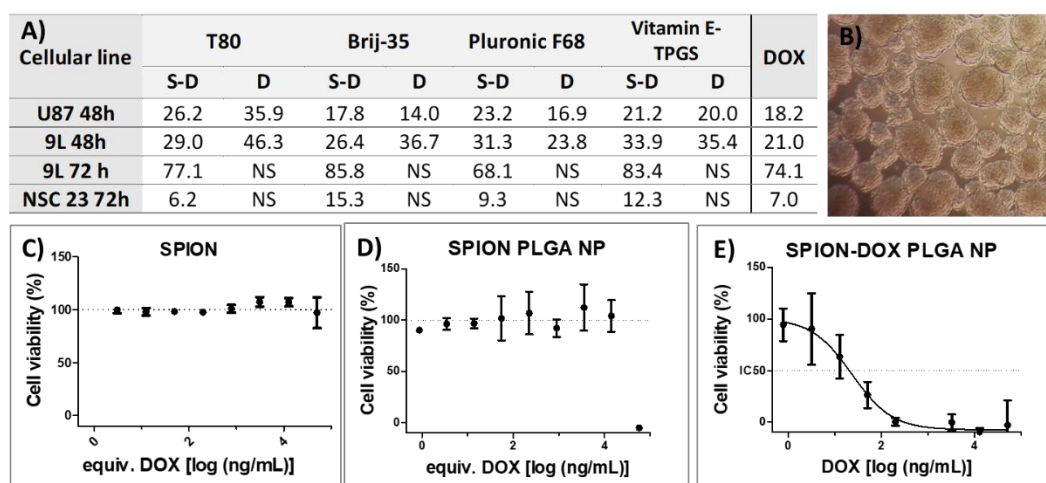


**Figure 9:** A) EC50 (ng/mL) of DOX, DOX PNP and SPION-DOX PNP formulated with the surfactants T80, Brij-35, Pluronic F68 or Vitamin E-TPGS. NS= not studied; S-D= SPION-DOX PNP; D= DOX PNP. B) Image of the patient-donated neurospheres NSC-23.

C, D, E) Cell viability representation vs DOX concentration in the treatment of U87-MG cells with SPION, SPION PNP or SPION-DOX PNP.

### Conclusions

In this chapter, surfactant-coated PNP with a high DOX and SPION encapsulation were obtained. The nanovehicles designed were stable at 4<sup>o</sup> C after being lyophilized and, in addition, they had low longitudinal and high transversal relaxations, indicating that they will be good contrast agents for MRI. On the other hand, the nanocarriers were efficiently internalized into glioma cells where the drug was released, providing a therapeutic effect in both normal tumor population cells and neuronal cells with stem cell properties. All told, 4 theranostic NP useful to treat and monitor glioma *in vitro* were developed successfully.

### Bibliography

1. Azzarelli R, Simons BD, Philpott A. The developmental origin of brain tumours: a cellular and molecular framework. *Development*. 2018;145:dev162693.
2. Huse JT, Holland EC. Targeting brain cancer: advances in the molecular pathology of malignant glioma and medulloblastoma. *Nat. Rev. Cancer*. 2010;10:319–31.
3. Search of: glioblastoma - List Results - ClinicalTrials.gov. (<https://clinicaltrials.gov/ct2/results?cond=glioblastoma&term=&cntry=&state=&city=&dist=>). Accessed 27 June 2018.
4. Stupp R, Mason WP, van den Bent MJ, Weller M, Fisher B, Taphoorn MJB et al. Radiotherapy plus Concomitant and Adjuvant Temozolomide for Glioblastoma. *N. Engl. J. Med*. 2005;352:987–96.
5. Ganipineni LP, Danhier F, Pr at V. Drug delivery challenges and future of chemotherapeutic nanomedicine for glioblastoma treatment. *J. Control. Release*. 2018;281:42–57.
6. Vanan MI, Eisenstat DD. DIPG in Children - What Can We Learn from the Past? *Front. Oncol*. 2015;5:237.
7. Peiris PM, Abramowski A, MCGinnity J, Doolittle E, Toy R, Gopalakrishnan R et al. Treatment of invasive brain tumors using a chain-like nanoparticle. *Cancer Res*. 2015;75:1356–65.
8. Hobbs SK, Monsky WL, Yuan F, Roberts WG, Griffith L, Torchilin VP et al. Regulation of transport pathways in tumor vessels: Role of tumor type and microenvironment. *Proc. Natl. Acad. Sci*. 1998;95:4607–12.
9. Luque-Michel E, Imbuluzqueta E, Sebasti an V, Blanco-Prieto MJ. Clinical advances of nanocarrier-based cancer therapy and diagnostics. *Expert Opin. Drug Deliv*. 2017;14:75–92.
10. Estella-Hermoso de Mendoza A, Preat V, Mollinedo F, Blanco-Prieto MJ. In vitro and in vivo efficacy of edelfosine-loaded lipid nanoparticles against glioma. *J.*

- Control. Release. 2011;156:421–6.
11. Singh D, Kapahi H, Rashid M, Prakash A, Majeed ABA, Mishra N. Recent prospective of surface engineered Nanoparticles in the management of Neurodegenerative disorders. *Artif. Cells, Nanomedicine Biotechnol.* 2016;44:780–91.
  12. Petri B, Bootz A, Khalansky A, Hekmatara T, Müller R, Uhl R et al. Chemotherapy of brain tumour using doxorubicin bound to surfactant-coated poly ( butyl cyanoacrylate ) nanoparticles : Revisiting the role of surfactants. *J. Control. Release.* 2007;117:51–8.
  13. Gidwani M, Singh A V. Nanoparticle enabled drug delivery across the blood brain barrier: in vivo and in vitro models, opportunities and challenges. *Curr. Pharm. Biotechnol.* 2014;14:1201–12.
  14. Hoosain FG, Choonara YE, Tomar LK, Kumar P, Tyagi C, du Toit LC et al. Bypassing P-Glycoprotein Drug Efflux Mechanisms: Possible Applications in Pharmacoresistant Schizophrenia Therapy. *Biomed Res. Int.* 2015;2015:484963.
  15. Gelperina S, Maksimenko O, Khalansky A, Vanchugova L, Shipulo E, Abbasova K et al. Drug delivery to the brain using surfactant-coated poly(lactide-co-glycolide) nanoparticles: Influence of the formulation parameters. *Eur. J. Pharm. Biopharm.* 2010;74:157–63.
  16. Schuster T, Mühlstein A, Yaghootfam C, Maksimenko O, Shipulo E, Gelperina S et al. Potential of surfactant-coated nanoparticles to improve brain delivery of arylsulfatase A. 2017;253:1–10.
  17. Collnot E-M, Baldes C, Wempe MF, Kappl R, Hüttermann J, Hyatt JA et al. Mechanism of Inhibition of P-Glycoprotein Mediated Efflux by Vitamin E TPGS: Influence on ATPase Activity and Membrane Fluidity. *Mol. Pharm.* 2007;4:465–74.
  18. Meng X, Liu J, Yu X, Li J, Lu X, Shen T. Pluronic F127 and D- $\alpha$ -Tocopheryl Polyethylene Glycol Succinate (TPGS) Mixed Micelles for Targeting Drug Delivery across The Blood Brain Barrier. *Sci. Rep.* 2017;7:2964.
  19. Kulkarni SA, Feng S-S. Effects of Particle Size and Surface Modification on Cellular Uptake and Biodistribution of Polymeric Nanoparticles for Drug Delivery. *Pharm. Res.* 2013;30:2512–22.
  20. Koziara JM, Lockman PR, Allen DD, Mumper RJ. In situ blood-brain barrier transport of nanoparticles. *Pharm. Res.* 2003;20:1772–8.
  21. Ferumoxytol in Improving MR Imaging in Patients With High-Grade Brain Tumors or Cerebral Metastases - Full Text View - ClinicalTrials.gov. (<https://clinicaltrials.gov/ct2/show/study/NCT00103038>). Accessed 3 July 2018.
  22. Zhou J, Zhang J, Gao W. Enhanced and selective delivery of enzyme therapy to 9L-glioma tumor via magnetic targeting of PEG-modified,  $\beta$ -glucosidase-conjugated iron oxide nanoparticles. *Int. J. Nanomedicine.* 2014;9:2905–17.
  23. Yi G, Gu B, Chen L. The safety and efficacy of magnetic nano-iron hyperthermia therapy on rat brain glioma. *Tumor Biol.* 2014;35:2445–9.
  24. Miguel-Sancho N, Bomati-Miguel O, Colom G, Salvador J-P, Marco M-P, Santamaría J. Development of Stable, Water-Dispersible, and Biofunctionalizable Superparamagnetic Iron Oxide Nanoparticles. *Chem. Mater.* 2011;23:2795–802.
  25. Friedrich RP, Janko C, Pöttler M, Tripal P, Zaloga J, Cicha I et al. Flow cytometry for intracellular SPION quantification: specificity and sensitivity in&nbsp;comparison with spectroscopic methods. *Int. J. Nanomedicine.*



- 2015;10:4185.
26. Sahoo SK, Panyam J, Prabha S, Labhasetwar V. Residual polyvinyl alcohol associated with poly (D,L-lactide-co-glycolide) nanoparticles affects their physical properties and cellular uptake. *J. Control. Release.* 2002;82:105–14.
  27. Velusamy P, Chia-Hung S, Shritama A, Kumar GV, Jeyanthi V, Pandian K. Synthesis of oleic acid coated iron oxide nanoparticles and its role in anti-biofilm activity against clinical isolates of bacterial pathogens. *J. Taiwan Inst. Chem. Eng.* 2016;59:450–6.
  28. Masur S, Zingsem B, Marzi T, Meckenstock R, Farle M. Characterization of the oleic acid/iron oxide nanoparticle interface by magnetic resonance. *J. Magn. Magn. Mater.* 2016;415:8–12.
  29. Li Z, Qiu L, Chen Q, Hao T, Qiao M, Zhao H et al. pH-sensitive nanoparticles of poly(l-histidine)–poly(lactide-co-glycolide)–tocopheryl polyethylene glycol succinate for anti-tumor drug delivery. *Acta Biomater.* 2015;11:137–50.
  30. Kalaria DR, Sharma G, Beniwal V, Ravi Kumar MN V. Design of Biodegradable Nanoparticles for Oral Delivery of Doxorubicin: In vivo Pharmacokinetics and Toxicity Studies in Rats. *Pharm. Res.* 2009;26:492–501.
  31. Ma Y-C, Wang J-X, Tao W, Qian H-S, Yang X-Z. Polyphosphoester-based nanoparticles with viscous flow core enhanced therapeutic efficacy by improved intracellular drug release. *ACS Appl. Mater. Interfaces.* 2014;6:16174–81.
  32. Schleich N, Sibret P, Danhier P, Ucakar B, Laurent S, Muller RN et al. Dual anticancer drug/superparamagnetic iron oxide-loaded PLGA-based nanoparticles for cancer therapy and magnetic resonance imaging. *Int. J. Pharm.* 2013;447:94–101.
  33. Jia Y, Yuan M, Yuan H, Huang X, Sui X, Cui X et al. Co-encapsulation of magnetic Fe<sub>3</sub>O<sub>4</sub> nanoparticles and doxorubicin into biodegradable PLGA nanocarriers for intratumoral drug delivery. *Int. J. Nanomedicine.* 2012;7:1697–708.
  34. Luque-Michel E, Larrea A, Lahuerta C, Sebastian V, Imbuluzqueta E, Arruebo M et al. A simple approach to obtain hybrid Au-loaded polymeric nanoparticles with a tunable metal load. *Nanoscale.* 2016;8:6495–506.
  35. Bteich J, Ernsting MJ, Mohammed M, Kiyota T, McKee TD, Trikha M et al. Nanoparticle Formulation Derived from Carboxymethyl Cellulose, Polyethylene Glycol, and Cabazitaxel for Chemotherapy Delivery to the Brain. *Bioconjug. Chem.* 2018;29:2009–20.
  36. Lin W-L, Liang P-C, Chen Y-C, Chiang C-F, Mo L-R, Wei S-Y et al. Doxorubicin-modified magnetic nanoparticles as a drug delivery system for magnetic resonance imaging-monitoring magnet-enhancing tumor chemotherapy. *Int. J. Nanomedicine.* 2016;11:2021.
  37. Dobrovolskaia MA, Patri AK, Zheng J, Clogston JD, Ayub N, Aggarwal P et al. Interaction of colloidal gold nanoparticles with human blood: effects on particle size and analysis of plasma protein binding profiles. *Nanomedicine Nanotechnology, Biol. Med.* 2009;5:106–17.
  38. Yang M, Lai SK, Yu T, Wang Y-Y, Happe C, Zhong W et al. Nanoparticle penetration of human cervicovaginal mucus: the effect of polyvinyl alcohol. *J. Control. Release.* 2014;192:202–8.
  39. Murakami H, Kobayashi M, Takeuchi H, Kawashima Y. Preparation of poly(dl-lactide-co-glycolide) nanoparticles by modified spontaneous emulsification solvent

- diffusion method. *Int. J. Pharm.* 1999;187:143–52.
40. Fonte P, Reis S, Sarmento B. Facts and evidences on the lyophilization of polymeric nanoparticles for drug delivery. *J. Control. Release.* 2016;225:75–86.
  41. Munnier E, Cohen-Jonathan S, Linassier C, Douziech-Eyrolles L, Marchais H, Soucé M et al. Novel method of doxorubicin-SPION reversible association for magnetic drug targeting. *Int. J. Pharm.* 2008;363:170–6.
  42. Mohan P, Rapoport N. Doxorubicin as a molecular nanotheranostic agent: effect of doxorubicin encapsulation in micelles or nanoemulsions on the ultrasound-mediated intracellular delivery and nuclear trafficking. *Mol. Pharm.* 2010;7:1959–73.
  43. Changenet-Barret P, Gustavsson T, Markovitsi D, Manet I, Monti S. Unravelling molecular mechanisms in the fluorescence spectra of doxorubicin in aqueous solution by femtosecond fluorescence spectroscopy. *Phys. Chem. Chem. Phys.* 2013;15:2937–44.
  44. Weinstein JS, Varallyay CG, Dosa E, Gahramanov S, Hamilton B, Rooney WD et al. Superparamagnetic Iron Oxide Nanoparticles: Diagnostic Magnetic Resonance Imaging and Potential Therapeutic Applications in Neurooncology and Central Nervous System Inflammatory Pathologies, a Review. *J. Cereb. Blood Flow Metab.* 2010;30:15–35.
  45. Malinovskaya Y, Melnikov P, Baklaushev V, Gabashvili A, Osipova N, Mantrov S et al. Delivery of doxorubicin-loaded PLGA nanoparticles into U87 human glioblastoma cells. *Int. J. Pharm.* 2017;524:77–90.
  46. Malinovskaya Y, Melnikov P, Baklaushev V, Gabashvili A, Osipova N, Mantrov S et al. Delivery of doxorubicin-loaded PLGA nanoparticles into U87 human glioblastoma cells. *Int. J. Pharm.* 2017;524:77–90.
  47. de Lencastre Novaes LC, Jozala AF, Mazzola PG, Júnior AP. The influence of pH, polyethylene glycol and polyacrylic acid on the stability of stem bromelain. *Brazilian J. Pharm. Sci.* 2014;50:371–80.
  48. Yang C, Wu T, Qi Y, Zhang Z. Recent advances in the application of vitamin E TPGS for drug delivery. *Theranostics.* 2018;8:464–85.
  49. Battaglia L, Gallarate M, Peira E, Chirio D, Muntoni E, Biasibetti E et al. Solid Lipid Nanoparticles for Potential Doxorubicin Delivery in Glioblastoma Treatment: Preliminary In Vitro Studies. *J. Pharm. Sci.* 2014;103:2157–65.
  50. González-Fernández Y, Brown HK, Patiño-García A, Heymann D, Blanco-Prieto MJ. Oral administration of edelfosine encapsulated lipid nanoparticles causes regression of lung metastases in pre-clinical models of osteosarcoma. *Cancer Lett.* 2018;430:193–200.
  51. Valenciano EV, Fisiología D De, Medicina E De, Universidad D, Rica DC, Costarricense C et al. Importancia de Células Madre TumORAles y Cultivos de Neuroesferas en Neurooncología. *Neuroeje.* 2012;25:55–60.
  52. Alicia M. Mihaliak, Candace A. Gilbert, Li Li, Marie-Claire Daou RPM, Andrew Reeves, Brent H. Cochran and AHR. Clinically relevant doses of chemotherapy agents reversibly block formation of glioblastoma neurospheres. *Cancer Lett.* 2010;296:168–77.
  53. Lazzari G, Couvreur P, Mura S. Multicellular tumor spheroids: A relevant 3D model for the: In vitro preclinical investigation of polymer nanomedicines. *Polym. Chem.* 2017;8:4947–69.





# **CHAPTER 3**

---

**Magnetic enhancement into brain tumor and MRI monitoring of SPION and doxorubicin-loaded PLGA nanocarriers with different surfactants**



## Magnetic enhancement in brain tumor and MRI monitoring of SPION and doxorubicin-loaded PLGA nanocarriers with different surfactants

Edurne Luque-Michel<sup>1,2</sup>, Laurent Lemaire<sup>3,4</sup>, Victor Sebastian<sup>5,6</sup> and Maria J. Blanco-Prieto<sup>1,2</sup>

<sup>1</sup> *Department of Pharmacy and Pharmaceutical Technology, School of Pharmacy, University of Navarra, C/Irunlarrea 1, E-31008 Pamplona, Spain*

<sup>2</sup> *Instituto de Investigación Sanitaria de Navarra (IdiSNA), Pamplona, Spain*

<sup>3</sup> *INSERM UMR-S 1066- CNRS 6021, Micro et Nanomédecines Biomimétiques – MINT Université d'Angers, 4 rue Larrey, Angers 49933, France*

<sup>4</sup> *PRISM – Plateforme de Recherche en Imagerie et Spectroscopie Métabolique, Université d'Angers, 4 rue Larrey, Angers 49933, France*

<sup>5</sup> *Institute of Nanoscience of Aragon (INA) and Department of Chemical, Engineering and Environmental Technology, University of Zaragoza, C/Mariano Esquillor, s/n, I+D+I Building, 50018 Zaragoza, Spain*

<sup>6</sup> *CIBER de Bioingeniería, Biomateriales y Nanomedicina (CIBER-BBN), Centro de Investigación Biomédica en Red, C/ Monforte de Lemos 3-5, Pabellón 11, 28029 Madrid, Spain*

### Abstract

Glioma is a type of cancer with a very poor prognosis. In the case of glioblastoma multiforme (GBM), this is around 15 months. In order to advance in personalized medicine, we developed polymeric nanoparticles (PNP) loaded with doxorubicin (DOX) and SPION (Superparamagnetic Iron Oxide Nanoparticles), in which could be able to treat the tumor and enable follow-up using magnetic resonance imaging (MRI). This could contribute to early detection of recurrences as well as disease monitoring and individual treatment adjustment. To this effect, the simple emulsion solvent and evaporation method was selected to develop PNP targeting the BBB with 4 different surfactant coatings (Tween 80, Brij-35, Pluronic F68 or Vitamin E-TPGS). Their capacity to cross through a model of the human blood-brain barrier (BBB), their function and their immune behavior using the complement activation (CH50) test were examined. Finally, the therapeutic and diagnostic (theranostic) efficiency of the Tween 80-PNP were studied in orthotopic tumor-bearing nude mice along with extra magnetic targeting. Our findings showed PNP tumor uptake with a significant slowdown in tumor growth.

**Keywords:** polymeric nanocarriers, Tween 80, Pluronic F68, Brij- 35, Vitamin E-TPGS, BBB, complement, MRI, tumor doubling time





## INDEX

<b>I. Introduction</b> .....	126
<b>II. Materials and methods</b> .....	128
1. SPION-DOX PNP synthesis and characterization .....	128
2. <i>In vitro</i> studies .....	129
2.1 Cell culture .....	129
2.2 BBB Permeability .....	129
2.3 BBB cells internalization .....	131
3. Complement activation (CH50) test .....	131
4. <i>In vivo</i> studies .....	132
1.1 Intracranial inoculation of human glioblastoma .....	132
1.2 Magnetic targeting and MRI monitoring .....	132
1.3 Efficacy studies .....	133
2. Statistical studies .....	134
<b>III. Results and discussion</b> .....	134
1. SPION-DOX PNP characterization .....	134
2. <i>In vitro</i> studies .....	135
2.1 BBB permeability .....	135
2.2 BBB cells internalization .....	137
3. Complement activation (CH50) test .....	138
4. <i>In vivo</i> studies .....	140
4.1 Magnetic targeting and MRI monitoring .....	140
<i>Continuous monitoring</i> .....	141
<i>Monitoring at 4 hours</i> .....	143
4.2 Efficacy studies .....	144
<i>Tumor growth monitoring</i> .....	144
<i>Survival rates</i> .....	145
<b>IV. Conclusions</b> .....	146
<b>V. References</b> .....	146

**Introduction**

Glioblastoma (GBM) is the most common and the most malignant variant in the wide spectrum of intrinsic glial brain tumors. Overall, the incidence of GBM is higher in

males than in females [1]. Although it can affect children, its incidence increases with age. In particular, the age at diagnosis tends to be higher for primary GBM (arise in the absence of prior disease) with a mean age of 55, than for secondary GBM (developed from low-grade astrocytoma) with a mean age of 40 years. To date, no uniform etiology has been identified, extracranial metastasis is rare and tumors are commonly located in the supratentorial region (frontal, temporal, parietal, and occipital lobes) and infrequently in the cerebellum. For spinal cord GBMs, the mean age of onset is 27 years, and 53 % of these tumors are found in those aged less than 18 years [1]. Morphologically, GBM is highly heterogeneous, being diffuse and infiltrative in nature, which makes surgical removal particularly difficult [2]. In parallel, the failure of chemotherapy to reach the brain and the presence of stem cells lead to tumor recurrence [2, 3]. Only 2-5 % of patients are long-term survivors living more than 3 years; in fact, it has been suggested that GBM recurrence is inevitable after a median survival time of 32–36 weeks [4]. In response to this, more effective and accurate treatments are being developed. For instance, implantable Gliadel® wafers improve the survival rate in gliomas but fail to prevent tumor recurrence and are limited by their low penetration (1–2 mm) into the distant regions of the remnant tumor [2]. In contrast to the intracranial treatments, many therapeutic drugs are excluded from entering the brain because they cannot cross the blood-brain barrier (BBB). In the area of cancer nanomedicine, drugs are encapsulated inside nanocarriers that provide controlled release of the drug once in the tumor. In this sense, nanoparticles (NP) designed to achieve BBB uptake could increase the drug concentration in glioma and then increase the effectiveness of treatment. This is the case with polymeric nanoparticles (PNP) made with surfactants like Tween 80 (T80), Pluronic F68, Brij 35 or Vitamin E-TPGS, which have been studied in some depth over the last few years. This type of strategy takes advantage, for example, of the adsorption of apolipoproteins across blood plasma onto the T80 nanoparticles' surface, promoting the recognition by LDL receptors in the brain capillary endothelial cells [5]; moreover, both neurons and glial cells express LDL receptors [6]. On the other hand, the term 'theragnosis' is defined as any 'material that combines the modalities of therapy and diagnostic imaging' into a single package [7]. In this perspective, we suggest a new combination approach, based on the association of doxorubicin (DOX) and SPION (superparamagnetic iron oxide nanoparticles) within

the surfactant-coated PNP. DOX was chosen as the vectorized drug because it is an antineoplastic agent widely used in the treatment of various cancers which, although toxic against glioma cells, does not cross the BBB [8, 9]. SPION were selected since they can be monitored by magnetic resonance imaging (MRI) and, moreover, they can be targeted to tumor with the use of magnets [10]. These theranostic SPION-DOX PNP would thus reflect the real-time characteristics of the tumor in each patient and could allow for earlier disease detection, more accurate prognostic information and an enhanced ability to monitor the efficacy of treatment [11]. Besides, the evaluation of the NP accumulation in healthy tissues would allow us to assess the risk of patients developing off-target side effects or to screen patients who are likely to respond positively to the treatment [12].

In this chapter, we study the role of the different surfactants in crossing the BBB by an *in vitro* model with the human hCMEC/D3 cell line. However, in real patients, actively or passively targeted NP would need time to reach the tumor area. During this time they could be affected by the immune system taking them out from the bloodstream, before reaching the tumor. Moreover, within and around malignant brain tumors a large number of macrophages and activated microglia have been reported to be present [11]. So, in order to improve the pharmacokinetic and biodistribution of DOX, an external magnetic field was used after an i.v. injection of SPION-DOX PNP in mice and the ability of DOX-SPION PNP to cross the BBB was studied, in comparison with a control group in which a magnet was not used.

## **Material and methods**

### **1. SPION-DOX PNP synthesis and characterization**

SPION-DOX PNP were formulated by the simple emulsion and solvent evaporation method. Briefly, the SPION were covered with oleic acid (10 mg of iron/mL of oleic acid) by a 24 hour incubation in continuous agitation, and after that, they were washed and dissolved in dichloromethane. Separately, 1 mg of DOX was

dissolved overnight in 0.8 mL of a mixture of triethylamine and ethyl acetate in the proportion 1: 1000. The follow day, 50 mg of polymer poly (Lactic-co-Glycolic Acid) (PLGA) (Resomer® RG 503H, PLGA 50:50) were dissolved in the same solution of DOX and 0.2 mL of SPION covered with oleic acid were added. All of this was poured into 2 mL of 1 % surfactant (T80, Brij-35, Pluronic F68 or Vitamin E-TPGS) and sonicated for 20 seconds at 20 Watts in a Microson Ultrasonic Cell Disruptor XL (Branson sonifier 450, Branson Ultrasonics corp., EEUU). Next, the sonicated solution was poured into an aqueous solution of 0.3 % surfactant (T80, Brij-35, Pluronic F68 or Vitamin E-TPGS) and 0.4 % polyvinyl alcohol (PVA) in continuous agitation for 1.5 hours. Once the organic solvent was evaporated, the formulation was washed three times (centrifugations at 17000 g for 10 min at 4°C) and lyophilized along with 37% (w/w with respect to the amount of PLGA) of the cryoprotector trehalose.

SPION-DOX PNP size and surface charge were characterized using a Zetasizer Nano ZS (Malvern Instruments, UK), and the size of the NP was confirmed by TEM images. The DOX loading efficiency was determined fluorimetrically in a Tecan GENios microplate reader (Tecan Group Ltd, Maennedorf, Switzerland) at an excitation and emission wavelength of 485 and 580 nm. In addition to this, the encapsulation of SPION was calculated and analyzed spectrophotometrically ( $\lambda=300$  nm) using a microplate PowerWave XS Microplate Spectrophotometer (BioTek). Fluorescence and absorbance were converted into  $\mu\text{g/mL}$  DOX or SPION using a calibration curve previously set.

## **2. *In vitro* studies**

### **2.1 Cell culture**

The immortalized human brain capillary endothelial cells hCMEC/d3 were purchased from CELLutions Biosystems inc. and grown in EBM-2 medium (Lonza) supplemented with 5 % FBS and 1 % (v/v) penicillin-streptomycin from Gibco®; hydrocortisone (1.4  $\mu\text{M}$ ), L-ascorbic acid (5  $\mu\text{g/mL}$ ) and basic FGF (1 ng/mL) from Sigma, and chemical defined lipid concentrate (1/100) and HEPES (10 mM) from

Fisher Scientific. Cells were cultured at 37°C and 5% CO<sub>2</sub> in flasks coated with 0.1 mg/ml rat tail collagen type I (BD Biosciences) for 1 h at 37 °C. For culturing, every 3-4 days when cells were approximately 80 % confluent, a 1:5 split was performed.

## 2.2 BBB permeability

Human brain microvascular endothelial cell line (hCMEC/d3) between passage 25 and 35 was used in all studies. In order to be sure that the DOX did not disrupt the barrier (due to toxicity), before assessing the permeability assay, a safe DOX dose was fixed by the means of the cell proliferation assay MTS (CellTiter 96® Aqueous One Solution Cell Proliferation Assay). For that, 20 x 10<sup>3</sup> cells/well were seeded in a 96-well plate and incubated at 37 °C and 5 % CO<sub>2</sub>. The following day, the toxicity of DOX, SPION and SPION-DOX PNP on the hCMEC/D3 cells was tested using an increasing concentration of DOX (0-50 µg/mL) for 4 hours. The highest harmless DOX concentration at 4 hours was 5 µg/mL DOX, a dose chosen for the permeation studies. After that, the permeability to free and encapsulated DOX was measured on hCMEC/D3 cells. For this, 5 X 10<sup>4</sup> cells/cm<sup>2</sup> were seeded and grown in 6-multiwell collagen pre-coated Transwell® (collagen-coated 0.4 µm pore PTFE membrane insert, Corning Life Sciences). Cells were grown for 7-10 days up to a Transendothelial Electrical Resistance (TEER) value of 120 Ω·cm<sup>2</sup> [13, 14], measured with a Millicell ERS-2 Epithelial Volt-Ohm meter (Millipore). Additionally, the cell monolayer was periodically inspected under a microscope. Once the monolayer was formed, the culture medium was replaced in the upper and lower chambers and the non-toxic DOX concentration of 5 µg/mL was added to the upper compartment. After 2 and 4 h, the medium in the lower chamber was collected and analyzed fluorimetrically for DOX determination. The initial quantity of DOX added to the upper compartment was considered 100% of DOX and the amount of DOX permeated was presented as the percentage of this initial quantity.

At the end of the experiment, the permeability to the highly hydrophilic and low molecular weight Lucifer yellow was calculated to confirm the integrity of the membrane after the DOX passage, as previously described by Poler B. *et al.* [15, 16]. To do this, the culture medium was removed and cells were washed twice with

Phosphate-Buffered Saline (PBS) before adding 20  $\mu\text{M}$  LY in the upper chamber for 1 h. The amount of LY in the lower chamber was measured fluorimetrically from 200  $\mu\text{L}$  collected at 0, 20, 40 and 60 minutes, at the excitation and emission wavelengths of 485 nm and 535 nm. Considering the values reported by others [17], only those monolayers with LY permeability below  $1.7 \times 10^{-3}$  cm/min were considered.

### 2.3 BBB cell internalization

The internalization of DOX from the SPION-DOX PNP was also studied in the hCMEC/D3 cell line using fluorescence microscopy (Zeiss, 120 Libra). To this end,  $1 \times 10^5$  cells were seeded on sterile glass coverslips placed inside a 24-well plate. After 24 h, the cells were treated for 4 h with 30  $\mu\text{g}/\text{mL}$  of DOX free or encapsulated inside the different types of NP. After the treatment, the cells were fixed with p-formaldehyde 4 % (5 min), permeated with Triton 0.1 % (10 min) and stained with DAPI (1:1000; 5 min). Cells were washed three times and the slides were prepared with a drop of fluorescence mounting media to be analyzed microscopically.

### 3. Complement activation (CH50) study

The activation of the complement system by the NP was quantified *in vitro* by the CH50 test. Complement consumption was assessed by calculating its residual hemolytic capacity after incubation with the NP. Specifically, the experiment consisted of exposing a fixed number of sheep erythrocytes [sensitized with rabbit (anti-sheep) erythrocyte antibodies (Eurobio, Courtaboeuf, France)] to proteins of normal human serum (NHS) previously incubated with SPION-DOX PNP. Then the systematic lysis of the erythrocytes was calculated from the hemoglobin released, which can be used as a dye in a colorimetric titration [18].

For testing, various NP suspensions (from 0 to 5 mg/mL) were added individually to 0.1 mL of NHS (0.4 mL final volume). After 1 h at 37 °C under gentle stirring, the suspensions were diluted (1:25 v/v) in VBS2+ (Veronal Buffered Saline containing 0.15 mM  $\text{Ca}^{2+}$  and 0.5 mM of  $\text{Mg}^{2+}$ ) and 0.2 mL of sensitized erythrocytes ( $10^8$  cells/mL) were added. After a second 45 min incubation at 37 °C with gentle stirring,

the reaction was stopped, adding ice-cold NaCl solution (0.15 M) and centrifuging 10 min at 800 g. As non-lysed erythrocytes precipitate, the absorption at 415 nm of the supernatant was determined using a microplate reader (Multiskan Anscnt, Labsystems SA, Cergy-Pontoise, France). A control of the spontaneous erythrocyte hemolysis due to NP alone was also measured. Finally, the amount of serum required to hemolyze 50 % of the erythrocytes added (CH50 units) was calculated. The results were plotted as the consumption of CH50 units vs. the NP surface area [19].

#### **4. *In vivo* studies**

Animal care and use were in accordance with the regulations of the French Ministry of Agriculture and approved by the Pays de la Loire Ethics in Animal Experimentation Committee under project number 01858.03. A scheme of the *in vivo* studies performed can be followed in the Figure 1.

##### **4.1 Intracranial inoculation of GBM cells**

Tumor implantation was performed via the stereotaxic inoculation of the human U87 glioma cells in 8 weeks old female nude mice. As described previously [20], mice were anesthetized with Xylazine/Ketamine (50/30 UI; 20  $\mu$ L/g) and placed in a stereotaxic holder with a heating pad to maintain the appropriate physiological temperature. First, a hole in the skull was opened to, secondly, inject 4  $\mu$ L (at 0.5  $\mu$ L/min) suspension of  $8 \times 10^4$  glioma cells, on the fixed coordinates according to the bregma: 0.5mm anterior, 2.5mm right lateral, and 4 mm depth. After surgery, mice received a single 30  $\mu$ g/kg subcutaneous injection of Buprecare (buprenorphin). *In vivo* experiments were performed 9-10 days later, after checking by MRI that the tumor had developed. The different groups of mice were formed maintaining an equitable distribution in function of tumor sizes.

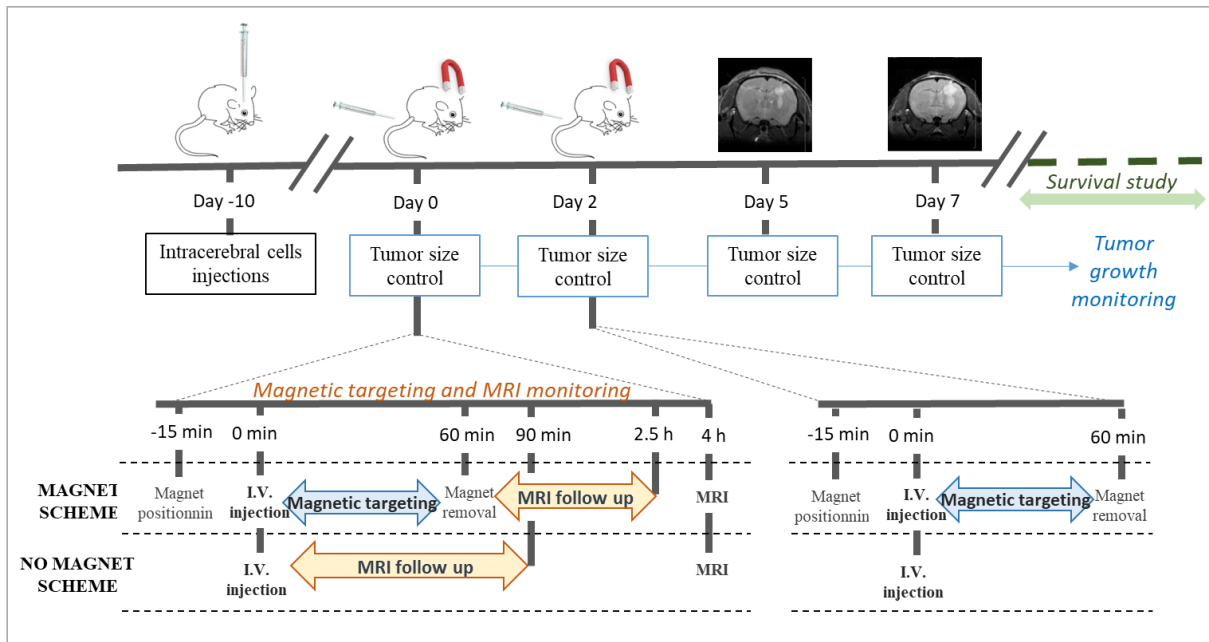


**Figure 1:** Diagram of the *in vivo* studies performed.

## 4.2 Magnetic targeting and MRI monitoring

To assess the magnetic and contrast capability of SPION-DOX PNP, 12 tumor-bearing animals were equitably divided into two treatment groups: NP targeted using a magnet (n=6) and NP not targeted using a magnet (n=6). Each group received intravenously 16 mg/kg of Fe and 5 mg/kg of DOX in SPION-DOX PNP synthesized with surfactant T80 and reconstituted in physiological serum (0.2 mL). As previously described [21], an external 0.4-T (190 Tm<sup>-1</sup> magnetic field gradient) targeting magnetic field, 8 mm diameter/4 mm high disk-shaped neodymium magnets (Supermagnete, Gottmadingen, Germany) were placed onto the top of the head of the mice for 1 hour. During the MR protocol, mice were anesthetized with 0.5 % isoflurane and respiration was monitored. Furthermore, animal body temperature was maintained throughout the experiment at 36.5–37.5 °C by using a feedback-regulated heating pad.

MRI was performed using a 7T scanner (Biospec 70/20 Avance III, Bruker Wissembourg, France) equipped with BGA12S gradient system (675 mT/m). Prior to



injection, animals were controlled to assess tumor sizes using a Rapid Acquisition with Relaxation Enhancement sequence (TR = 3200 ms; TE = 33 ms, RARE factor 4, matrix size = 256 x 128; FOV = 2 x 1 cm, slice thickness = 1 mm). A multiple gradient echo image, using the same geometrical parameters were also used to produce T2\* maps prior injection; susceptibility weighted images (SWI) were also collected before NP injection (TR=350 ms; TE=18 ms; Slice thickness 1 mm; matrix size=384 X 192; FOV=2 x 1 cm). Half of each group (3 mice/group) was continuously analyzed by MRI for 2.5 hours and the other half (the rest 3 mice/group) was imaged only 4 hours after the injection. SPION-DOX PNP deposition was qualitatively observed using susceptibility weighted images (SWI) and quantitatively objectivate from the multiple gradient echo set of images by calculating the relaxation rate of transverse magnetization ( $R2^*=1/T2^*$ ).

### 4.3 Efficacy studies

To determine the efficacy of the treatment with SPION-DOX PNP, tumor-bearing mice were treated twice with a time interval of 48 h by intravenous injection of SPION-DOX PNP (at a DOX dose of 5 mg/kg). One group was exposed to 1 h external magnet targeting after each injection (n=7), the other being unexposed to the external magnet (n=5). To monitor the efficacy of the treatment, tumor size were calculated prior to the first injection, two days later, i.e. prior the second injection and then on days 5 and 7. Afterwards, the tumor volume growth curves were fitted with an exponential function using the least squares methods; and then the time constant of the exponential was converted into a doubling time value to compare the two groups [20]. Finally, to assess the survival, the body weight and mobility of each mouse was measured daily. Survival time was calculated from day 0 (tumor inoculation) to the day of sacrifice when experimental limits points were reached.

### 5. Statistical analysis

All results are expressed as mean  $\pm$  standard deviation (SD). To demonstrate statistical differences, two-way ANOVA, unpaired two-tailed t-test or log-Rank

(mantel-Cox) survival tests were performed, using the software GraphPad Prism 5 for Windows.

## Results

### 1. SPION-DOX PNP characterization

As shown previously, the NP developed had a uniform size distribution for all surfactants used; their physiochemical characteristics are detailed in Figure 2A. The mean size was around 219 nm by DLS and 143 nm measured on TEM images, and a representative TEM image is presented in Figure 2B. In this context, the amount of Fe and DOX encapsulated in SPION-DOX PNP was around 10  $\mu\text{g}/\text{mg}$  of DOX and 20  $\mu\text{g}/\text{mg}$  of Fe, in both cases corresponding to more than 80 % encapsulation efficacy.

A) Surfactant used	Size		PDI (DLS)	Z potential (mV)	DOX ( $\mu\text{g}/\text{mg}$ form.)	Fe ( $\mu\text{g}/\text{mg}$ form.)
	DLS	TEM				
T80	227,4 $\pm$ 18,2	116,2 $\pm$ 37,4	0.066 $\pm$ 0.021	-13.8 $\pm$ 3.3	11.2 $\pm$ 1.9	17.8 $\pm$ 1.8
Brij- 35	209.1 $\pm$ 26.5	120,3 $\pm$ 38,4	0.077 $\pm$ 0.019	-16.8 $\pm$ 2.9	10.7 $\pm$ 0.8	20.3 $\pm$ 1.5
Pluronic F68	211.9 $\pm$ 7.7	109,2 $\pm$ 27,5	0.076 $\pm$ 0.017	-15.8 $\pm$ 2.1	10.7 $\pm$ 0.9	17.7 $\pm$ 3.9
Vitamin E- TPGS	227.9 $\pm$ 55.8	226,3 $\pm$ 57,9	0.107 $\pm$ 0.019	-17.8 $\pm$ 1.7	11,1 $\pm$ 2,8	21.9 $\pm$ 3.6

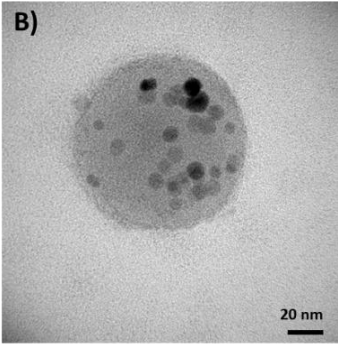


**Figure 2:** A) Characterization of SPION-DOX PNP developed with 4 different surfactants (T80, Brij-35, Pluronic F68 and Vitamin E-TPGS): size, polydispersity (PDI) and Z potential measured by DLS; size of minimum 150 NP measured on TEM images; and DOX and Fe loading inside the PNP. B) TEM image of a representative SPION-DOX PNP synthesized with the surfactant T80.

### 2. *In vitro* studies

## 2.1 BBB permeability

The brain is protected from exogenous and endogenous substances and from harmful organisms by the dynamic barrier BBB. The BBB is mainly formed by brain capillary endothelial cells, although its function is regulated by various cells, including astrocytes, neurons and pericytes [2, 22]. The rapid vessel formation accompanying the growth of the tumor leads to the so-called “blood brain tumor barrier” (BBTB) which is more permeable than the BBB. Nevertheless, therapeutics are rarely effective in patients with brain tumors because the permeability of the BBTB is still selective [8, 23]. The utilization of the surfactants T80, Brij-35, Pluronic F68 and Vitamin E-TPGS was selected as a strategy to facilitate the NP permeation through the BBB [24]. For this reason, the permeation through the endothelial hCMEC/D3 cell monolayer, assumed as a model of the BBB, of the SPION-DOX PNP developed with different surfactant was used to select the one with the best penetration. This assay was performed using Transwell® devices in which the cells were grown up to monolayer formation and then free or encapsulated DOX was placed in the upper compartment. The dose of 5 ug/mL (9.2 μM) was chosen since it had been found not to cause any cytotoxicity to hCMEC/D3 cells in a previous MTS assay. The quantitative fluorimetric analysis of DOX in the lower compartment at 2 and 4 hours after 3 independent experiments is shown in Figure 3. As can be seen, except in the case of Vitamin E-TPGS, more than 90 % of DOX, either free or encapsulated, crossed the transwell membrane without cells after 4 hours (Figure 3A). Therefore, no interaction of DOX, T80, Brij-35 and Pluronic F-68 with the membrane was considered. With the cellular monolayer formed on the transwell membrane (Figure 3B), Brij-35 was the one with the highest permeability and Vitamin E the one with the lowest permeability, since this last surfactant interacts with the membrane (Figure 3A). However, the amount of DOX that permeated through the cellular monolayer did not significantly differ between the different types of SPION-DOX PNP NP, or between free or encapsulated DOX (Figure 3B). Unfortunately, this *in vitro* model was not able to detect the better coating strategy.

As it has been demonstrated that the permeation of DOX is time and dose dependent in this BBB model [8, 17], higher doses or longer times should be tested. However,

these conditions will break the integrity of the BBB, as it was confirmed by a permeability study using lucifer yellow (a low molecular weight paracellular diffusion marker). Moreover, the prolongation of the transport studies may raise issues concerning the validity of the *in vitro* model. Nevertheless, Battaglia L. *et al.* studied the BBB permeation to DOX using 0.1 and 1  $\mu\text{M}$  DOX concentrations for 3 and 24h-experiments [8] and Pinzón-Daza ML. *et al.* used 5  $\mu\text{M}$  DOX concentration for a 3h-experiment, both using the same BBB model and obtaining differences between the treatments studied. Therefore, as these results are not in agreement with ours, the route of SPION-DOX PNP internalization was tested (below) in order to explain the equal BBB permeation to all treatments.

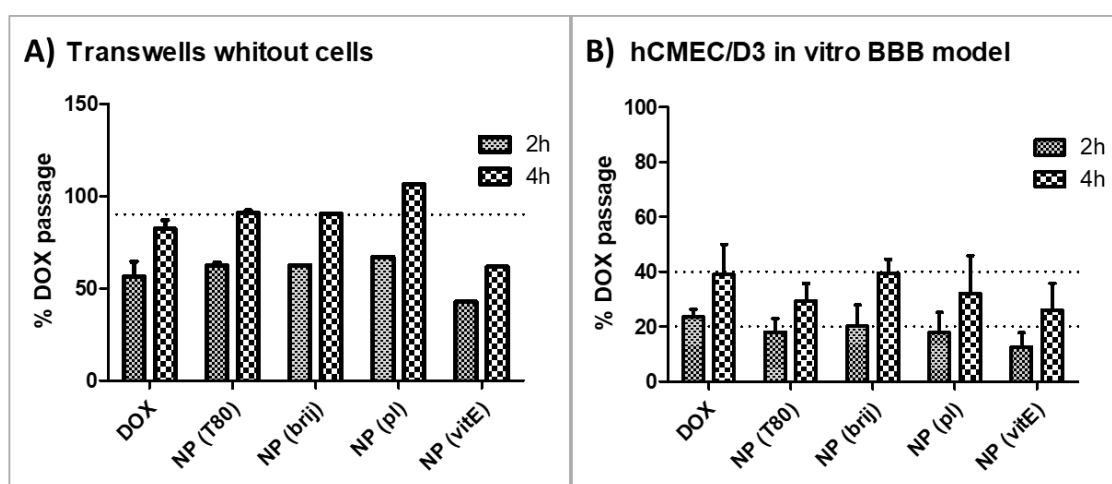


**Figure 3:** DOX permeated through A) Transwell membranes without cells and B) hCMEC/d3 cell monolayers; percentages with respect to the initial amount added in the upper compartment. Free DOX or DOX encapsulated inside SPION-DOX PNP (developed with the surfactants T80, Brij-35, Pluronic F68 or Vitamin E-TPGS) are shown.

## 2.2 BBB cells internalization

At the BBB, the paracellular route is truly restricted and, consequently, nanocarriers enhance brain delivery by promoting any of the transcellular pathways [25]. Receptor-mediated transcytosis should be the main pathway used by our PNP due to the surfactants' coatings, which competitively inhibit substrate binding and efflux pump ATPase, and alter membrane fluidity [26, 27]. In this route, the complex formed by the NP and the cellular receptor is invaginated into the cytoplasm as a vesicle, called endosome. Then, the acidification of the endosome leads to the breakage of this complex releasing the NP, which can cross to the other side of the membrane thereby entering the brain. In our case, this acidic environment of the endosome could release the drug from the NP, mostly entering the nucleus of the endothelial cell instead of crossing to the other side of the Transwell® device. For that reason, a microscopy study of the NP internalization inside the hCMEC/D3 cells was performed. In Figure 4, it can be seen that after 4 hours of treatment with free or encapsulated DOX, the fluorescence drug (in red) was located inside the nucleus (in blue) and not in the cytoplasm, thus confirming our hypothesis.

Taken all together, the release of the drug inside the BBB cells' lysosomes prevented its monolayer passage and it was not possible to identify differences between the different NP-coatings. It should be mentioned that even though the DOX was mainly released inside the endothelial cell, this is an *in vitro* static study that might not be correlated with what happens *in vivo*.

## 3. Complement activation (CH50) test

Before reaching the BBB, other agents have to be bypassed by the NP. The complement system is an important component of the innate immune system that comprises more than 30 proteins. Unfortunately, whenever synthetic particles are injected into the bloodstream, the complement system is activated [28, 29]. Therefore, complement activation experiments were a major concern in our studies.

Specifically, the first event that takes place when NP enter the blood stream is opsonization, which consists of protein adsorption onto the nanoparticle surface. This opsonization depends on NP physico-chemical properties, such as their size, charge or surface composition [30]. In this way, the protein corona formed determines the *in vivo* physiological responses, including pharmacokinetics, biodistribution, cellular uptake and intracellular trafficking [12]. At that point, if the protein corona is rich in opsonins, it can trigger the recognition and clearance by macrophages that rapidly intercept and guide the NP to the liver and the spleen [29, 31]; while with a protein corona of dysopsonin proteins (such as apolipoproteins and albumin), NP can avoid phagocytic uptake, interact with the BBB and reach the GBM [2, 12, 24].

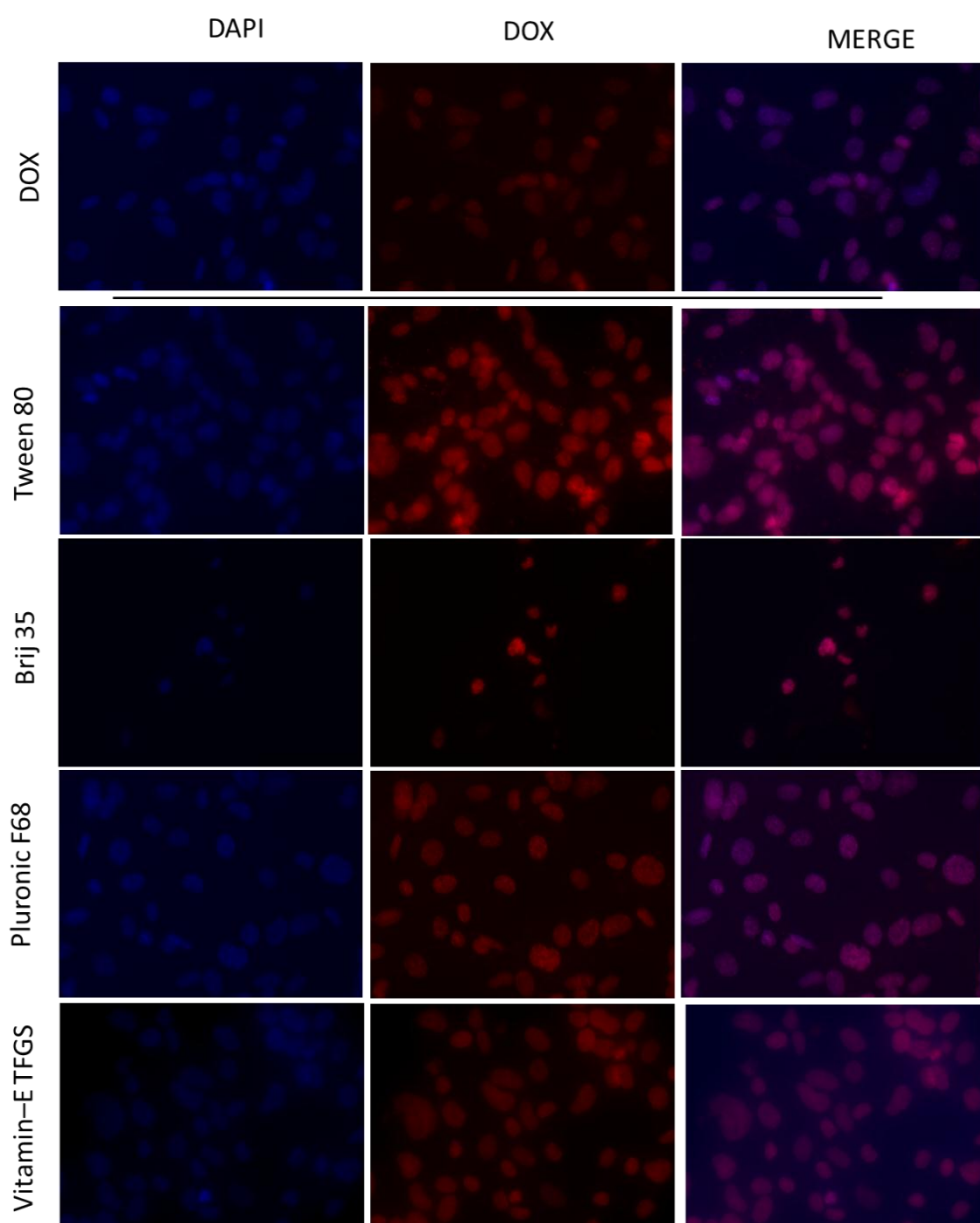


**Figure 4:** Fluorescence microscopy images of hCMEC/D3 cells uptake of DOX and SPION-DOX PNP formulated with the surfactants T80, Brij-35, Pluronic F68 or Vitamin E-TPGS. Cells were cultured for 24 h, followed by incubation with the treatments for 4 h at 37 °C and 5 % CO<sub>2</sub>. DAPI indicates nucleus location in blue and DOX fluorescence is detected in red.

The consumption of CH50 units was measured at a fixed amount of erythrocytes in human serum previously incubated at increasing NP concentrations. Figure 5 shows CH50 consumption as a function of the NP surface area for SPION-DOX PNP synthesized with T80, Brij-35, Pluronic F68 or Vitamin E-TPGS. As expected, an increase in the CH50 consumption with the amount of NP, when the surface area in contact with the proteins is increased, is observed. Unfortunately, this increment is indicative of complement activation. In detail, the results revealed a CH50 consumption of around 80-90 % for a NP surface area around 350 cm<sup>2</sup>/mL in the case of the SPION-DOX PNP made with the surfactants T80, Brij-35 and Pluronic F68; whereas this was around 40 % in the case of Vitamin E-TPGS. Vitamin E-tocopheryl polyethylene glycol succinate (TPGS) is a derivative of the natural vitamin E ( $\alpha$ -tocopherol) that comprises a lipophilic alkyl tail and a hydrophilic polyethylene glycol (PEG) chain [32, 33]. It is acknowledged that PEG coating provides NP with a more hydrophilic surface that can reduce plasma opsonization via hydrophilicity and steric repulsion [31, 34–36]. For instance, Cieslak *et al.* obtained a total CH50 consumption of around 4 times less with PEG-modified liposomes than with non-modified liposomes [19]. Nonetheless, in our case, Vitamin E-TPGS NP seem to have a better complement consumption at low NP surface areas but, in the end, 100 % consumption was found for a surface area of around 500 cm<sup>2</sup>/mL, similar to the rest of surfactants. In agreement with our results, Vrignaud S *et al.* had a CH50 consumption of around 90 % for a NP surface area of 300 cm<sup>2</sup>/mL with the positive complement control PMMA NP [37]. And Bustele K. *et al.* obtained 100 % consumption for a very low surface area of 100 cm<sup>2</sup> for protonated micelles, consistent with strong complement activation by the polycations. However, they solved this high consumption by modifying the micelles with a novel biotinylated triblock copolymer [38]. Overall, our NP also had a high complement consumption

[39, 40], so a rapid bloodstream clearance by the liver and the spleen was expected in future *in vivo* studies.

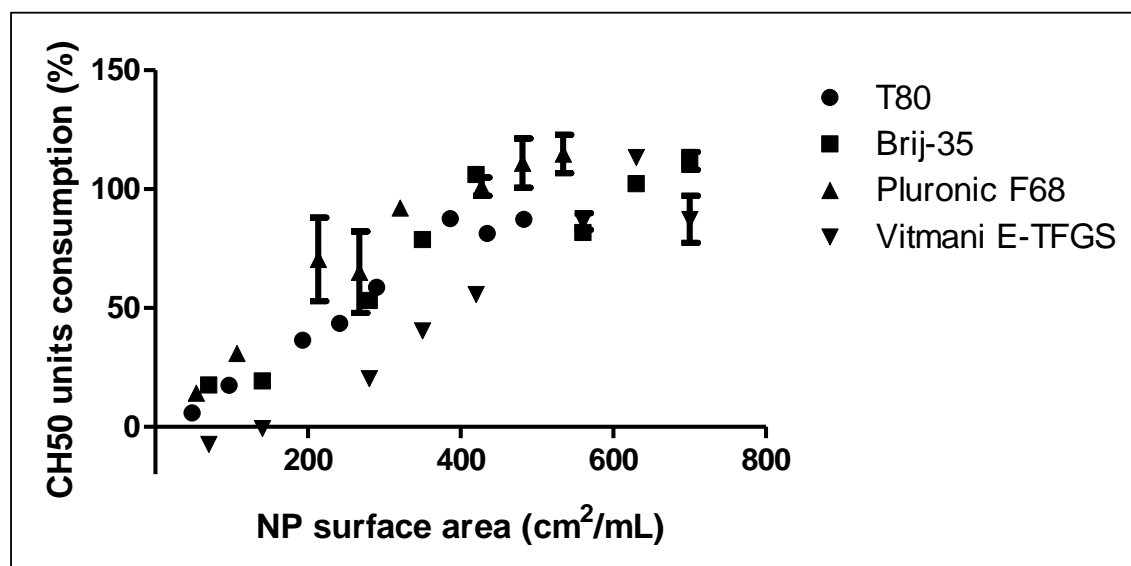


**Figure 5:** SPION-DOX PNP complement activation. CH50 unit consumption versus NP surface area of the 4 different NP developed with the surfactants T80, Brij-35, Pluronic F68 or Vitamin E-TPGS.

#### 4. *In vivo* studies

##### 4.1 Magnetic targeting and MRI monitoring

On the basis of the above results, potent NP guiding to the tumor was required; therefore, taking advantage of the magnetic properties of our NP, the use of an external magnetic field was selected as the best alternative to ensure correct targeting of the treatment. An orthotopic U87 glioma model in female nude mice was used to evaluate whether the magnetic field influenced or not the retention of the NP inside the tumor. For that, we compared by MRI the GBM deposition of non-targeted and magnetically-targeted SPION-DOX PNP (at 16 mg Fe/kg body weight). NP developed with the surfactant T80, the surfactant coating most widely studied in the



literature [26, 41, 42] and the one used in our previous study [43], was chosen for these *in vivo* studies.

#### *Continuous monitoring*

As can be seen in the Figure 6, targeted NP were more likely to be retained in the tumor area. Non-targeted NP could be detected in the tumor tissues immediately after the treatment (15-20 minutes after administration); however, 60 minutes later this contrast disappeared (Figure 6A). In contrast, targeting the NP with an external magnet for one hour led to a significant accumulation at the tumor level that last throughout the 2.5 h (Figure 6B). This accumulation was objectivated by R2\* relaxation calculation in the tumor and the non-tumor bearing hemisphere of mice (Figures 6C and E). In mice treated with NP but not targeted with magnet (Figure 6C) we observed that during the first minutes after administration the tumor tissue had a higher R2\* than the control brain; however, after one hour both had the same value. The higher vascularity of the tumor could explain this greater contrast in the short term; NP are in the bloodstream and are rapidly cleared by the mononuclear phagocyte system (MPS). This was confirmed by acquiring transversal TE images over the liver and spleen of one mouse that revealed a high contrast and therefore accumulation of SPION-DOX PNP (Figure 6D). Close analysis of R2\* curves with times (Figure 6E) showed that after 15-20 min after magnet removal (but 75-80 minutes after NP injection), the R2\* of both the tumor and the control tissues were still increased as compared to the values measured before injection. This indicates that the magnet retained the SPION-DOX PNP throughout the entire brain area. Meanwhile, once the NP of the cerebral bloodstream receded, SPION-DOX PNP extravasation was observed only at the tumor region, the R2\* value in the healthy region decreasing rapidly whereas the R2\* in the tumor area remained higher for the entire experimental time. This sustained difference between both tissues during the entire experimental period was found to be very significant in a two-tailed ANOVA statistical study ( $p = 0.0017$ ). As previously described in detail, it would be possible for a SPION-DOX PNP to cross the BBTB after being trapped within its endothelial cells due to a SPION mutual dipole-dipole attraction developed in a continuous magnetic field, which would lead to NP internalization by the malignant cells [21].

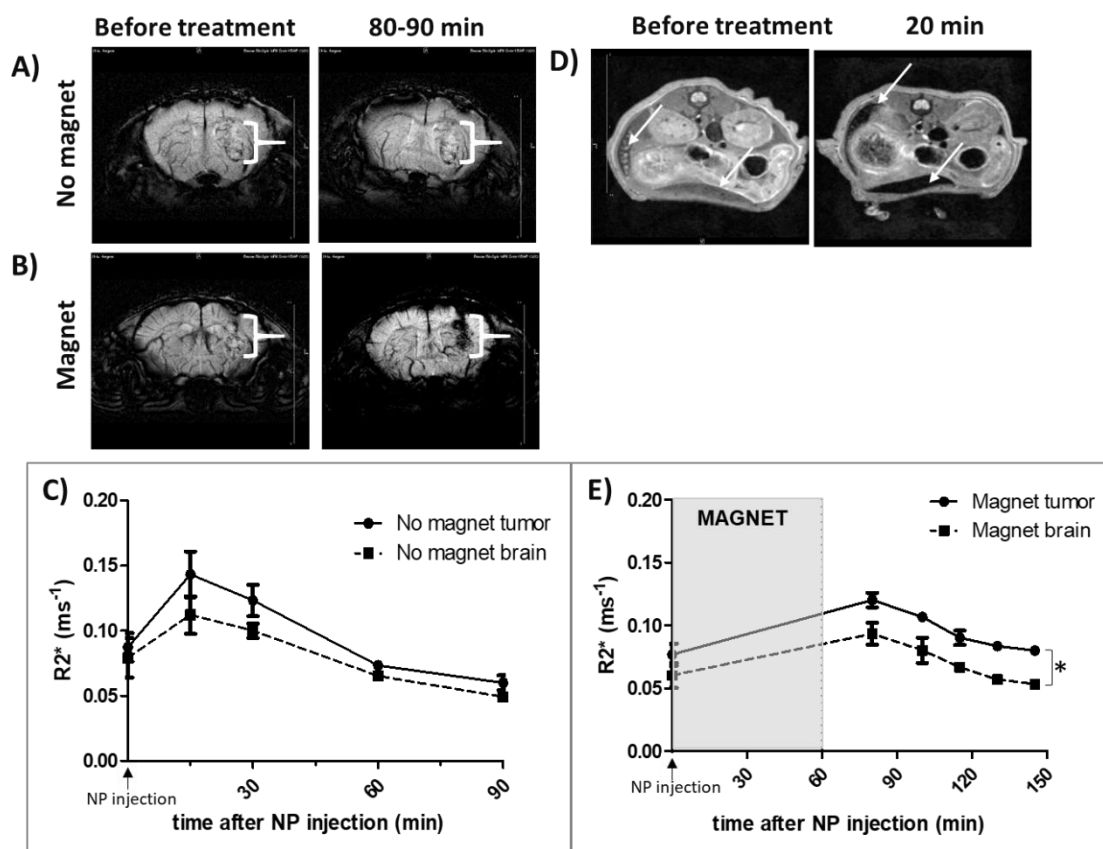


**Figure 6:** NP brain uptake evaluation in tumor-bearing mice. A) Brain SWI images before and 80 minutes after i.v. injection of SPION-DOX PNP. B) Brain SWI images before and 90 minutes after i.v. injection of magnetically targeted SPION-DOX PNP. C) Relaxation rate ( $R2^*$ ) in tumor and non-tumor tissue after i.v. injection of SPION-DOX PNP ( $n = 3$ ). D) Body transverse T2 images before and after i.v. injection of SPION-DOX PNP ( $n = 1$ ). E) Relaxation rate ( $R2^*$ ) in tumor and non-tumor tissue after i.v. injection of magnetically targeted SPION-DOX PNP; significant differences detected (statistical study ANOVA 2 tails ( $P = 0.0017$ )). White brackets indicate the tumor location, plain white arrow the liver and dash white arrow the spleen.

### Monitoring at 4 hours

To evaluate the long/median term retention of the NP in the GBM with external magnetic targeting, SWI images were acquired 4 hours after i.v. injection in 3 mice (Figure 7). Results appeared heterogeneous as in one mouse the susceptibility effects of NP were still observed at the tumor site (Figure 7A), in another there was a slight

susceptibility effect (Figure 7B) and in the third one, no effect was detected (Figure 7C). Therefore, although this should be studied in more detail, 4 hours seemed to be the limit of NP retention when intravenous SPION-DOX PNP were directed to GBM with a limited one hour of magnet guidance. No contrast was detected in non-targeted tumors at 4 hour (n=3).

Thus, all results demonstrated the effectiveness of magnetic targeting to enhance preferential accumulation of the SPION-DOX PNP within brain tumors in an amount properly perceptible by MRI; and not within the healthy cerebral areas. Moreover, this study establishes the effectiveness of SPION-DOX PNP as contrast agent *in vivo* as well as the usefulness of MRI imaging in non-invasive *in vivo* monitoring.

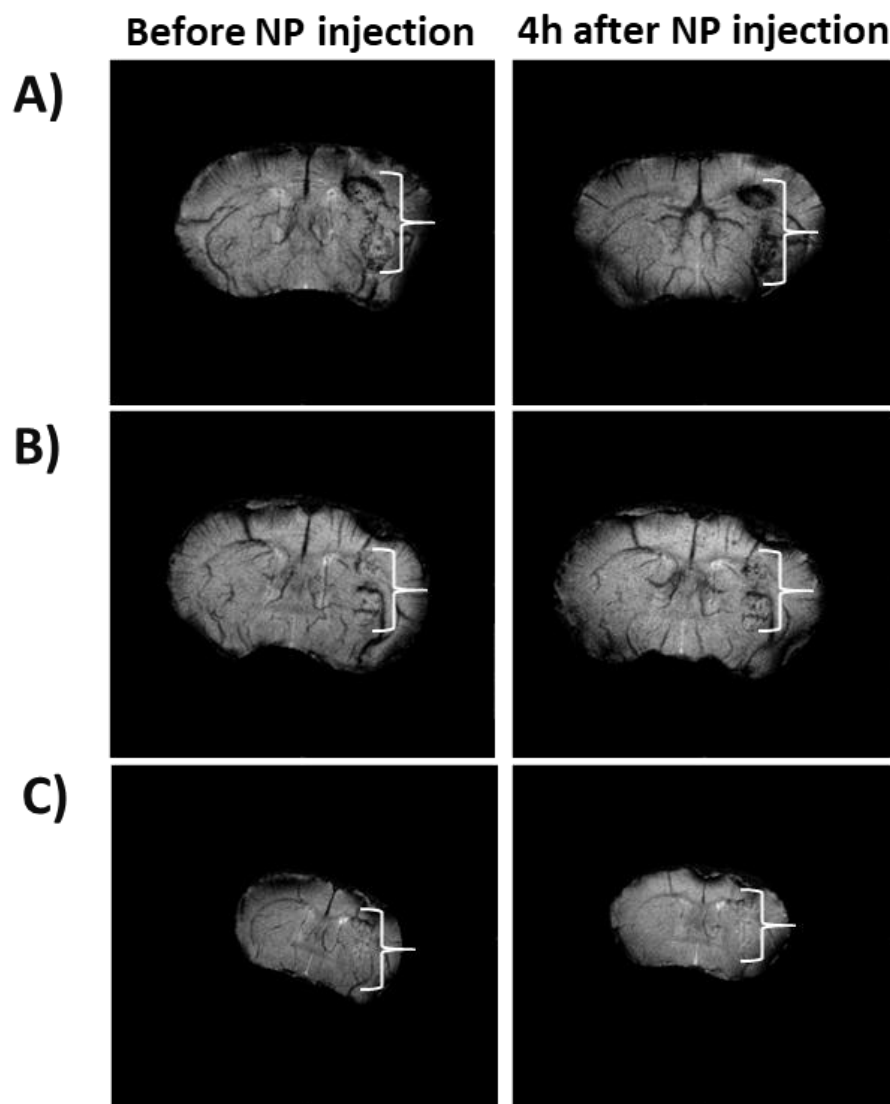


**Figure 7:** SWI images of 3 magnet-exposed GMB before and 4 h after i.v. injection of SPION-DOX PNP. White brackets indicate tumor location.

## 4.2 Efficacy studies

The therapeutic effectiveness of SPION-DOX PNP magnetically targeted to the brain in an orthotopic U87 nude mice was evaluated. The final goal was to investigate whether magnetic targeting could further improve the efficiency of DOX delivery and tumor growth inhibition as well as survival rates. For that, SPION-DOX PNP (at 5 mg DOX/kg body weight) developed with the surfactant T80 were administered twice on alternate days. In one group the NP were targeted with the use of 1 hour of magnet (n=7) and in a second group the NP were not targeted magnetically (n=5).

### *Tumor growth monitoring*

To assess treatment efficiency, tumor progression was monitored by MRI using T2-weighted imaging (Figure 8A and B); from which the tumor doubling time was calculated (Figure 8C). SPION-DOX PNP magnetically-targeted tumors needed  $4.4 \pm 1.5$  days to double their size, whereas non-targeted tumors doubled in size in only  $2.3 \pm 1.2$  days without significant improvement as compared to results reported in the literature [20]. Besides, the slower growth of the tumor when treated with magnetically-targeted SPION-DOX PNP was significantly different (two-tailed unpaired t-test study ( $P < 0.05$ )). These results indicated a therapeutic effect in the tumor as well as the enormous potential of the magnetically targeted-SPION-DOX PNP to deliver DOX to glioma cells, as free DOX displays very poor penetration into gliomas and cannot gain access to brain tumor cells [44]. Therefore, like other authors [45], we demonstrate therapeutic benefits based on the superparamagnetic characteristics of SPION that allow guidance by an external magnet and simultaneously provide contrast in MRI.

### Survival rate

As expected, magnetically targeted treatment slightly prolonged the median survival time despite non-significant (Figure 8D). Indeed, the survival rates of mice with magnetically targeted NP was slightly higher than the untargeted group, with a median survival of 31 and 28 days, respectively. To improve the survival rates, a larger number of doses [46–48] or a longer magnet exposure [45, 49] could be used to reach a higher DOX concentration in the tumor. Importantly, contrary to what is usually thought, intra-tumor complement activation could help tumor growth and progression. As our NP activate the complement, we should also consider whether the nanocarriers eventually shift the balance in favor of tumor growth [50, 51]. On the other hand, the similar survival rate for both treatments could also be explained by the fact that non-magnetically targeted NP could be retained within the tumor area in a non-detectable concentration by MRI, but would still be therapeutically effective. Unless according to the high proliferative rate of U87-glioma cell [20] and the two-doses therapeutic schedule explored, checking the therapy impact through mice survival is not fine enough. Therefore, in future survival studies free DOX control should be added, as in the study by Sun Z. *et al* who obtained median survival times of 17 days with free DOX and 35 days with their dual targeted DOX NP (single treatment of 10 mg DOX/kg) [46].

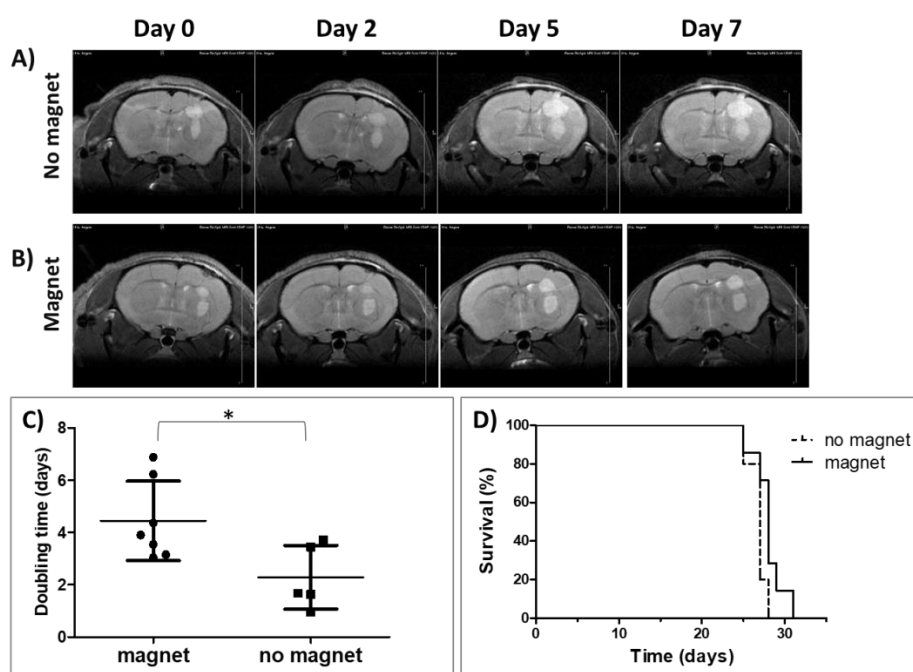


**Figure 8:** Tumor bearing mice brains intravenously treated with SPION-DOX PNP (2 times, in alternative days); in one group the NP were directed magnetically (n=7) and in other group the NP were not directed with a magnet (n=5). A, B) T2-weighted images on days 0, 2, 5 and 7 after the first injection C) Representation of the time needed for the tumors to double their size; significant difference detected between magnet-exposed GBM and non-targeted tumor (unpaired two-tailed t-test study ( $P < 0.05$ )). D) Survival rates.

## Conclusions

The objective of this study was to show that these new theranostic SPION-DOX PNP could provide an interesting solution for treating and monitoring GBM. Although these investigations focus on the surfactant covering of the PNP, rapid endosomal DOX release could explain the absence of differences in the *in vitro* permeation through the hCMEC/D3 cell monolayer. On the other hand, complement activation was confirmed when SPION-DOX PNP coated with T80 were tested associated with a fast clearance from the bloodstream after their intravenous injection in GBM-bearing mice. Taking advantage of the magnetic properties of the SPION, a significant enhancement of SPION-DOX PNP uptake in the tumor was obtained after their magnetic targeting, with a significant decrease in the growth rate of the tumors. Further *in vivo* studies are needed to better the posology required to enhance survival rates, but magnetically targeted SPION-DOX PNP proved to be a promising drug delivery system to enhance DOX uptake by brain tumours while also making possible the non-invasive monitoring by MRI.

## Bibliography

1. Vleeschouwer S De. Glioblastoma. Codon Publications. 2017. doi:10.15586/CODON.GLIOBLASTOMA.2017.
2. Gaikwad PS, Banerjee R. Nanotechnology-based strategies as novel therapies in gliomas. *Ther. Deliv.* 2018;9:571–92.
3. Valenciano EV, Fisiología D De, Medicina E De, Universidad D, Rica DC, Costarricense C et al. Importancia de Células Madre TumORAles y Cultivos de Neuroesferas en Neurooncología. *Neuroeje.* 2012;25:55–60.
4. Gutkin A, Cohen ZR, Peer D. Harnessing nanomedicine for therapeutic intervention in glioblastoma. *Expert Opin. Drug Deliv.* 2016;13:1573–82.
5. Neves AR, Queiroz JF, Reis S. Brain-targeted delivery of resveratrol using solid lipid nanoparticles functionalized with apolipoprotein E. *J. Nanobiotechnology.* 2016.

- doi:10.1186/s12951-016-0177-x.
6. Pinzón-Daza M, Garzón R, Couraud P, Romero I, Weksler B, Ghigo D et al. The association of statins plus LDL receptor-targeted liposome-encapsulated doxorubicin increases in vitro drug delivery across blood-brain barrier cells. *Br. J. Pharmacol.* 2012;167:1431–47.
  7. Luque-Michel E, Imbuluzqueta E, Sebastián V, Blanco-Prieto MJ. Clinical advances of nanocarrier-based cancer therapy and diagnostics. *Expert Opin. Drug Deliv.* 2017;14:75–92.
  8. Battaglia L, Gallarate M, Peira E, Chirio D, Muntoni E, Biasibetti E et al. Solid Lipid Nanoparticles for Potential Doxorubicin Delivery in Glioblastoma Treatment: Preliminary In Vitro Studies. *J. Pharm. Sci.* 2014;103:2157–65.
  9. Rousselle C, Clair P, Lefauconnier JM, Kaczorek M, Scherrmann JM, Temsamani J. New advances in the transport of doxorubicin through the blood-brain barrier by a peptide vector-mediated strategy. *Mol. Pharmacol.* 2000;57:679–86.
  10. Shen W Bin, Anastasiadis P, Nguyen B, Yarnell D, Yarowsky PJ, Frenkel V et al. Magnetic enhancement of stem cell-targeted delivery into the brain following MR-guided focused ultrasound for opening the blood-brain barrier. *Cell Transplant.* 2017;26:1235–46.
  11. Weinstein JS, Varallyay CG, Dosa E, Gahramanov S, Hamilton B, Rooney WD et al. Superparamagnetic Iron Oxide Nanoparticles: Diagnostic Magnetic Resonance Imaging and Potential Therapeutic Applications in Neurooncology and Central Nervous System Inflammatory Pathologies, a Review. *J. Cereb. Blood Flow Metab.* 2010;30:15–35.
  12. Li H, Jin H, Wan W, Wu C, Wei L. Cancer nanomedicine: mechanisms, obstacles and strategies. *Nanomedicine.* 2018;13:1639–56.
  13. Sano, Yasuteru; Kashiwamuea, Yoko; Abe, Masaaki; Dieu, Le-Ha; Huwlyler, Jörg; Shimizu, Fumitaka; Haruki, Hiroyo; Maeda, Toshihiko; Saito, Kazuyuki; Tasaki, Ayako; Kanda T. Stable human brain microvascular endothelial cell line retaining its barrier-specific nature independent of the passage number. *Neuroimmunology.* 2013;4:92–103.
  14. Daniels BP, Cruz-Orengo L, Pasioka TJ, Couraud PO, Romero IA, Weksler B et al. Immortalized human cerebral microvascular endothelial cells maintain the properties of primary cells in an in vitro model of immune migration across the blood brain barrier. *J. Neurosci. Methods.* 2013;212:173–9.
  15. R. Poller, H. Gutman, S. Krahenbuhl, B. Weksler, I. Romero, P.O. Couraud G, Tuffin, J. Drewe JH. The human brain endothelial cell line hCMEC/D3 as a human blood-brain barrier model for drug transport studies. *J. Neurochem.* 2008;107:1358–68.
  16. Cecchelli R, Dehouck B, Descamps L, Fenart L, Duhem C, Lundquist S et al. In vitro model for evaluating drug transport across the blood-brain barrier. *Adv. Drug Deliv. Rev.* 1999;36:165–78.
  17. Markoutsas E, Pampalakis G, Niarakis A, Romero IA, Weksler B, Couraud P et al. European Journal of Pharmaceutics and Biopharmaceutics Uptake and permeability studies of BBB-targeting immunoliposomes using the hCMEC / D3 cell line. *Eur. J. Pharm. Biopharm.* 2011;77:265–74.
  18. Vonarbourg A, Passirani C, Saulnier P, Simard P, Leroux JC, Benoit JP. Evaluation of pegylated lipid nanocapsules versus complement system activation and macrophage uptake. *J. Biomed. Mater. Res. Part A.* 2006;78A:620–8.
  19. Cieślak A, Wauthoz N, Nieto Orellana A, Lautram N, Béjaud J, Hureauux J et al. Stealth nanocarriers based sterosomes using PEG post-insertion process. *Eur. J. Pharm. Biopharm.* 2017;115:31–8.
  20. Lemaire L, Nel J, Franconi F, Bastiat G, Saulnier P. Perfluorocarbon-Loaded Lipid Nanocapsules to Assess the Dependence of U87-Human Glioblastoma Tumor pO<sub>2</sub> on In Vitro Expansion Conditions. *PLoS One.* 2016;11:e0165479.
  21. Marie H, Lemaire L, Franconi F, Lajnef S, Frapart Y-M, Nicolas V et al. Superparamagnetic Liposomes for MRI Monitoring and External Magnetic Field-

- Induced Selective Targeting of Malignant Brain Tumors. *Adv. Funct. Mater.* 2015;25:1258–69.
22. Hobbs SK, Monsky WL, Yuan F, Roberts WG, Griffith L, Torchilin VP et al. Regulation of transport pathways in tumor vessels: Role of tumor type and microenvironment. *Proc. Natl. Acad. Sci.* 1998;95:4607–12.
  23. Peiris PM, Abramowski A, McGinnity J, Doolittle E, Toy R, Gopalakrishnan R et al. Treatment of Invasive Brain Tumors Using a Chain-like Nanoparticle. *Cancer Res.* 2015;75:1356–65.
  24. Singh D, Kapahi H, Rashid M, Prakash A, Majeed ABA, Mishra N. Recent prospective of surface engineered Nanoparticles in the management of Neurodegenerative disorders. *Artif. Cells, Nanomedicine Biotechnol.* 2016;44:780–91.
  25. Aparicio-blanco J, Martín-sabroso C, Torres-su A. In vitro screening of nanomedicines through the blood brain barrier : A critical review. *Biomaterials.* 2016;103:229–55.
  26. Schuster T, Mühlstein A, Yaghootfam C, Maksimenko O, Shipulo E, Gelperina S et al. Potential of surfactant-coated nanoparticles to improve brain delivery of arylsulfatase A. 2017;253:1–10.
  27. Collnot E-M, Baldes C, Wempe MF, Kappl R, Hüttermann J, Hyatt JA et al. Mechanism of Inhibition of P-Glycoprotein Mediated Efflux by Vitamin E TPGS: Influence on ATPase Activity and Membrane Fluidity. *Mol. Pharm.* 2007;4:465–74.
  28. Parekh G, Shi Y, Zheng J, Zhang X, Leporatti S. Nano-carriers for targeted delivery and biomedical imaging enhancement. *Ther. Deliv.* 2018;9:451–68.
  29. Moghimi SM, Simberg D. Complement activation turnover on surfaces of nanoparticles. *Nano Today.* 2017;15:8–10.
  30. Fornaguera C, Calderó G, Mitjans M, Vinardell MP, Solans C, Vauthier C. Interactions of PLGA nanoparticles with blood components: protein adsorption, coagulation, activation of the complement system and hemolysis studies. *Nanoscale.* 2015;7:6045–58.
  31. Huang J, Li Y, Orza A, Lu Q, Guo P, Wang L et al. Magnetic Nanoparticle Facilitated Drug Delivery for Cancer Therapy with Targeted and Image-Guided Approaches. *Adv. Funct. Mater.* 2016;26:3818–36.
  32. Liu B-Y, Wu C, He X-Y, Zhuo R-X, Cheng S-X. Multi-drug loaded vitamin E-TPGS nanoparticles for synergistic drug delivery to overcome drug resistance in tumor treatment. *Sci. Bull.* 2016;61:552–60.
  33. Yang C, Wu T, Qi Y, Zhang Z. Recent advances in the application of vitamin E TPGS for drug delivery. *Theranostics.* 2018;8:464–85.
  34. Gu G, Xia H, Hu Q, Liu Z, Jiang M, Kang T et al. PEG-co-PCL nanoparticles modified with MMP-2/9 activatable low molecular weight protamine for enhanced targeted glioblastoma therapy. *Biomaterials.* 2013;34:196–208.
  35. Xin H, Chen L, Gu J, Ren X, wei Z, Luo J et al. Enhanced anti-glioblastoma efficacy by PTX-loaded PEGylated poly( $\epsilon$ -caprolactone) nanoparticles: In vitro and in vivo evaluation. *Int. J. Pharm.* 2010;402:238–47.
  36. Jiang X, Xin H, Sha X, Gu J, Jiang Y, Law K et al. PEGylated poly(trimethylene carbonate) nanoparticles loaded with paclitaxel for the treatment of advanced glioma: in vitro and in vivo evaluation. *Int. J. Pharm.* 2011;420:385–94.
  37. Vrignaud S, Anton N, Passirani C, Benoit J-P, Saulnier P. Aqueous core nanocapsules: a new solution for encapsulating doxorubicin hydrochloride. *Drug Dev. Ind. Pharm.* 2013;39:1706–11.
  38. Butsele K Van, Cajot S, Vlierberghe S Van, Dubruel P, Passirani C, Benoit JP et al. pH-responsive flower-type micelles formed by a biotinylated poly(2-vinylpyridine)-block-poly(ethylene oxide)-block-poly(caprolactone) triblock copolymer. *Adv. Funct. Mater.* 2009;19:1416–25.
  39. Carla V, Mosqueira F, Legrand P, Gulik A, Bourdon O, Gref R et al. Relationship between complement activation , cellular uptake and surface physicochemical aspects of novel PEG-modi " ed nanocapsules. *Biomaterials.* 2001;22:2967–79.



40. Vittaz M, Bazile D, Spenlehauer G, Verrecchia T, Veillard M, Puisieux F et al. Effect of PEO surface density on long-circulating PLA-PEO nanoparticles which are very low complement activators. *Biomaterials*. 1996;17:1575–81.
41. Gelperina S, Maksimenko O, Khalansky A, Vanchugova L, Shipulo E, Abbasova K et al. Drug delivery to the brain using surfactant-coated poly(lactide-co-glycolide) nanoparticles: Influence of the formulation parameters. *Eur. J. Pharm. Biopharm.* 2010;74:157–63.
42. Gidwani M, Singh A V. Nanoparticle enabled drug delivery across the blood brain barrier: in vivo and in vitro models, opportunities and challenges. *Curr. Pharm. Biotechnol.* 2014;14:1201–12.
43. Estella-Hermoso de Mendoza A, Pr at V, Mollinedo F, Blanco-Prieto MJ. In vitro and in vivo efficacy of edelfosine-loaded lipid nanoparticles against glioma. *J. Control. Release.* 2011;156:421–6.
44. Peiris PM, Abramowski A, Mcginnity J, Doolittle E, Toy R, Gopalakrishnan R et al. Treatment of invasive brain tumors using a chain-like nanoparticle. *Cancer Res.* 2015;75:1356–65.
45. Schleich N, Po C, Jacobs D, Ucakar B, Gallez B, Danhier F et al. Comparison of active, passive and magnetic targeting to tumors of multifunctional paclitaxel/SPIO-loaded nanoparticles for tumor imaging and therapy. *J. Control. Release.* 2014;194:82–91.
46. Sun Z, Yan X, Liu Y, Huang L, Kong C, Qu X. Application of dual targeting drug delivery system for the improvement of anti-glioma efficacy of doxorubicin. *Oncotarget.* 2017;8:58823–34.
47. Chen Y, Huang Y, Liu W, Gao F, Fang X. c(RGDyK)-decorated Pluronic micelles for enhanced doxorubicin and paclitaxel delivery to&nbsp;brain glioma. *Int. J. Nanomedicine.* 2016;11:1629.
48. Liu S, Guo Y, Huang R, Li J, Huang S, Kuang Y et al. Gene and doxorubicin co-delivery system for targeting therapy of glioma. *Biomaterials.* 2012;33:4907–16.
49. Shen W-B, Anastasiadis P, Nguyen B, Yarnell D, Yarowsky PJ, Frenkel V et al. Magnetic Enhancement of Stem Cell-Targeted Delivery into the Brain Following MR-Guided Focused Ultrasound for Opening the Blood-Brain Barrier. *Cell Transplant.* 2017;26:1235–46.
50. Moghimi SM. Cancer nanomedicine and the complement system activation paradigm: Anaphylaxis and tumour growth. *J. Control. Release.* 2014;190:556–62.
51. Coty J-B, Noiray M, Vauthier C. Assessment of Complement Activation by Nanoparticles: Development of a SPR Based Method and Comparison with Current High Throughput Methods. *Pharm. Res.* 2018;35:129.



## **DISCUSSION AND OUTLOOK**

---



Early diagnosis and selective eradication of cancer cells are the two major challenges in cancer management. Different protocols have been established for each type of neoplasia. Overall, chemotherapy is a widespread and effective way of treating cancerous tissues, consisting in drugs named cytostatics which cause cell death by decreasing the cell's proliferation capacity and stopping the progression of the tumor. The main drawback of cytostatics is that they do not differentiate the diseased from the healthy cells and they are more effective in cells with rapid proliferation. This lack of selectivity results in low drug concentration at the tumor site and numerous side effects like vomiting, stomatitis, depression of the bone marrow and alopecia. As a matter of fact, these treatments are applied intermittently to allow the patient's immune system to recover and reduce the risk of serious infections. Apart from that, each type of cytostatic drug has specific adverse effects, such as cardiotoxicity, in the case of doxorubicin (DOX) [1]. In this context and in order to obtain optimal therapeutic effects, the right drugs should be delivered to the right location of the right patient at the right time with the right concentration. Nanomedicine, which has emerged as one of the most promising anti-cancer strategies, is offers advantages over conventional medicine in modifying the biodistribution and the clearance of cytostatic drugs, making it possible to target the cytotoxic drug to the tumor and reduce the adverse effects. Nanoparticles (NP) are defined as colloidal systems with an average diameter between 1 and 1000 nm that can carry the drug of interest encapsulated inside a matrix or adsorbed on its surface [2]. Since the early approval in 1995 of the doxorubicin-liposomal formulation Doxil® /Caelyx (Jansenn) for Kaposi's sarcoma, the Food and Drug Administration (FDA) has approved more than 50 new nanomedicines and almost 80 are currently in clinical trials [3]. DOX is one of the most commonly used therapeutic agents and is the drug model in numerous published studies on nanocarriers, mainly due to the central anthracycline group (Figure 1) responsible for its intrinsic fluorescence, that allows us to visualize DOX in tissues or cells by fluorescence-based microscopy and imaging [4]. DOX cytotoxic effect is attributed to two different mechanisms that result in the disruption of DNA causing cell death: the intercalation between the bases of DNA that block its synthesis and transcription; and the inhibition of topoisomerase II that stops the replication process.

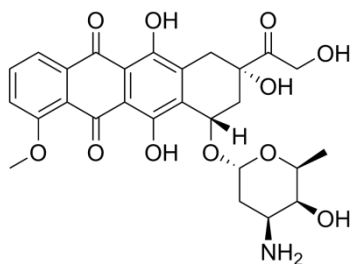


**Figure 1:** Chemical structure of DOX

In brief, one of the most important missions of nanotechnology is research on NP with high efficacy in clinical fields [5]. In contrast to the great advances made by nanomedicine in cancer treatment, the development of effective ways to treat central nervous system (CNS) disorders is still faced with difficulties. In fact, the effects of a pegylated liposomal DOX (Doxil or Caelyx) have been also investigated in glioblastoma (GBM), but the results obtained are unconvincing [6–8]. GBM is one of the most aggressive tumors occurring in the CNS [9]. This aggressiveness is characterized by highly proliferating infiltrative cells, indistinct tumor margins, high intra- and intertumor heterogeneity, peritumoral edema and inflammation [10]. As a large volume of research has shown, the difficulties of treating GBM can be attributed to the blood–brain barrier (BBB), to the difficulty of removing the entire tumor and to the presence of resistant stem cells. The BBB was first discovered by Ehrlich in 1885, who found that intravenously injected dye could stain most organs except the brain [11]. With its function to protect the brain from damage caused by unwanted blood borne molecules, the BBB represents one of the most tightly regulated and complex biological barriers in mammals (Figure 2). As a consequence, it is the most important barrier in brain-targeted delivery. In fact, the failure of many sophisticated conventional treatments have led investigators to explore new local and regional routes of administration such as focused ultrasound (FUS), Convection Enhanced Delivery (CED), intranasal, intra-arterial infusion of osmotic agents and receptor mediated agents [12]. In our group, previous studies revealed that edelfosine, an

alkyl-lysophospholipid that affects the cell membrane and the apoptotic machinery of the cancer cell [13] when it is administered orally in solid lipid NP (SLN) formulated with Tween 80 (T80), was accumulated in the brain and had anti-tumor efficacy in a glioma-bearing xenograft mouse animal model [14]. This result led us to hypothesize that T80 influenced the passage of the drug through the BBB, a point which was confirmed by evidence from the literature [14–16]. In addition to these previous studies, in the MINT laboratory (Micro et Nanomédecines Translationnelles) in Angers (France) where the work for the last part of this thesis was carried out, Marie H. and collaborators successfully directed magnetic liposomes to the brain tumors with the use of magnets, crossing the BBB [17].

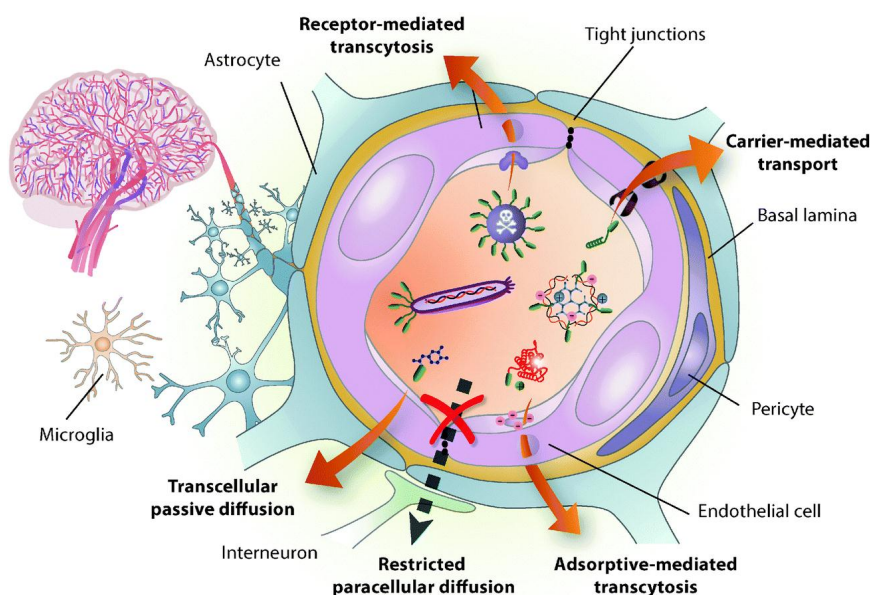


**Figure 2:** BBB structure and possible transport pathways for NP. The BBB is formed mainly by the tight brain endothelium, which is surrounded by the basal lamina and regulated by the other cells in the neurovascular unit, including pericytes, glial cells and neurons [18].

Overall, nanocarriers have potential for improving cancer therapy significantly by encapsulating cytostatic drugs and delivering them to the tumor site. They are also

useful in disease prevention and diagnosis [19]. Since X-rays were discovered by W.C. Roentgen in 1895, medical imaging techniques have contributed to accurate diagnosis [20]. In the past decade, enormous advances have been made in research on imaging sciences, such as the application of many new technologies (positron emission tomography (PET), computed tomography (CT) or magnetic resonance imaging (MRI)) and imaging agents based on nanosystems to oncology research and clinical trials [21]. These days, the demand for personalized therapies is growing; for instance, the 2016 revision of the World Health Organization (WHO) classification of brain tumors introduces the possibility of evaluating the overall prognosis and making a choice about the therapeutic management. This new classification not only relies on the histological profile of the cells (pure astrocytoma, oligoastrocytoma, and neuro-astrocytoma) but also on the genetic profile of the tumor [12, 22]. The most notable changes are in the isocitrate dehydrogenase (IDH) status (mutated vs. wild type) and the detection of the chromosomal 1p19q co-deletion; though it has been noted that these diagnostic approaches fall short of predicting the therapeutic response of individual tumors [23]. On the topic of personalized medicine, in the near future theranostic nanomedicine would certainly revolutionize the therapeutic concept from site-specific therapy to patient-specific therapy (deliver right drug to right patient) [24]. Theranostic NP are multifunctional entities that bring therapeutic and diagnostic aspects together in one setting, facilitating specific and personalized therapies for diseases [25]. All of this will enable clinicians to target drug delivery with minimal out-of-target toxicity and to adapt the therapy to the needs of the patient, avoiding overdosing non-responders. For these reasons theragnosis could provide non-invasive monitoring of drug distribution and accumulation at the tumor site together with early feedback on disease progression. In addition, non-invasive imaging may serve to identify potential recurrences, which could prompt further changes in therapy [21].

Owing to the aforesaid advantages of theranostic nanomedicine for cancer, in the present project we have focused on two main objectives: the coencapsulation of diagnostic and therapeutic agents to attain GBM monitored treatments; and simultaneously, the monitoring of the influence of surfactants or magnetic targeting in BBB uptake. The main findings of this research have been summarized in three



chapters. The first one describes the design, preparation and characterization of polymeric NP (PNP) encapsulating gold NP (AuNP) (AuNP PNP) along with its *in vitro* evaluation as contrast agent by CT. The second chapter involves the design, preparation and characterization of PNP synthesized with different surfactants and encapsulating superparamagnetic iron oxide NP (SPION) and DOX; along with its *in vitro* therapeutic and diagnostic capability evaluation by MRI. And finally, the third chapter includes the *in vivo* evaluation of the therapeutic and diagnostic efficacy of the PNP encapsulating both SPION and DOX, synthesized with the surfactant T80 and magnetically targeted to the brain with magnets.

## CHAPTER 1

Evidence of the clinical interest of AuNP is revealed by the number of AuNP that have progressed into clinical trials (NCT03020017, NCT01270139 NCT02755870, NCT01420588 and NCT02782026). For example, NU-0129, now being tested in an early Phase I trial, is composed of siRNA arranged on the surface of Au nanospheres. The Au nanocomplexes can penetrate the BBB and deliver siRNA into tumor cells, knocking down the expression of oncoprotein Bcl2Like12 and, therefore, inhibiting GBM or gliosarcoma tumor growth [25]. As another example, CYT-6091 is recombinant human tumor necrosis factor (rhTNF) bound to colloidal gold, which is in a Phase I clinical trial for solid tumor treatment. Conversely, the capacity of AuNP as contrast agent is not being clinically investigated. Up to now, there are no gold-based nanomedicines approved by the American food and drug administration (FDA) [3], even though AuNP are well represented in a range of research fields. They are described in bibliography as a good CT contrast agent due to their high X-ray attenuation, simple surface chemistry and biocompatibility. CT is among the most popular medical imaging modalities since it provides high resolution images, fast scan time, low cost and compatibility with all patients. The images obtained by CT provide anatomical information by X-ray equipment, in some cases using a contrast material based on iodine. The literature states that gold has a high atomic number and electronic density, which provides greater X-ray attenuation than iodine-based

contrast agents and, consequently, a sensitivity approximately 2.7 times higher in CT image [4]. For these reasons, we focus our efforts on encapsulating AuNP in PNP in order to finally co-encapsulate them together with the cytostatic drug DOX.

The polymer poly (lactic-co-glycolic acid) PLGA is biocompatible and biodegradable and its use in humans is approved by the FDA. In the presence of physiological water, the PLGA undergoes hydrolysis releasing the original monomers (lactic acid and glycolic acid) (Figure 3), which are natural metabolites easily metabolized in the body via the Krebs cycle without any systemic toxicity [26]. In addition, this polymer has the possibility of modulating its rate of degradation by varying the molecular weight and the ratio of the monomers in the copolymer. Lactic acid is more hydrophobic than glycolic acid and, therefore, PLGA enriched in lactic acid is less hydrophilic, absorbs less water and consequently degrades more slowly. The two first numbers of the name of the polymer indicate this proportion, and if the terminal group is an acid group instead of an ester, this is indicated with a final H [27, 28]. For AuNP PNP synthesis we use the PLGA 504, so we use the proportion 50:50 of monomer with an ester final group. On the other hand, the higher the last number (4) that appears in the name, the higher the molecular weight is.

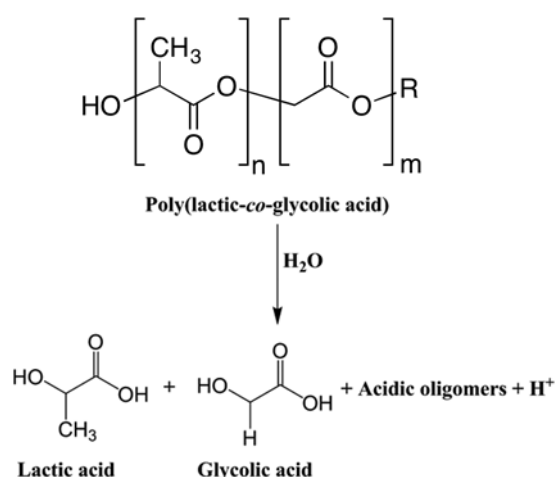


**Figure 3:** Structure and degradation of the polymer PLGA.

As explained in Chapter 1 and Annex 1, we used two synthesis methods by multiple emulsions ( $W_1/O/W_2$ ): the direct encapsulation of preformed AuNP (Figure 3A) or the *in situ* reduction of Au ions inside the PNP (Figure 3B), using heat to activate the reductive effect of citrate ions. We used the last of these to attain a homogeneous encapsulation of AuNP, although a large influence on the type of the surfactant used was detected. In fact, T80 could not stabilize electrostatically either the polymeric or the gold NP. However, it is important to point out that to the best of our knowledge this is the first case of a one-pot fabrication of highly monodisperse PLGA NPs with a tuneable Au NP payload, with the surfactants sodium taurocholate (STC) and sodium collate (SC).

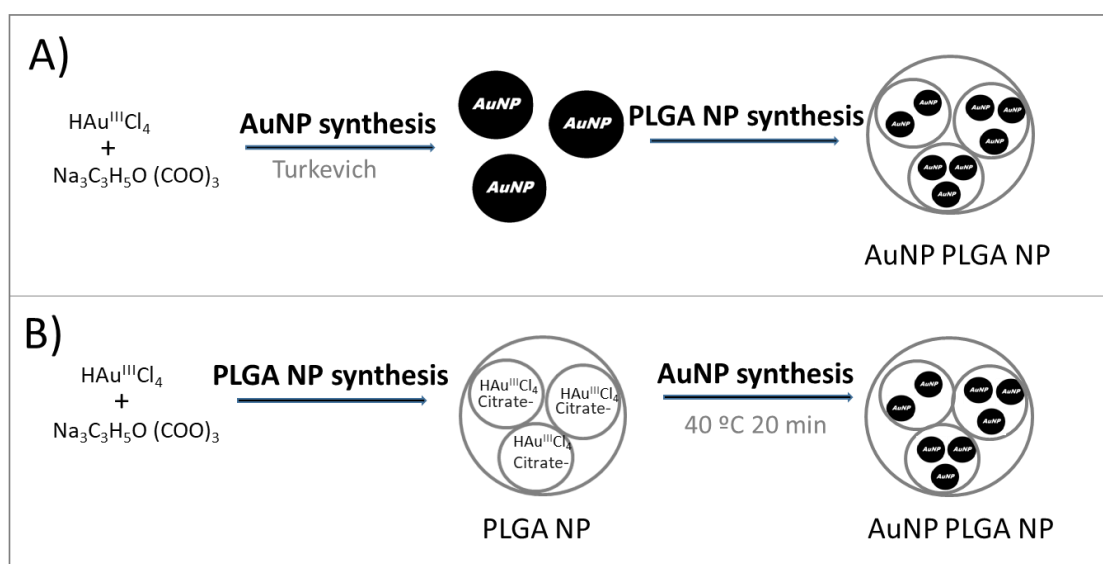


**Figure 4:** Schematic illustration of the two AuNP PNP synthesis methods explored: A) direct encapsulation method and B) the *in situ* reduction method.

As also displayed in chapter 1, these AuNP PNP proved to be non-toxic and good contrast agents in *in vitro* techniques (Figure 5). Prior to the *in vivo* assay, the nanovehicles were examined to confirm their capacity as contrast agents by micro-CT. Unfortunately, the AuNP PNP developed did not have sufficient X-ray attenuation

to be used *in vivo*. The most important limitation was the relatively high mass concentration, at millimolar concentration, of contrast agent necessary [29], an amount of Au that could not be attained with our synthesis method. Moreover, we noticed that *in vivo* cytotoxicity has not been studied rigorously and, generally, it has been investigated at doses below the range utilized in the studies that investigate AuNP as X-ray contrast agent. Hence, due to the fact that AuNP concentration depends on both X-ray attenuation and toxicity, it is absolutely necessary to determine the minimum effective and safe dose of AuNP for X-ray imaging [29].

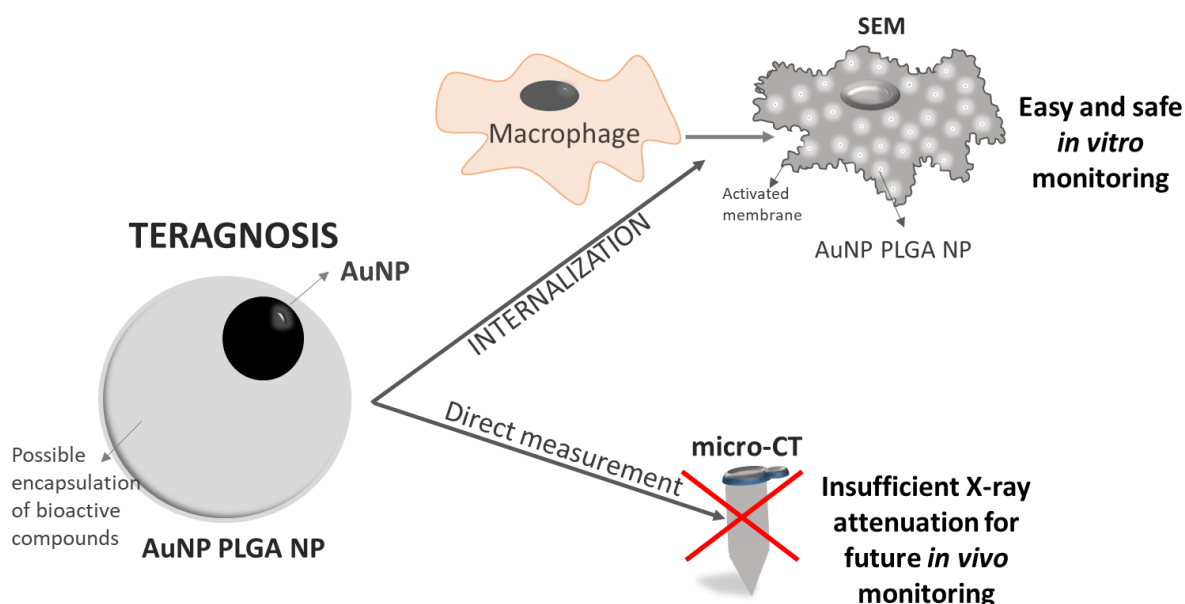


**Figure 5:** Visualization of hybrid gold-loaded PNP in cells using scanning electron microscopy. Journal of Drug Delivery Science and Technology (Chapter 1).

In parallel with the previous CT imaging studies and with the aim of achieving the combination of AuNP and DOX in PNP, the subsequent co-encapsulation with DOX was studied. As described in chapter 1 concerning the encapsulation of the pyrene drug model, after the synthesis of AuNP-DOX PNP the fluorescence of the DOX disappeared (data not shown). In this case, we hypothesized that it might be

impossible to coencapsulate them in the same PNP. Several studies were conducted to confirm this hypothesis; for example, the drug was quantified directly (inside the PNP) and indirectly (in the washing-water) but it was not detected in any of these; the NP were dialyzed to measure the DOX released, but no drug was released; we tried to separate the hypothetical complex formed by DOX and AuNP by pH changes (because of the high affinity of DOX to acidic conditions) or by using 2-mercaptetanol (Brust M. *et al.* exploited the high affinity of thiol for gold producing AuNP-thiolates (Au-S) [30]). In addition to the previous tests, the composition of the formulation ( $W_1/O/W_2$ ) was changed to keep the drug and AuNP precursors separate in different phases of the emulsion (DOX in phase  $W_1$  vs. in phase O), but none of these assays detected the drug once the PNP were formed. Afterwards, a satisfactory stability study of DOX at 40 °C over one week discarded DOX degradation as a result of the high temperature used in the synthesis AuNP PNP. And finally, the individual mixing of DOX with the AuNP precursors revealed a high and irreversible interaction between DOX and gold hydrochloride, confirming the impossibility of co-encapsulating DOX and AuNP by the *in situ* procedure.

All in all, our findings encouraged us to keep working with PLGA NP as potent candidates for nanocarriers design; however, we dismissed the idea of working with gold due to the low sensitivity of CT to this contrast agent and the impossibility of its coencapsulation with DOX. Regarding the encapsulation of DOX in PNP (Annex 2), an encapsulation efficacy around 80 % with a simple emulsion (O/W) method using PLGA 503H was achieved. NP were developed with the use of different surfactants (Figure 6): the anionic surfactants previously used (STC and SC) and the non-ionic surfactants Tween 80, PVA and, moreover, Brij-35 [31, 32], Pluronic F68 [33, 34] and Vitamin E-TPGS [35–38], which were described in the literature as glycoprotein P (pgP) inhibitor and BBB uptake enhancers. Moreover, the multidrug efflux pump pgP is expressed not only in the BBB but also in brain glioma cells where it collaborates in the intracellular drug concentration reduction and multidrug resistance (MDR) effect. On the other hand, the cationic surfactant didodecyldimethylammonium bromide (DDAB) had 0 % of DOX encapsulation due to the electrostatic interaction with DOX, which was positively charged.

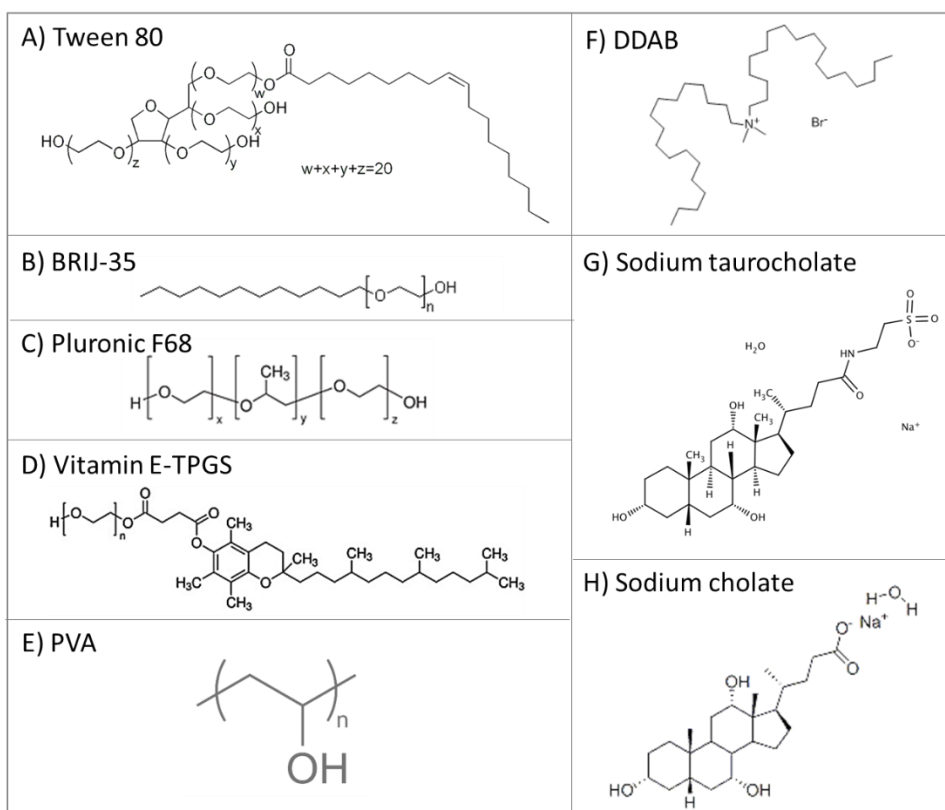


**Figure 6:** Chemical structure of the different surfactants used to synthesize DOX PNP. A, B, C, D and E) non-ionic surfactants. F) Cationic surfactant DDAB. G and H) Anionic surfactants.

## CHAPTER 2:

From here, our second key diagnostic agent to encapsulate was superparamagnetic iron oxide NP (SPION) as MRI contrast agent. In the studies presented in chapter 2 and 3, PLGA NP were used as a dual action carrier for DOX and SPION encapsulation. MRI is a non-invasive, non-radiation and tomographic imaging modality that offers good resolution of soft tissue such as brain, and actually it is normally used in glioma diagnosis [11]. MRI provides excellent temporal and spatial resolution, although there is a desire to develop contrast agents with higher efficiency for small tissue lesions, molecular activity or cellular activities, where there is less sensitivity than

other techniques [20]. Here, SPION offer various desirable features: small size, safety, biocompatibility and super paramagnetism in exposure to external magnetic fields. Moreover, SPION are considered the first generation of preclinical theranostic nanomedicines for the management of malignant brain tumors [21]. A number of similar SPION have been granted FDA approval (Resovist®, Feridex®, Abdoscan®, etc.). Although these have been discontinued for reasons that remain unclear, nowadays the one named Ferumoxytol is being investigated in phase I (NCT00660543) as MRI contrast agent in patients with glioma, and Nanotherm™ was designed for glioma therapy using local tissue hyperthermia; in actual fact, it has increased the overall survival of patients by up to 12 months [3]. SPION are reportedly associated with minimal to no toxicity and are well known as a T2-MRI diagnostic agent and for their magnetic properties. These last properties could be used, for example, for targeting by the application of an external magnetic field. Moreover, this may synergize with the pre-existing enhanced permeability and retention (EPR) effect of nanocarriers, improving their therapeutic effectiveness [5, 10]. Some more studies using PLGA nanocarriers encapsulating SPION and DOX are shown in Table 1. The first author, Jia Y. *et al.* synthesized SPION-DOX PNP of 280 nm by a different simple emulsion (O/W) method using Pluronic F127 as surfactant. The NP were injected directly into a subcutaneous Lewis lung carcinoma in mice and the antitumor activity was enhanced when NP were kept magnetically [39]. Jun-Qing S. *et al.* in 2016, published the therapeutic and diagnostic efficacy of SPION-DOX PLGA micelles of 50 nm functionalized with the peptide A54 to treat hepatocellular carcinoma [40]. Finally, the last authors Mosafer J. and colleagues in 2017, synthesized SPION-DOX PNP of 130 nm using a modified multiple emulsion ( $W_1/O_{1,2}/O_2$ ) method with the surfactant PVA and the aptamer AS1411 to target nucleolin proteins. They showed an enhancement of the contrast of MRI in the tumor site [41, 42]. Moreover, Mosafer J. has published in 2018 an article based only on the influence of 4 different fabrication methods (O/W;  $W_1/O/W_2$ ;  $W_1/O_{1,2}/W_2$  and  $O_1/W_1/O_2/W_2$ ) in the encapsulation of DOX and SPION, concluding that the modified multiple emulsion used in the previous articles produced better results in terms of particle size, drug loading, release profile and magnetic properties [43].

Author (year) [ref]	Vehicle type	Size (nm)	Cancer type	SPION purpose
Jia Y. <i>et al.</i> (2012) [39]	PLGA NP	280	- Lewis lung carcinoma	- NP kept in the tumor magnetically
Schleich N. <i>et al.</i> (2013) [44]	PLGA NP	285	- Colon carcinoma (only <i>in vitro</i> data; <i>in vivo</i> data with drug Paclitaxel)	- MRI
Niu C. <i>et al.</i> (2013) [45]	PLGA microbubbles	800-900	- Lymph nodes tumor	- MRI
Jun-Qing S. <i>et al.</i> (2016) [40]	PLGA micelles	50	- Hepatocellular carcinoma	- MRI
Mosafer J. <i>et al.</i> (2017-2018) [41-43]	PLGA NP	130-170	- Colon carcinoma - Glioma (only <i>in vitro</i> data)	- MRI
Our study (2018)	PLGA NP	228	- Glioma	- MRI - Magnetic targeting

**Table 1:** PLGA nanocarriers encapsulating DOX and SPION

In the present thesis (chapter 2), the encapsulation of preformed SPION inside PNP was satisfactory when SPION were covered with oleic acid and incorporated in the organic phase of a simple (O/W) emulsion. Contrary to the encapsulation of AuNP precursors, we did not see a surfactant influence, probably because the encapsulation used preformed metallic NP. Likewise, the coencapsulation of DOX and SPION in a simple emulsion (O/W) formed with the PLGA 503H was satisfactory with all surfactants selected as BBB uptake enhancers: T80, BRIJ-35, Pluronic F68 and Vitamin E-TPGS. The SPION-DOX PNP developed had a homogeneous average size of  $228.4 \pm 38.5$  nm with negative charge ( $-17.7 \pm 3.5$  mV), the 100 % of SPION were encapsulated inside the PNP and an encapsulation efficacy higher than 80 % was achieved for DOX. In view of the conservation of the NP developed, their lyophilization was chosen and the NP were stable as lyophilized powder for 3 months at 4 °C. In order to use an easy, quick and routine iron quantification method, the use of the colorimetric method published by Calatayud MP. *et al.* was considered [46]. This method is based on acidic digestion (HCl 6 M-HNO<sub>3</sub> (65%) at 50–60 ° C during 2 h) of the SPION followed by potassium thiocyanate addition to form iron–thiocyanate



complexes, which has strong absorbance at wavelength 478 nm [46]. However, the color obtained was not stable over time and other techniques were engaged. In keeping with the literature, the direct absorbance of SPION was quantified by spectrophotometry. The iron concentration was then determined by comparing the sample absorbance to a calibration curve. Various articles verified a similar spectrophotometric SPION quantification method inside the cells [47, 48] but in order to confirmed this, two samples at 8.0 and 48.5 ppm were re-quantified with an ICP external masses team, which showed a real concentration of 12.6 and 44.3 ppm. Therefore, an exhaustive validation should be performed to delimit the trustworthy range with this quantification method.

Once we had set the SPION-DOX PNP, their ability as contrast agents to MRI was studied by nuclear magnetic resonance. From suspensions containing superparamagnetic NP, low longitudinal ( $r_1 < 1.85 \text{ mM}^{-1} \text{ s}^{-1}$ ) and high transverse relaxations ( $r_2 172.0 \pm 18.3 \text{ mM}^{-1} \text{ s}^{-1}$ ) were obtained, which were equivalent to the values of commercialized SPION [49]. To date, the double amount of SPION inside PNP did not trigger differences in the relaxivity parameters, although in our forthcoming studies it would be interesting to test if it has an influence on magnetic targeting. After that, the *in vitro* release of DOX from SPION-DOX PNP was studied. At first, DOX adsorption on the NP surfaces was detected when using independent samples for each time of the release study. Then, dialysis devices were used (chapter 2) to mimic better a real intravenous injection. In this method, the free DOX was slightly attached to the dialysis membrane but it could be possible to see the release of DOX from the NP at different pH values. Mosafer *et al.*, as already mentioned in Table 1, also found the same pH influence with their SPION-DOX PNP: the release rates were accelerated in buffer at acidic pH due to the improved solubility of protonated DOX. Since the pH of cellular organelles such as endosomes is acid, this is beneficial for increasing the cytotoxicity effect of the drug inside the cells while its low release at neutral pH limits the release in blood circulation [41, 42]. With the use of these dialysis devices, those NP formulated with vitamin E did not show any DOX release at acidic pH: these results are not consistent with either the literature [50] or the cellular studies of these NP (below). So this unexpected effect suggested an interaction between the surfactant and the dialysis membrane that prevents DOX

permeation. In fact, the detection of DOX in the nucleus of human glioma U87 cells after 4 hours of treatment by fluorescence microscopy, confirmed the rapid DOX release from all types of NP at the acidic condition of cell endosomes. As a consequence, all NP developed had high toxicity against the glioma cell lines 9L and U87, as well as against the neurosphere stem cells obtained from a patient from the hospital *Clínica de Navarra*. The toxicities were equivalent to the non-encapsulated drug, so the encapsulation of DOX in PNP along with SPION does not modify its activity. To confirm the localization of the vehicle inside cellular organelles, the iron from the NP could be stained through the method of Perl's Prussian Blue (PB) [5, 10].

### CHAPTER 3:

The confirmation of that controlled drug release was taking place led us to evaluate the influence of the surfactant coatings in BBB permeation (chapter 3). This experiment was assessed by a human BBB functional *in vitro* model learned in a short stay in the laboratory of Professor Karine Andrieux ("Unité de technologies chimiques et biologiques pour la santé") at the University of Paris Descartes. The hCMEC/D3 cell monolayers used possess functional intercellular junctions with highly restrictive permeability properties [51, 52]. To perform the experiment, cell were seeded on a precoated Transwells (Figure 7) and once the monolayer was formed, free or encapsulated DOX were added to the upper compartment. Unexpectedly, the amount of DOX permeated did not significantly differ between free or encapsulated DOX; or between the different surfactant-coated SPION-DOX PNP NP. After several hypotheses had been ruled out, a microscopy study of DOX distribution inside the cytoplasm revealed that DOX was mainly in the nucleus. This finding suggested that, as had occurred previously with glioma cells, DOX was released inside endosomes at acidic pH showing the same BBB permeation profile as the free DOX. Unfortunately, all these unexpected results hindered the study of the surfactant influence. In this context, it must be mentioned that to overcome the BBB and treat brain tumors, more than only one targeting could be used. For instance, the drug delivery system design with trans-BBB targeting and brain tumor cell targeting is common. However, to date

there is no specific targeting vector available that solely reacts with one kind of cell [53]. Other strategies can be also explored, for example, Qiu Y. *et al.* shown that the use of electromagnetic pulses induce BBB permeability via regulating protein kinase C signalling and translocation of the tight junction protein ZO-1 [54]. In our case, taking advantage of magnetic properties of SPION, is commonly used an external magnet to target the NP [55, 56].

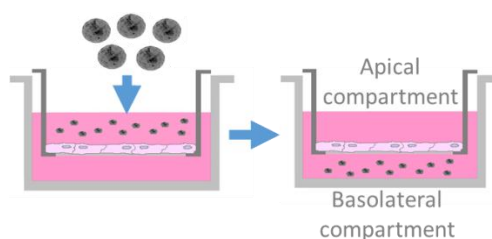


**Figure 7:** Illustration of the transwell devices where the cells are seeded to form the monolayer that mimics the BBB endothelium.

Before starting an *in vivo* experiment, it should be considered that as soon as NP are introduced into biological fluids, complement proteins are deposited on the surface of NP in a process called opsonization that leads to a premature elimination of the nanocarrier by the reticuloendothelial system [57]. The protein corona formed modifies the NP distribution and may cover the targeting ligand (as our cover ships with surfactants) hindering the specific reaction between ligands and their targets [11]. In this context, because there is no good way to prevent the formation of protein corona, recent studies have been focusing on its characterization (in terms of composition, density, conformation, thickness, affinity and dynamics) to figure out how to use it to our advantage [24]. In our study, a complement (CH50) test confirmed this complement activation by all the surfactant-coated NP, so magnetic external targeting could be used to overcome this inconvenience. Ucakar *et al.* (in 2018) [10] did not show a significant difference between the brain accumulation of T80-coated and uncoated SPION-paclitaxel PNP. But, interestingly, the magnetic

targeting enhanced the brain accumulation of these NP, the antitumor efficacy and the survival rate (Table 2). We should note that Ukacar *et al.* ensure that their study is the first to evaluate targeting strategies in terms of antitumor efficacy with polymeric nanotheranostic particles in an orthotopic GBM model.

In clinical practice, although it has only been tested in a few trials to date, magnetic targeting remains important for targeted drug delivery and has been presented as a promising strategy in a number of studies [58]. Lubbe and coworkers [59] have performed the first clinical trial of magnetically-targeted drug delivery where an epidoxorubicin magnetic-carrier was effectively targeted to solid tumors in 6 out of 14 patients. A second clinical trial was performed by Kodaand and co-workers [60] and 30 out of 32 patients were successfully targeted for hepatocellular carcinoma with a DOX magnetic-carrier; in a later clinical study they showed that up to 91 % of the tumor volume was affected by DOX [61]. Thus, magnetically responsible nanocarriers do not need affinity ligands on their surface to be targeted to a specific site in the body. Consequently, the design of magnetically responsible nanocarriers allows more freedom for the surface optimization to avoid undesired interactions with blood components, such as formation of protein corona [58]. As a result, various targeting strategies previously used such as the adsorption of acid hyaluronic (HA), a ligand for the cell surface glycoprotein CD44 overexpressed on glioma cells [9], or apolipoprotein E (ApoE) that will bind to low-density lipoprotein receptors on the BBB endothelial cells [62], have been discarded.

All the results discussed previously, along with what the literature states, led us to propose the SPION-DOX PNP developed as a new personalized therapy for glioma with the use of an external magnetic targeting. For that reason, we evaluated the diagnostic and anti-glioma efficacy of the magnetically targeted T80-coated SPION-DOX PNP injected intravenously in a GBM murine model (Figure 8). All the results concerning the *in vivo* studies of biodistribution, therapeutic efficacy and tracking capacity by means of MRI, are compiled in chapter 3.

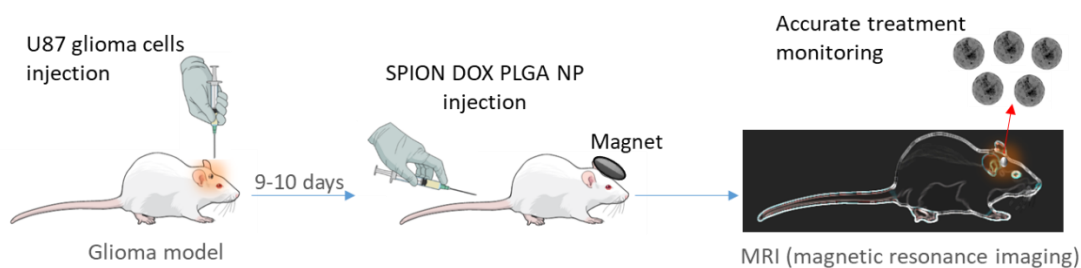


**Figure 8:** Schematic illustration of the studies performed.

First, after a single SPION-DOX PNP intravenously injection followed by a magnetic targeting for 1 hour ( $n=6$ ), the NP were detected inside the tumor for 2.5 hour monitoring and, moreover, the presence was also detected at 4 h in 2 out of 3 tumors. Importantly, the SPION-DOX PNP were detected in the tumor area and not in the healthy brain indicating blood brain tumor barrier (BBTB) permeation, which is more permeable than the healthy BBB. When the SPION-DOX PNP were not directed magnetically to the tumors ( $n=6$ ), the normal tumor contrast was recovered 1 h after NP injection, indicating a vascular effect without BBTB penetration. Thus, the effectiveness of using a magnet to retain the NP inside the tumor was confirmed. In the same way (Table 2), Chertok B. *et al.* used 30 min of magnet to satisfactorily target their magnetic nanocarriers to tumors in a 9L-glioma bearing rat [63]. Likewise, Zhou J. and colleges magnetically targeted their NP in mice bearing subcutaneous 9L-glioma tumors confirming the targeting by MRI [64]. And Marie H., in the laboratory MINT where our experiment were done, used a 4 hour magnet exposure to satisfactorily target SPION-loaded liposomes to brain tumors, using the same U87 glioma model [17]. In fact, Marie H. explained the magnetic targeting effectiveness by the development of dipolar interactions between SPION in a continuous magnetic field. This interaction would trigger SPION concentration in the tumor area with a more heterogeneous vasculature (the BBTB) allowing the passage.

Author (year) [ref]	Glioma model	Fe dose (mg/kg)	Magnet time (h)	Magnet force (T)	Cytotoxic drug	Drug dose (mg/kg)	Number of doses
Chertok B. <i>et al.</i> (2007) [63]	Orthotopic 9L glioma (rat)	12	0.5	0.4	None	-	-
Zhou J. <i>et al.</i> (2014) [64]	Subcutaneous 9L glioma (mice)	12	1	Not specified	None	-	-
Marie H. <i>et al.</i> (2015) [17]	Orthotopic U87 glioma (mice)	Not specified	4	0.4	None	-	-
Ucakar B. <i>et al.</i> (2018) [10]	Orthotopic U87 glioma (mice)	14	4	1.4	Paclitaxel	5	6
Our study (2018)	Orthotopic U87 glioma (mice)	16	1	0.4	DOX	5	2

**Table 2:** Studies with magnetic targeting to glioma bearing mice with SPION.

As efficient trafficking to the target site is a key process that determines the therapeutic effect, we then studied the therapeutic influence of the same magnetic targeting conditions (Table 2). Two doses of 5 mg /kg of DOX encapsulated in SPION-DOX PNP were administered on alternate days: in one group the tumors were magnetically targeted (n=7) and in the other group the tumors were not targeted with magnets (n=5). As a result, the magnet-exposed tumors slowed their growth significantly (doubling time of  $4.4 \pm 1.5$  days in comparison to  $2.3 \pm 1.2$  days of non-targeted tumors). The magnetically-targeted mice prolonged their survival slightly (from 28 to 31 days). In Ucakar B. *et al.* (Table 2), the only study that analyzed the therapeutic influence of magnetic targeting (with the drug paclitaxel) in a orthotopic glioma mice model, obtained a significant prolongation in the survival rates of mice but using a longer targeting time (4h vs. 1h), a stronger magnet (1.4 T vs. 0.4 T) and a larger number of doses (6 vs. 2). Similarly, although the dose of DOX used (5mg / kg; 2 doses) is within what is usually used in glioma therapy in mice (1-10 mg/kg), more

than 2 doses are normally administered [65–71]. Therefore, to increase the therapeutic effects with our SPION-DOX PNP, in future studies a longer or stronger magnetic targeting conditions should be used as well as more doses on alternate days. To sum up, we must just highlight the theranostic efficacy of the NP developed since they were monitored by MRI at the same time as they treated the tumors.

## FUTURE PERSPECTIVES

Personalized medicine is attracting increasing attention and it is expected that the integration of nanotechnology will take on special importance. In this context, theranostic NP provide imaging and therapy at the same time, which makes them a significant target for investigation. These nano-therapeutics could facilitate clinical efficacy and toxicity studies, as well as affording a better understanding of various important aspects of the drug delivery process. Moreover, their study would allow individual treatment adjustment depending on the patient response. For instance, by the observation of NP distribution, the treatment could be discarded for patients that do not retain the NP at the target site; or if the NP are retained for a short period, they could be administered more frequently. Most notably, the encapsulation of the diagnostic agent alone could be used to study the future therapeutic response of a specific patient or to check the stage of the diseases.

It is important to mention that despite all the studies cited, the translation of oncological nanomedicines into clinical practice is proving slow. Some major reasons for this could be the lack of reliable technology to scale up the production of advanced nanomaterials, the regulatory hurdles, and market forces [72]. In truth, the simple emulsion and solvent evaporation methods used in this project would not be easy to adapt for large-scale production since the batches obtained are small (about 100 mg/batch) and larger volumes may not be well homogenized with the sonotrode. As a solution to scale-up these kinds of NP, Larrea A. and colleagues in the INA have

demonstrated the effectiveness of microfluidic systems to produce nanoscale materials by continuous microchannel emulsification (Annex 3), which is able to multi-stage processing such as used for the production of AuNP PNP [73]. Regarding regulatory hurdles and market forces, the employment of clinically validated nanomaterials, such as the FDA-approved PLGA, T80, SPION or DOX, could possibly accelerate the clinical translation of theranostic NP.

Apart from the above mentioned points, further *in vivo* research efforts are still needed to achieve safe and efficacious clinical platforms. At present, many FDA-approved nanotherapeutic agents still offer a modest overall survival increment and, although less toxic than conventional therapies, are associated with adverse effects. For example, liposomal DOX (Doxil and Caelyx) are associated with stomatitis and palmar-plantar erythrodysesthesia and the albumin-bound paclitaxel (Abraxane) is associated with sensory neuropathy and nausea [24]. In this context, magnetic targeting would efficiently concentrate the therapeutic agent at the target site, reducing or eliminating new systemic side effects [74]. Consequently, it is expected that magnetic targeting will find important clinical uses in the future and our findings might have potential applications in the pharmacological therapy for different CNS (epilepsy, stroke or neurodegenerative diseases) [75–77]. This leads us to mention that in recent years, only a minor number of brain-directed pharmaceuticals have reached the market (3–5 %), since most of the proposed drugs were incapable of crossing the BBB *in vivo* [78]. As a matter of fact, the development of new strategies to treat brain diseases is one of the most challenging and expensive market niches for pharmaceutical companies, and it is of utmost importance that these should prove effective in the development phase [78]. On the whole, SPION, with their magnetic and contrast characteristics, have already been successfully applied in disorders in the brain, cardiovascular system, liver, blood vessels and other vital organs. In coming years, multifunctional SPION would be an attractive material for biomedical applications and may change the usual business model in the pharmaceutical industries [79].



To end the discussion, it is important to mention that there are multiple barriers preventing these new nanosystems from entering clinical practice, but we are confident that intense interdisciplinary research combining nanotechnology, material sciences, cancer biology and clinical medicine along with a focus on clinical translation and legislative bodies will ultimately lead to tangible benefits for our patients [72, 80].

### **Bibliography**

1. Lorenzo-Velázquez B, Lorenzo Fernández P. *Farmacología básica y clínica. Médica Panamericana*. 2017.
2. Strambeanu N, Demetrovici L, Dragos D, Lungu M. *Nanoparticles: Definition, Classification and General Physical Properties. Nanoparticles' Promises and Risks*. Cham: Springer International Publishing. 2015:3–8.
3. Bobo D, Robinson KJ, Islam J, Thurecht KJ, Corrie SR. *Nanoparticle-Based Medicines: A Review of FDA-Approved Materials and Clinical Trials to Date*. *Pharm. Res.* 2016;33:2373–87.
4. Gautier J, Allard-Vannier E, Munnier E, Souce M, Chourpa I. *Recent advances in theranostic nanocarriers of doxorubicin based on iron oxide and gold nanoparticles*. *J. Control. Release.* 2013;169:48–61.
5. Gholami L, Tafaghodi M, Abbasi B, Daroudi M, Kazemi Oskuee R. *Preparation of superparamagnetic iron oxide/doxorubicin loaded chitosan nanoparticles as a promising glioblastoma theranostic tool*. *J. Cell. Physiol.* 2018. doi:10.1002/jcp.27019.
6. Glas M, Koch H, Hirschmann B, Jauch T, Steinbrecher A, Herrlinger U et al. *Pegylated Liposomal Doxorubicin in Recurrent Malignant Glioma: Analysis of a Case Series*. *Oncology.* 2007;72:302–7.
7. Ananda S, Nowak AK, Cher L, Dowling A, Brown C, Simes J et al. *Phase 2 trial of temozolomide and pegylated liposomal doxorubicin in the treatment of patients with glioblastoma multiforme following concurrent radiotherapy and chemotherapy*. *J. Clin. Neurosci.* 2011;18:1444–8.
8. Beier CP, Schmid C, Gorlia T, Kleinletzenberger C, Beier D, Grauer O et al. *RNOP-09: pegylated liposomal doxorubicine and prolonged temozolomide in addition to radiotherapy in newly diagnosed glioblastoma--a phase II study*. *BMC*

- Cancer. 2009;9:308.
9. Gutkin A, Cohen ZR, Peer D. Harnessing nanomedicine for therapeutic intervention in glioblastoma. *Expert Opin. Drug Deliv.* 2016;13:1573–82.
  10. Ucakar B, Joudiou N, Bianco J, Danhier P, Danhier F. Magnetic targeting of paclitaxel-loaded poly ( lactic- co -glycolic acid ) -based nanoparticles for the treatment of glioblastoma. *Int. J. Nanomedicine.* 2018;13:4509–21.
  11. Gao H. Progress and perspectives on targeting nanoparticles for brain drug delivery. *Acta Pharm. Sin. B.* 2016;6:268–86.
  12. Tosi U, Marnell CS, Chang R, Cho WC, Ting R, Maachani UB et al. Advances in molecular imaging of locally delivered targeted therapeutics for central nervous system tumors. *Int. J. Mol. Sci.* 2017. doi:10.3390/ijms18020351.
  13. Estella-Hermoso de Mendoza A, Campanero MA, Lana H, Villa-Pulgarin JA, de la Iglesia-Vicente J, Mollinedo F et al. Complete inhibition of extranodal dissemination of lymphoma by edelfosine-loaded lipid nanoparticles. *Nanomedicine.* 2012;7:679–90.
  14. Estella-Hermoso de Mendoza A, Preat V, Mollinedo F, Blanco-Prieto MJ. In vitro and in vivo efficacy of edelfosine-loaded lipid nanoparticles against glioma. *J. Control. Release.* 2011;156:421–6.
  15. Singh D, Kapahi H, Rashid M, Prakash A, Majeed ABA, Mishra N. Recent prospective of surface engineered Nanoparticles in the management of Neurodegenerative disorders. *Artif. Cells, Nanomedicine Biotechnol.* 2016;44:780–91.
  16. Petri B, Bootz A, Khalansky A, Hekmatara T, Müller R, Uhl R et al. Chemotherapy of brain tumour using doxorubicin bound to surfactant-coated poly ( butyl cyanoacrylate ) nanoparticles : Revisiting the role of surfactants. *J. Control. Release.* 2007;117:51–8.
  17. Marie H, Lemaire L, Franconi F, Lajnef S, Frapart Y-M, Nicolas V et al. Superparamagnetic Liposomes for MRI Monitoring and External Magnetic Field-Induced Selective Targeting of Malignant Brain Tumors. *Adv. Funct. Mater.* 2015;25:1258–69.
  18. Oller-Salvia B, Sánchez-Navarro M, Giralt E, Teixidó M. Blood–brain barrier shuttle peptides: an emerging paradigm for brain delivery. *Chem. Soc. Rev.* 2016;45:4690–707.
  19. Shi J, Kantoff PW, Wooster R, Farokhzad OC. Cancer nanomedicine: progress, challenges and opportunities. *Nat. Rev. Cancer.* 2017;17:20–37.
  20. Jeong Y, Hwang HS, Na K. Theranostics and contrast agents for magnetic resonance imaging. *Biomater. Res.* 2018;22:20.
  21. Aparicio-Blanco J, Torres-Suárez AI. Towards tailored management of

- malignant brain tumors with nanotheranostics. *Acta Biomater.* 2018;73:52–63.
22. Louis DN, Perry A, Reifenberger G, von Deimling A, Figarella-Branger D, Cavenee WK et al. The 2016 World Health Organization Classification of Tumors of the Central Nervous System: a summary. *Acta Neuropathol.* 2016;131:803–20.
  23. Vleeschouwer S De. Glioblastoma. Codon Publications. 2017. doi:10.15586/CODON.GLIOMASTOMA.2017.
  24. Li H, Jin H, Wan W, Wu C, Wei L. Cancer nanomedicine: mechanisms, obstacles and strategies. *Nanomedicine.* 2018;13:1639–56.
  25. Guo J, Rahme K, He Y, Li L-L, Holmes JD, O’Driscoll CM. Gold nanoparticles enlighten the future of cancer theranostics. *Int. J. Nanomedicine.* 2017;12:6131–52.
  26. Lü J-M, Wang X, Marin-Muller C, Wang H, Lin PH, Yao Q et al. Current advances in research and clinical applications of PLGA-based nanotechnology. *Expert Rev. Mol. Diagn.* 2009;9:325–41.
  27. Jain RA. The manufacturing techniques of various drug loaded biodegradable poly(lactide-co-glycolide) (PLGA) devices. *Biomaterials.* 2000;21:2475–90.
  28. Ignatius AA, Claes LE. In vitro biocompatibility of bioresorbable polymers: poly(L, DL-lactide) and poly(L-lactide-co-glycolide). *Biomaterials.* 1996;17:831–9.
  29. Cole LE, Ross RD, Tilley JM, Vargo-Gogola T, Roeder RK. Gold nanoparticles as contrast agents in x-ray imaging and computed tomography. *Nanomedicine.* 2015;10:321–41.
  30. Brust M, Walker M, Bethell D, Schiffrin DJ, Whyman R. Synthesis of thiol-derivatised gold nanoparticles in a two-phase Liquid–Liquid system. *J. Chem. Soc., Chem. Commun.* 1994;0:801–2.
  31. Koziara JM, Lockman PR, Allen DD, Mumper RJ. In situ blood-brain barrier transport of nanoparticles. *Pharm. Res.* 2003;20:1772–8.
  32. Hoosain FG, Choonara YE, Tomar LK, Kumar P, Tyagi C, du Toit LC et al. Bypassing P-Glycoprotein Drug Efflux Mechanisms: Possible Applications in Pharmacoresistant Schizophrenia Therapy. *Biomed Res. Int.* 2015;2015:484963.
  33. Gelperina S, Maksimenko O, Khalansky A, Vanchugova L, Shipulo E, Abbasova K et al. Drug delivery to the brain using surfactant-coated poly(lactide-co-glycolide) nanoparticles: Influence of the formulation parameters. *Eur. J. Pharm. Biopharm.* 2010;74:157–63.
  34. Schuster T, Mühlstein A, Yaghootfam C, Maksimenko O, Shipulo E, Gelperina S et al. Potential of surfactant-coated nanoparticles to improve brain delivery of

- arylsulfatase A. 2017;253:1–10.
35. Collnot E-M, Baldes C, Wempe MF, Kappl R, Hüttermann J, Hyatt JA et al. Mechanism of Inhibition of P-Glycoprotein Mediated Efflux by Vitamin E TPGS: Influence on ATPase Activity and Membrane Fluidity. *Mol. Pharm.* 2007;4:465–74.
  36. Meng X, Liu J, Yu X, Li J, Lu X, Shen T. Pluronic F127 and D- $\alpha$ -Tocopheryl Polyethylene Glycol Succinate (TPGS) Mixed Micelles for Targeting Drug Delivery across The Blood Brain Barrier. *Sci. Rep.* 2017;7:2964.
  37. Kulkarni SA, Feng S-S. Effects of Particle Size and Surface Modification on Cellular Uptake and Biodistribution of Polymeric Nanoparticles for Drug Delivery. *Pharm. Res.* 2013;30:2512–22.
  38. Collnot EM, Baldes C, Schaefer UF, Edgar KJ, Wempe MF, Lehr CM. Vitamin e TPGS P-glycoprotein inhibition mechanism: Influence on conformational flexibility, intracellular ATP levels, and role of time and site of access. *Mol. Pharm.* 2010;7:642–51.
  39. Jia Y, Yuan M, Yuan H, Huang X, Sui X, Cui X et al. Co-encapsulation of magnetic Fe<sub>3</sub>O<sub>4</sub> nanoparticles and doxorubicin into biodegradable PLGA nanocarriers for intratumoral drug delivery. *Int. J. Nanomedicine.* 2012;7:1697–708.
  40. Situ JQ, Wang XJ, Zhu XL, Xu XL, Kang XQ, Hu JB et al. Multifunctional SPIO/DOX-loaded A54 Homing Peptide Functionalized Dextran-g-PLGA Micelles for Tumor Therapy and MR Imaging. *Sci. Rep.* 2016;6:1–14.
  41. Mosafer J, Abnous K, Tafaghodi M, Mokhtarzadeh A, Ramezani M. In vitro and in vivo evaluation of anti-nucleolin-targeted magnetic PLGA nanoparticles loaded with doxorubicin as a theranostic agent for enhanced targeted cancer imaging and therapy. *Eur. J. Pharm. Biopharm.* 2017;113:60–74.
  42. Mosafer J, Teymouri M, Abnous K, Tafaghodi M, Ramezani M. Study and evaluation of nucleolin-targeted delivery of magnetic PLGA-PEG nanospheres loaded with doxorubicin to C6 glioma cells compared with low nucleolin-expressing L929 cells. *Mater. Sci. Eng. C.* 2017;72:123–33.
  43. Mosafer J, Teymouri M. Comparative study of superparamagnetic iron oxide/doxorubicin co-loaded poly (lactic-co-glycolic acid) nanospheres prepared by different emulsion solvent evaporation methods. *Artif. Cells, Nanomedicine Biotechnol.* 2018;46:1146–55.
  44. Schleich N, Sibret P, Danhier P, Ucakar B, Laurent S, Muller RN et al. Dual anticancer drug/superparamagnetic iron oxide-loaded PLGA-based nanoparticles for cancer therapy and magnetic resonance imaging. *Int. J. Pharm.* 2013;447:94–101.
  45. Niu C, Wang Z, Lu G, Krupka TM, Sun Y, You Y et al. Doxorubicin loaded superparamagnetic PLGA-iron oxide multifunctional microbubbles for dual-mode US/MR imaging and therapy of metastasis in lymph nodes. *Biomaterials.*

- 2013;34:2307–17.
46. Calatayud MP, Riggio C, Raffa V, Sanz B, Torres TE, Ibarra MR et al. Neuronal cells loaded with PEI-coated Fe<sub>3</sub>O<sub>4</sub> nanoparticles for magnetically guided nerve regeneration. *J. Mater. Chem. B*. 2013;1:3607.
  47. Friedrich RP, Janko C, Pöttler M, Tripal P, Zaloga J, Cicha I et al. Flow cytometry for intracellular SPION quantification: specificity and sensitivity in&nbsp;comparison with spectroscopic methods. *Int. J. Nanomedicine*. 2015;10:4185.
  48. Dadashzadeh ER, Hobson M, Jr LHB, Dean DD, Frank JA. Rapid Spectrophotometric Technique for Quantifying Iron in Cells Labeled with Superparamagnetic Iron Oxide Nanoparticles: Potential Translation to the Clinic. *Contrast Media Mol Imaging*. 2014;8:50–6.
  49. Weinstein JS, Varallyay CG, Dosa E, Gahramanov S, Hamilton B, Rooney WD et al. Superparamagnetic Iron Oxide Nanoparticles: Diagnostic Magnetic Resonance Imaging and Potential Therapeutic Applications in Neurooncology and Central Nervous System Inflammatory Pathologies, a Review. *J. Cereb. Blood Flow Metab*. 2010;30:15–35.
  50. Yang C, Wu T, Qi Y, Zhang Z. Recent advances in the application of vitamin E TPGS for drug delivery. *Theranostics*. 2018;8:464–85.
  51. R. Poller, H. Gutman, S. Krahenbuhl, B. Weksler, I. Romero, P.O. Couraud G, Tuffin, J. Drewe JH. The human brain endothelial cell line hCMEC/D3 as a human blood-brain barrier model for drug transport studies. *J. Neurochem*. 2008;107:1358–68.
  52. Daniels BP, Cruz-Orengo L, Pasiaka TJ, Couraud PO, Romero IA, Weksler B et al. Immortalized human cerebral microvascular endothelial cells maintain the properties of primary cells in an in vitro model of immune migration across the blood brain barrier. *J. Neurosci. Methods*. 2013;212:173–9.
  53. Wei X, Chen X, Ying M, Lu W. Brain tumor-targeted drug delivery strategies. *Acta Pharm. Sin. B*. 2014;4:193–201.
  54. Chen Y, Liu L. Modern methods for delivery of drugs across the blood-brain barrier. *Adv. Drug Deliv. Rev*. 2012;64:640–65.
  55. Hua MY, Liu HL, Yang HW, Chen PY, Tsai RY, Huang CY et al. The effectiveness of a magnetic nanoparticle-based delivery system for BCNU in the treatment of gliomas. *Biomaterials*. 2011;32:516–27.
  56. Liu H-L, Hua M-Y, Yang H-W, Huang C-Y, Chu P-C, Wu J-S et al. Magnetic resonance monitoring of focused ultrasound/magnetic nanoparticle targeting delivery of therapeutic agents to the brain. *Proc. Natl. Acad. Sci*. 2010;107:15205–10.
  57. Chen F, Wang G, Griffin JI, Brennehan B, Banda NK, Holers VM et al.

- Complement proteins bind to nanoparticle protein corona and undergo dynamic exchange in vivo. *Nat. Nanotechnol.* 2017;12:387–93.
58. Kralj S, Potrc T, Kocbek P, Marchesan S, Makovec D. Design and Fabrication of Magnetically Responsive Nanocarriers for Drug Delivery. *Curr. Med. Chem.* 2017;24:454–69.
59. Lübke AS, Bergemann C, Riess H, Schriever F, Reichardt P, Possinger K et al. Clinical experiences with magnetic drug targeting: a phase I study with 4'-epidoxorubicin in 14 patients with advanced solid tumors. *Cancer Res.* 1996;56:4686–93.
60. Koda, J.; Venook, A.; Walser, E.; Goodwin S. A multicenter, phase I/II trial of hepatic intra-arterial delivery of doxorubicin hydrochloride adsorbed to magnetic targeted carriers in patients with hepatocellular carcinoma. *Eur. J. Cancer.* 2002;38:S18.
61. Wilson MW, Kerlan RK, Fidelman NA, Venook AP, LaBerge JM, Koda J et al. Hepatocellular Carcinoma: Regional Therapy with a Magnetic Targeted Carrier Bound to Doxorubicin in a Dual MR Imaging/ Conventional Angiography Suite—Initial Experience with Four Patients. *Radiology.* 2004;230:287–93.
62. Neves A, Queiroz J, Weksler B. Solid lipid nanoparticles as a vehicle for brain-targeted drug delivery: two new strategies of functionalization with apolipoprotein E. .... 2015;26:495103.
63. Chertok B, David AE, Huang Y, Yang VC. Glioma selectivity of magnetically targeted nanoparticles: A role of abnormal tumor hydrodynamics. *J. Control. Release.* 2007;122:315–23.
64. Zhou J, Zhang J, Gao W. Enhanced and selective delivery of enzyme therapy to 9L-glioma tumor via magnetic targeting of PEG-modified,  $\beta$ -glucosidase-conjugated iron oxide nanoparticles. *Int. J. Nanomedicine.* 2014;9:2905–17.
65. Sun Z, Yan X, Liu Y, Huang L, Kong C, Qu X. Application of dual targeting drug delivery system for the improvement of anti-glioma efficacy of doxorubicin. *Oncotarget.* 2017;8:58823–34.
66. Zhang Y, Zhai M, Chen Z, Han X, Yu F, Li Z et al. Dual-modified liposome codelivery of doxorubicin and vincristine improve targeting and therapeutic efficacy of glioma. *Drug Deliv.* 2017;24:1045–55.
67. Li Y, Baiyang L, Leran B, Zhen W, Yandong X, Baixiang D et al. Reduction-responsive PEO-SS-PCL micelle with tailored size to overcome blood–brain barrier and enhance doxorubicin antiglioma effect. *Drug Deliv.* 2017;24:1782–90.
68. Belhadj Z, Ying M, Cao X, Hu X, Zhan C, Wei X et al. Design of Y-shaped targeting material for liposome-based multifunctional glioblastoma-targeted drug delivery. *J. Control. Release.* 2017;255:132–41.

69. Fang Y, Jiang Y, Zou Y, Meng F, Zhang J, Deng C et al. Targeted glioma chemotherapy by cyclic RGD peptide-functionalized reversibly core-crosslinked multifunctional poly(ethylene glycol)- b -poly( $\epsilon$ -caprolactone) micelles. *Acta Biomater.* 2017;50:396–406.
70. Liu S, Guo Y, Huang R, Li J, Huang S, Kuang Y et al. Gene and doxorubicin co-delivery system for targeting therapy of glioma. *Biomaterials.* 2012;33:4907–16.
71. Chen Y, Huang Y, Liu W, Gao F, Fang X. c(RGDyK)-decorated Pluronic micelles for enhanced doxorubicin and paclitaxel delivery to&nbsp;brain glioma. *Int. J. Nanomedicine.* 2016;11:1629.
72. Li K, Nejadnik H, Daldrup-Link HE. Next-generation superparamagnetic iron oxide nanoparticles for cancer theranostics. *Drug Discov. Today.* 2017;22:1421–9.
73. Larrea A, Clemente A, Luque-Michel E, Sebastian V. Efficient production of hybrid bio-nanomaterials by continuous microchannel emulsification: Dye-doped SiO<sub>2</sub> and Au-PLGA nanoparticles. *Chem. Eng. J.* 2017;316:663–72.
74. Polyak B, Friedman G. Magnetic targeting for site-specific drug delivery: applications and clinical potential. *Expert Opin. Drug Deliv.* 2009;6:53–70.
75. Pinzón-Daza M, Garzón R, Couraud P, Romero I, Weksler B, Ghigo D et al. The association of statins plus LDL receptor-targeted liposome-encapsulated doxorubicin increases in vitro drug delivery across blood-brain barrier cells. *Br. J. Pharmacol.* 2012;167:1431–47.
76. Silva LHA, Cruz FF, Morales MM, Weiss DJ, Rocco PRM. Magnetic targeting as a strategy to enhance therapeutic effects of mesenchymal stromal cells. *Stem Cell Res. Ther.* 2017;8:58.
77. Marcus M, Smith A, Maswadeh A, Shemesh Z, Zak I, Motiei M et al. Magnetic Targeting of Growth Factors Using Iron Oxide Nanoparticles. *Nanomaterials.* 2018;8:707.
78. Saraiva C, Praça C, Ferreira R, Santos T, Ferreira L, Bernardino L. Nanoparticle-mediated brain drug delivery: Overcoming blood-brain barrier to treat neurodegenerative diseases. *J. Control. Release.* 2016;235:34–47.
79. Vallabani NVS, Singh S. Recent advances and future prospects of iron oxide nanoparticles in biomedicine and diagnostics. *3 Biotech.* 2018;8:279.
80. Luque-Michel E, Imbuluzqueta E, Sebastián V, Blanco-Prieto MJ. Clinical advances of nanocarrier-based cancer therapy and diagnostics. *Expert Opin. Drug Deliv.* 2017;14:75–92.





**CONCLUSIONS**

---

**CONCLUSIONES**



The experimental work compiled in this volume has been focused on the development of theragnostic nanoparticles for glioma therapy and diagnosis, as well as the study of different strategies to cross the blood brain barrier (BBB) that protects the brain. All the results obtained during this PhD have led us to conclude as follows:

1. Polymeric NP (PNP) encapsulating gold nanoparticles (AuNP PNP) of around 102 nm and negative surface were developed by the multiple emulsion ( $W_1/O/W_2$ ) and solvent evaporation method.
2. The AuNP PNP designed were good as *in vitro* contrast agents by scanning electron microscopy (SEM) since their internalization in macrophages could be monitored. However, the AuNP PNP designed did not have sufficient X-ray attenuation to be used as *in vivo* contrast agent by computed tomography (CT).
3. PNP encapsulating doxorubicin (DOX), superparamagnetic iron nanoparticles (SPION) or both (SPION-DOX PNP) of around 230 nm with negative charge were developed by a simple emulsion (O/W) and solvent evaporation method with the use of the surfactants: Tween 80, Brij-35, Pluronic F68 and Vitamin E-TPGS, all of them BBB permeation enhancers. 100 % of SPION were encapsulated inside the PNP and an encapsulation efficacy higher than 80 % was obtained for DOX.
4. The SPION-DOX PNP designed were stable as lyophilized powder for 3 months at 4 °C and showed low longitudinal and high transverse relaxations, indicating their usefulness as contrast agent by magnetic resonance imaging (MRI).
5. The SPION-DOX PNP designed showed an accelerated DOX release under acidic conditions, corresponding to the cellular endosomes and lysosomes pHs. Consequently, *in vitro* toxicities equivalent to the free DOX were observed in the glioma cell lines 9L and U87, as well as in neuronal stem cells obtained from a patient from the hospital Clínica Universidad de Navarra.
6. Using a human BBB *in vitro* model, it was not possible to detect differences between all surfactant-coated SPION-DOX PNP designed and, moreover, all of them showed a high complement activation, leading us to expect a rapid systemic clearance.

7. *In vivo* biodistribution studies by MRI in a glioma murine model confirmed that 1 hour of magnetic targeting after the intravenous injection of the SPION-DOX PNP designed (at 16 mg Fe/kg) was effective to retain the NP for 4 hours in the tumor area and not in healthy brain, indicating blood brain tumor barrier (BBTB) permeation. On the other hand, tumors not directed magnetically recovered the normal contrast in 1 hour indicating a vascular effect without BBTB permeation.
8. *In vivo* theranostic efficacy studies by MRI in a glioma murine model confirmed the effectiveness of targeting magnetically the SPION-DOX PNP designed for 1 hour. After 2 doses on alternate days at 5 mg DOX/kg and 16 mg Fe/kg, the tumor growths were slowed significantly (4.4 vs. 2.3 days of doubling time) and the survival rates of mice were prolonged (28 vs. 31 days) when a magnet was used.

El trabajo experimental recopilado en esta memoria se ha centrado en el desarrollo de nanopartículas (NP) teragnósticas para la terapia y el diagnóstico de glioma, así como en el estudio de diferentes estrategias para superar la barrera hematoencefálica (BHE) que protege el cerebro. Los resultados obtenidos en este trabajo nos permiten concluir:

1. Mediante el método de emulsión múltiple ( $A_1/O/A_2$ ) y evaporación del disolvente se han desarrollado NP poliméricas que encapsulan NP de oro (AuNP PNP) con un tamaño aproximado de 102 nm y carga superficial negativa.
2. Las AuNP PNP diseñadas son buenos agentes de contraste *in vitro*; su internalización en macrófagos pudo ser monitorizada por microscopía electrónica de barrido. Sin embargo *in vivo*, dichas nanopartículas no muestran contraste suficiente para poder ser utilizadas en tomografía computarizada.
3. Mediante el método de emulsión simple (O/A) y evaporación de disolvente, se han desarrollado NP poliméricas con distintos surfactantes: Tween 80, Brij-35, Pluronic F68 o Vitamina E-TPGS, todos ellos potenciadores del paso a través de la BHE. Estas NP encapsulan doxorubicina (DOX), NP de hierro superparamagnéticas (SPION) o ambas (SPION-DOX PNP) con un tamaño de alrededor de 230 nm, carga superficial negativa y una eficacia de encapsulación superior al 80 % para la DOX y del 100 % para las SPION.
4. Las SPION-DOX PNP liofilizadas fueron estables durante 3 meses a 4 °C. Además, han mostrado poseer las características adecuadas para ser monitorizadas *in vivo* mediante imagen por resonancia magnética (IRM).
5. La liberación de DOX desde las SPION-DOX PNP fue más rápida a pH 4 que a pH 7. Debido a la rápida liberación del fármaco en condiciones ácidas (simulando el pH de los lisosomas y endosomas celulares), la toxicidad de las SPION-DOX PNP fue equivalente a la del fármaco no encapsulado en todas las líneas celulares estudiadas.
6. Las distintas SPION-DOX PNP desarrolladas no mostraron diferencias en su paso a través de un modelo *in vitro* de BHE. Además, todas las NP mostraron una alta activación del sistema del complemento, sugiriendo su rápida eliminación sistémica por parte del sistema monocítico nuclear.

7. Los estudios de biodistribución en un modelo murino de glioma, confirmaron que tras 1 hora de direccionamiento magnético, las SPION-DOX PNP son retenidas durante 4 horas en el tumor y no en el cerebro sano, indicando que las NP atraviesan las barrera hematoencefálica tumoral (BHET). Por otro lado, aquellas SPION-DOX PNP no dirigidas magnéticamente no son retenidas durante más de 1 hora en la zona tumoral, sugiriendo que éstas se encuentran en el torrente sanguíneo y no atraviesan la BHET.
8. La administración en el modelo murino de glioma de dos dosis intravenosas en días alternos de SPION-DOX PNP dirigidas magnéticamente, ralentizó el crecimiento tumoral de manera significativa (con un tiempo de duplicación tumoral de 4.4 días frente a 2.3 días) y prolongó la supervivencia de los ratones (con una supervivencia de 28 días frente a 31 días), en comparación con el mismo tratamiento no dirigido.

# **ANNEX 1**

---

**Supplementary Material of chapter 2: A simple approach to obtain hybrid Au-loaded polymeric nanoparticles with tunable metal load.**





Electronic Supplementary Material (ESI) for Nanoscale.  
This journal is © The Royal Society of Chemistry 2015

**A simple approach to obtain hybrid Au-loaded polymeric nanoparticles with tunable metal load.**

*Eduarne Luque-Michel, Ane Larrea, Celia Lahuerta, Víctor Sebastian, Eduarne Imbuluzqueta, Manuel Arruebo, María J. Blanco-Prieto and Jesús Santamaría.*

Supporting Information

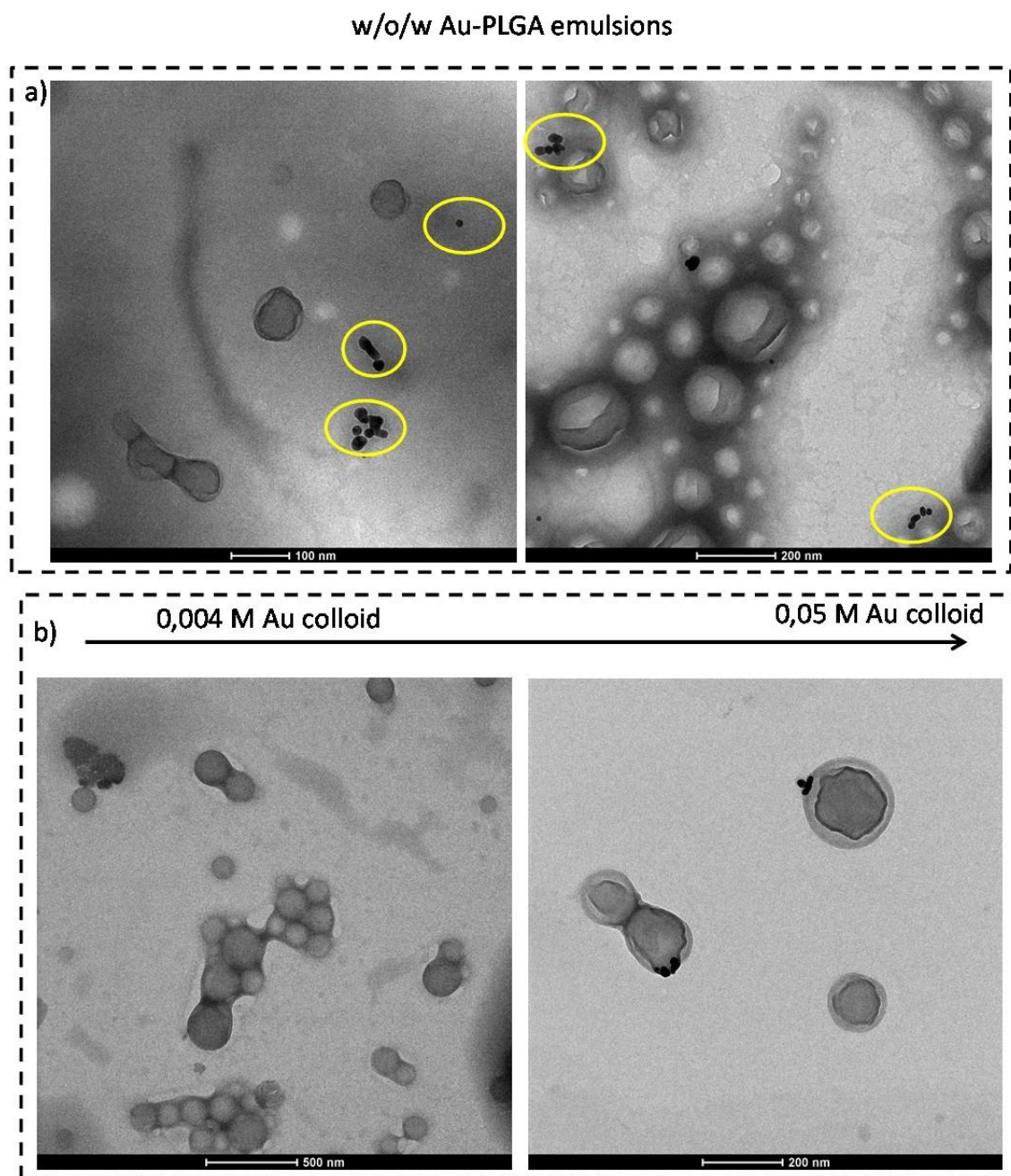
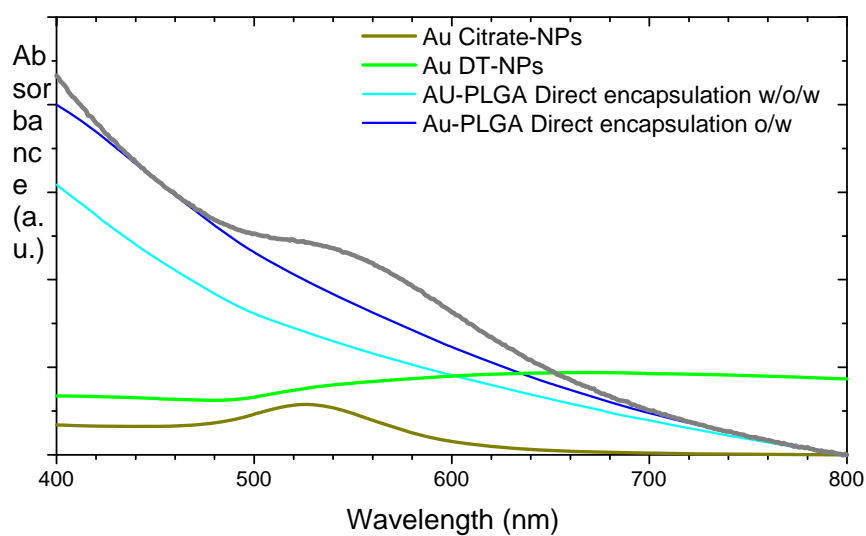


**Figure S1.-** TEM micrographs of Au- PLGA hybrid nanoparticles produced by the direct encapsulation method in w/o/w emulsion. a) Marked areas show the location of Au- NPs outward from the PLGA- NPs; b) Au aggregation as the concentration of Au colloid is increased.



## a) Direct Encapsulation-Preformed Au Nanoparticles



## b) In-situ formation

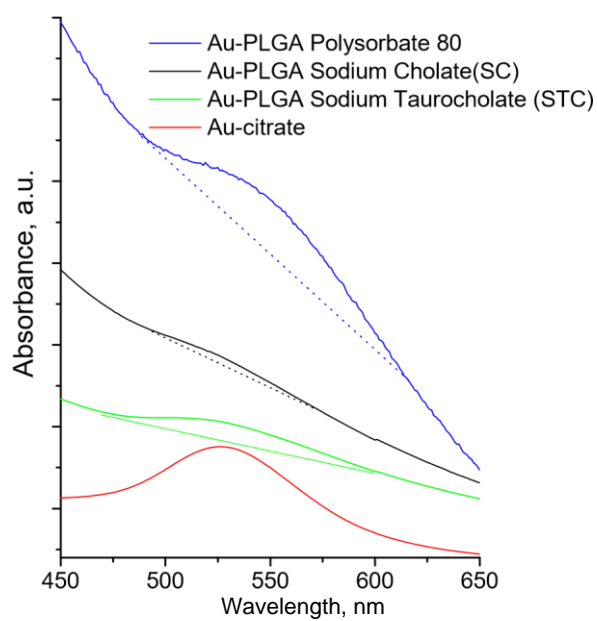


**Figure S3.-** UV- VIS spectra of the Au- NPs and Au- PLGA NPs produced in this work: a) Direct encapsulation approach, b) *In- situ* reduction.

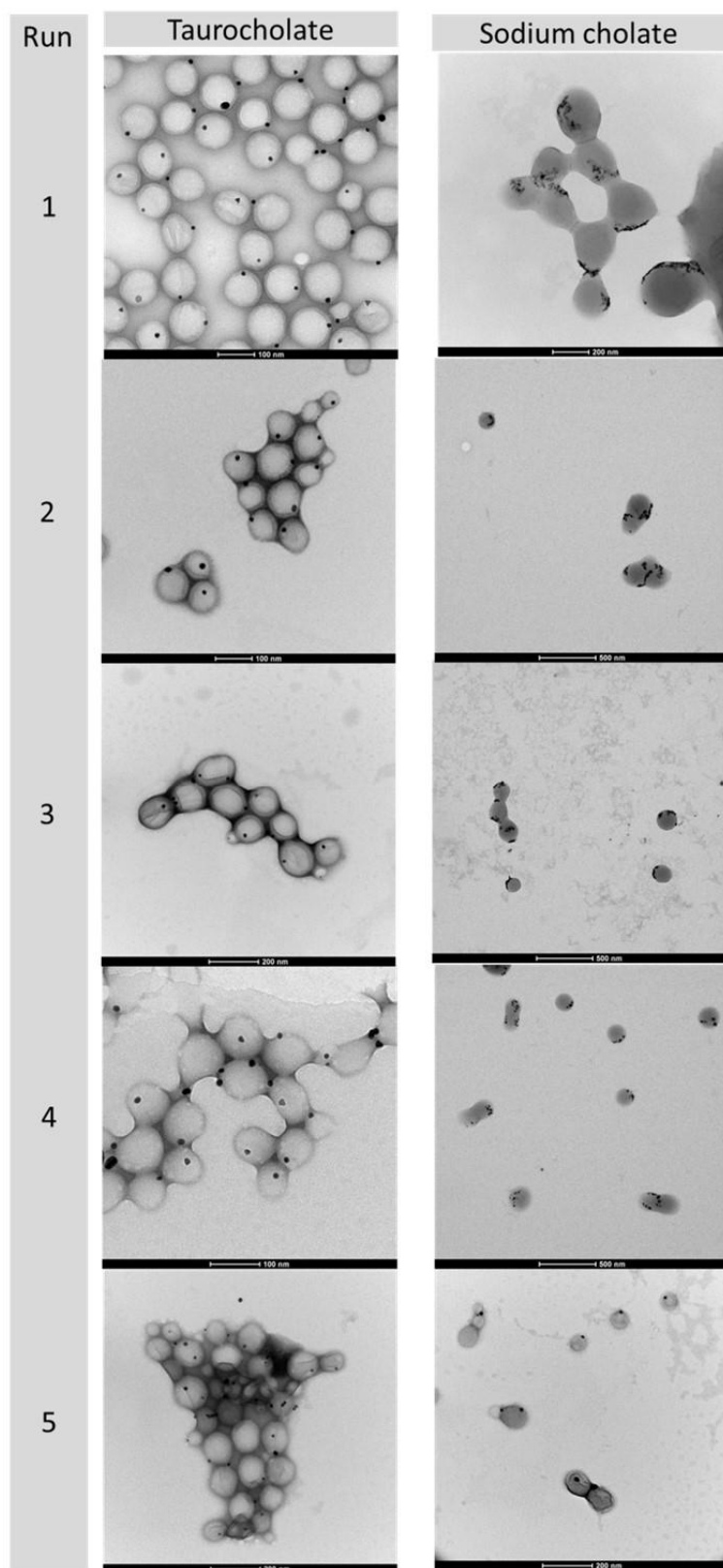


**Figure S4.-** TEM micrographs of Au- PLGA hybrid nanoparticles produced by the *in-situ* reduction method in w/o/w emulsion with STC and SC in 5 different batches to show the synthesis procedure reproducibility.

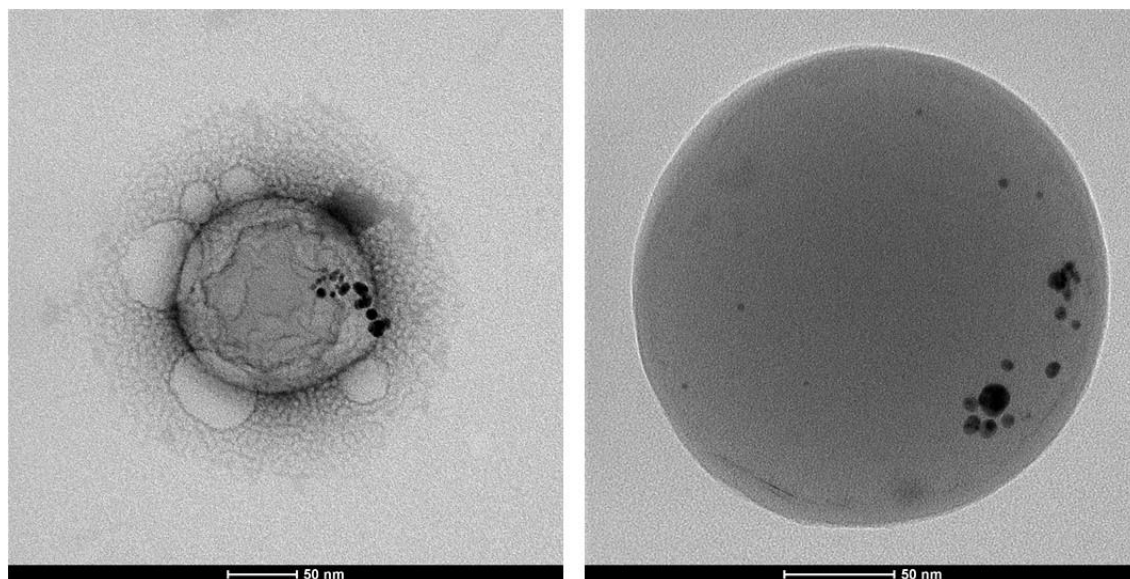


**Figure S5.-** TEM micrographs of Pyrene- Au- PLGA hybrid nanoparticles produced by the “in- situ reduction method” in w/o/w emulsion with SC after laser radiation for 15 min.



## **ANNEX 2**

---

**Optimization of doxorubicin (DOX) encapsulation into polymeric nanoparticles (PNP) using Lactic-co-Glycolic Acid (PLGA) as polymer.**





**ANNEX 2:** Optimization of doxorubicin (DOX) encapsulation into polymeric nanoparticles (PNP) using Poly Lactic-co-Glycolic Acid (PLGA) as polymer.

Annex 2 consists of one table that shows the different DOX encapsulation efficiencies (EE; as % with respect to the weight of the entire formulations), size, polydispersity index (PDI) or Z potential when modifying the composition of the organic and aqueous phases of the NP. First, different PLGAs (Resomer® 502, 503, 752 with free carboxylic or ester end groups) were tested. Then, the use of different solvent mixtures (ethyl acetate (EA), dichloromethane (DM) or acetone) and the proportions of these or of the surfactant used (1 or 2 %) were tuned. Moreover, to be able to dissolve the DOX in the organic phase, triethylamine (TEA) or oleic acid was added to the organic phase in different proportions (1:100 or 1:1000). After all these tests, the best DOX encapsulation efficacy was reached with PLGA 503H, EA: TEA (1:1000) and 1 % of surfactant and different surfactants were used to synthesize the NP with this composition (in bold).

TCS: taurocholate sodium; CS: cholate sodium; PVA: polyvinyl alcohol; T80: Tween 80; DDAB: Didodecyldimethylammonium bromide; VIT E: Vitamine E- Tocopheryl polyethylene glycol 1000

## ANNEX 2

ORGANIC PHASE			WATER PHASE		SOLVENT EVAPORATION		EE DOX (%)	Characterization		
PLGA (50 mg)	DOX (mg)	SOLVENT (1 mL)	Surfactant type (2 mL)	Surfactant (%)	Surfactant type (10 mL)	Surfactant (%)		SIZE (Z average)	PDI	POT Z
503	1	TEA:AcEt (1:1000)	TC	1	TC	0.3	77,6 ± 6,3	133,5 ± 16,8	0,14 ± 0,06	-33,6 ± 6,9
503	1	[TEA:DM (1:1000)]: AcEt (3:1)	TC	1	TC	0.3	81,8 ± 12,6	142,1 ± 28,5	0,12 ± 0,02	-30,7 ± 8,5
503	1	[TEA:DM (1:100)]: AcEt (3:1)	TC	1	TC	0.3	62,6	122,8	0,09	-39,8
503	1	[TEA:DM (1:1000)]: Acetone (3:1)	TC	1	TC	0.3	68,0	118,2	0,10	-31,3
503	1	Oleic acid:AcEt (1:1000)	TC	1	TC	0.3	67,1 ± 17,5	126,5 ± 8,7	0,14 ± 0,09	-37,0 ± 8,8
503	1	[Oleic acid:DM (1:1000)]: Acetone (3:1)	TC	1	TC	0.3	51,5	132,5	0,15	-32,9
503	1	[oleic acid:DM (1:1000)]: AcEt (3:1)	TC	1	TC	0.3	67,4	151,6	0,12	-37,0
<b>503H</b>	<b>1</b>	<b>TEA:AcEt (1:1000)</b>	<b>TC</b>	<b>1</b>	<b>TC</b>	<b>0.3</b>	<b>82,2 ± 9,6</b>	<b>120,8 ± 16,9</b>	<b>0,10 ± 0,03</b>	<b>-32,2 ± 5,6</b>
503H	1	TEA:AcEt (1:100)	TC	1	TC	0.3	78,5	148,5	0,07	
503H	1	Oleic acid:AcEt (1:1000)	TC	1	TC	0.3	52,2	114,5	0,08	-37,3
502	1	TEA:AcEt (1:1000)	TC	1	TC	0.3	45,8 ± 5,4	97,1 ± 9,4	0,10 ± 0,01	-29,2 ± 3,5
502	1	[TEA:DM (1:1000)]: AcEt (3:1)	TC	1	TC	0.3	31,1	170,0	0,13	-17,5
502H	1	TEA:AcEt (1:1000)	TC	1	TC	0.3	61,6 ± 10,0	90,2 ± 1,9	0,12 ± 0,02	-26,2 ± 4,9
752	1	TEA:AcEt (1:1000)	TC	1	TC	0.3	46,3 ± 2,4	105,7 ± 24,0	0,15 ± 0,06	-33,1 ± 3,5
752	1	[TEA:DM (1:1000)]: AcEt (3:1)	TC	1	TC	0.3	30,4	235,7	0,22	-17,8

752H	1	TEA:AcEt (1:1000)	TC	1	TC	0.3	47,3 ± 17,4	92,5 ± 3,9	0,12 ± 0,03	-24,5 ± 5,8
PEG-PLGA 50105	1	TEA:AcEt (1:1000)	TC	1	TC	0.3	61,22 ± 10,4	153,4 ± 4,7	0,14 ± 0,01	-25,2 ± 4,9
PEG-PLGA 5055	1	TEA:AcEt (1:1000)	TC	1	TC	0.3	57,9 ± 5,9	149,0 ± 29,9	0,09 ± 0,00	-32,1 ± 5,8
503H	1	TEA:AcEt (1:1000)	TC	2	TC	0,6	63,1 ± 5,7	91,1 ± 12,6	0,15 ± 0,07	-30,0 ± 8,5
<b>503H</b>	<b>1</b>	<b>TEA:AcEt (1:1000)</b>	<b>CS</b>	<b>1</b>	<b>CS</b>	<b>0.3</b>	<b>53,8 ± 4,5</b>	<b>94,5 ± 3,0</b>	<b>0,15 ± 0,04</b>	<b>-30,0 ± 12,1</b>
503H	1	TEA:AcEt (1:1000)	CS	2	CS	0,6	59,5 ± 15,1	86,1 ± 5,8	0,14 ± 0,02	-37,2 ± 6,5
<b>503H</b>	<b>1</b>	<b>TEA:AcEt (1:1000)</b>	<b>PVA</b>	<b>1</b>	<b>PVA</b>	<b>0.3</b>	<b>75,7 ± 7,2</b>	<b>208,1 ± 36,9</b>	<b>0,07 ± 0,01</b>	<b>-13,5 ± 2,1</b>
503H	1	TEA:AcEt (1:1000)	PVA	2	PVA	0,6	63,2 ± 13,6	190,0 ± 31,1	0,11 ± 0,01	-13,1 ± 4,1
<b>503H</b>	<b>1</b>	<b>TEA:AcEt (1:1000)</b>	<b>T80</b>	<b>1</b>	<b>T80</b>	<b>0.3</b>	<b>83,7 ± 3,7</b>	<b>132,5 ± 47,2</b>	<b>0,11 ± 0,03</b>	<b>-28,45 ± 7,1</b>
503H	1	TEA:AcEt (1:1000)	T80	2	T80	0,6	46,9 ± 22,5	117,1 ± 44,9	0,17 ± 0,01	-31,8 ± 14,6
<b>503H</b>	<b>1</b>	<b>TEA:AcEt (1:1000)</b>	<b>T80 (pH 7.4)</b>	<b>1</b>	<b>T80 (pH 7.4)</b>	<b>0.3</b>	<b>101,5 ± 15,3</b>	<b>94,5 ± 4,5</b>	<b>0,13 ± 0,01</b>	<b>-24,3 ± 7,1</b>
503H	1	TEA:AcEt (1:1000)	T80 (pH 7.4)	2	T80 (pH 7.4)	0,6	68,9 ± 3,3	76,2 ± 10,8	0,17 ± 0,00	-30,7 ± 8,2
<b>503H</b>	<b>1</b>	<b>TEA:AcEt (1:1000)</b>	<b>BRIJ 35</b>	<b>1</b>	<b>BRIJ 35</b>	<b>0.3</b>	<b>70,2 ± 6,8</b>	<b>71,3 ± 3,6</b>	<b>0,17 ± 0,01</b>	<b>-29,7 ± 2,5</b>
503H	1	TEA:AcEt (1:1000)	BRIJ 35	2	BRIJ 35	0,6	57,1 ± 7,4	60,5 ± 1,8	0,21 ± 0,02	-27,8 ± 5,7
<b>503H</b>	<b>1</b>	<b>TEA:AcEt (1:1000)</b>	<b>PLURONIC</b>	<b>1</b>	<b>PLURONIC</b>	<b>0.3</b>	<b>77,56 ± 9,10</b>	<b>91,23 ± 3,90</b>	<b>0,09 ± 0,00</b>	<b>-30,8 ± 7,0</b>
503H	1	TEA:AcEt (1:1000)	PLURONIC	2	PLURONIC	0,6	91,4 ± 10,2	90,5 ± 10,2	0,09 ± 0,01	-31,2 ±

ANNEX 2

---

										5,1
<b>503H</b>	<b>1</b>	<b>TEA:AcEt (1:1000)</b>	<b>LECITIN</b>	<b>1</b>	<b>LECITIN</b>	<b>0.3</b>	<b>1,9 ± 2,7</b>	<b>434,4 ± 145,2</b>	<b>0,61 ± 0,19</b>	<b>-37,45 ± 0,1</b>
<b>503H</b>	<b>1</b>	<b>TEA:AcEt (1:1000)</b>	<b>DDAB</b>	<b>1</b>	<b>DDAB</b>	<b>0.3</b>	<b>0,0</b>	<b>52,6</b>	<b>0,33</b>	<b>14,9</b>
503H	1	TEA:AcEt (1:1000)	DDAB	2	DDAB	0,6	0,0	64,9	0,16	39,3



## ANNEX 3

---

**Efficient production of hybrid bio-nanomaterials by continuous microchannel emulsification: Dye-doped SiO<sub>2</sub> and Au-PLGA nanoparticles.**



Larrea A, Clemente A, Luque-Michel E, Sebastian V. Efficient production of hybrid bio-nanomaterials by continuous microchannel emulsification: Dye-doped SiO<sub>2</sub> and Au-PLGA nanoparticles. *Chemical Engineering Journal*, 2017, 316: 663-672.

<https://doi.org/10.1016/j.cej.2017.02.003>